EVALUATION OF LIQUEFACTION POTENTIAL OF SOILS BY USING PROBABILISTIC AND MACHINE LEARNING METHODS

A Thesis Submitted

in partial fulfilment of the requirements for the award of the degree of

DOCTOR OF PHILOSOPHY

In

CIVIL ENGINEERING

By

Nerusupalli Dinesh Kumar Reddy

(Roll No.: 2K18/Ph.D./CE/01)

Under the supervision of

Prof. Ashok Kumar Gupta

&

Prof. Anil Kumar Sahu

DEPARTMENT OF CIVIL ENGINEERING

DELHI TECHNOLOGICAL UNIVERSITY

SHAHBAD DAULATPUR, BAWANA ROAD, DELHI - 110042 (INDIA)

SEPTEMBER 2024

DELHI TECHNOLOGICAL UNIVERSITY

(Formerly Delhi College of Engineering)

Shahbad Daulatpur, Bawana road, Delhi- 110042

DECLARATION

I hereby declare that the research work presented in this thesis entitled "Evaluation of Liquefaction Potential of Soils by Using Probabilistic and Machine Learning Methods" is original and carried out by me under the supervision of Prof. Ashok Kumar Gupta and Prof. Anil Kumar Sahu, Department of Civil Engineering, Delhi Technological University, Delhi, and being submitted for the award of Ph.D. degree to Delhi Technological University, Delhi, India. The content of this thesis has not been submitted either in part or whole to any other university or institute for the award of any degree or diploma.

Date: 17/09/2024 **(Nerusupalli Dinesh Kumar Reddy)**

Place: DTU, Delhi **Roll no.: 2K18/Ph.D./CE/01**

DELHI TECHNOLOGICAL UNIVERSITY

(Formerly Delhi College of Engineering)

Shahbad Daulatpur, Bawana road, Delhi- 110042

Date: 17/09/2024

CERTIFICATE

This is to certify that the PhD thesis entitled “Evaluation of Liquefaction Potential of Soils by Using Probabilistic and Machine Learning Methods " is being submitted by Mr. Nerusupalli Dinesh Kumar Reddy, for the fulfilment of the requirements for the award of the degree of Doctor of Philosophy in Civil Engineering to the Department of Civil Engineering, Delhi Technological University, Delhi, India. He has a bonafide record of original research work carried out by him under my guidance and supervision. The results embodied in this thesis have not been submitted to any other university or institution for the award of any degree or diploma.

(Prof. Ashok Kumar Gupta)
Supervisor
Dept. of Civil Engineering
DTU, Delhi

(Prof. Anil Kumar Sahu)
Joint-Supervisor
Dept. of Civil Engineering
DTU, Delhi

ACKNOWLEDGEMENT

It is my proud privilege to express my heartfelt indebtedness to my research supervisors Prof. Ashok Kumar Gupta, Professor, Department of Civil Engineering, DTU Delhi and Prof. Anil Kumar Sahu, Department of Civil Engineering, DTU Delhi, for their excellent guidance, valuable suggestions and encouragement in the course of the study and preparation of this thesis. Indeed, I am greatly honoured to be their research student and greatly influenced by their penchant for excellence. Their unwavering support and help in the face of all kinds of odds and uncertainties are humbly acknowledged. I avail this opportunity to express my deep sense of gratitude and sincere thanks to my research supervisors for their inspiration, expert guidance, moral support and continuous encouragement, which were vital factors in the successful completion of the present work.

With stupendous ecstasy and profundity of complacency, I pronounce utmost gratitude to Sh. Kewal Singh, retired senior lab technician, Mr. Anil Agnihotri, Mr. Sunil Tirkey, lab technician, and Nitesh, Inder Singh, lab attendant, Department of Civil Engineering, for their valuable help. I also express my gratitude to my colleagues and friends, Kumar Shashwat, Diksha, Deepak Singh, Rahul Kumar Meena, Vijay Kaushik, Srijan, Istuti, Preeti, Sandeep Baghel, Shivangi Bhardwaj, Abhishek Paswan, Yakshansh, Rahul Kumar, Salila Bharati, Shailesh Kumar Gupta, Saurabh Saha, Ruchika Dabas, Noopur Awasthi and Ashwani Sharma for providing me helpful advice, kind cooperation, and friendly discussion at various stages of the work.

Sincere thanks are due to Hon'ble Shri Vinai Kumar Saxena, Chancellor, Delhi Technological University, Delhi and Prof. Prateek Sharma, Hon'ble Vice-Chancellor, Delhi Technological University, Delhi. I would like to thank Prof. K. C. Tiwari, Professor and Head, Department of Civil Engineering, Delhi Technological University, Delhi. Prof. Vijay K. Minocha), the DRC Chairman, and all the faculty members, especially Prof. Nirendra Dev, Prof. A. K. Shrivastava, Dr. Shilpa pal, Prof. Raju Sarkar, Dr. Ritu Raj, and Mr. Hrishikesh Dubey for providing me sensible guidance, faultless planning, helpful advice, and kind cooperation at various stages of the work. I am also thankful to the lab staff and office staff of the Civil Engineering Department for providing the kind cooperation and necessary facilities to carry out the study and grateful to the University for providing financial assistance and support during my degree program.

I am thankful to the Delhi Technological University for providing an opportunity for research through its research fund and sponsoring me to pursue my research. I would also like to thank the DTU Library for providing me with the literature of research content and online journals. The co-operation and encouragement of my colleagues at Delhi Technological University, Delhi, are gratefully acknowledged. I express my special thanks to my friends for their help and valuable support. I express my warm regards and profound gratitude to my esteemed father and my family members for their moral support, encouragement and blessings. I humbly thank all those who, in any manner, directly or indirectly, put a helping hand to complete this research work.

(Nerusupalli Dinesh Kumar Reddy)

ABSTRACT

Soil liquefaction is a substantial seismic hazard that endangers both human life and infrastructure. This research specifically examines the occurrence of soil liquefaction events in past earthquakes, with a special emphasis on the 1964 Niigata, Japan and 1964 Alaska, USA earthquakes. These occurrences were important achievements in the comprehension of harm caused by liquefaction. Geotechnical engineers often use in-situ experiments, such as the standard penetration test (SPT) to evaluate the likelihood of liquefaction. The attraction for this option arises from the difficulties connected in acquiring undisturbed samples of superior quality, as well as the related expenses. Although shear wave velocity tests and Baker penetration tests are alternative in-situ testing, they are less often used in this assessment procedure. Geotechnical engineering specialists choose the deterministic framework for liquefaction assessment because of its clear mathematical approach and low needs for data, time, and effort. This work emphasises the need of integrating probabilistic and reliability methodologies into the design process of crucial life line structures to enable well-informed risk-based decision-making. This research investigates the several methodologies and protocols used by scholars to construct prediction models for evaluating the likelihood of liquefaction. Recently, many models like as Artificial Neural Networks (ANN), Support Vector Machines (SVM), Random Forests (RF), Genetic Programming (GP), Ensemble models, and SVM-Grey Wolf Optimisation (SVM-GWO) have been extensively used to assess the likelihood of liquefaction. Furthermore, the use of probability-based models that include reliability analysis has shown its effectiveness in this matter. This research investigates the constraints of certain models, such as their sluggish convergence rate, vulnerability to model overfitting, and dependence on the inclusion of a single variable. The primary objective of this work is to investigate the nonlinearity of liquefaction and improve existing techniques for assessing liquefaction susceptibility. This initiative adds to the area of geotechnical engineering by helping to reduce the dangers associated with liquefaction.

The objective of this project is to create machine learning models that use deterministic, probabilistic, and reliability-based methods to evaluate the likelihood of soil liquefaction. The work presents a new equation that combines Bayes conditional probability with Genetic Programming (GP). In addition, a novel soil liquefaction prediction model is presented, which improves the correlation features, chi-square, relief characteristics, and technical indicators. This research examines the efficacy of ensemble classifiers, including Deep Belief Networks (DBN), Long Short-Term Memory (LSTM), and Support Vector Machines (SVM), when

integrated with an optimised Bidirectional Gated Recurrent Unit (Bi-GRU), to improve the accuracy of predictions. This research suggests using a new technique called Average Cat and Salp swarm algorithm (AC-SSO) and an Opposition-based self-adaptive shark smell optimizer (OSA-SSO) model to find the best weights in the Bi-GRU model.

This research aims to analyse post-liquefaction and borehole data obtained from the National Capital Region (NCR), with a special emphasis on Delhi. The data used in this study is obtained from the Standard Penetration Test (SPT) database. This research aims to assess the potential for liquefaction and provide performance metrics for liquefaction in the field. The created models are used to construct SPT CRR models. The suggested deterministic approaches use genetic programming (GP) to create CRR models in combination with the commonly employed CSR7.5 model. This research evaluates the effectiveness of deterministic models specifically designed for SPT by comparing them to established statistical approaches utilising separate datasets. This research aims to assess the likelihood of liquefaction occurring by using probabilistic assessment methods. It especially focuses on determining the probability of liquefaction (PL) and measuring the level of caution inherent in deterministic models when it comes to PL. This thesis investigates the correlation between the Fs and PL by using mapping functions derived from the Bayesian theory of conditional probability. This work evaluates the predictive accuracy of created SPT-based probabilistic models over different PL limitations, in comparison to current probabilistic models.

The study presents a sophisticated soil liquefaction prediction model that integrates improved correlation features, chi square analysis, relief characteristics, and technical indicators. This thesis investigates the incorporation of ensemble classifiers, such as Deep Belief Networks (DBN), Long Short-Term Memory (LSTM), and Support Vector Machines (SVM), with an optimised Bidirectional Gated Recurrent Unit (Bi-GRU) to get dependable prediction results. This study presents a new method for calculating the best weights in Bi-GRU by using an innovative AC-SSO and OSA-SSO model. The suggested models are then assessed and contrasted with pre-existing models, including both augmented correlation properties and those without such enhancements. This study presents a strategy that efficiently decreases the percentage of false negatives, which is a crucial part of evaluating the model. By acknowledging the possibility of failure and integrating safety measures, significant improvements have been noticed.

CONTENTS

LIST OF TABLES

LIST OF FIGURES

ABBREVIATIONS AND SYMBOLS

A	Material Attenuation Factor
AC-SSO	Averaged Cat and SSO
AFOSM	Advanced First Order Second Moment
amax	Peak Horizontal Ground Surface Acceleration
ANN	Artificial Neural Networks
Ar	Area replacement ratio
ATR	Average True Range
BA	Balanced Accuracy
Bi-GRU	Bidirectional Gated Recurrent Unit
BN	Bayesian Network
BPNN	Back Propagation NN
BPT	Becker Penetration Test
XGboost	Extreme Gradient Boosting
C_B	Correction Factor for Bore Hole Diameters
CDC	Curiosity-Driven Exploration
C_E	Energy Correction Factor Provided by The Hammer
CMF	Chaikin Money Flow
C_N	Correction Factor for Overburden Pressure
CNN	Convolutional NN
COV	Coefficient of Variation
CPT	Cone Penetration Test
C_R	Rod Correction Factor
CRR	Cyclic Resistance Ratio

C_S	Correction Factor for Using Split Spoons with Space for Liners
CSR	Cyclic Stress Ratio
CSR7.5	Cyclic Stress Ratio Adjusted to A Benchmark Earthquake of Moment Magnitude of 7.5
D50	Mean Grain Size
d	Critical Depth
DBN	Deep Belief Network
DE	Differential Evolution
DGC	Drainage Geo Composite
DT	Decision Tree
DNN	Deep Neural Network
EC	Ensemble Classifiers
ELM	Extreme Learning Machine
EmBP	Emotional Backpropagation Neural Network
EML	Explainable Machine Learning
EPR	Evolutionary Polynomial Regression
ERm	Energy Provided by The Hammer
FC	Fines Content
$f_L(x)$	Probability Density Function of Liquefied
$f_{NL}(x)$	Probability Density Function of Non-Liquefied
FN	False Negative
FORM	First Order Reliability Method
FP	False Positive
FNR	False Negative Rate
FOR	False Omission Rate
FPR	False Positive Rate

Frq	Loading Frequency
Fs	Factor of Safety
g	Acceleration Due to Gravity
$G_{(mean)error}$	Mean Absolute Percentage Error
GA	Genetic Algorithm
GBM	Gradient Boosting Machine
GI	Gini Index
GP	Genetic Programming
GWO	Grey Wolf Optimization
K_σ	Overburden Correction Factor
$K_\propto$	Correction for Static Shear Stress
KNN	K-Nearest Neighbours
LI	Liquefaction Index
$L_{a,l}$	Weights Amid Neurons
LSTM	Long Short-Term Memory
LSSVM	Least Squares SVM
LP	Learning Percentage
LPI	Liquefaction Potential Index
LR	Logistic Regression
LSI	Liquefaction Severity Index
M	Earthquake Magnitude on the Richter Scale
MLR	Multi-Linear Regression
MCC	Matthews Correlation Coefficient
ML-FCN	Multi-Layer Fully Connected Network

MSF	Magnitude Scaling Factor
MVFOSM	Mean Value First-Order Second Moment
(N1)60cs	Corrected Standard Penetration Value of The Site Soil Layer Under Investigation
Neq	Number Of Uniform Stress Cycles
N_m	Measured SPT Blow Count
NN	Neural Networks
NPV	Negative Predictive Value
NB	Naive Bayes
OSA-SSO	Opposition Based Self Adaptive SSO
$\overline{PO}$	output
$\bar{P}_q(\zeta)$	Possibility Function
PCA	Principal Component Analysis
PFEMs	Performance Fitness and Error Metrics
PGA	Peak Ground Acceleration
PI	Plasticity Index
$P\left(L/F_s\right)$	Probability Of Liquefied
P_L	Probability of Liquefaction
$P\left(NL/F_s\right)$	Probability Of Non-Liquefied
PPV	Proportion Of Predicted Positives
PSO	Particle Swarm Optimization
qc	CPT-Cone Resistance
r	Distance of The Site from The Centre of Energy Release
RBFNN	Radial Basis Function Neural Network
RBMs	Restricted Boltzmann Machines

r_d	The Stress Reduction Factor
RF	Random Forest
RMSE	Root Mean Square Error
RNN	Recurrent Neural Network
SHAP	Shapley Additive exPlanations
SMP	Standardised Mean Difference
SPC	Statistical Process Control
SPT	Standard Penetration Test
SRD	Self-Regulated Decision-Making
SSA	Salp Swarm Optimization
SVM	Support Vector Machine
t^P	Pseudo-Temperature
TN	True Negative
TP	True Positive
TPR	True Positive Rate
Vs	Shear Wave Velocity
WT	Water Table Depth
z_d	Vertical Depth from The Ground Surface
θ_a	Biases
$\Delta(N_1)_{60}$	Correction for Equivalent Clean Sand
Δu	Change in Pore Pressure
σ'_{3c}	Effective Confining Pressure
σ_{dc}	Cyclic Deviator Stress
σ_v	The Cumulative Vertical Pressure
σ'_v	Effective Vertical Stress
γ_{cyc}	Cyclic Shear Strain

γ_t	Threshold Shear Strain
τ_{av}	Mean Shear Stress
τ_{cyc}	Maximal Cyclic Shear Stress
τ_{max}	Maximum Shear Stress
λ	Scale Parameter
k	Shape Parameter
μ	Sigmoid Activation Function
$\Re 1, \Re 2, \Re 3$	Randomly Parameters
LI_P	Predicted Value of The Liquefaction Performance Index
F	Liquefaction Index Function Created by the GP
X	Vector of Input Variables
Ci	Constant GP Tree
f	User-Defined Functions
n	Number of Terms in The Target Expression
$C0$	Bias Term
θ_a	Bias Term in DBN
PR^F	Partition Terms in DBN
$K^{\hat{H}}$	Input Vector in DBN
$U^{\hat{H}}$	Output Vector in DBN
$SE_{\hat{H}}$	Square Error in DBN
$L_{a,l}$	Weights Amid in DBN
(M_t, D_t)	Output Layer in LSTM
(X_t, D_{t-1}, M_{t-1})	Input Layer in LSTM
F_t	Sorting The Data to Ignore in LSTM
(J_{MF}, B_{MF})	Weight And Bias to Hidden Layer in LSTM
(J_{IF}, B_{IF})	Weight And Bias to Input Layer in LSTM
ut	Update Gate in Bi-GRU
W_r	Correspond to Weight Matrix of rt
f_r	Correspond to Bias Matrix of rt
R_t	Linear Interruption

R_{t-1}	Hidden State at The Previous Time Step
μ	Sigmoid Activation Function
C, γ, r, d	Constant Parameters SVM
w^T	Transpose of the Weight Vector in SVM
α_i	Lagrange Multipliers
x_i	Training Data Points in SVM
φ_i	Feature Mapping Function in SVM
Ψ	Random Integer
$V_{j,\ell}$	Cat Velocity
$Z_{j,\ell,old}$	Position of Cats
$Z_i^1 = i^{th}$	Initial Population

CHAPTER 1

INTRODUCTION

1.1 General

Natural disasters are devastating occurrences caused by natural phenomena, including earthquakes, floods, hurricanes, tornadoes, and firestorms, among others. These natural calamities have the capacity to cause significant damage to property and result in loss of life. Irrespective of location on the planet, natural disasters have the potential to occur. Natural hazards have been a persistent aspect of human settlement since the inception of human civilization. Such narratives may be found in archival documents, ancient religious texts, and folklore originating from many places worldwide. These tales are believed to have originated thousands of years ago. It is reasonable to assume that the frequency of natural disasters recorded in history, along with the resulting impact on human life and property, has increased in tandem with the expansion of human populations and the decrease in hazard-prone areas (Chaudhary and Piracha, 2021).

Natural catastrophes represent a significant threat to both human lives and the environment. Following a natural disaster, there are immediate and significant consequences on both the social and economic aspects. Conversely, emerging countries with large populations and socio-economic situations that compel people to reside in vulnerable areas have heightened adverse effects from natural disasters. Each week, natural disasters cause over one billion dollars in damages and are forecasted to result in the deaths of one thousand individuals. As to the website www.em-dat.net/ngdc.noaa.gov, earthquakes accounted for around 30% of all deaths and 60% of all property destruction caused by many catastrophic natural disasters worldwide in the past century. While natural catastrophes are no longer seen as a punishment from a higher power, they may still be reduced via the use of effective detection, evaluation, and analytic systems. The simultaneous occurrence of rapid digital computer advancements, the creation of innovative computational algorithms, and their application in hitherto uncharted domains of science and engineering all transpired simultaneously. Recent years have witnessed a substantial surge in the incidence of such activities. Next section aims to provide a succinct rationale for assessing seismic hazard and using machine learning techniques for liquefaction

susceptibility assessments. This is done to ascertain the trajectory that research will follow in this thesis.

1.2 Current patterns of natural disasters

An investigation was carried out to analyse current patterns in natural disasters with the aim of assessing the need for the ongoing research. Records of notable natural calamities that had place globally and in India from 1911 to 2020 are gathered from reputable international and national catastrophe databases, including Wikipedia, national disaster management organizations, and sarc-2 sdc.nic.in, among others". Upon assessing the reliability of the database, the conflicting statistics have been verified. The primary natural dangers are earthquakes, tsunamis, floods, cyclones, and landslides. The table below provides a comprehensive analysis and presentation of the frequency, fatalities, and property damage resulting from the natural catastrophes during the last century (1911-2020). Over the course of the previous century, there has been a consistent rise in the occurrence of severe natural disasters, accompanied by a decline in the number of deaths resulting from these events (Figure 1.1). This exemplifies that the enhanced readiness, The implementation of early warning systems and other incremental preventative actions by the world community has effectively prevented loss of life. Nevertheless, the extent of damage to property resulting from significant natural disasters has increased throughout the same timeframe (Figure 1.1). This suggests that the current measures for reducing the impact of disasters are insufficient in safeguarding facilities against the extreme severity of the risks.

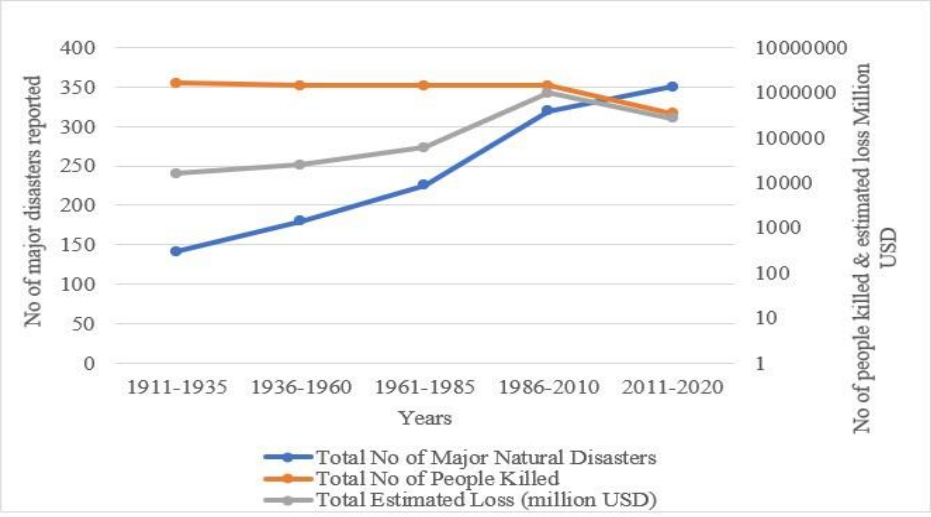

Figure 1.1 Depicts significant natural disasters worldwide. From 1911 to 2020, the recorded casualties and property damage were measured in millions of US dollars

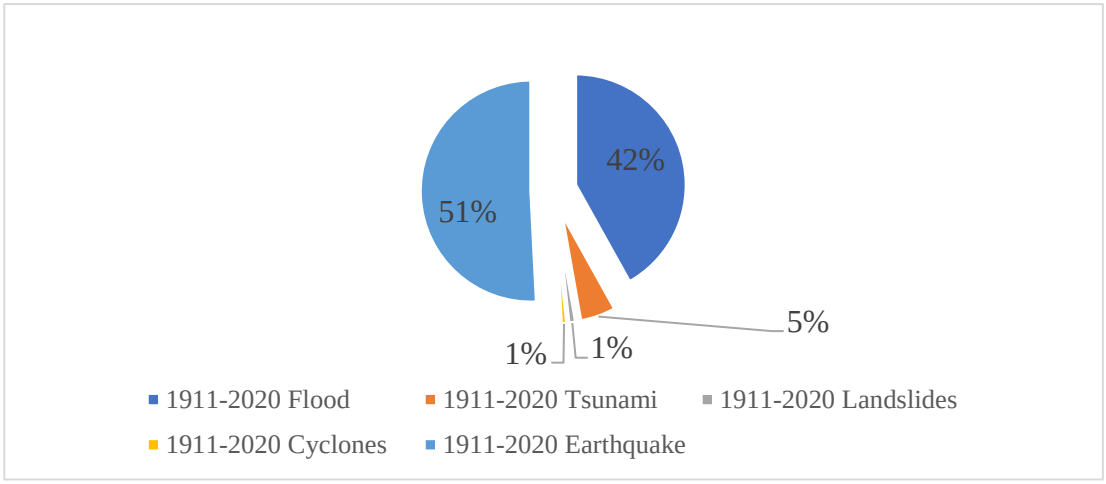

Figure 1.2 Illustrates the global distribution of catastrophic disasters resulting in human fatalities from 1911 to 2020

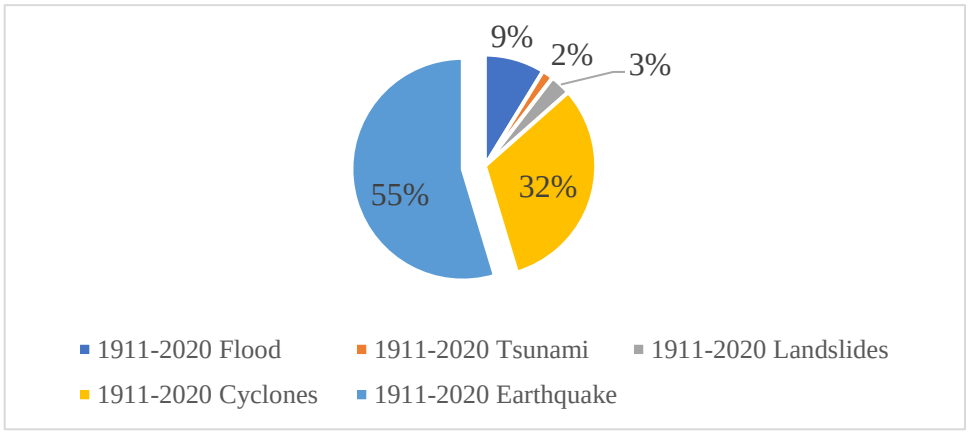

Figure 1.3 Illustrates the global distribution of property damage resulting from significant disasters between 1911 and 2020

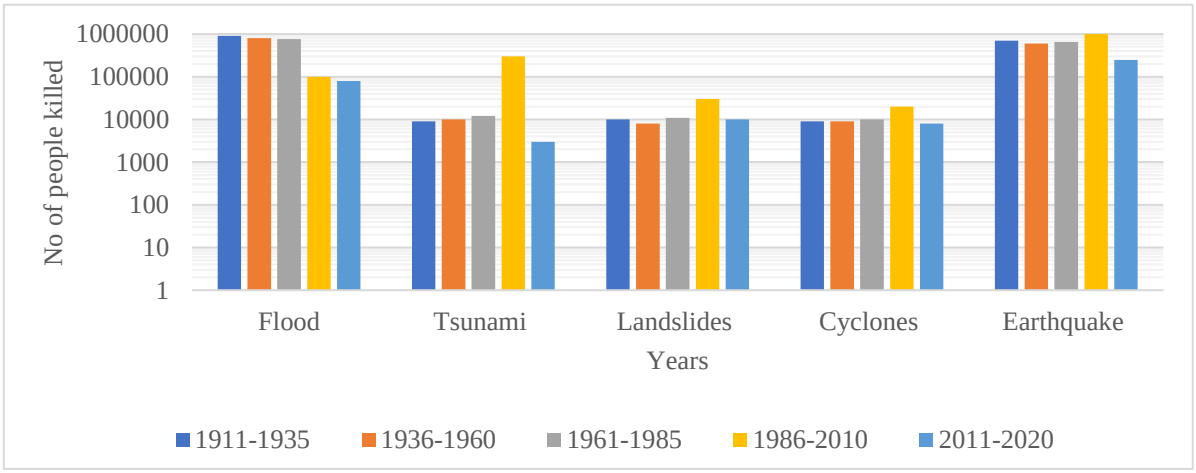

Figure 1.4 Displays the global count of fatalities resulting from significant natural disasters between 1911- 2020

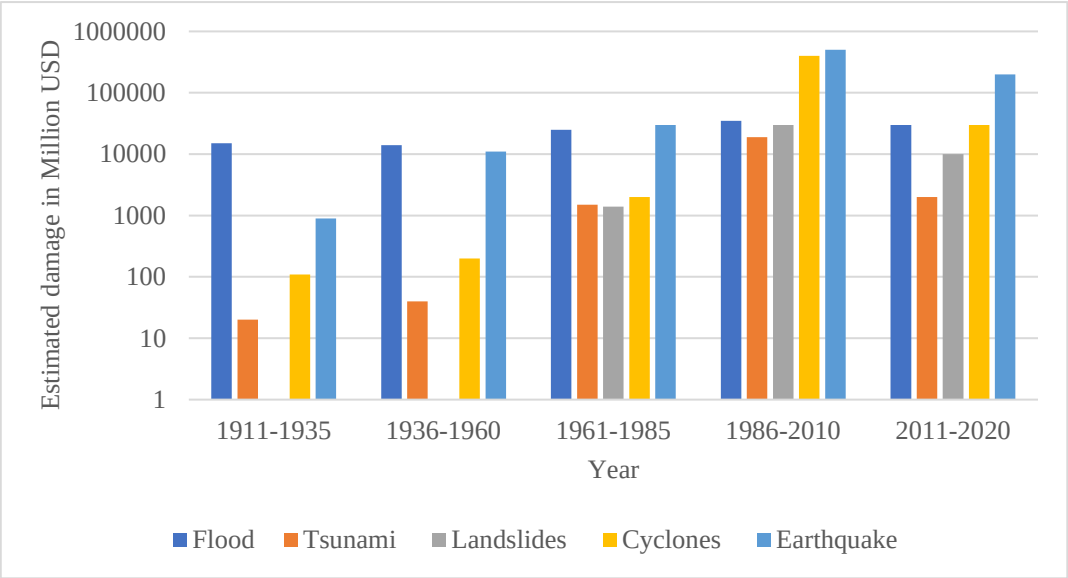

Figure 1.5 Illustrates the extent of property damage caused by significant global disasters from 1911-2020

Figures 1.2 and 1.3 illustrate the varying trends in human mortality and property losses resulting from important natural catastrophes throughout the last century. The flood is responsible for the greatest number of fatalities, while the earthquake inflicts the greatest amount of property damage. Nevertheless, when the data is presented in terms of a 25-year period for human fatalities (Figure 1.4) and property damage (Figure 1.5), it was seen that the impact of the flood on human deaths and property loss has diminished over the last 50 years. Nevertheless, the number of deaths and destruction of property caused by earthquakes has constantly risen over this period. This might be attributed to the enhanced precision of flood prediction models and warning systems, as well as the increased resilience of society against this disaster. The destructive capacity of earthquakes has escalated because of heightened urbanisation and the lack of a sufficient mitigation strategy.

1.3 Soil liquefaction

Seismic hazards include many threats such as ground shaking, structural vulnerabilities, liquefaction, landslides, failures of retaining structures, dangers to essential infrastructure, and tsunamis. The primary cause of both human casualties and infrastructure damage is the liquefaction of soil triggered by seismic activity. Terzhagi and Peck (1948) were the first to recognise and describe the occurrence of soil liquefaction, which refers to the abrupt decrease in strength of loose sand deposits. This discovery played a crucial role in the early development of soil mechanics. However, it was the occurrence of severe earthquakes in various parts of the world, such as Niigata and Alaska (1964), Loma Prieta (1989), Kobe (1995), Kocaeli (1999),

and Chi-Chi (1999), that drew the attention of engineers, seismologists, and the scientific community to this phenomenon (Baziar and Jafarian, 2007). Additional research undertaken in both field and laboratory settings has shown that soil liquefaction may be more accurately described as a catastrophic collapse phenomenon. Soil liquefaction is phenomenon of a saturated soil which is experiencing reduction in effective stress due increases in pore pressure under dynamic condition. The formation of sand boils, major landslides, surface sinking, lateral spreading, movement of bridge supports, settling and swaying of buildings, collapse of maritime structures, and substantial damage to lifeline systems are some of the repercussions that may be caused by soil liquefaction.

There are two types of liquefaction occur, which are flow liquefaction and cyclic liquefaction. Both types of liquefaction are distinct from one another. If the shear force necessary to maintain a soil in a condition of static equilibrium is higher than the residual strength of the soil when it is in a liquefied state, a phenomenon that is referred to as flow liquefaction may take place.

The occurrence of cyclic liquefaction is possible even in situations where the static shear stress is smaller than the shear strength of the soil that has been liquefied. This instance is one in which the distortions that are produced are impacted by shear force that is both recurrent and steady. In most cases, the deformations are brought about suddenly because of the vibrations caused by earthquakes. Shaking caused by earthquakes may lead to considerable and long-lasting deformations or changes. When compared to flow liquefaction, cyclic liquefaction may be seen as occurring in a much wider range of soil and site circumstances. The evaluation of liquefaction hazard includes the study of liquefaction susceptibility, the evaluation of liquefaction effect (that is, the degree to which ground collapse occurs because of liquefaction), and the investigation of the reaction of different foundations in liquefied soil. The evaluation of liquefaction potential, which is a method that assesses the chance of liquefaction happening in each kind of soil after a certain earthquake, is the primary focus of the current research project. One of the most important initial steps in limiting the damage caused by liquefaction is to determine the degree to which the soil is susceptible to liquefaction under seismic stress conditions. Additionally, there are different ways like as cyclic strain-based, energy-based, and cyclic stress-based techniques are also used in the process of evaluating the potential for soil liquefaction the stress-based strategy is more often used than other techniques (Krammer, 1996), and in this study, a cyclic stress-based approach was used to determine the likelihood of liquefaction.

There are two types of cyclic stress-based techniques used to evaluate the possibility for liquefaction. The cyclic tri-axial test and the cyclic simple shear test are two kinds of laboratory tests that may be performed on soil that have not been in any way disrupted and the alternative way is based on empirical connections that relate observed field behaviour with in-situ testing. Some examples of these tests are the standard penetration test (SPT), the cone penetration test (CPT), the shear wave velocity measurement (V_S), and the Becker penetration test (BPT). Liquefaction analysis makes use of sophisticated techniques such as finite element, finite difference, and statistically-derived analytical processes. These approaches are based on the assessment of seismic case histories that are received from the field. In comparison to the other approaches stated, the techniques of finite element and finite difference evaluations are the ones that display the highest level of precision and complexity. Nevertheless, due to the significant variability of liquefied sediments within proximity, a comprehensive site characterization is necessary to establish a precise site model that can be used for a full numerical analysis. Despite doing thorough laboratory testing, it is very difficult to get the right composition of liquefiable soil. Therefore, in-situ investigations and post-liquefaction case histories calibrated with empirical connections are widely used worldwide. Geotechnical engineers across the globe prefer to use cyclic stress-based simpler approaches, including as SPT, CPT, V_S measures, and BPT, to assess the possibility for soil liquefaction. The simplified approach based on the Standard Penetration Test (SPT), first devised by Seed and Idriss in 1971, has undergone many updates and improvements (Seed and Idriss 1982; Seed et al. 1983; Seed et al. 1985; Youd et al. 2001) it remains the most often used method globally. Robertson and Campanella (1985) pioneered the development of a CPT -based technique for assessing the likelihood of liquefaction this method involves converting the SPT-based approach by using an empirical correlation between SPT - CPT and it follows a stress-based approach like the one proposed by Seed and Idriss (1971) and further improvement done to the cone penetration testing (CPT) by Seed and de Alba (1986), Olsen (1988), Shibata and Teparaksa (1988), Mitchell and Tseng (1990), Stark and Olson (1995), Suzuki et al. (1995), Olsen (1997), Robertson and Wride (1998), and Youd et al. (2001) utilising statistical and regression analysis techniques. Multiple simpler procedures using shear wave velocity VS have been developed (Stokoe et al. 1988; Tokimatsu and Uchida 1990; Addo and Robertson 1992; Kayen et al. 1992; Andrus and Stokoe 2000; Juang et al. 2000a; Juang et al. 2001; Andrus et al. 2003) and which are widely using to determine the soil liquefaction. Nevertheless, there are only a limited number of simpler techniques based on the BPT (Becker Penetration Test) technique, including

the ones proposed by Harder and Seed in 1986 and Youd et al. in 2001. These methods, however, are only applicable to soils with a gravelly composition.

The revised Standard Penetration Test (SPT) blow count provides a measure of a soil's ability to withstand liquefaction. The calculation considers elements such as overburden pressure and is correlated with the cyclic resistance ratio (CRR), which indicates the soil's ability to endure cyclic loading. Graphically representing this correlation facilitates the evaluation of soil liquefaction vulnerability during seismic events, providing guidance for building decisions in regions prone to earthquakes. Evaluation of the factor of safety (F_S), which is established by the ratio of the cyclic resistance ratio (CRR) to the cyclic stress ratio (CSR), is required to ascertain the liquefaction potential of a soil when it is exposed to seismic loading. The seismic loading is commonly stated as CSR. The deterministic technique, which involves quantifying the liquefaction potential of soil in terms of the factor of safety (F_S), is preferred by geotechnical specialists for its simplicity in implementation. Parametric and model inaccuracies may lead to situations where $F_S>1$ does not always indicate the absence of soil liquefaction, nor does it guarantee a complete absence of the risk of liquefaction. Furthermore, it should be noted that Fs does not always result in liquefaction and does not guarantee complete liquefaction, as stated by Juang et al. (2000b). The boundary between liquefaction and non-liquefaction situations in deterministic techniques is referred to as a "limit state function." This function is often meant to be cautious, including most cases that have been converted into a liquid state. In recent decades, some geotechnical researchers have successfully forecasted the probability of liquefaction by using reliability analysis, taking into consideration mistakes in models and parameters (Haldar and Tang 1979; Toprak et al. 1999; Juang et al. 2006). Liao et al. (1988) performed a logistic regression analysis on the available case histories to ascertain the probability of liquefaction (P_L). This study presents a straightforward regression equation that may be used to estimate the nominal probability, which serves as a metric for the model's degree of uncertainty. Juang et al. (1999) developed a dependable technique for estimating the likelihood of liquefaction (P_L) using a Bayesian mapping function. Juang et al. (2002) further developed their previously suggested approach for creating a mapping function that relates P_L and F_S. The construction of this mapping function was based on the methods presented by Youd and Idriss in 2001. Goharzay et al. (2017) built upon the first proposal of the first order reliability-based Bayes probability function by Muduli and Das (2013). The Bayesian network (BN) approach has been shown to be a very effective tool for engineers to assess the probability of earthquake-induced liquefaction. In 2021, Hu introduced an innovative approach for

forecasting the liquefaction of soil containing gravel. This technique relies on the use of two Bayesian network models. Hu et al. (2022) developed a hybrid Bayesian network (BN) model to predict liquefaction caused by earthquakes. The model is based on shear wave velocity (Vs) and builds upon previous studies by Hu and Liu (2019), Hu (2021), and Hu et al. (2022), as well as the work of Pirhadi et al. (2023). In their study, Cetin et al. (2004) used an updated database of case histories to establish a new collection of probabilistic and deterministic connections. Their objective was to predict the likelihood of liquefaction start by using the maximum likelihood function inside a Bayesian framework. Subsequently, Idriss Boulanger (2010) and Boulanger and Idriss (2014) devised a method that combines deterministic and probabilistic approaches using SPT data, therefore enhancing the methodology established by Seed and Idriss (1971). The determination of liquefaction potential relies on a set of assumptions and approximations, which form the basis of all suggested conventional techniques and empirical linkages. Fundamentally, difficulties related to assessing liquefaction are very nonlinear. Some of geotechnical researchers developed machine learning methods to overcome the challenges posed by nonlinearity and other complexities in forecasting the likelihood of liquefaction. Goh (1994) developed a neural network model to predict and evaluate the likelihood of liquefaction in saturated, cohesionless soil. Subsequently, additional scholars in the geotechnical domain developed various machine learning techniques, such as neural networks, support vector machine (SVM), genetic programming (GP), least square support vector machine (LSSVM), and stochastic gradient boosting (SPG), for the purpose of conducting liquefaction analysis (Pal 2006; Samui and Karthikeyan 2013; Hanna et al. 2007; Samui et al. 2011; Samui and Hariharan 2015; Xue and Liu 2017). Zhang et al. (2015) devised a non-parametric, multivariate adaptive regression spline (MARS) method to assess the likelihood of liquefaction in sands and granular soils using the energy concept. Zhang et al. (2021) used CPT data to introduce the extreme learning machine (ELM) as a method for assessing the susceptibility of soil deposits to liquefaction. The Artificial Neural Network (ANN) model, which is widely recognised as a leading machine learning approach in this field, has shown good use in the prediction of liquefaction (Samui and Sitharam 2011; Ramakrishnan et al. 2008). ANN models have some significant limitations, such as limited generalisation capacity, slow convergence rate, and susceptibility to overfitting. These shortcomings may adversely affect the accuracy of result prediction. The existing liquefaction assessment methods based on machine learning are fundamentally opaque since they favour accuracy at the expense of explainability. The existing liquefaction datasets are quite small and have a higher

percentage of liquefaction events compared to non-liquefaction events. As a result, these models exhibit distinct performance characteristics when compared to databases from other areas of the world. Subsequently, additional scholars have introduced novel machine learning techniques such as random forest (RF), extreme gradient boosting (XGBoost), and gradient boosting machine (GBM) (Kumar et al. 2022; Kohestani et al. 2015; Zhang et al. 2021a; Zou et al. 2022). Zhang and Wang (2001) have devised an improved ensembled and hybrid method using genetic algorithms, while Zhang et al. (2021b) have developed a hybrid model by incorporating SVM − GWO. Machine learning models that already exist are better options for handling enormous amounts of data and enhancing the accuracy of predictions. Every machine learning approach has its own limitations and constraints due to parameters and model ambiguity (Momeni et al. 2015).

1.4 Motivation of research

According to the literature study discussed in Chapter 2, numerous methodologies and processes have been used by academics throughout the years to build prediction models for evaluating liquefaction potential. In recent years, basic models such as ANN, SVM, RF, GP, Ensemble models, and SVM − GWO, as well as probability-based models with reliability analysis, have been widely used to estimate liquefaction potential. These models have a sluggish convergence rate, suffer from model overfitting, and include just one variable. Due to the nonlinear nature of liquefaction, any improvement in the methodologies that are currently used to evaluate liquefaction potential is a contribution to the area of geotechnical engineering for the purpose of lowering the risks associated with liquefaction that are present. The present study introduces a unique probabilistic approach that combines Genetic Programming (GP) and utilises Bayes conditional probability to suggest a novel equation. Additionally, it presents a unique soil liquefaction prediction model that enables the creation of enhanced correlation features, chi square, relief characteristics, and technical indicators. Dependable prediction outputs may be achieved by combining ensemble classifiers, including Deep Belief Networks (DBN), Long Short-Term Memory (LSTM), and Support Vector Machines (SVM), with an optimised Bidirectional Gated Recurrent Unit (Bi − GRU). This study introduces a novel approach for determining the optimal weights in Bi − GRU. It utilises a distinctive Average Cat and Salp swarm algorithm (AC − SSO) and Opposition based self-adaptive shark smell optimizer (OSA − SSO) model.

1.5 Research objectives and scope

The current research work aims to construct a deterministic, probabilistic, and unique soil liquefaction prediction model to determine the liquefaction potential of soil by using liquefaction SPT database.

- Post-liquefied and site-liquefaction data collection from various sources and sites.
- To develop Probability based model for liquefaction data set.
- To develop python-based industrial useable machines learning algorithm for liquefaction data set.
- To make a comparison among the all-developed models and optimize the best model for a data set.

1.6 Structure of thesis

This thesis is divided into seven chapters. which have been arranged in the following sequence.

- **Chapter 1** of this thesis begins with a concise introduction, followed by an examination of the current trend in natural disasters and a study on liquefaction. The chapter then proceeds to Summarise the motivation, scope, and objectives of the research activity, so establishing the foundation for the whole thesis.
- **Chapter 2** of this study provides a comprehensive literature review on the topic of liquefaction susceptibility analysis. This chapter discusses the several methodologies used in the study of liquefaction triggering, as well as the in-situ test-based procedures utilised for evaluating the susceptibility to liquefaction. Additionally, the chapter explores the numerous methods of analysis and analytical tools that are often employed in this field.
- **Chapter 3** focuses on providing a comprehensive account of the approaches used, namely genetic programming (GP), to construct several models for the purpose of assessing the potential for liquefaction. It provides an overview of the basic concept and practical use of Genetic Programming (GP), as well as the type known as Multi-Gene Genetic Programming (MGGP)). Additionally, the incorporation of a novel soil liquefaction prediction model enhances the correlation features, chi-square values, relief characteristics, and technical indicators. Classifiers such as Deep Belief Networks (DBN), Long Short-Term Memory (LSTM), and Support Vector Machines (SVM), and optimised Bidirectional Gated Recurrent Unit (Bi − GRU). are often used

in many applications. The study introduces two innovative optimization algorithms: the Average Cat and Salp swarm algorithm (AC − SSO) and the Opposition-based self-adaptive shark smell optimizer (OSA − SSO) model.

- **Chapter 4** presents an analysis conducted on the liquefaction SPT database data visualisation. The purpose of this analysis was to examine the entropy and dependence of variables. Additionally, deterministic models were created using the MGGP approach. The created model was verified by using an independent database. When discussing the use of GP as an alternative predictive tool, it is important to consider several elements such as the selection and tuning of GP parameters. Additionally, it is necessary to explore different statistical measures that may be used to evaluate the performance of different prediction approaches.
- **Chapter 5** of this study examines the assessment of liquefaction susceptibility using a probabilistic approach. This chapter discusses the construction of a Bayesian mapping function for the liquefaction studied data. The function utilises the deterministic models of Standard Penetration Test (SPT) described in Chapter 4. This chapter presents a comparison of the efficiency of the produced models with the existing SPT probabilistic models.
- **Chapter 6** of this study introduces a novel soil liquefaction prediction model that enables the creation of enhanced correlation features, chi square, relief characteristics, and technical indicators. The combination of ensemble classifiers, including Deep Belief Networks (DBN), Long Short-Term Memory (LSTM), and Support Vector Machines (SVM), and optimised Bidirectional Gated Recurrent Unit (Bi − GRU). enhances the achievement of reliable prediction results. This chapter presents a novel approach for determining the optimal weights in Bi − GRU, using the Average Cat and Salp swarm algorithm (AC − SSO) and Opposition based self-adaptive shark smell optimizer (OSA − SSO) model.
- **Chapter 7** of this thesis presents generalized conclusions derived from a range of investigations, while also indicating the area of future study.

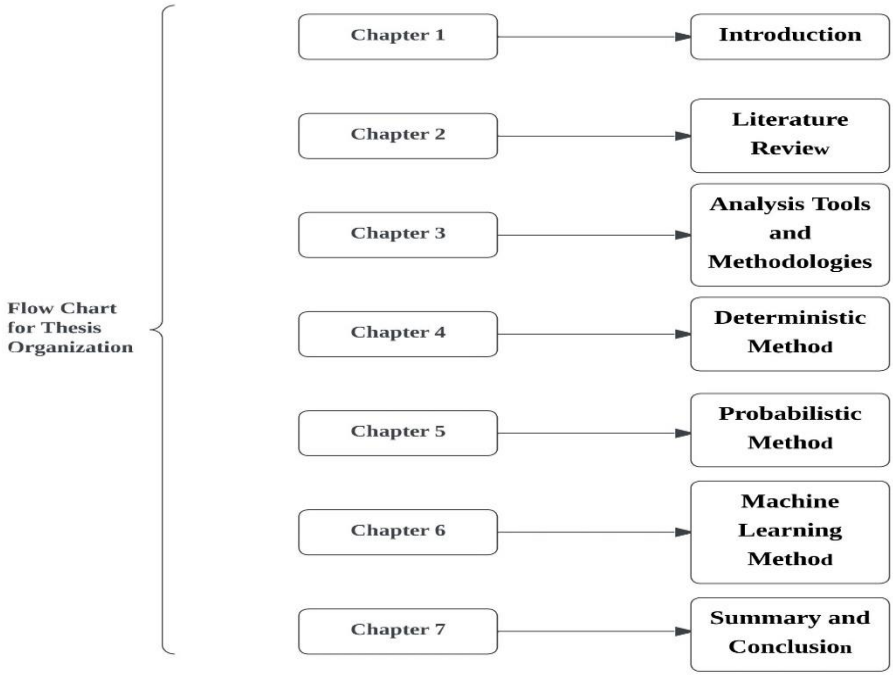

Figure 1.6 Presents a flow diagram illustrating the structure and arrangement of the thesis

The Figure 1.6 illustrates the overall framework and approach for determining the liquefaction potential of soil via the use of SPT data and probabilistic and machine learning methodologies.

CHAPTER 2

LITERAURE SURVEY THE STUDY AREA

2.1 Introduction

The process of assessing liquefaction danger includes analysing the susceptibility of liquefaction, evaluating the potential for liquefaction, assessing the impact of liquefaction (i.e., the degree of ground collapse induced by liquefaction), and studying the reaction of different foundations in soil that has undergone liquefaction. The following are the primary issues of geotechnical engineers. However, the current work primarily examines the assessment of liquefaction potential, which involves determining the probability of liquefaction initiation in a specific soil during each seismic event. This chapter provides an overview of several methodologies used to assess the possibility for liquefaction. The accessible research papers are provided in four distinct sections. Part I examines several ways for assessing the possibility for liquefaction, whereas Part II specifically examines the stress-based approach, with a focus on in-situ test-based methodologies. Part III discusses the many ways of analysis used to estimate liquefaction potential within the stress-based approach framework. These approaches include the deterministic, probabilistic, and machine learning methods. The last section provides a description of the several analytical approaches used in model creation to evaluate the possibility for liquefaction.

2.2 Liquefaction potential evaluation

After identifying a certain soil as liquefiable using several susceptibility criteria outlined by Kramer (1996), the subsequent step in the assessment of liquefaction hazard involves examining the potential for liquefaction, which is the main objective of the present study. The liquefaction potential of a saturated cohesion-less soil in level ground is primarily determined by the intensity and duration of earthquake loading, as well as the engineering properties of the soil. Various methodologies, including as the energy-based approach, the cycle stress-based strategy, and the cyclic strain-based methodology, may be used to analyse the likelihood of liquefaction. The following subsections provide succinct explanations of each of the three strategies that are described farther down in this article.

2.2.1 Energy-oriented strategy

The energy-oriented strategy is highly suitable for evaluating the liquefaction potential, since it accurately captures both the cyclic stress and strain amplitudes via the dissipated energy. When a dry soil undergoes cyclic loading, it undergoes densification by expending energy to reorganise its individual particles. In saturated soil, densification leads to an elevation in pore water pressure when the soil grains need less energy to reorganise owing to a reduction in contact pressures under un-drained conditions. Davis and Berrill (1982) devised an energy-based approach, as seen in equation 2.1, where the accumulation of pore water pressure is attributed to the dissipated seismic energy at a specific location. They also proposed an expression as a criterion for liquefaction. Berrill and Davis (1985) modified their previous model and derived an equation that considers the non-linear correlation between pore pressure increase and dissipated energy, the influence of natural attenuation, and a revaluation of the relationship between the magnitude of an event and the total radiated energy.

$$\frac{\Delta u}{\sigma'_v} = \frac{120A^{0.5}10^{0.75M}}{rN_1^{1.5}\sigma_0'^{0.75}} \tag{2.1}$$

Where;

Δu = change in pore pressure, σ'_v = effective vertical stress, N1 = The adjusted SPT value of the soil layer situated at the location under study, A = the attenuation factor of the substance, M = magnitude of the earthquake, r = measures the distance between the site and the place of energy release or earthquake formed.

Law et al. (1990) used the energy concepts and formulated a criterion for the manifestation of liquefaction in sands, as shown below.

$$\frac{10^{1.5M}}{2.28\times10^{-10}N_1^{11.5}r^{4.3}} \geq 1.0 \tag{2.2}$$

Previous studies have shown connections between the increase in pore pressure and the amount of energy released during ground shaking (Figueroa et al. 1994; Ostadan et al. 1996). The initiation of liquefaction may be determined by comparing the estimated unit energy obtained from the time series data of a design earthquake with the energy-based resistance to liquefaction, which is determined by the in-situ parameters of the soil (Lianget al. 1995; Dief

2000). The energy-oriented strategy, nonetheless, are used less often owing to the lack of high-quality data required for calibrating these methods.

2.2.2 The methodology based on cyclic strain

This method relies on concrete evidence suggesting that the compaction of dry sands is mainly influenced by cyclic strain. A further point to consider is that there is a certain threshold volumetric strain beyond which compaction does not take place. There is a clear correlation between the dry density of sand and its capacity to create additional pore pressure when it reached saturation. This shows that pore pressure formation is primarily linked to cyclic strains rather than cyclic stress. This technique expresses the loads caused by earthquakes in terms of cyclic strains. The temporal evolution of the repetitive shear deformation may be approximated by the examination of the ground reaction. Dorby et al. (1982) devised a simpler approach to estimate uniform cyclic shear strain (γ_{cyc}) based on the amplitude of uniform cyclic stress, as first suggested by Seed and Idriss (1971). After calculating γ_{cyc}, it is then compared to the threshold shear strain (γ_t). If the $\gamma_{cyc}$is smaller than the γ_t, there will be no generation of pore water pressure, and as a result, liquefaction cannot be begun. If the γ_{cyc} is greater than the γ_t, then liquefaction may occur. The liquefaction potential may be evaluated by comparing the earthquake-induced cyclic loading, which is quantified in terms of the amplitude of a series of uniform strain cycles, with the resistance to liquefaction. This comparison can ensure that the liquefaction potential is accurately determined. This resistance is represented as the cyclic strain amplitude that must be present to induce liquefaction in the same number of cycles. Liquefaction may occur when the amount of pressure applied surpasses the resistance to liquefaction at certain depths.

Dorby et al. (1984), devised a torsional tri-axial test with the purpose of measuring liquefaction resistance. This test was carried out by applying strain controlled cyclic torsion to a cylindrical tri-axial specimen to impose cyclic stresses under circumstances of un drained. As a result, there is an increase in pore pressure in the specimen. As compared to the cycle stress technique, the cyclic 16 strain approach is not employed by a significant number of industries. This is because cyclic strain amplitudes are not as accurately predicted as cyclic stress amplitudes, and the cyclic strain-controlled testing equipment is not as readily available as the cyclic stress-controlled testing equipment (Kramer and Elgamal, 2001). As a result, the assessment of

liquefaction potential via the use of cyclic stress-based methodologies is the primary emphasis of this chapter.

2.2.3 The methodology based on cyclic stress

The seismic loading is quantified in relation to the cyclic shear stress using this approach. Next, a comparison is conducted between the stress and the soil's liquefaction resistance, which is determined using the cyclic shear stress. Liquefaction is anticipated once the load exceeds the soil's resistance. The assessment of earthquake loading may be done by two distinct methods: (i) undertaking a thorough analysis of ground reaction; and (ii) utilising the simplified strategy first proposed by Seed and Idriss (1971) and its subsequent modifications. The simplified approaches are much more popular in comparison to the first approach. The simplified model proposed by Seed and Idriss (1971) used to predict the uniform cyclic shear stress amplitude induced by seismic loading on flat or gently sloping terrain. The model is shown in equation 2.3 below.

$$\tau_{av} = 0.65 \frac{a_{max}}{g} \sigma_v r_d \tag{2.3}$$

Where:

τ_{av} = Mean shear stress; σ_v = The cumulative vertical pressure at the specified depth; a_{max}= Maximum horizontal acceleration; and g = Acceleration due to gravity and r_d = The stress reduction factor (e.g., r_d= 1 relates to rigidity behaviour), as shown in Figure 2.1. and r_d can be written as:

$$r_d = \frac{(\tau_{max})_d}{(\tau_{max})_r} \tag{2.4}$$

The $(\tau_{max})_d$ indicates maximum shear stress for deformable soil element, whereas $(\tau_{max})_r$ indicates maximum shear stress rigid soil element. so, factor 0.65 is to accurately reflects the actual condition of the field.

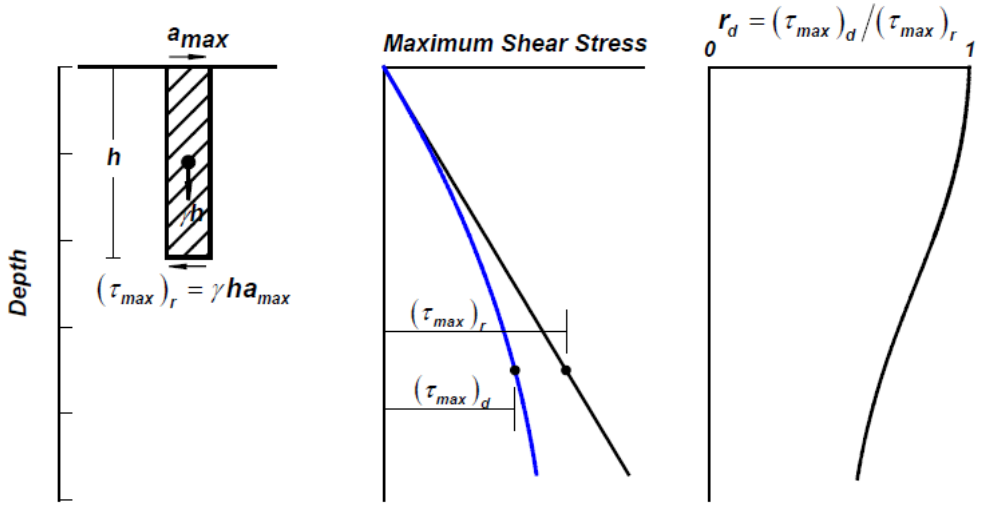

Figure 2.1 Illustrating the process of calculating the maximum shear stress (τ_{max}), and the stress reduction coefficient, (r_d) (Seed and Idriss in 1971)

The liquefaction resistance of a soil element is defined by its closeness to the failure state and the kind of force required to transfer it from its original state to the failure state. The cyclic stress-based technique is often used for evaluating the possibility for liquefaction, and there are two approaches within this approach that may be utilised. The first method involves evaluating undisturbed samples in a laboratory setting. The second strategy is based on empirical linkages, which create a relationship between the behaviour of soil in the field and tests that are conducted in the field.

2.2.3.1 The methodology-based laboratory

In the laboratory, there are two different kinds of tests that may be employed to evaluate the liquefaction resistance. The cyclic tri-axial test and the cyclic simple shear test are the two exams that are being performed here. These tests may be performed on materials that have not been altered in any way. For the purposes of these tests the moment at which the initial process of liquefaction is finished or when a certain cyclic strain amplitude limit is achieved is the point when liquefaction failures happen. The results of the laboratory tests reveal that the number of loading cycles necessary for liquefaction failure reduces as the shear stress increases and the density of the soil decreases. A normalisation of the cyclic strength is achieved using the initial effective overburden pressure, which ultimately results in the production of the cyclic stress ratio (CSR). Within the framework of the cyclic simple shear test, the CSR is the ratio of cyclic shear stress and initial vertical effective stress, represented as $(\mathrm{CSR})_{ss} = \tau_{cyc}/\sigma'_y$. The cyclic

tri-axial test evaluates the ratio of maximal cyclic shear stress and the two times of effective confining pressure. The ratio may be represented as $(\mathrm{CSR})_{\mathrm{tx}} = \sigma_{\mathrm{dc}}/2\sigma'_{3\mathrm{c}}$.

Where:

σ_{dc} is cyclic deviator stress and $\sigma'_{3\mathrm{c}}$ is the effective confining pressure. It is not possible to compare the CSRof the two tests that were discussed before since they apply quite different loads,

$$(\mathrm{CSR})_{\mathrm{ss}} = \mathrm{cr}\ (\mathrm{CSR})_{\mathrm{tx}} \qquad (2.5)$$

Seed and Lee (1966) found that the earliest occurrence of liquefaction in saturated sands under cyclic loading occurs when the increase in pore pressure matches the original effective confining pressure. This definition was obtained from their research. Seed and Idriss (1967) devised an empirical method to evaluate the susceptibility of soil deposits to liquefaction by integrating laboratory-derived pore water pressure data with seismic response predictions of shear stress over time. This approach was developed to assess the susceptibility of soil deposits to liquefaction. Seed et al. (1975) established a model to calculate the number of uniform stress cycles, Neq, required to produce the same rise in pore pressure as an irregular time history. This model is derived using an amplitude that corresponds to 65% of the maximum cyclic shear stress is represented as $\tau_{\mathrm{avg}} = 0.65\tau_{\mathrm{max}}$. It was possible to do this by applying a weighting mechanism to a collection of shear stress time records that were derived from the severe ground motions that were documented. It was established by Ishihara and Koseki (1989) that penalties have a little impact on the resistance to liquefaction when the plasticity indices are lower than 10. A mathematical model was created by Chern and Chang in 1995 with the purpose of evaluating the liquefaction qualities of soil that has been subjected to cyclic stress via the occurrence of earthquakes, derived from the results of cyclic triaxial testing. It is possible to estimate the cyclic shear strength, by the number of cycles required for liquefaction, and the formation of excess pore pressure. Bray and Sancio (2006) demonstrated the susceptibility of these soils to liquefaction by cyclic testing of a wide range of soils with a fine-grained texture. The liquefaction of these soils at Adapazari (1999) was seen following the Kocaeli earthquake. Gratchev et al. (2006) examined the reliability of the plasticity index (PI) as a criterion for assessing the liquefaction potential of clayey soils under rotating stress. It was found that an increase in PI led to a decrease in the soil's ability to liquefy, and soil with a PI higher than 15 appear to be non-liquefiable. This finding aligns with the outcomes of previous investigations. Given the substantial challenges and costs associated with obtaining undisturbed samples from

cohesion-less soil deposits, several engineers choose to use the field performance correlation-based approach. This is despite the fact that assessment of liquefaction potential based on laboratory test gives satisfactory findings. In this research, the emphasis is placed on in-situ test-based approaches that are currently accessible for evaluating liquefaction potential.

2.2.3.2 Methods based on in-situ tests

The possibility of soil liquefaction may be determined by conducting in-situ tests, including the standard penetration test (SPT), the cone penetration test (CPT), the shear wave velocity (Vs) measurement, and the Becker penetration test (BPT). Because obtaining undisturbed soil samples and performing precise laboratory tests on granular soils pose significant challenges, geotechnical engineers often rely on in-situ tests and calibrated empirical relationships based on case histories to assess the likelihood of soil liquefaction. The simpler approach developed by Seed and Idris (1971) relies mostly on a boundary curve. This boundary curve establishes a threshold that distinguishes between instances of liquefaction and non-liquefaction in soil during earthquakes, using field observations and data collected on-site. Typically, the barrier is carefully established by ensuring that any occurrences of liquefaction are positioned above it. The earthquake loading parameters in this approach often use the cycle stress ratio (CSR), while the in-situ test parameters are employed to indicate the cyclic resistance ratio (CRR), This indicates the engineering properties of the soil and its ability of generate pore pressure. The SPT and CPT-based strategies are often used to evaluate the vulnerability of soil to liquefaction, rendering them the favoured in-situ techniques among the several alternatives previously discussed.

Methodology derived from the CPT

Despite its significance in assessing liquefaction resistance, the SPT-based technique does possess a few limitations. The primary reason of these problems is the fluctuating character of the SPT, as shown by Robertson and Campanella (1985) and Skempton (1986). The cone penetration test (CPT) is gaining popularity in contemporary times because to its reliability, reproducibility, and capacity to ascertain an uninterrupted soil profile. The Cone Penetration Test (CPT) is used as a valuable tool to assess several soil characteristics, together with the soil's susceptibility to liquefaction. A conventional Cone Penetration Test (CPT) involves inserting a conical penetrometer with a diameter of 35.7 millimetres into the ground at a consistent speed of 2 centimetres per second. Simultaneously, electronic transducers measure

the force exerted on the conical tip, To determining the tip resistance, qc, the force that is applied at the tip of the penetrometer is divided by the cross-sectional area of the instrument. A similar calculation is used to determine the sleeve friction, which is indicated by the symbol fs, is the ratio of force of drag on the sleeve to the surface area of the sleeve. Compared to the SPT, the CPT has many advantages, with the most significant being its ability to provide a continuous measurement of penetration resistance and its reduced vulnerability to operational errors. The primary limitations of the CPT include its inability to penetrate strata containing gravels or with high penetration resistance, as well as its reliance on companion borings or soundings to get authentic soil samples.

Zhou was the pioneer in 1980 to provide a direct link between liquefaction and the case history CPT database of the Tangshan earthquake in 1978. At a depth of fifteen metres, he showcased the significant significance of cone penetration resistance, which may distinguish between situations that can be liquefied and those that cannot. Seed and Idriss (1981) as well as Douglas et al. (1981) suggested using correlations between the SPT and CPT to convert the existing SPT-based charts for use with CPT data. Robertson et al. (1985) established a CPT approach for measuring liquefaction potential. This approach is a transformation from an SPT –based method that use empirical correlation of SPT – CPT data. Furthermore, it adheres to the stress-based methodology introduced by Seed and Idriss (1971). Seed and de-Alba (1986), Shibata and Teparaksa (1988), Stark and Olson (1995), Suzuki et al. (1995), Olsen (1997), and Robertson and Wride (1998) are among the experts who have modified and improved this technique.

The fundamental methodologies utilizing CPT are outlined in figure 2.2, showcasing the limit state function, often called the boundary curve. This figure also presents a graph illustrating the relationship between the cyclic resistance ratio (CRR) and the corrected CPT tip resistance (QC), effectively delineating between liquefied and non-liquefied conditions. These techniques need the inclusion of further data, such as the average particle size (D50) and the proportion of fine particles (FC). Solely relying on CPT measures is insufficient to get this information. To ascertain the values of D50 and FC, it is important to gather samples from further boreholes. Regarding the assessment of liquefaction resistance in silty sands with more than 5% fines, Ishihara (1993) suggested that the effects of fines could be estimated by adding certain increments to the measured tip resistance. This would result in an equivalent tip resistance for clean sand. This would enable the calculation of the impacts of penalties. Olsen (1997) developed a CRR model that used the parameters qc, $\sigma'v$, and friction ratio (Rf) only to assess

the probability for liquefaction, relying solely on CPT data. The NCEER workshop in 1998 recommended its usage, and it is also included in the summary piece by Youd et al. (2001). Robertson and Wride (1998) devised a unique methodology that use the soil behaviour type index, denoted as Ic. The CRR for clean sands, characterised by a fines content (FC) of 5% or less, is determined by analysing the CPT data, as seen in Figure 2.2. Only the earthquake with a magnitude of 7.5 may be used for the purpose of validating this graphic, namely Figure 2.2.

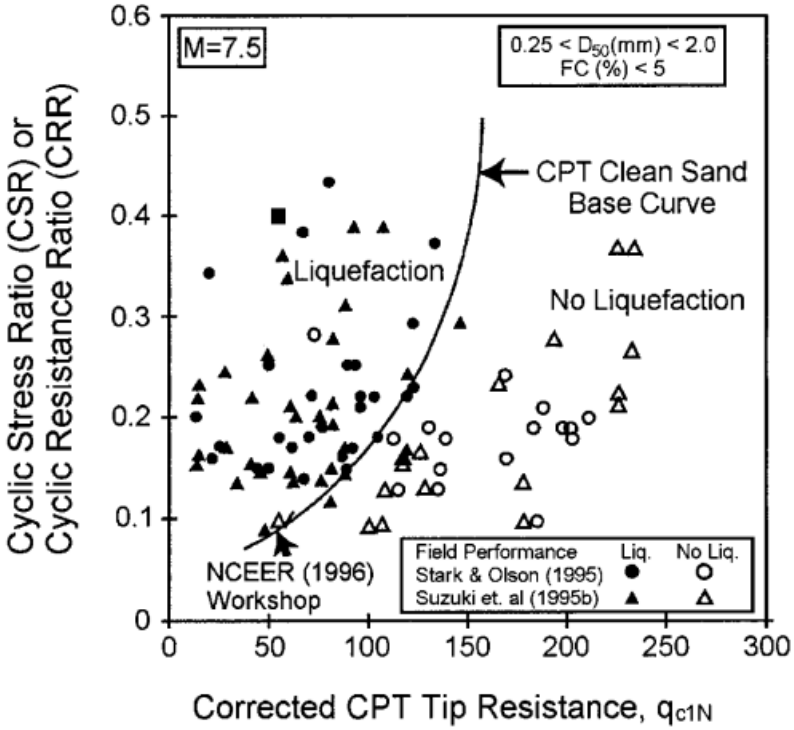

Figure 2.2 Curve recommended for calculation for CRR from CPT data (Robertson and Wride 1998)

Methods using the shear wave velocity (V_s)

The use of shear wave velocity (Vs) as an in-situ measurement to assess the soil's resistance to liquefaction is well acknowledged. This is because both Vs and CRR are similar, yet they do not exhibit a straight proportionality but several parameters, including the void ratio (e), effective confining loads, stress history, and geologic age, have an impact on them. The enumeration presents a concise overview of the main advantages derived from use Vs for assessing liquefaction potential. (i) shear wave velocity (Vs) method conducted in soils that provide difficulties for penetration using SPT and CPT methods or for extracting undisturbed samples, such as sandy and gravelly soils. They are also useful in regions where drilling or probing may not be allowed. The small-strain shear modulus plays a crucial role in analytical

methods used to forecast the dynamic behaviour of soil and assess the interaction between soil and structures. (ii) shear wave velocity (Vs) method is a fundamental mechanical characteristic of soil materials, and it is closely linked to the small-strain shear modulus in the context of soil materials. However, the use of Vs for assessing liquefaction resistance is coupled by some disadvantages: Initially, seismic wave velocity measurements are conducted at low degrees of deformation, but the development of pore-water pressure and the onset of liquefaction occur at medium to high levels of deformation. Seismic testing does not yield samples suitable for soil classification or the identification of clay-rich soft soils that do not liquefy. Additionally, if the measurement interval is extended, it is possible that thin layers with low seismic wave velocities may go undetected. Hence, it is advisable to conduct an adequate number of boreholes and perform in-situ tests (such as SPT or CPT) to distinguish and classify thin liquefiable layers, Some of the simpler techniques that have been created and are currently being used include the methodologies developed by Dobry et al. (1981), Stokoe et al. (1988), Tokimatsu and Uchida (1990), Robertson et al. (1992), Kayen et al. (1992), Lodge (1994), Andrus and Stokoe (1997), Andrus and Stokoe (2000), Juang et al. (2000a), Juang et al. (2001), and Andrus et al. (2003). The use of the Vs-based approach is much less frequent as compared to the SPT-based methodology and the CPT-based method. This is in opposition to the SPT-based approach and the CPT −based approach. The reason for this is because the Vs technique is still in its infancy and has not yet undergone validation against the historical post-liquefaction database. This is the cause-and-effect relationship.

Methods derived from the Becker penetration test (BPT)

In most cases, the capacity of non-gravelly soils to endure liquefaction has been evaluated via the use of the Standard Penetration Test (SPT) and the Cone Penetration Test (CPT), On the other hand, measurements of shear wave velocity (Vs) are only carried out in very unusual circumstances. Penetrometers with a big diameter have been used by a number of researchers in order to circumvent these challenges. The Becker penetration test, often known as the BPT, is widely acknowledged as a highly efficient and frequently used method for large-scale investigation. In the late 1950s, Canada was the location where the Bottom Pressure Recorder, often known as the BPT, was invented. The structure is made up of a cylindrical casing that is three metres in length and has a diameter of 168 millimetres or three metres. Within the casing, there are two walls that come together to form a building that has two walls. A dual-action pile hammer that is powered by diesel is used to force the pile into the ground on the ground. The hammer hits are administered at the base of the casing, and the penetration continues without

interruption for the whole of the process. In order to determine the Becker penetration resistance, the number of blows that are necessary to drive the casing through an increment of 300 mm. There is a lack of standards within the BPT, which has led to the use of a wide variety of apparatus and processes during the history of its development. In the present moment, only a limited number of liquefaction sites have been used for the purpose of collecting BPT data. As a result, the BPT cannot be directly connected with the conduct experienced in the field. In its place, it is of the utmost importance to compute comparable SPT Nm-values by making use of the information obtained from the BPT. As a consequence of this, assessment approaches that are founded on the SPT may be used in order to establish the relationship with field behaviour. The calculation of the CRR is subject to a significant amount of extra uncertainty as a result of the use of this indirect technique. However, only a small number of less complicated approaches that depend on BPT have been developed (Harder and Seed 1986 and Youd et al. 2001). This is mostly due to the fact that BPT is only appropriate for soil that has a gravelly character.

SPT based method which used for study

A stress-based technique to evaluate the likelihood for liquefaction triggering was first devised by Seed and Idriss (1967). This approach was presented in the year 1967. This methodology has been employed extensively over the course of the previous 45 years (for instance, Seed and Idriss 1971, Shibata 1981, Tokimatsu and Yoshimi 1983, NRC 1985, Seed et al. 1985, Youd et al. 2001, Cetin et al. 2004, Idriss and Boulanger 2004). The cyclic stress ratios (CSR) that are created by earthquakes and the cyclic resistance ratios (CRR) of the sediment are compared in the basic framework, which has been recognised by a significant number of scholars. This comparison is necessary in order to understand the relationship between the two. The components of this framework were built in order to provide a methodical assessment of the many factors that have an effect on the cycle resistance and the penetration resistance of the material. The following provides a concise description of these components for understanding. At a certain depth, z, inside the soil profile, the earthquake-induced concrete shear resistance (CSR) is often defined as a typical or consistent value that is equivalent to 65% of the cyclic shear stress ratio, represented as:

$$\mathrm{CSR}_{\mathrm{M},\sigma'_{\mathrm{v}}} = 0.65\,\frac{\tau_{\max}}{\sigma'_{\mathrm{v}}} \tag{2.6}$$

Where:

The symbol τ_{max} denotes the highest shear stress caused by an earthquake, σ'_v represents the vertical effective stress, earthquake M is magnitude and in-situ σ'_v. The reference stress level, represented by the factor 0.65, was first determined by Seed and Idriss (1967) and has remained unchanged in subsequent use. It is possible that selecting a different reference stress level may result in changes to the values of certain components and relationships; nevertheless, this will not have any impact on the definitive outcomes of the liquefaction evaluation technique. Assuming that the same stress level is used consistently throughout the whole process, including forward computations. To estimating the value of τ_{max}via the use of dynamic response studies, it is necessary to include a considerable quantity of input acceleration time series and trustworthy site characterisation information. This is done to guarantee that the study is sufficiently robust. There is also the possibility of calculating the maximum shear stress by using the equation that is obtained from the Seed and Idriss Simplified Liquefaction Procedure.

$$CSR_{M,\sigma'_v} = 0.65 \frac{\sigma_v}{\sigma'_v} \frac{a_{max}}{g} r_d \quad (2.7)$$

Where $\sigma_v =$ vertical total stress at defined depth z, $\frac{a_{max}}{g}$ = maximum horizontal acceleration, and r_d = The shear stress reduction factor incorporates the dynamic behaviour of the soil profile.

Cyclic resistance ratio (CRR)

The Cyclic resistance ratio (CRR) of the soil is often linked to an in-situ measurement, such as the number of blows per depth in the Standard Penetration Test (SPT), the penetration resistance in the Cone Penetration Test (CPT), or the velocity of shear waves (Vs). The SPT blow counts are affected by many procedural elements, such as the length of the rods, the energy of the hammer, the specifications of the sampler, and the size of the borehole, as well as the effective overburden stress. Consequently, the link to CRR relies on the modified penetration resistance.

$$(N_1)_{60} = C_N C_E C_R C_B C_S N_m \quad (2.8)$$

The C_N represents the correction factor for overburden pressure. The C_E = ER_m/60%, ER_m. ERm represents the energy provided by the hammer as a the proportion of the hammer's energy that is theoretically free-falling. In order to compensate for the diminution in energy ratios that is associated with shorter rod lengths, the rod correction factor, also known as C_R, is used. The correction factor for nonstandard borehole diameters is denoted as C_B. C_S represents the

correction factor for using split spoons with space for liners. Lastly, N_m refers to the measured SPT blow count. If conventional processes are followed, the factors C_B and C_S are assigned a value of 1.

The soil's cyclic resistance ratio (CRR) is influenced by the magnitude scaling factor (MSF), and the effective overburden stress, which is represented by the K_σ factor. The correlation for CRR is first derived using a reference value of M = 7.5 and $\sigma'_v = 1$ atm. the modified CRR is represented as :

$$CRR_{M,\sigma'_v} = CRR_{M=7.5,\sigma'_v=1} \,.\, MSF.\, K_\sigma \quad (2.9)$$

The soil's critical shear strength (CRR) is also influenced by the existence of continuous static shear pressures, such as those that may occur under foundations or inside slopes. The impact, quantified by the K_α coefficient, is often minimal in virtually flat terrain conditions. The reason it is not included here is because the case history database is mostly composed of flat or very level ground conditions. The relationship between the cone resistance ratio CRR to $(N_1)_{60}$ is influenced by the fines content (FC) of the soil. This relationship represented as:

$$CRR_{M=7.5,\sigma'_v=1} = f[(N_1)_{60}, FC] \quad (2.10)$$

To simplify mathematical calculations, this correlation may also be represented in reference to an analogous clean-sand $(N_1)_{60CS}$, which can be derived using the following equation:

$$(N_1)_{60cs} = (N_1)_{60} + \Delta(N_1)_{60} \quad (2.11)$$

The updated CRR in terms of $(N_1)_{60cs}$ i.e.:

$$CRR_{M=7.5,\sigma'_w=1} = f[(N_1)_{60cs}] \quad (2.12)$$

Where:

The adjustment $(N_1)_{60CS}$ varies based on the value of fines content (FC).

Key characteristics of a liquefaction analysis methodology

For a liquefaction analysis approach to be conducted within the stress-based framework outlined above, two essential qualities are required:

For instance, the liquefaction analysis technique may be used to a diverse range of critical real-world scenarios. This encompasses a wide range of structures, ranging from minor lateral

expansions to massive earth embankments. Given that practice often necessitates extrapolating beyond the confines of case history experiences, to make it easier to make extrapolations of this kind, it is vital that the framework be supported by reliable experimental and theoretical underpinnings. Additionally, the mechanics are consistent with those that are used in the process of generating companion correlations to other in-situ measurements, such as the SPT blow count, the CPT penetration resistance, and the shear wave velocity (Vs). The consistency of the mechanics makes it easier to include data from a variety of sources in a cohesive manner. Additionally, it offers a firm foundation for the modification of constitutive models that are used in nonlinear dynamic studies.

There are five functions or connections that are included in stress-based analysis. These functions and linkages outline basic components of dynamic site response, penetration resistance, and soil characteristics.

$$r_d = f(\text{depth; earthquake and ground motion characteristics; dynamic soil properties}) \tag{2.13}$$

$$C_N = f(\sigma'_v; D_R; FC) \tag{2.14}$$

$$C_R = f(\text{depth; rod stick} - \text{up length}) \tag{2.15}$$

$$MSF = f(\text{earthquake and ground motion characteristics; soil characteristics}) \tag{2.16}$$

The use of a combination of empirical, experimental, and theoretical approaches is the most effective way for the construction of various forms of function. In order to apply the obtained correlations to situations that are not well represented in the case history database, the resilience of these functions is of the utmost importance. In order to evaluate liquefaction analytical techniques and investigate a variety of options, statistical analysis and regression processes are very useful tools. Nevertheless, the statistical models need to be limited and led by both the experimental evidence that is now available and the appropriate theoretical considerations. When considering correlations that cause liquefaction, it is not advisable to depend simply on regression models in order to establish physical links. This is due to the following reasons:

- The available case history data is often inadequate to establish such relationships

- The correlations are activated by the occurrence of liquefaction
- The establishment of such a link will depend on the anticipated forms of the other functions, particularly when considering that four out of the five listed functions heavily rely on depth
- Using regression to build functions that describe basic behaviours does not ensure the production of a function that can consistently be used to extrapolate the resultant correlation to situations that are insufficiently represented in the database, such as extremely deep depths. This is because regression is a technique that is used to generate functions that depict fundamental behaviours. These criteria are crucial in understanding the explanations for the inconsistencies that exist between different liquefaction analysis approaches now in use.

Overview of the Idriss-Boulanger method

The following section offers a succinct overview of the elements of the analytical methodology used or produced by Idriss and Boulanger (2004, 2006, 2008) as part of their liquefaction triggering correlation.

Shear stress reduction parameter (r_d)

Expanding upon the research conducted by Golesorkhi (1989), Idriss (1999) conducted several site response evaluations with varying parameters. As a result, Idriss concluded that the parameter r_d may be expressed in multiple ways when developing liquefaction evaluation procedures.

$$r_d = \exp\left[\propto (z_d) + \beta(z_d) * M\right] \tag{2.17}$$

$$\propto (z_d) = -1.0120 - 1.1260 \sin\left(\frac{z_d}{11.73} + 5.1330\right) \tag{2.18}$$

$$\beta(z_d) = 0.1060 + 0.1180 \sin\left(\frac{z_d}{11.28} + 5.1420\right) \tag{2.19}$$

where z_d is the vertical depth in metres from the ground surface. The resultant correlation is plotted in Figure 2.3.

Additional interdependent links, such as the probabilistic associations shown by Cetin et al. (2004) and Kishida et al. (2009b), have been suggested. The last two variables are derived from extensive site response assessments conducted under different site conditions and ground

movements. The impact of a site's average shear wave velocity and shaking intensity is taken into consideration by these respective relationships.

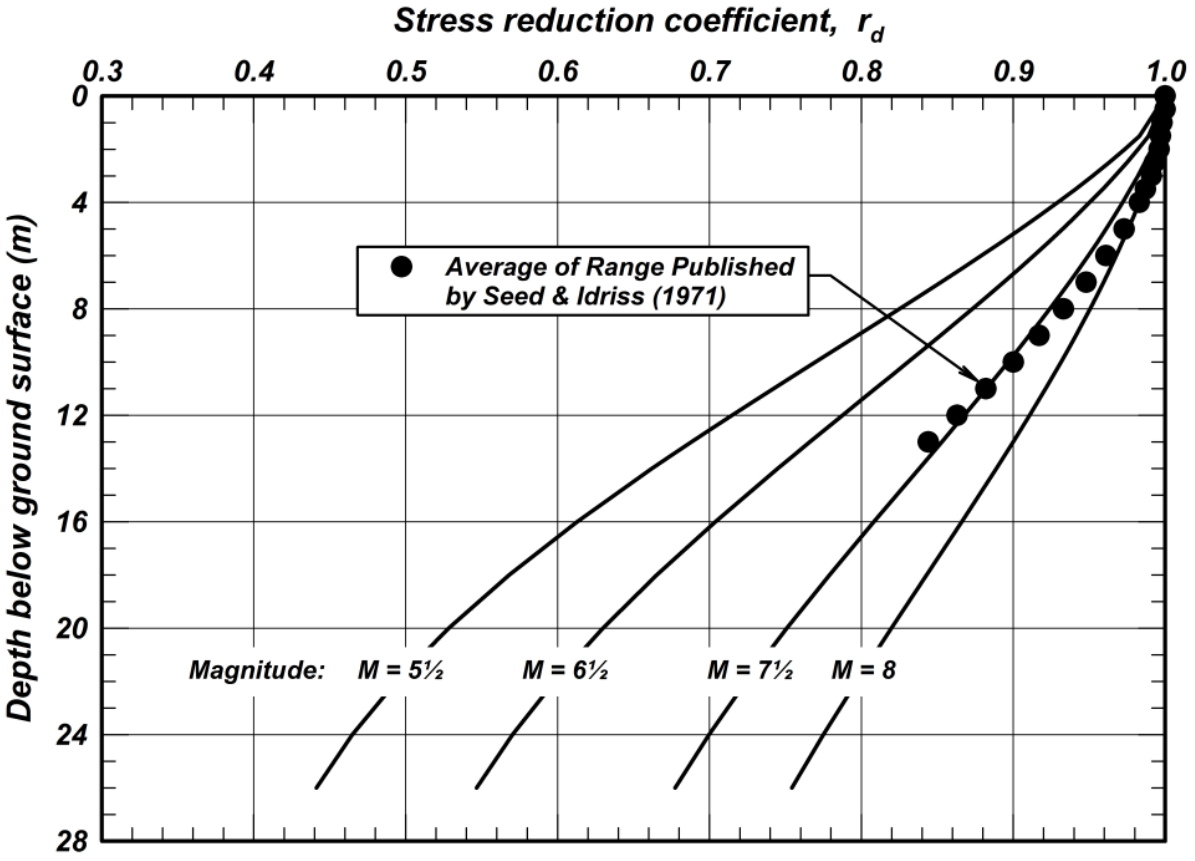

Figure 2.3 Illustrates the connection between the reduction factor (r_d) and the shear stress

Adjustment for the Overburden correction factor, C_N

The C_N relationship, originally established by Boulanger (2003), was derived from two distinct datasets: (1) a reassessment of published SPT calibration chamber test data spanning a range of σ'_v values from 0.7 to 5.4 atm (Marcuson and Bieganousky 1977a, 1977b); and (2) the findings of analyses conducted on σ'_v values ranging from 0.2 to 20 atm using the cone penetration theory proposed by Salgado et al. (1997a, 1997b). The cone penetration theory demonstrated excellent correlation with a comprehensive database of more than 400 CPT calibration chamber experiments, including σ'_v values of up to 7 atm. The further suggestion made by Idriss and Boulanger (2003, 2008) was that the dependency of the $C_N$relationship on DR may be shown in terms of $(N)_{60}$ as follows:

$$C_N = \left(\frac{P_a}{\sigma'_v}\right)^m \leq 1.7 \qquad (2.20)$$

$$m = 0.784 - 0.0768\sqrt{(N)_{60}} \quad (2.21)$$

Where $(N)_{60} = C_E C_R C_B C_S N_m$

The necessary iteration for this expression may be easily executed by using the automatic iteration mechanism provided in an Excel spreadsheet system. The diagram in Figure 2.4a illustrates the arrangement of this link, considering different values of $(N)_{60}$ and effective overburden stresses up to 10 atm. The connection is then compared to the relationship shown by Liao and Whitman (1986) in Figure 2.4b, specifically for effective overburden stresses of up to 2 atm.

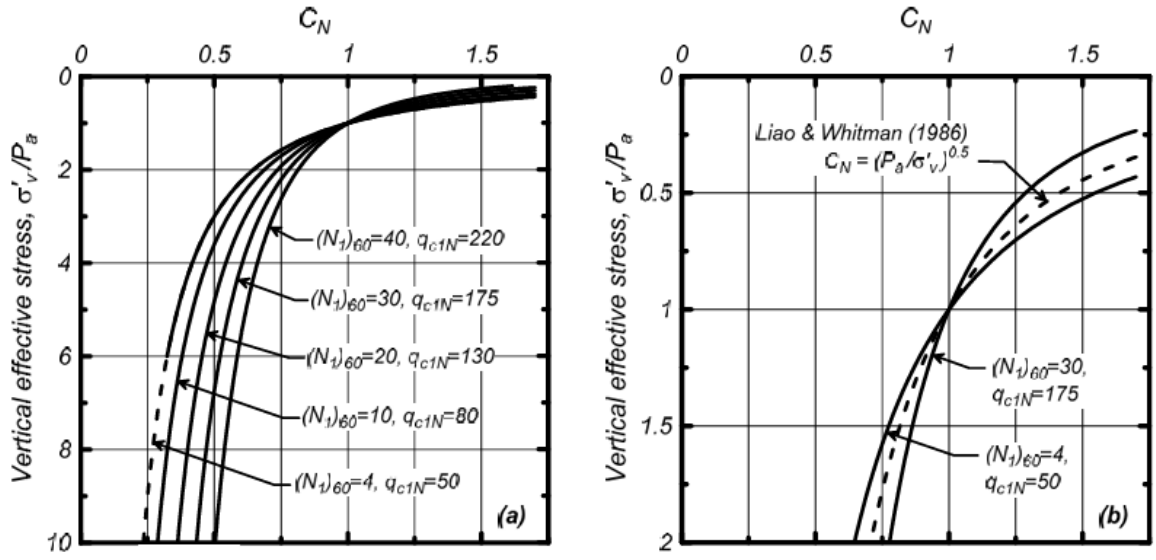

Figure 2.4 Illustrates the correlation between the overburden correction factor C_N and the SPT penetration resistance

The highest value of C_N is restricted to 1.7 where the vertical effective stresses are less than 35 kPa, corresponding to depths less than about 2 metres. Since these expressions were not developed or verified for very low effective stresses, this constraint has been applied. In absence of this restriction, the assumed functional form would provide C_N values that are abnormally large as the vertical effective stress approaches zero. Several research have proposed that the boundaries should range from 1.6 to 2.0.

A recent field study conducted at Perris Dam by the California Department of Water Resources (Wehling and Rennie 2008) allowed for the development of a site-specific C_N relationship for

an alluvial layer consisting of silty and clayey sand (FC = 30-45%). This relationship was derived while considering a range of σ'_v values from 0.2 to 8.5 atm over the dam segment.

Adjustment for the short rod (C_R)

The impact of the rod's length on the energy delivered to the sample rods during the primary hammer impact prompts consideration of the short rod adjustment factor. If the effective reflectivity (ERm) of a SPT-system is assessed for rod lengths beyond around 10 metres, Consequently, the ER would be reduced while using shorter rod lengths. The short rod adjustment factor, C_R, would be less than one for rod lengths less than 10 metres. The C_R values proposed by Youd et al. (2001) have been included into this research and are shown in the following table for different rod lengths:

Length of rod < 3 m	$C_R = 0.75$	(2.22)
Length of rod 3-4 m	$C_R = 0.80$	(2.23)
Length of rod 4-6 m	$C_R = 0.85$	(2.24)
Length of rod 6-10 m	$C_R = 0.95$	(2.25)
Length of rod 10-30 m	$C_R = 1.00$	(2.26)

The length of the rod is equivalent to the sum of the rod's stick-up length (the distance above the ground surface) and the depth of the sample. The measurements of rod protrusions in liquefaction case studies are often not given or unknown, requiring estimate via the use of established methods and common equipment configurations. Cetin et al. (2004) used a length of 1.2 metres for donut hammers and USGS safety hammers, and a length of 2.1 metres for all other safety hammers when the rod stick-up length was unspecified. Idriss and Boulanger (2004) used the values employed by Seed et al. (1984) and the values suggested by Cetin et al. (2000) for the cases that were not addressed in Seed et al. (1984). In the present reappraisal, a uniform rod protrusion length of 2.0 m was used for all instances from Japan, while a length of 1.5 m was utilised for all other scenarios. In addition, it is shown that the modification of the anticipated length of the rod stick-up has a small impact on the analysis of the liquefaction case histories. Recent investigations have left some uncertainty regarding the specifics of the short rod adjustment as proposed by Daniel et al. in 2005. They suggested that the energy transfer during successive hits could potentially aid in advancing the development of the sampler. It

beneficial to determining the combined effect of the short rod correction factor and the overburden correction factor at shallow depths.

Utilising the magnitude scaling factor (MSF) allows for the evaluation of the ways in which time and the number of loading cycles influence the beginning of the liquefaction process. The link between the MSF and the magnitude of the earthquake was established by combining two different kinds of relationships: (1) laboratory-based connections between the CRR and the number of equivalent uniform loading cycles, and (2) correlations between the number of equivalent uniform loading cycles and the magnitude of the earthquake. It is common practice to assume that the value of M is 7.5, and the MSF factor is applied to the predicted CSR value for each case history to standardise it to that value. Following a reevaluation of the MSF for sands, Idriss (1999) brought up the following hypothesis on the link between the two variables:

$$\mathrm{MSF} = 6.9 \,.\, \exp\left(\frac{-\mathrm{M}}{4}\right) - 0.058 \leq 1.8 \qquad (2.27)$$

For earthquakes of relatively minor size, which are distinguished by the likelihood that a single peak stress may dominate the whole time series, an upper limit for the MSF has been set. This limit is referred to as the MSF upper limit. A seismic event that is referred to be a "small magnitude" earthquake is precisely the kind of earthquake that meets this specific definition. The value of 1.8 is derived by considering the time series of stress resulting from a moderate magnitude earthquake as primarily influenced by a single pulse of stress, which corresponds to half to one entire cycle depending on its symmetry. This enables the attainment of the importance. This assumes that all other stress cycles are sufficiently insignificant in magnitude to be ignored. Figure 2.5 presents a visual representation of the link that was identified because of the research.

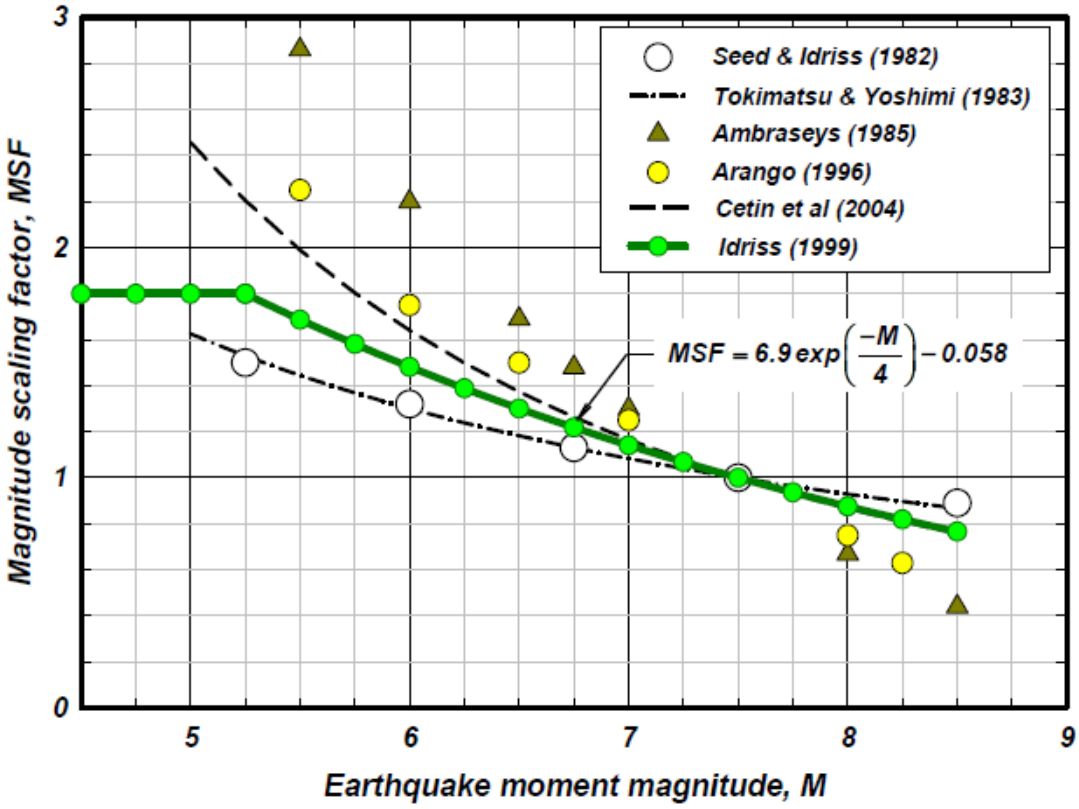

Figure 2.5 Illustrates the relationship between the magnitude scaling factor (MSF) and earthquake magnitude (M)

Overburden correction factor, K_σ

The K_σ relationship used in this work was formulated by Boulanger (2003) based on three fundamental discoveries. Initially, Boulanger established a connection between the critical state stress ratio (CRR) of a pure reconstituted sand in a controlled laboratory setting and the sand's relative state parameter index, ξ_R. Furthermore, Boulanger demonstrated that the K_σ correlation for these uncontaminated sands could be readily deduced from the CRR-ξ_R correlation. Finally, Boulanger established a K_σ connection that aligned including the use of field-based methods CRR-$(N_1)_{60cs}$ correlations generated from the comparing field-based CRR-ξ_R relationships. Idriss and Boulanger (2008) suggested that the relationship between K_σ should be expressed in terms of the values of $(N_1)_{60cs}$ in the following manner:

$$K_\sigma = 1 - C_\sigma \ln\left(\frac{\sigma'_v}{P_a}\right) \leq 1.1 \tag{2.28}$$

$$C_\sigma = \frac{1}{18.9 - 2.55\sqrt{(N_1)_{60cs}}} \leq 0.3 \tag{2.29}$$

The correlation achieved is shown in Figure 2.6, illustrating a range of values for $(N_1)_{60cs}$. The maximum value of K_σ reaches its upper limit of 1.1 when the vertical effective stresses are less than about 40 kPa. This constraint must be imposed since there is no derivation or validation of these equations for extremely low effective stresses, and the hypothesised mathematical expression becomes undefined as the vertical effective stress approaches zero. As a result, the implementation of this limitation is required. The use of the limit of 1.1 for the highest value of K_σ in the analysis of the liquefaction case histories is further shown to be insignificant, hence contributing to the insignificance mentioned earlier.

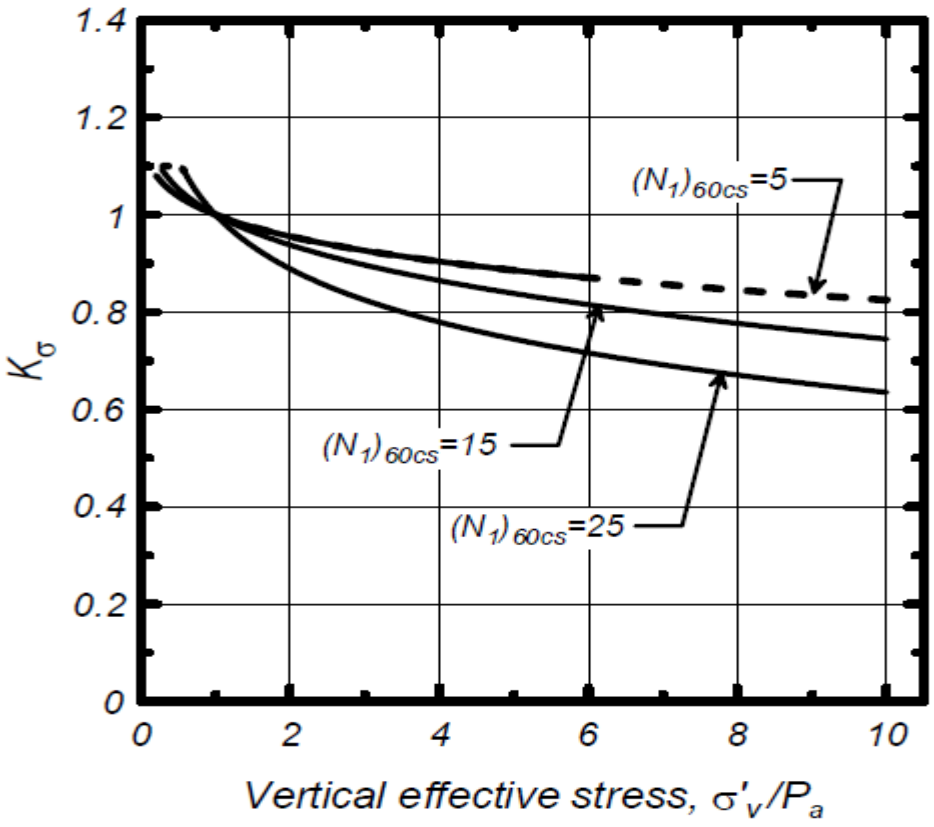

Figure 2.6 Illustrates the relationship between the overburden correction factor K_σ

The K_σ and C_N relations are essential in applications requiring extrapolation for depths beyond the scope of the case history database. A variety of potential combinations of these two connections are investigated with the help of the in-situ test and the data from the frozen sand sample taken from Duncan Dam.

The correction for equivalent clean sand $\Delta(\mathbf{N_1})_{60}$

The adjustment for clean and, $\Delta(N_1)_{60}$, is established by empirical analysis using historical data on instances of liquefaction. This analysis considers the influence of fines content of the blow count of the standard penetration test (SPT). Analysis of liquefaction case histories reveals a clear trend, as the fines content (FC) increases, the correlation for triggering liquefaction shifts towards the left. This phenomenon may be shown by adjusting the SPT $(N_1)_{60}$values to equivalent clean sand $(N_1)_{60CS}$ values, as outlined in equation 2.11. Subsequently, the CRR can be expressed as $(N_1)_{60CS}$. The clean sand modifications suggested by Idriss and Boulanger (2004, 2008) is shown in the following manner:

$$\Delta(N_1)_{60} = \exp\left(1.63 + \frac{9.7}{FC+0.1} - \left(\frac{15.7}{FC+0.01}\right)^2\right) \quad (2.30)$$

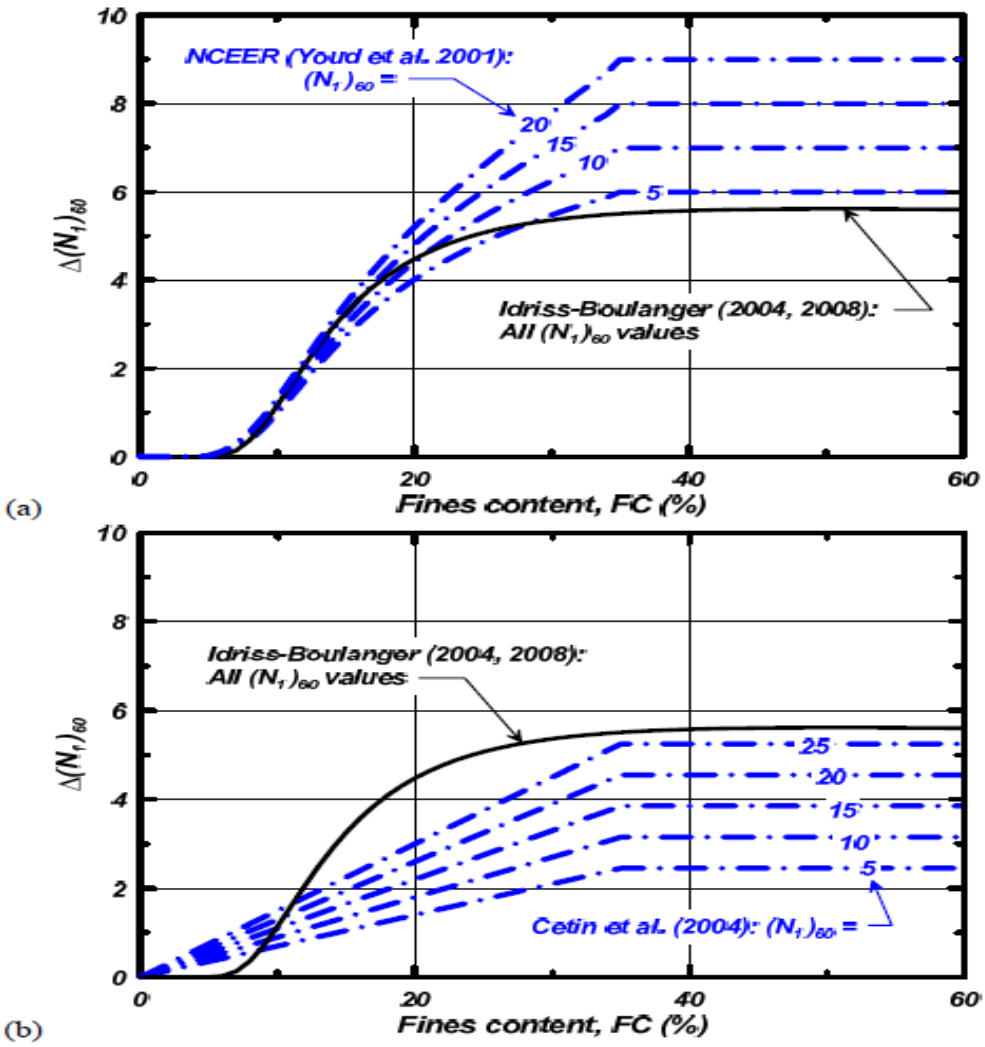

Figure 2.7 The relation between fineness content (FC) and correction for equivalent clean sand $\Delta(N_1)_{60}$

FC is shown as a percentage. The relationships obtained are plotted in Figure 2.7, along with the suggested modifications for equivalent clean sand proposed by Youd et al. (2001) using the original curves published by Seed et al. (1984), and the recommended adjustments for equivalent clean sand proposed by Cetin et al. (2004). The recalibration for the equivalency of clean sand is being reviewed with the most up-to-date database.

The correlation between the cyclic resistance ratio (CRR) adjusted to a magnitude of 7.5 (M = 7.5) and the effective vertical stress ($\sigma'_v = 1$) and the corresponding value of the normalised SPT No $(N_1)_{60CS}$ for cohesionless soils, as determined by Idriss and Boulanger in 2004 and 2008, can be expressed as:

$$CRR_{M=7.5,\sigma'_v=1atm} = \exp\left(\left(\frac{(N_1)_{60cs}}{14.1}\right) + \left(\frac{(N_1)_{60cs}}{126}\right)^2 - \left(\frac{(N_1)_{60cs}}{23.6}\right)^3 + \left(\frac{(N_1)_{60cs}}{25.4}\right)^4 - 2.8\right) \quad (2.31)$$

2.3 Analysis methods

In liquefaction potential assessment, the primary analytical criteria are to assess the soil's resistance (CRR) in relation to the loading effects (CSR). The liquefaction triggering assessments are conducted using three approaches, which are selected dependent on the project's significance.

- Deterministic methods
- Probabilistic methods
- Machine learning methods

A concise overview and relevant scholarly works about the aforementioned methodologies are provided individually.

2.3.1 Deterministic methods (F_S)

In the approach, the F_S parameter, which signifies the ratio of CRR to CSR, is determined by forecasting individual values of load (CSR) and resistance (CRR) without considering the uncertainty related to the prediction of loading and resistance. Figure 2.8 illustrates this. The computed CRR and CSR are considered to have a probability of occurrence of 100%. Within a deterministic approach, a factor of safety (F_S) beyond 1 signifies the absence of liquefaction, whereas a F_S value of 1 or below indicates the occurrence of liquefaction. This approach employs a single component to include all uncertainties associated with the load and resistance

characteristics, relying only on prior knowledge and experience. Nevertheless, despite its shortcomings in obtaining a thorough understanding of the processes that contribute to liquefaction, this analytical method continues to be highly preferred by geotechnical specialists because to its simple mathematical approach that requires little data, time, and effort.

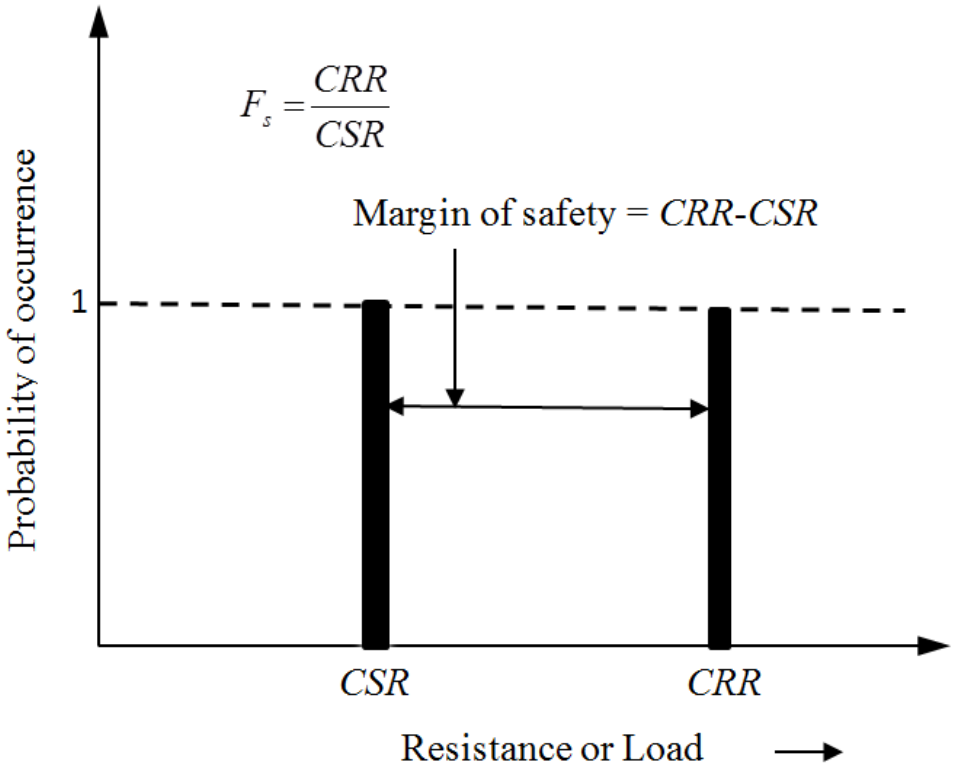

Figure 2.8 Illustrates the deterministic technique used to evaluate liquefaction potential, as described by Becker in 1996

The "simplified procedure" first introduced by Seed and Idriss (1971), and further explained in preceding sections, is the most definitive method for assessing the likelihood of liquefaction at a given site. This technique has been modified and improved several times to make it suitable for different in-situ testing scenarios (Seed et al. 1983; Seed et al. 1985; Robertson and Campanella, 1985; Shibata and Teparaksa, 1988; Olsen, 1997; Robertson and Wride, 1998). The 1998 workshop conducted by the National Centre for Earthquake Engineering Research (NCEER) resulted in a comprehensive assessment of deterministic methods that use in-situ testing to evaluate the potential occurrence of soil liquefaction (Youd et al. 2001). The equation (Youd et al. 2001) may be used to compute the factor of safety (Fs) against liquefaction during an earthquake.

$$F_S = \left(\frac{CRR_{M=7.5,\sigma'_V=1atm} K_\sigma K_\alpha}{CSR * MSF}\right) \quad (2.32)$$

Where:

CSR is an acronym for determined cyclic stress ratio. K_σ is the component used to adjust for overburden, while K_α denotes the factor used to correct for static shear stress. MSF, however, is the factor utilised to modify the value for magnitudes that are either lower or bigger than 7.5.

2.3.2 Probabilistic methods

It is crucial to recognise that a factor of safety (F_S) value greater than one does not always mean that liquefaction is not possible when assessing its likelihood (Juang et al.2000b). This is due to the inherent uncertainties associated with the parameters and models. In essence, it is unfeasible to guarantee the complete absence of liquefaction. It is important to note that the occurrence of liquefaction is not always indicated by a factor of safety (F_S) value that is less than or equal to 1. As per Figure 2.5 to get insight into the fluctuation of CRR and CSR. By using the average values of CRR and CSR in the calculation of F_S, it may be inferred that F_S exceeds 1.0. The possibility exists that the CRR may be lower than the CSR, as seen by the shaded region in Figure 2.9, which displays the distributions of CSR and CRR. This is seen by the presence of the shaded area in the diagram. This would lead to a scenario where the value of F_S is smaller than 1, contradicting the previous prediction and perhaps causing the change of a non-liquefied case into a liquefied one. Considering this, substantial efforts have been undertaken in recent decades to assess the chance of liquefaction, often known as the probability of liquefaction (P_L).

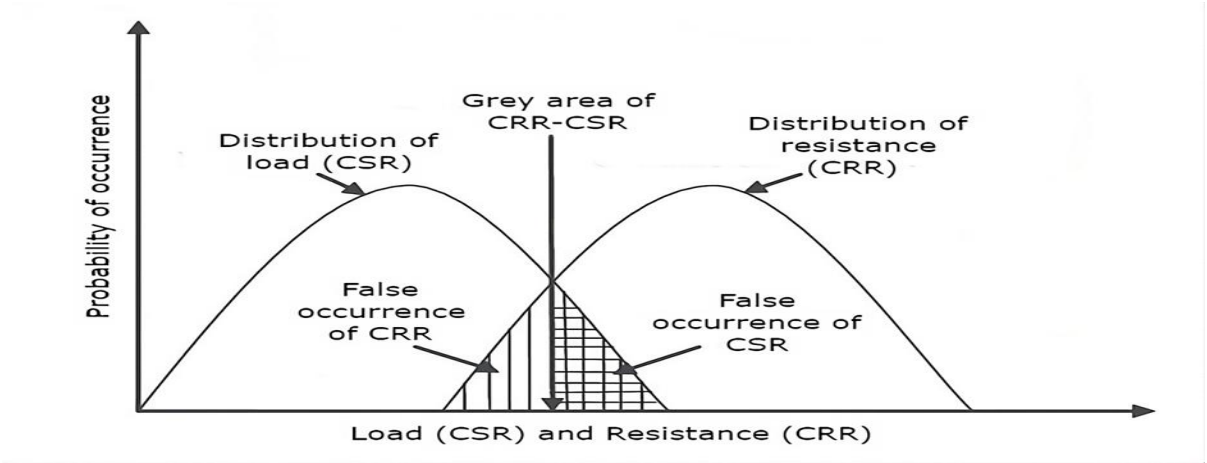

Figure 2.9 Illustrates the prospective distribution of CRR (Cyclic Resistance Ratio) and CSR (Cyclic Stress Ratio) in the assessment of liquefaction potential

Haldar and Tang (1979) performed statistical analyses on the variance of the limit state proposed by Seed and Idriss (1971), using the Standard Penetration Test (SPT), in order to ascertain the likelihood of failure. Fardis and Veneziano (1981) used a Bayesian regression approach to develop a model for evaluating the susceptibility of sands to liquefaction. Their model was developed by using the results of 192 cyclic simple shear instances, while accounting for the uncertainties arising from sample processing, system compliance, and stress deviations. Therefore, the model that has been offered is only relevant to sands that are relatively uncontaminated and homogenous. Fardis and Veneziano (1982) presented a probabilistic method to analyse the occurrence of liquefaction in horizontally layered sand deposits when vertically propagating S waves are present. The approach accurately forecasted the probability of liquefaction by analysing the historical SPT data after the occurrence of liquefaction. Liao et al. (1988) developed logistic regression models by using a database of post-liquefaction field performance. These models were utilised to quantify the probability of liquefaction based on multiple variables, such as earthquake location, peak horizontal acceleration at the level of the ground, normalised cyclic stress ratio (CSR), groundwater table depth, total vertical stress, effective vertical stress, and corrected field. The Standard Penetration Test (SPT) measures the N-value, fines content, clay content, and gravel. Hwang and Lee (1991) used a liquefaction potential probability matrix and a fragility curve that depended on the moment magnitude to determine the chance of experiencing no, slight, moderate, or severe liquefaction incidents. In order to develop alternative earthquake-site models, they considered the uncertainty associated with both site features and seismic parameters. For the purpose of determining the ground displacements for each scenario, the Fourier Acceleration amplitude spectrum, which combines non-linear site response analysis, was used. SPT N −values are used in the calculation of the factor of safety, which is used to quantify the chance of liquefaction. The shear stresses calculated using this method roughly correspond to those obtained using the less complex stress-based methodology described by Seed and Idriss (1971). Youd and Nobble (1997b) and Toprak et al. (1999) used logistic regression analysis to develop empirical equations for assessing post-liquefaction field performance based on data. The term "plural" refers to a grammatical form that indicates the presence of more than one of a particular noun or pronoun. Juang et al. (2000b) proposed a Bayesian mapping function that use the SPT dataset to build a correlation between Fs and PL. In their study, Juang et al. (2002a) found that the Bayesian mapping function method outperforms the logistic regression approach in assessing the site-specific likelihood of

liquefaction. The equation used in logistic regression for assessing liquefaction probability is unaffected by any deterministic methodologies. Conversely, The Bayesian mapping function allows for a seamless transition from Fs-based design to P_L-based design, while keeping the characteristics of the deterministic technique under consideration. Considering this, the Bayesian mapping function is the preferred approach based on the research conducted by Juang et al. (2002b). The study examined three simplified techniques, all of which were based on Cone Penetration Testing (CPT). There are three approaches are available by Bayesian mapping function, 'the Robertson method, the Olsen method, and the Juang method.' A Bayesian mapping function was developed for each of the deterministic approaches to facilitate the comparison. The research included case studies from the 1999 Chi-Chi earthquake in Taiwan and was carried out using a probabilistic approach. The researchers showed that the Juang et al. (2003) methodology outperforms the other two techniques Regarding its precision in forecasting the susceptibility of soils to liquefaction which was developed based on more basic method using Cone Penetration Testing (CPT) that use the Bayesian mapping functional approach to demonstrate a correlation between Fs and P_L.

2.3.3 Probabilistic technique based on reliability

The probabilistic models are solely based on data, since they depend on statistical evaluations of liquefaction data. The computation of P_L using these empirical models just considers the mean values, without considering the uncertainty in the parameters and the model itself throughout the investigation. If there is significant parameter and model uncertainty, the resultant prediction limit may be prone to error. To address these problems, one might use a reliability-based probabilistic analysis of liquefaction, which considers uncertainties in both the model and variables.

Juang et al. (1999b) used the advanced first order second moment (AFOSM) method to calculate the dependability index (β) for both liquefied and non-liquefied situations in the database. They established a connection between β and P_L by using a Bayesian mapping function that depended on the post-liquefaction database. The minimization study for computing the dependability index was performed using the ellipsoid technique, as proposed by Low and Tang (1997). The authors of the reliability research assumed about the coefficient of variation (COV) of the soil and seismic parameters. Nevertheless, the absence of regard for model uncertainty was apparent. Juang et al. (2000d) used the AFOSM technique in conjunction with Monte Carlo simulation to ascertain the minimum β value for both liquefied and non-liquefied situations. In

addition, they proposed a P_L-Fs connection using a Bayesian mapping function technique, but neglecting to include model uncertainty. Cetin (2000) and Cetin et al. (2004) developed probabilistic models using the Standard Penetration Test (SPT) to evaluate the probability of liquefaction. The First Order Reliability Method (FORM) and a Bayesian updating technique were used for evaluation. Moss (2003) and Moss et al. (2005) presented a probabilistic model using the Cone Penetration Test (CPT) to evaluate the probability of liquefaction. The researchers used a mean value first-order second moment (MVFOSM) reliability technique together with a Bayesian updating strategy. Hwang and Yang (2004) used MVFOSM reliability analysis to construct a model that measures the relationship between the probability of liquefaction, the factor of safety, and the reliability index. Juang et al. (2006) used the first order reliability technique (FORM) together with the Bayesian mapping function approach to do a probabilistic assessment of soil liquefaction potential. In addition, they performed comprehensive sensitivity analyses to measure the uncertainty associated with their created CRR model.

2.3.4 Recent development of machine learning and deep learning methods

Galupino and Dungca (2023) investigated the use of machine learning techniques to evaluate the susceptibility to liquefaction in Metro Manila, Philippines. The objective of this research was to include underutilised geotechnical data in order to extract valuable information about the detection of potential difficulties, such as liquefaction. The study assessed certain characteristics of the site, such as, level of the groundwater table, the SPT N-value, the kind of soil, and the fines content. The analysis used a linear model to estimate the Peak Ground Acceleration (PGA), revealing a importance of accurately prediction ($R^2 = 0.89$) between PGA, M, and the distance from the earthquake epicentre. The inquiry also assessed the possible hazard of liquefaction for a predicted magnitude of 7.5 M and generated a graph that had been validated by previous research. The study was deficient in providing a thorough examination of the current body of knowledge.

Jas and Dodagoudar (2023) created a machine learning model that offered a concise justification for the predictions it made. XGBoost – SHAP was the method that the researchers used in order to analyse the liquefaction of the soil. According to the authors, the bulk of the methodological methods to machine learning that are used for evaluating soil liquefaction are opaque. A database that was not balanced was used in the earlier study in order to develop these models. Through the incorporation of the essential layer thickness and coefficient of

permeability into the database, this research included both previously collected data and new information. Through the use of the eXtreme Gradient Boosting (XGBoost) machine learning approach, probabilistic models were effectively generated. It was suggested that the k-means synthetic minority oversampling approach, also known as SMOTE, may be used as a tool to improve the accuracy of models by addressing imbalanced datasets. In order to improve the hyperparameters, search approaches were used, which ultimately led to an improvement in the accuracy of the model. For this particular piece of work, an explainable machine learning (EML) technique known as SHapley Additive exPlanations (SHAP) was used. Obtaining a more in-depth comprehension of the XGBoost model was accomplished via the use of the SHAP (Shapley Additive exPlanations) approach. The cone penetration resistance and the permeability coefficient were identified as the first and fourth most important input qualities that influence the potential for liquefaction, respectively, according to the data provided by SHAP.

Cai et al. (2022) hybrid intelligence models were built in order to provide predictions on the possibility of soil liquefaction in this paper, the Least Squares Support Vector Machine (LSSVM) and the Radial Basis Function Neural Network (RBFNN) are employed. Furthermore, to enhance the performance of these models, three different optimisation procedures were used. These strategies are known as Grey Wolves Optimisation (GWO), Differential Evolution (DE), and Genetic Algorithm (GA). The evaluation of the models that were developed was carried out with the use of statistical markers, one of which was the root mean square error. When compared to other models that have been suggested in the literature, the RBFNN − GWO and LSSVM − GWO models have shown superior performance in terms of their ability to predict the potential for soil liquefaction. The purpose of this study was to determine whether or not the Grey Wolves Optimisation (GWO) method is successful in the training of Radial Basis Function Neural Network (RBFNN) and Least Squares Support Vector Machine (LSSVM) models. It was discovered via the study that the cyclic stress ratio had the most significant influence on the liquefaction of the soil in the scenario that was examined.

Kumar et al. (2022a) It was suggested that five distinct machine learning models be used in order to provide an accurate prediction of the likelihood of soil liquefaction. For the purpose of training the models, data acquired from conventional penetration testing was used. XGBoost, RF, GBM, SVR, and GMDH were some of the models that were used in the research. Within the scope of this research, six different input factors were evaluated. These variables included the depth, the corrected SPT No., the total vertical stress, the fine content (FC), the

maximum horizontal acceleration, the total effective stress, and the magnitude of the earthquake. Using several statistical factors, this study conducted an evaluation of the degree to which the presented models were successful in predicting the likelihood of liquefaction. It was clear that the XGBoost model has superior predictiveness than the other four models. The models that are provided have the capability of functioning as a reliable tool that can properly estimate the possibility of liquefaction in complex earthquake engineering circumstances that occur in the real world.

Kumar et al. (2022b) Several techniques, such as the factor of safety approach (FOS), the liquefaction potential index approach (LPI), and the liquefaction severity index approach (LSI), were used to assess the probability of soil liquefaction. The objective of this research was to analyse a dataset consisting of measurements from traditional penetration tests conducted at different depths under the surface of the earth. The dataset included 834 unique locations. During the inquiry, a liquefaction analysis was conducted, considering seven essential input characteristics. The criteria considered, in addition to the corrected SPT − N values, were the maximum horizontal acceleration, fine content (FC), total vertical stress, total effective stress, magnitude moment, and depth. This research assessed the efficacy of several approaches in predicting the vulnerability to liquefaction by analysing performance metrics and error matrices. The study's results indicate that the FOS-based strategy exhibited superior accuracy in predicting the probability of liquefaction, as compared to the LSI and LPI techniques. This article specifically examined the regional differences in important measurements such unit weight and fine content. It aimed to offer a better understanding of the main elements that caused uncertainty when evaluating the likelihood of liquefaction.

Ozsagir et al. (2022) The purpose of this study was to evaluate the appropriateness of seven different machine learning techniques for predicting the likelihood of soil liquefaction. Metrics like as accuracy, recall, precision, F1 score, and receiver operating characteristic were used in order to assess the effectiveness of these algorithms. When applied to the dataset, the decision tree strategy demonstrated superior performance compared to other methods, with an accuracy rate of 90% across the board. This study was conducted with the intention of providing decision-makers with an approach that is both comprehensive and applicable for determining the likelihood of ground liquefaction. The feature of the soil known as the mean grain size (D50) was found to be the most important factor that had the largest influence on the chance of liquefaction. Through the use of neural networks and classification trees, the objective of this research was to achieve the construction of a database that has the capability to anticipate

liquefaction. It is important in order to grasp the ambiguous area that exists between the several suggested transition zones (the zone that is liquefiable and the zone that is not liquefiable).

Carlos et al (2021) a probabilistic model was created in order to estimate the probability of liquefaction start in granular soil profiles that had been levelled, stratified, and saturated, and that had been enhanced with dense granular columns (DGCs). For the purpose of developing the model, the findings of a full numerical parametric analysis were used. This analysis was confirmed via the utilisation of a dynamic centrifuge experiment. A further evaluation of the model was carried out by making use of previously conducted case studies that were pertinent to the use of deep ground development techniques for the goal of reducing the risk of liquefaction. One of the distinguishing features of the proposed probabilistic model was that it took into account variations in a great deal of important components. For the drainage geo composite (DGC), the characteristics that were taken into consideration were the area replacement ratio (Ar), the stiffness, and the drainage capacity. Furthermore, the model takes into consideration the range of hydraulic conductivity, as well as the thickness, depth, and relative density of each layer under consideration. In addition to this, it took into account the evolutionary characteristics of ground vibrations as well as the inherent unpredictability that is present when attempting to estimate pore pressures and shear stresses inside each stratum. The major objective of this study was to investigate the patterns and factors that had a significant role in the liquefaction of layered soil deposits that had been subjected to deep ground improvements (DGIs). With the help of this study, a design approach for DGIs was developed with the intention of considering the influence of various mitigation mechanisms, soil nonlinearity, soil-DGI interactions, layer-to-layer interactions, the optimum intensity measure and the degree of softening in crucial layers.

Ghani and Kumari (2021) performed a multi-linear regression analysis, which resulted in the creation of a new equation. The factor of safety against liquefaction (F_S) in fine-grained soil that is situated inside seismically active regions of Bihar, India, may be determined with the use of this equation. The flexibility of fine-grained soil was explored in this research to see how it influences the liquefaction qualities of the soil. Using reliability analysis that was based on the First Order Second Moment (FOSM) approach, it was also possible to establish a link between the factor of safety (F_S), the reliability index (b), and the likelihood of liquefaction (P_L). During the early stages of the construction of many civil engineering projects that were prone to liquefaction, the equation that was constructed functioned as a vital tool for making important technical choices. This research was conducted with the intention of making a

significant contribution to the area of predicting liquefaction in fine-grained soils that have moderate to high flexibility. Additionally, the study aimed to contribute academically to the existing body of knowledge on liquefaction research studies.

Ghorbani and Eslami (2021) presented a complete energy-based model with the purpose of predicting the susceptibility of several types of sandy soils, including clean, silty, and clayey sands, to undergo liquefaction. Plasticity Index (PI) and loading Frequency were not taken into consideration by earlier energy-based models despite their potential influence. The model that is being explained, on the other hand, takes these factors into consideration. A novel methodology, Evolutionary Polynomial Regression (EPR), was implemented during the model's development. The validation of the model was successfully accomplished by analysing a diverse collection of one hundred case studies originating from a variety of locations all over the globe. These case studies included a broad range of soil properties. When compared to earlier energy-based models, the findings showed that the current model had a significant advantage over other models. The results of the parametric analysis showed that the fine content (FC) and plasticity index (PI) of the soil were the most important factors in determining the amount of energy required for liquefaction in sandy soils that included a substantial number of fine particles.

Hu (2021) conducted dynamic penetration and shear wave velocity studies to greatly augment the existing datasets on field outcomes case histories of gravelly soil liquefaction. The study enhanced data quality by using screening, correction, and repair procedures on the provided data case histories. This study presented a novel method for detecting the key elements that lead to the development of liquefaction in soil containing gravel. This study proposed revised criteria for two factors contributing to liquefaction in gravelly soil: Hn, which refers to the impervious layer with a minimum thickness of 0 m, and Dn, which represents the unsaturated zone among the groundwater table and the impervious layer with a maximum thickness of 4 m. The objective of this study was to enhance the precision of a model via the use of data cleansing techniques and the identification of influential elements.

Kumar et al. (2021) a deep learning model that was meant to classify the dependability of soil in relation to liquefaction was shown. In this study, a comparative analysis was carried out between a deep learning model that was suggested and the emotional backpropagation neural network (EmBP). The purpose of this study was to determine whether or not it would be worthwhile to use a deep learning model in order to conduct an analysis of a database that

included cone penetration test results from the Chi-Chi earthquake investigation. For the purpose of determining the degree to which soil is susceptible to liquefaction, cone resistance (qc) and peck ground acceleration were used as measures. When evaluating the performance of the models that were built, a number of different measurements were used. These variables included the receiver operating features, sensitivity, specificity, the Phi correlation coefficient, and the Precision-Recall F measure. Therefore, the success of the approaches that were used is shown by the fact that the deep learning framework that was constructed in this research demonstrated greater performance in comparison to EmBP. The evaluation of the models that were built by utilising seismic data from across the world revealed favourable findings that were in accordance with fitness metrics. The present investigation was conducted with the intention of developing a decision-making tool that is both clear and effective in the field of engineering design. For the purpose of conducting a statistical analysis of the probability of liquefaction, this method was used. The results of this research have the potential to improve understanding of the connection that exists between the characteristics of the soil and the parameters relevant to earthquakes.

Pirhadi et al. (2021) investigated the phenomena of earthquake liquefaction in gravelly soils, which is a phenomenon that has been seen in the past in connection with sandy soils. Creating a comprehensive database of case histories that chronicle instances of liquefaction in gravelly soil in various locations around the world was the purpose of this study. The database was established with the intention of achieving this aim. The primary objective was to make use of this data in order to build empirical, semi-empirical, and probabilistic models that were capable of properly predicting the possibility of soil liquefaction under these conditions. During the course of this research, a comprehensive investigation of the phenomenon of soil liquefaction in gravelly soil as a result of seismic events was carried out. In order to take into account, the uncertainties that were associated with the models and parameters that were used in the evaluation process, it utilised probabilistic models. Within the scope of this study, classifier curves were developed via the use of Bayesian mapping and logistic regression techniques in order to anticipate the likelihood of liquefaction events. For the purpose of determining the extent to which the bias sample weighting factor affects the accuracy of the model's predictions, this study carried out a sensitivity analysis on the factor. The findings of this study brought to light the need of using probabilistic models rather than deterministic models in order to account for variations in the data.

Zhang et al. (2021a) presented a new method called Extreme Learning Machine (ELM) to forecast soil liquefaction based on Cone Penetration Test (CPT) data. This research conducted an analysis to identify and categorise seven predictive characteristics. Subsequently, a total of 226 CPT samples were divided into distinct training and test sets. This work performed a comparative analysis on the training accuracy and speed of the Extreme Learning Machine (ELM) model, considering differences in the number of neurons and activation functions. The goal was to choose the most efficient model in accordance with performance criteria. This research assessed the effectiveness of the newly constructed Extreme Learning Machine (ELM) model on the test dataset and showcased its higher performance in comparison to the prediction model based on the Standard Penetration Test (SPT). The research presented data to substantiate the viability of using ELM and advancing it for in situ evaluation objectives. This study introduced an innovative method for scholars to construct prediction models for soil liquefaction by using Cone Penetration Test (CPT) data.

Zhang et al. (2021b) The study used a multi-layer fully connected network (ML − FCN) to enhance the performance of the deep neural network (DNN). The ML − FCN was utilised to a prediction model for soil liquefaction using the shear wave velocity (Vs) and standard penetration (SPT) dataset. The article demonstrated that the ML − FCN DNN trained model exhibited superior accuracy in predicting liquefaction potential compared to Hanna's suggested model. The article emphasised the significance of include the parameter of Vs to enhance the model's performance. The work made a significant contribution to the area of earthquake engineering by presenting a refined prediction model for soil liquefaction. This model has shown to be more precise, hence aiding in the prevention of natural catastrophes and engineering failures resulting from soil liquefaction.

Zhang and Wang (2021) At every level of the design process for building projects, it was essential to assess the liquefaction susceptibility induced by seismic activity. Using a hybrid ensemble technique, this study presented a unique approach to enhance the capability of classification models to be applied to a broad variety of scenarios. Using a weighted voting mechanism, the proposed method accomplished the integration of the predictions of seven basic classifiers. The BPNN, SVM, DE, k-nearest neighbours, logistic regression, multiple linear regression, and naive Bayes were the primary classifiers that were used in this inquiry. Optimisation of the hyperparameters and weights of the core classifiers was accomplished using the evolutionary method. The performance evaluation of the suggested classifier ensemble was carried out on three datasets that were obtained from research publications that

had been published in the past. All three datasets were examined, and the results showed that the ensemble performed better than the basic classifiers in terms of a various of metrics. These measurements included accuracy, precision, recall, F1 score, AUC, and ROC. The ensemble of classifiers was able to successfully demonstrate the significance of important characteristics in three different datasets, which ultimately led to an improvement in the effectiveness of future data collection efforts. The present ensemble technique has shown a substantial amount of resilience, and it has the potential to be developed to address more categorization challenges in the field of civil engineering.

Zhao et al. (2021) In order to determine whether soil liquefaction is possible, a unique assessment approach was devised. The data acquired from the observations conducted during the cone penetration test (CPT) and the shear wave velocity test (Vs) were utilized. During the study, a novel hybrid machine learning model known as the PSO − KELM model was presented. The kernel extreme learning machine (KELM) and particle swarm optimisation (PSO) are both components of this model, which is used to determine whether or not soil liquefaction is possibly occurring. In order to investigate the nonlinear relationship that exists between the cyclic stress ratio (CRR) and the cone penetration test (CPT), as well as the measurements of shear wave velocity (Vs), the PSO − KELM search method was used. The development of a novel probabilistic model that takes into account both model uncertainty and sample bias via the use of weighted estimate of maximum likelihood was the major purpose of this study. The PSO − KELM model suggested using a number of factors as inputs. These variables included the cycle stress ratio, the equivalent clean sand standardised cone tip resistance, the normalised friction ratio, the fines content, and the soil behaviour type. The empirical findings indicated that the PSO − KELM model outperformed many alternative machine learning methodologies. The proposal to combine CPT and Vs data showed potential for improving prediction accuracy by offering a more inclusive depiction of soil liquefaction events. The primary objective of this research was to improve the effectiveness of seismic cone penetration testing (SCPT) in evaluating the likelihood of soil liquefaction.

Zhao et al. (2021) In order to improve the performance of support vector machine (SVM) models, it was suggested that two different optimisation strategies, namely the genetic algorithm (GA) and the grey wolf optimizer (GWO), be used. The purpose of these improved models was to provide an accurate prediction of the likelihood of soil liquefaction occurring because of seismic events. Using field observation data acquired from cone penetration test (CPT), standard penetration test (SPT), and shear wave velocity test (Vs), the purpose of this

research was to evaluate the applicability of the GA − SVM model as well as the GWO − SVM model. It is proposed that many datasets be used to improve the reliability of the comparison between the newly suggested model and the GA − SVM model. In this study, it was vital to include extra measurement indicators in order to completely assess the classification performance of the two hybrid models. This was done to strengthen the dependability of the newly proposed GWO − SVM model.

2.4 Conclusions

The following inferences may be made based on the literature review that was presented before.

- While the energy-based technique is theoretically more suitable for assessing liquefaction studies, it is not widely used compared to the cyclic stress-based approach. This is primarily because there is a lack of reliable data to calibrate the models built for the energy-based approach.
- The cycle strain-based technique is less often implemented compared to the cyclic stress-based methodology owing to less precise prediction of cyclic strain amplitudes and the lack of equipment for cyclic strain-controlled testing.
- Many researchers prefer to use the field performance correlation-based approach to evaluate liquefaction potential in cohesionless soil deposits. This is because of the challenges and expenses associated with obtaining better quality undisturbed samples through laboratory testing.
- Among the several in-situ approaches, SPT and CPT-based methods are extensively used for analysing the possibilities of soil to liquefaction. This is because there is a substantial amount of post-liquefaction data available for these methods.
- While geotechnical specialists often favour a deterministic approach to assess liquefaction potential, probabilistic assessment is essential in practical applications to make risk-based design choices.
- Based on the literature study, academics have used various methodologies and processes throughout the years to develop prediction models for evaluating the likelihood of liquefaction. Common models include ANN, SVM, RF, Genetic Programming (GP), Ensemble models, and Support Vector Machines with Grey Wolf

Optimisation ($SVM - GWO$). These models have a sluggish rate of convergence, are prone to model overfitting, and only include a single variable. Due to the nonlinearity of liquefaction, it is necessary to utilise strong models for assessing liquefaction potential and mitigating liquefaction hazards.

CHAPTER 3

MACHINE LEARNING AND GENETIC PROGRAMMING IS USED AS A TOOL FOR ANALYSIS

3.1 Introduction

In the present study a new equation using a revolutionary probabilistic model that incorporates Genetic Programming (GP) and Bayes conditional probability. It also includes a unique soil liquefaction prediction model that makes it easier to generate enhanced correlation features, chi square, relief characteristics, and technical indicators. The combination of ensemble classifiers such as Deep Belief Networks (DBN), Long Short-Term Memory (LSTM), and Support Vector Machines (SVM) in conjunction with an optimised Bidirectional Gated Recurrent Unit (Bi − GRU) facilitates the achievement of trustworthy prediction outputs. This study describes a novel technique for determining the optimal weights in Bi − GRU, which employs a novel Average Cat and Salp swarm algorithm (AC − SSO) and an Opposition based self-adaptive shark smell optimizer (OSA − SSO) model.

3.2 Genetic programming (GP)

Genetic Algorithms (GA) are adaptive heuristic search algorithms that are classified within the broader category of evolutionary algorithms. Genetic algorithms derive their principles from the concepts of natural selection and genetics. These techniques include using previous data to guide a random search towards areas of the solution space that are likely to provide higher performance. They are often used to provide superior remedies for optimisation and search challenges. Genetic algorithms mimic the process of natural selection, wherein organisms who exhibit the capacity to adopt to changes in the environment can survive, reproduce, transmit their characteristics to future generations. In essence, these simulations use the principle of "survival of the fittest" to ascertain the most prosperous people in each generation as they strive to solve a challenge. Each generation consists of individuals who represent points in the search space and possible solutions. Every individual is represented as a series of letters, integers, floats, or bits. This string has similarity to the Chromosome.

Genetic Programming (GP) is an approach to pattern recognition that entails constructing a model via adaptive learning utilising many instances of input data. The invention may be

attributed to Koza in the year 1992. It employs the concepts of genetic algorithms (GA) and replicates the natural development of live creatures in order to analyse their behaviour. Within the context of conventional regression analysis, the user is required to manually provide the structure of the model. However, in Genetic Programming (GP) regression, both the model's structure and parameters are automatically determined. The response is shown in either a hierarchical arrangement or a succinct mathematical expression, depending on the given information. The GP model, characterised by its hierarchical tree structure of nodes, is sometimes referred to as a GP tree. A functional set, commonly referred to as a terminal set, consists of nodes that act as its central components. The expression may have math operators (-,+, ×, ÷), math functions (e.g., sin, cos, tanh, or ln), Boolean operators (e.g., 'AND, OR, NOT', etc.), logical statements (e.g., 'IF or THEN'), or any other user-supplied functions. The ultimate collection consists of variables (e.g., x1, x2, x3, etc.) or numerical values (e.g., 3, 5, 6, 9, etc.), or a combination of both. A GP tree is created by the stochastic selection of functions and terminals, resulting in a total of 44 terminals. Figure 3.1 illustrates the hierarchical structure of the tree, with a central node and subordinate nodes that extend from each functional node to terminal nodes. Figure 3.1 displays a mathematical equation represented as a GP tree. The equation (x4+x5-x1*(x2/x3)) may be simplified to improve comprehension. The variables x1, x2, x3, x4, and x5 represent the terminal nodes. This subject encompasses the mathematical function and the math operations of addition (+), subtraction (-), multiplication (×), and division (/).

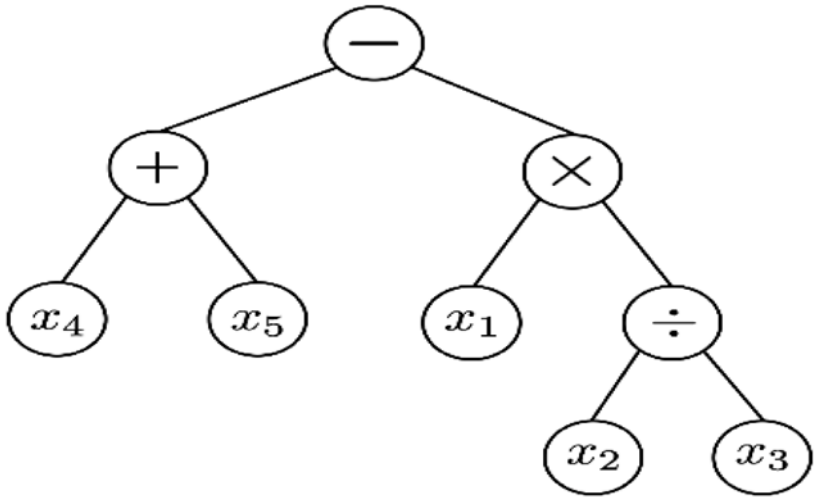

Figure 3.1 A typical GP tree encoding a mathematical equation: (x4+x5-x1*(x2/x3)

Initially, a set of GP trees is generated according to the population size supplied by the user. The development of these trees is random, with the user providing several functions and terminals. The fitness criteria are determined by the objective function and assesses the comparative excellence of each person within the population. Subsequent generations are created via the deliberate breeding of individuals from the original population based on their degree of adaptation. Subsequently, numerous evolutionary techniques such as reproduction, crossover, and mutation are applied on the functions and terminals of the chosen GP trees. The newly arrived population replaces the existing population. This procedure is repeated until the termination criteria are met, which may be defined as either attaining a certain fitness value or achieving the greatest number of generations. The result of genetic programming is decided by picking the GP model with the best fitness value across all generations. Presented here is a succinct summary of several evolutionary techniques used in genetic programming (GP).

3.2.1 Space search in genetic programming

The genetic programming starts by generating a population, which comprises a collective of individuals. Every individual function as a resolution to the provided issue. An individual has or is characterised by a set of elements referred to as Genes. Genes are linked together to create a sequence and generate chromosomes, which function as the solution to the problem. An extensively used technique for initialization involves the utilisation of randomly generated binary strings.

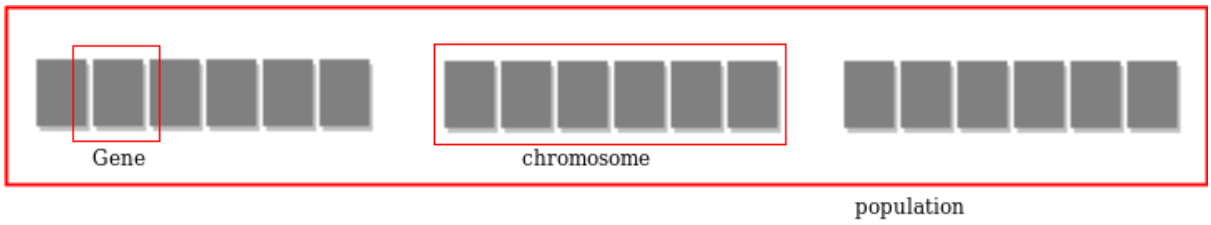

Figure 3.2 Illustrated the search space in genetic programming

3.2.2 Fitness assignment in genetic programming

A fitness function is implemented to evaluate an individual's degree of physical fitness. Competitiveness is the ability of a person to successfully compete with others. During each iteration, people are assessed according to their fitness function. The fitness function assigns a fitness score to each person. This score further impacts the likelihood of being chosen for

reproduction. The greater the fitness score, the higher the likelihood of being chosen for reproduction.

3.2.3 Selection in genetic programming

The selection phase entails the process of choosing people to produce children. Subsequently, the chosen people are paired together to enhance the process of reproduction. Subsequently, these people pass on their genetic material to the next generation.

There are three types of Selection methods available, which are:

- Tournament selection
- Roulette wheel selection
- Rank-based selection

3.2.3.1 Tournament selection

Throughout this procedure of selection, a certain quantity of GP trees engages in tournaments. The tournament size is determined by the number of GP trees that participate in the competition. The winner persists and obtains a larger number of reproductions, while the loser is prevented from advancing to the subsequent offspring.

3.2.3.2 Roulette wheel selection

Parents are selected depending on their degree of appropriateness. The chromosomes with better quality have a larger probability of getting selected. The method is shown by the example of a Roulette wheel, where the genetic programming chromosomes in the population are arranged. The magnitude of each division on the Roulette wheel is closely correlated to the fitness function value of each chromosome. Put simply, the size of the segment on the wheel increases proportionally with the fitness function value, as seen in Figure 3.1. A marble is propelled into the roulette wheel, and the chromosome upon which it lands is selected. Without a doubt, chromosomes that possess greater fitness values will be selected more often.

The procedure may be delineated by the following phases:

Phase 1. Determine the total fitness of all chromosomes in the population; sum =S.
Phase 2. Generate a random number, denoted as r, from a given interval (0, S)

Phase 3. Iterate across the population and calculate the total fitness by summing the values from 0 to the sum of Si. Terminate and output the i^{th} chromosome when the total Si exceeds r.

Phase 4. Perform steps 2 and 3 again

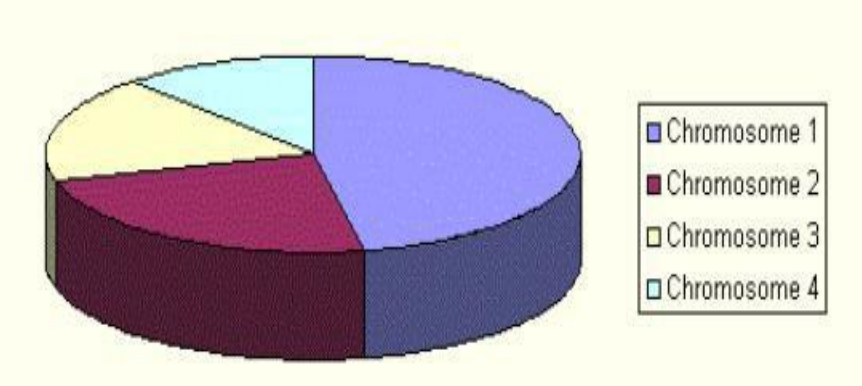

Figure 3.3 Roulette wheel selection in genetic programming

3.2.3.3 Rank-based selection

The prior selection process will encounter difficulties when there is a significant disparity in fitness levels. For instance, if the highest level of fitness among the chromosomes is more than half of the whole roulette wheel, then the other chromosomes will have lesser opportunities for selection. Rank selection involves first sorting the population based on their fitness levels, and then assigning each chromosome a fitness value based on this ranking. The person exhibiting the least level of fitness will be awarded a numerical value of 1, the second lowest will have a fitness of 2, and so on. The person with the utmost level of fitness will be given a value equivalent to the overall count of chromosomes within the population. Subsequently, all the chromosomes are given an opportunity to be chosen. The likelihood of selecting a chromosome is directly related to its position in the sorted list, rather than its level of fitness. However, using this approach may result in delayed convergence due to the little disparity between the superior chromosomes and the rest.

3.2.4 Reproduction in genetic programming

After the selection process, the reproduction stage involves the creation of offspring. At this step, the genetic algorithm utilises two variation operators to alter the parent population. The two operators involved in the reproduction phase.

3.2.5 crossover

The crossover operation plays a vital role in the reproductive phase of the genetic algorithm. Within this technique, a random location is selected within the genetic material. The crossover operator facilitates the exchange of genetic information between two parents in the current generation, leading to the creation of a new individual that symbolises the offspring.

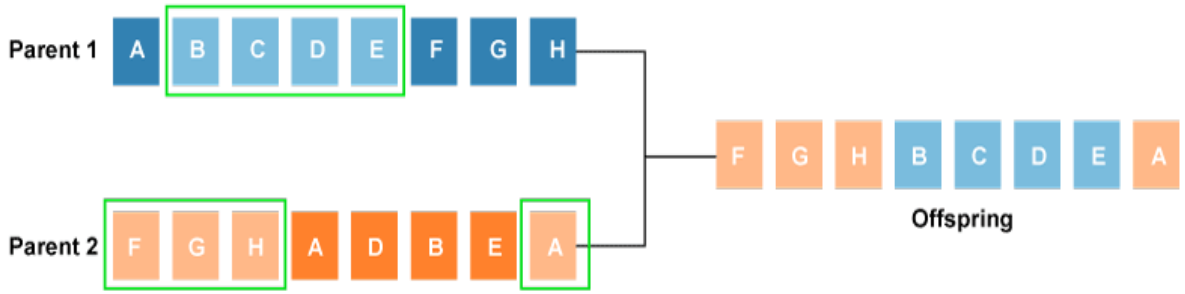

Figure 3.4 A typical crossover operation in GP

3.2.6 Mutation

The mutation operator imparts stochastic genetic variants into the progeny to maintain diversity throughout the population. The technique may be accomplished by modifying particular segments inside the chromosomes. Mutation enhances the ability to overcome early convergence and encourages the presence of a wide range of variations. The figure 3.6 depicts the process of mutation.

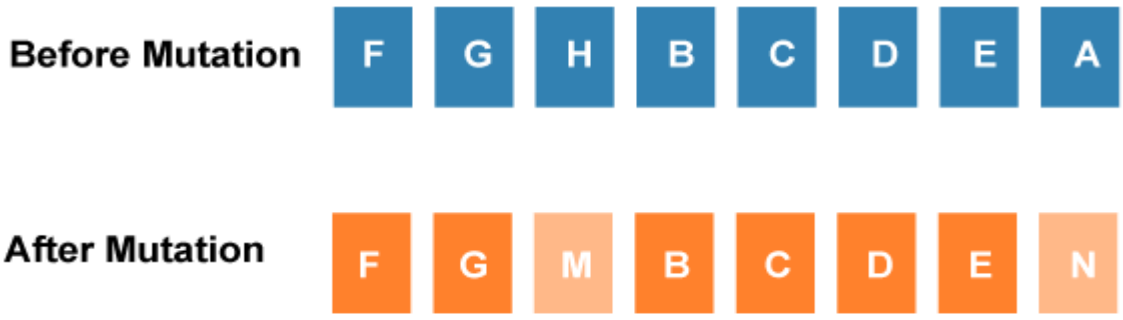

Figure 3.5 The mutation process

3.2.7 Termination in genetic programming

After the reproduction phase, a termination criterion is used to determine when the process should terminate. The method terminates after it achieves the fitness solution that satisfies the set threshold. The final alternative will be designated as the optimum solution among the people. The GP predictive algorithm considers various controlling parameters, such as the function collection, the size of the population, number of several generations, greatest gene count per individual (Gmax), greatest tree depth (dmax), tournament size, likelihood of crossover events, higher level crossover, minimal crossover, mutation incidents, sub-tree mutation, replacement of input terminal by another random terminal, Gaussian perturbation of randomly selected constants, reproduction, and ephemeral random constants.

These parameters are used to ascertain the results of the algorithm. The choice of these regulatory parameters impacts the model's ability to generalise, which will be generated by GP. The selection of these parameters is determined using a trial-and-error approach, Considering the specific problem at hand and considering some values previously suggested by Searson et al. in 2010. The user has the discretion to choose the function set, which may include arithmetic operators, mathematical functions, and other functions, based on their comprehension of the physical system under investigation. The population size directly influences the number of individuals included in the population. Before run concludes, the number of generations corresponds to the frequency at which the algorithm is used during the run. The complexity of the challenges often determines the optimal population size and the number of generations required. Multiple generations and populations undergo rigorous testing to ascertain the most efficient model. As a result of over-fitting the training data to the testing data, the fitness value of the training data has reduced, while the fitness value of the testing data has grown. The reason for this is the rise in Gmax and dmax values. The previously generated model is seeing a decrease in its ability to generalise. Hence, while constructing the MGGP model, it is crucial to find a harmonious equilibrium between the attained levels of accuracy and complexity in relation to Gmax and dmax. Research has shown the existence of optimum values for both Gmax and dmax, leading to the development of a highly efficient model (Searson et al. 2010). Using optimal values that exceed the regulatory parameters often leads to an enhancement in the effectiveness of the GP algorithm.

During the process of Genetic Programming (GP), a multitude of potential models are created at random. Subsequently, every model undergoes training and evaluation utilising the

appropriate training and testing data. Each model's fitness is evaluated by minimizing the root mean square error (RMSE) between the predicted and observed values of the output variable (LI) through the employment of the objective function (f).

$$\mathrm{RMSE} = \sqrt{\frac{\sum_{i=1}^{n}(\mathrm{LI}-\mathrm{LI_{Pre}})^2}{n}} \tag{3.1}$$

Let n be the total amount of incidences within the fitness group. If the errors calculated using Equation (3.1) for all models in the present population don't satisfy the termination criteria, the cycle of generating a new population continues until the desired optimal model is attained, as previously detailed.

The current study's GP-based model is presented in the following general manner:

$$\mathrm{LI_P} = \sum_{i=1}^{n} \mathrm{F}[\mathrm{X}, \mathrm{f(X)}, \mathrm{C_i}] + \mathrm{C_o} \tag{3.2}$$

where $\mathrm{LI_P}$ represents the predicted value of the liquefaction performance index, F is the liquefaction index function created by the GP, X is the vector of input variables, Ci is a constant, f represents the user-defined functions, n is the number of terms in the target expression, and C0 is the bias term. The GP, as described by Searson et al. (2010), is used in the development and implementation of the current models utilising gene expo 5.0.

3.3 Deep belief network (DBN) classifier

A Deep Belief Network (DBN) is a kind of deep learning network that consists of Multiple strata of interconnected units. Each stratum is composed of visible and hidden units. DBNs are designed to precisely capture complex patterns in data by collecting hierarchical representations of the incoming data. These models are categorised as generative models and are particularly well-suited for tasks such as unsupervised feature learning, dimensionality reduction, and generative modelling. The notion of Deep Belief Networks (DBN) was first proposed by Hinton et al (2006) and has since been successfully used in several fields, including feature learning, classification, and collaborative filtering (Chen et al 2014). The main constituent of DBN is a section focused on unsupervised learning, which employs restricted boltzmann machines (RBMs) as its essential components. In addition, DBN includes a logistic regression layer for the purpose of making predictions.

Restricted boltzmann machines (RBMs):

Restricted Boltzmann Machines (RBMs) are the fundamental elements of a Deep Belief Network (DBN). A RBM is a kind of neural network architecture that is both generative and stochastic in nature. The structure has two distinct layers: the visible layer and the concealed layer. The visible layer represents the input data, while the buried layer encodes the collected information. Each unit in a Restricted Boltzmann Machine (RBM) is encoded as a binary unit, capable of assuming values of either 0 or 1. The interconnections among these components are defined by weights, which ascertain the magnitude of the relationships. RBMs are trained using a technique called contrastive divergence or a similar training approach. Through the training process, The Restricted Boltzmann Machine (RBM) acquires the capacity to represent the combined probability distribution of the visible and hidden units. RBMs has the capacity to detect and understand patterns and relationships within the data, making them highly suitable for the task of gaining new characteristics and simplifying the complexity of dimensions.

Stacking and architecture:

A Deep Belief Network (DBN) consists of many layers of RBMs that are placed on top of each other. The hidden layer of one RBM acts as the visible layer for the next RBM in the sequence. By stacking layers in this fashion, the network is able to progressively gain increasingly intricate and abstract features from the raw input data. DBNs typically include an input layer, commonly referred to as the visible layer, many hidden layers, and an optional output layer. The number of hidden layers may vary depending on the complexity of the information and the purpose being shown in Figure 3.4.

Pretraining and fine-tuning:

DBNs are characterised by a unique training procedure consisting of two phases: pretraining and fine-tuning.

Pretraining:

Each Restricted Boltzmann Machine (RBM) layer undergoes separate unsupervised pretraining. Consequently, each Restricted Boltzmann Machine (RBM) acquires the ability to recreate its input data by leveraging the patterns it identifies within the data. The DBN is initialised using the pretrained weights of these RBMs.

Fine-tuning:

Following the pretraining process, the complete Deep Belief Network (DBN) undergoes fine-tuning via supervised learning. This process entails using annotated data to modify the weights and biases of the network, usually via backpropagation and optimisation approaches based on gradients. The process of fine-tuning involves modifying the Deep Belief Network (DBN) to suit a particular goal, such as classification or regression.

Hierarchical feature learning:

DBNs have a significant benefit in their capacity to acquire hierarchical representations of data. As data flows through the layers of Restricted Boltzmann Machines (RBMs), each following layer acquires the ability to encode more intricate and conceptual characteristics, building upon the properties learnt by the preceding layer. This hierarchical style is very suitable for capturing intricate patterns in intricate data.

Generative and discriminative capabilities:

DBNs has the ability to perform both generative and discriminative tasks. In order to generate new data samples, the hidden layers are stimulated and their stimulations are then sent to the visible layer. This attribute renders them very advantageous for jobs such as generating original images or data samples that bear similarity to the training data. Furthermore, DBNs may be enhanced to perform discriminative tasks, such as classification or regression, by adjusting the network parameters to reduce the prediction error on labelled data.

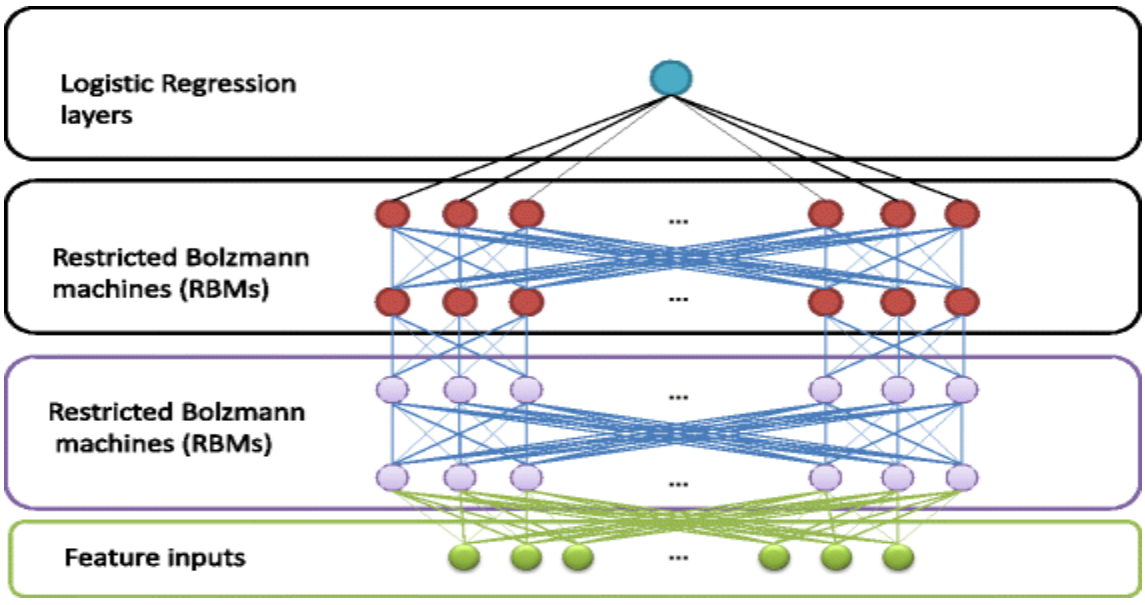

Figure 3.6 Deep belief network (DBN) architecture

DBN contain varied layers involving visible as well as hidden neurons and is specified in Eq. (3.5). The output denoted by $\overline{\mathrm{PO}}$is modeled in Eq. (3.4) and possibility function$\bar{\mathrm{P}}_{\mathrm{q}}(\zeta)$ is modeled in Eq. (3.3), wherein, pseudo-temperature is symbolized by t^{P}.

$$\bar{\mathrm{P}}_{\mathrm{q}}(\zeta) = \frac{1}{1+\mathrm{e}^{\frac{-\zeta}{\mathrm{t}^{\mathrm{P}}}}} \tag{3.3}$$

$$\overline{\mathrm{PO}} = \begin{Bmatrix} 1 & \mathrm{with} 1-\bar{\mathrm{P}}_{\mathrm{q}}(\zeta) \\ 0 & \mathrm{with} \bar{\mathrm{P}}_{\mathrm{q}}(\zeta) \end{Bmatrix} \tag{3.4}$$

$$\lim_{\mathrm{t}^{\mathrm{P}}\to 0^{+}} \bar{\mathrm{P}}_{\mathrm{q}}(\zeta) = \lim_{\mathrm{t}^{\mathrm{P}}\to 0^{+}} \frac{1}{1+\mathrm{e}^{\frac{-\zeta}{\mathrm{t}^{\mathrm{P}}}}} = \begin{cases} 0 & \text{for} \quad \zeta < 0 \\ \frac{1}{2} & \text{for} \quad \zeta = 0 \\ 1 & \text{for} \quad \zeta > 0 \end{cases} \tag{3.5}$$

The binary statebiis revealed in Eq. (3.6) and (3.7), wherein "θ_{a} implies biases and $\mathrm{L}_{\mathrm{a,l}}$ implies weights amid neurons".

$$\mathrm{EN}(\mathrm{bi}) = -\sum_{\mathrm{a}} \mathrm{bi}_{\mathrm{a}} \theta_{\mathrm{a}} - \sum_{\mathrm{a}<\mathrm{l}} \mathrm{bi}_{\mathrm{a}} \mathrm{L}_{\mathrm{a,l}} \mathrm{bi}_{\mathrm{l}} \tag{3.6}$$

$$\Delta\mathrm{EN}(\mathrm{bi}_{\mathrm{a}}) = \sum_{\mathrm{l}} \theta_{\mathrm{a}} + \mathrm{L}_{\mathrm{a,l}} \mathrm{bi}_{\mathrm{l}} \tag{3.7}$$

The energy for visible and hidden neuron (x, y) is in Eq. (3.8) - (3.10), "where$\mathrm{iny}_{\mathrm{l}}$and x_{a}implies a binary state of the hidden unitl and visible unita,$\mathrm{k}_{\mathrm{a}}$and C_{l} implies biases".

$$\mathrm{EN}(\mathrm{x}, \mathrm{y}) = -\sum_{(\mathrm{a,l})} \mathrm{L}_{\mathrm{a,l}} \mathrm{x}_{\mathrm{a}} \mathrm{y}_{\mathrm{l}} - \sum_{\mathrm{a}} \mathrm{k}_{\mathrm{a}} \mathrm{x}_{\mathrm{a}} - \sum_{\mathrm{l}} \mathrm{C}_{\mathrm{l}} \mathrm{y}_{\mathrm{l}} \tag{3.8}$$

$$\Delta\mathrm{EN}(\mathrm{x}_{\mathrm{a}}, \bar{\mathrm{y}}) = \sum_{\mathrm{l}} \mathrm{L}_{\mathrm{al}} \mathrm{y}_{\mathrm{l}} + \mathrm{k}_{\mathrm{a}} \tag{3.9}$$

$$\Delta\mathrm{EN}(\vec{\mathrm{x}}, \mathrm{y}_{\mathrm{l}}) = \sum_{\mathrm{a}} \mathrm{L}_{\mathrm{al}} \mathrm{x}_{\mathrm{a}} + \mathrm{C}_{\mathrm{l}} \tag{3.10}$$

weights are shown in Eq. (3.11).

$$\mathrm{M}_{(\widehat{\mathrm{m}})} = \max_{\mathrm{M}} \prod_{\vec{\mathrm{x}}\in\mathrm{N}} \mathrm{c}(\vec{\mathrm{x}}) \tag{3.11}$$

The RBM energy function is in Eq. (3.12), PR^{F}implies partition terms as in Eq. (3.13).

$$\mathrm{c}(\vec{\mathrm{x}}, \vec{\mathrm{y}}) = \frac{1}{\mathrm{PR}^{\mathrm{F}}} \mathrm{e}^{-\mathrm{EN}(\vec{\mathrm{x}}, \vec{\mathrm{y}})} \tag{3.12}$$

$$\mathrm{PR}^{\mathrm{F}} = \sum_{\vec{\mathrm{x}}, \vec{\mathrm{y}}} \mathrm{e}^{-\mathrm{EN}(\vec{\mathrm{x}}, \vec{\mathrm{y}})} \tag{3.13}$$

Let training pattern be $\left(\mathrm{K}^{\widehat{\mathrm{H}}}, \mathrm{U}^{\widehat{\mathrm{H}}}\right)$, wherein $\mathrm{K}^{\widehat{\mathrm{H}}}$and $\mathrm{U}^{\widehat{\mathrm{H}}}$indicate input and output vector, and$1 \leq \widehat{\mathrm{H}} \leq \mathrm{V}$, Vpoint out training pattern count. All neuron errors at the output are delineated by Eq. (3.14). Subsequently, the square error of $\widehat{\mathrm{H}}$ pattern is specified in Eq. (3.15)

$$\mathrm{e}_{\mathrm{l}}^{\widehat{\mathrm{H}}} = \mathrm{K}^{\widehat{\mathrm{H}}} - \mathrm{U}^{\widehat{\mathrm{H}}} \tag{3.14}$$

$$\mathrm{SE}_{\widehat{\mathrm{H}}} = \frac{1}{\tilde{\mathrm{o}}_{\mathrm{y}}} \sum_{\mathrm{l}=1}^{\tilde{\mathrm{o}}_{\mathrm{y}}} \left(\mathrm{e}_{\mathrm{l}}^{\widehat{\mathrm{H}}}\right)^{2} = \frac{1}{\tilde{\mathrm{o}}_{\mathrm{y}}} \sum_{\mathrm{l}=1}^{\tilde{\mathrm{o}}_{\mathrm{y}}} \left(\mathrm{K}^{\widehat{\mathrm{H}}} - \mathrm{U}^{\widehat{\mathrm{H}}}\right)^{2} \tag{3.15}$$

$$\mathrm{SE}_{\mathrm{avg}} = \frac{1}{\mathrm{V}} \sum_{\widehat{\mathrm{H}}=1}^{\mathrm{V}} \mathrm{SE}_{\widehat{\mathrm{H}}} \tag{3.16}$$

3.4 Long short-term memory (LSTM) classifier

The Recurrent Neural Network (RNN) is designed to address sequential time-series challenges by using its ability to retain and use past knowledge. Nevertheless, the limited applicability of the gradient vanishing and exploding phenomenon in long-term dependencies is mostly attributed to the singular structure and parameter solution technique used in Back Propagation Through Time (Hochreiter and Munchen, 1998). LSTM (Hochreiter and Schmidhuber, 1997) is a kind of neural network that addresses the limitations of RNN. Figure 3.7 depicts the internal cellular composition of RNN and LSTM. The Long Short-Term Memory (LSTM) model incorporates memory cells and three gates ('forget gate, input gate, and output gate') into the Recurrent Neural Network (RNN). These gates control the transmission of data inside the LSTM cells and govern the input, storage, and output of information, respectively.

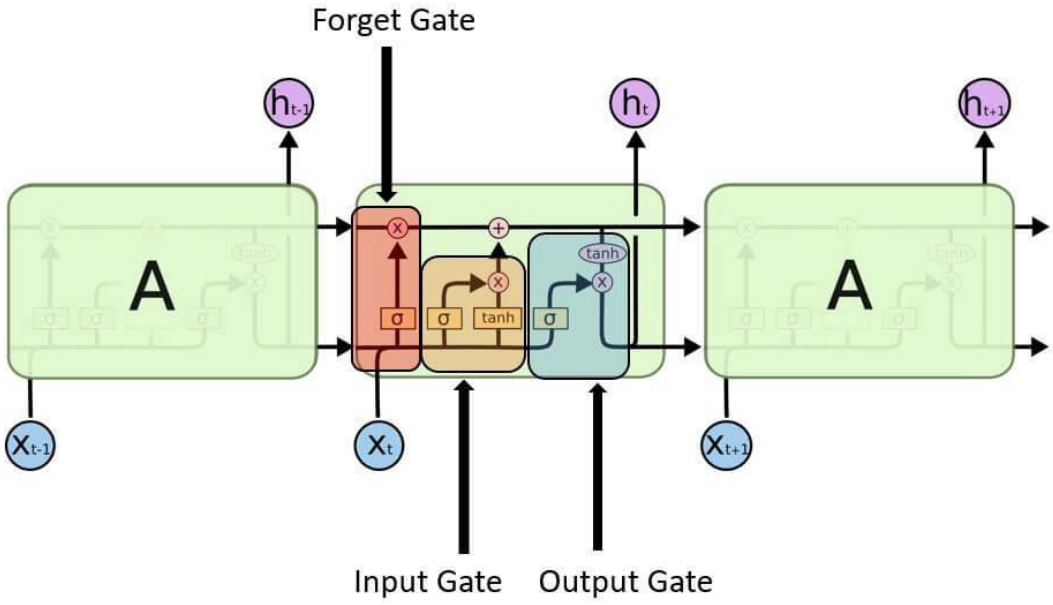

Figure 3.7 Long short-term memory (LSTM) architecture

LSTM encompassed 3 units, such as "forget gate, the input gate, and the output gate". Assume M and D as hidden and cell states. (M_t, D_t) and (X_t, D_{t-1}, M_{t-1})→ output and input layer.
At the "time t, the output, input and forget gate impliesO_t, I_t, F_t". LSTM is primarily employs F_t for sorting the data to ignore. $F_t$is formulated as specified in Eq. (3.17).

$$F_t = \sigma(J_{IF}X_t + B_{IF} + J_{MF}M_{t-1} + B_{MF}) \quad (3.17)$$

In Eq. (3.17)," $(J_{MF}, B_{MF})$and (J_{IF}, B_{IF}) Apply weight and bias constraints to connect the hidden and input layers to the forget gate, while also applying the activation function byσ.

Input gate in LSTM as shown in Eq. (3.18) - Eq. (3.20), where, $(J_{MG}, B_{MG})$and(J_{IG}, B_{IG}) Apply weight and bias constraints to provide a mapping between the hidden and input layers and the cell gate, respectively. (J_{MI}, B_{MI}) and (J_{II}, B_{II}) imply weight and bias constraint to map hidden and input layers to I_t".

$$G_t = \tanh(J_{IG}X_t + B_{IG} + J_{MG}M_{t-1} + B_{MG}) \quad (3.18)$$

$$I_t = \sigma(J_{II}X_t + B_{II} + J_{MI}M_{t-1} + B_{MI}) \quad (3.19)$$

$$D_t = F_tD_{t-1} + I_tG_t \quad (3.20)$$

$$O_t = \sigma(J_{IO}X_t + B_{IO} + J_{MO}M_{t-1} + B_{MO}) \quad (3.21)$$

$$M_t = O_t \tanh(D_t) \quad (3.22)$$

Further, the LSTM cell obtains the output hidden layer from the output gate as revealed in Eq. (3.21) and Eq. (3.22), wherein, (J_{MO}, B_{MO}) & (J_{IO}, B_{IO}) implies weight and bias to map the hidden and input layer to O_t.

3.5 Bidirectional GRU (BI-GRU)

The Recurrent Neural Network (RNN) is designed to address sequential time-series challenges by using its ability to retain and use past knowledge. Nevertheless, the limited applicability of the gradient vanishing and exploding phenomenon in long-term dependencies is mostly attributed to the singular structure and parameter solution technique used by Back Propagation Through Time (Hochreiter and Munchen, 1998). GRU (Cho et al. 2014) is a kind of recurrent neural network (RNN) that addresses the limitations of traditional RNNs. The GRU employs certain gates, including the update and reset gates, to mitigate gradient dispersion, hence facilitating long-term memory and minimising computational loss. The update gate (zT) supplants the input and forget gates of LSTM, dictating the extent to which the prior information is retained in the current predicting. This is seen in the accompanying Figure 3.8.

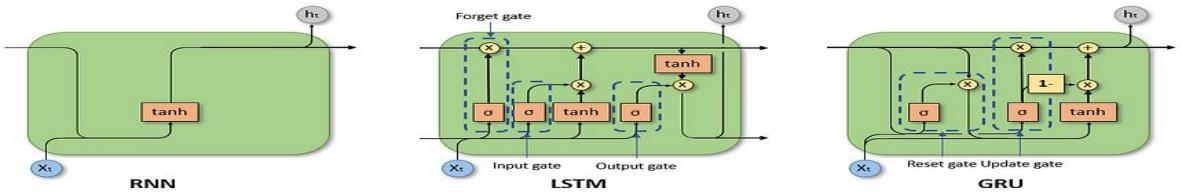

Figure 3.8 Bidirectional GRU (BI-GRU) architecture

Depending upon RNN, and 3 gates named 'forget gate, input gate and output gate and memory cell' in the LSTM. Likewise, GRU exploits 'special gates, called reset and update gates', to reducing gradient dispersal with lesser calculative deficits. The update gate (ut)same as forget and input gates in LSTM, portraying the retention degree of preceding data as shown in Eq. (3.23).

$$\mathrm{ut} = \mu(W_u.[R_{t-1}, Fea_t] + f_u) \tag{3.23}$$

In Eq. (3.23), μ correspond to sigmoid activation function among 0 and 1, Fea_t correspond to input matrix at time step t, R_{t-1} correspond to hidden state at the previous time step $t-1$. W_u correspond to weight matrix of ut and f_u correspond to bias matrix of ut. The reset gate (rt) regulates how much chronological data have to be disregarded that is shown in Eq. (3.24), wherein, W_r correspond to weight matrix of rt and f_r correspond to bias matrix of rt.

$$\mathrm{rt} == \mu(W_r.[R_{t-1}, Fea_t] + f_r) \tag{3.24}$$

Subsequently, the candidate's hidden state shown in Eq. (3.25), wherein, $\tanh$ correspond to $\tanh$activation function. f_R and W_R correspond to bias matrix and weight matrix of the new cell state, $*$ implies dot multiplication function.

Thus, the output (R_t) implies linear interruption amid $(\widetilde{R}_t)$and R_{t-1}.

$$\widetilde{R}_t = \tanh(W_R.[R_{t-1} * rg, Fea_t] + f_R) \tag{3.25}$$

$$R_t = (1 - \mathrm{ut}) * R_{t-1} + \mathrm{ut} * \widetilde{R}_t \tag{3.26}$$

The forward GRU encodes the preceding information of the input data, whereas the reverse GRU captures the subsequent information of the input data. The Bi-GRU is modelled a sin Eq. (3.27), wherein, $\overleftarrow{R}_t$and $\overrightarrow{R}_t$ correspond to hidden state of backward and forward GRU in that order, Ct correspond to Integration of outputs at 2 directions.

$$\mathrm{Yt} = \mathrm{Ct}(\overrightarrow{R}_t, \overleftarrow{R}_t) \tag{3.27}$$

3.6 Support vector machine (SVM)

The support vector machines (SVM) approach is a widely used machine learning technique for classification. However, it may also be used to predict a continuous output variable based on input data. The fundamental premise of Support Vector Machines (SVM) is to identify a function that can precisely map input variables to output variables, while minimising mistakes and satisfying a certain margin. In order to accomplish this objective, the input variables are converted into a space with a greater number of dimensions by the use of a kernel function.

Subsequently, the regression line that optimises the margin while ensuring that the error remains below a predetermined tolerance level is determined (Drucker et al. 1997). The SVR method is advantageous because to its ability to efficiently handle non-linear relationships among input and output variables. To achieve this goal, 'kernel functions such as polynomial, radial basis function (RBF), and sigmoid functions' are used. These functions aid in the learning of intricate relationships between variables (Smola and Schölkopf 2004). Support Vector Regression (SVR) has shown effective in several domains, including banking (Sharma et al. 2012), transportation (Yeh et al. 2010), and medical imaging (Borges et al. 2016). Optimum performance may be achieved by meticulously selecting and optimising the kernel function and other associated parameters. A frequently used technique for converting a linear classifier into a non-linear classifier entail using a non-linear function to translate the input space x onto a feature space F. An alternative method is using a non-linear function to carry out the mapping procedure.

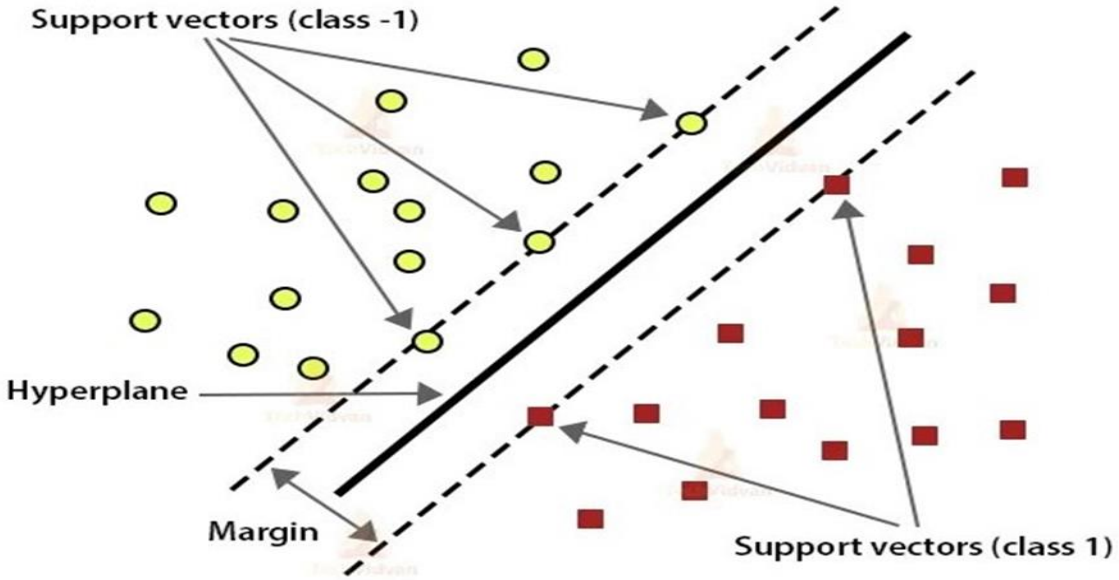

Figure 3.9 Support vector machine

The spatial partitioning function in space F may be mathematically represented as:

$$f(x) = w^T \varphi(x) + b \tag{3.28}$$

The statistical approach represented by the algebraic function f (x, w) may be described inside the subspace as follows:

$$w = \sum_{i=1}^{n} \alpha_i x_i \tag{3.29}$$

$$f(x, w) = \sum_{j=1}^{n} \alpha_i x_i \varphi_i(x) + b \quad (3.30)$$

$$f(x) = \sum_{i=1}^{n} \alpha_i x_i^T x + b \quad (3.31)$$

$$f(x) = \sum_{i=1}^{n} \alpha_i \varphi(x_i)^T \varphi(x) + b \qquad 0 \le \alpha_i \le C \quad (3.32)$$

$$k(x, x') = \varphi(x)^T \varphi(x') \quad (3.33)$$

$$f(x) = \sum_{i=1}^{n} \alpha_i k(x, x_i) + b \quad (3.34)$$

On the other hand, there is a wide variety of additional kernel functions that may be used in different situations to improve performance.

Linear kernel: $k(x_i, x_j) = x_i^T x_j$

Polynomial kernel: $k(x_i, x_j) = (\gamma x_i^T x_j + r)^d, \ \gamma > 0$

RBF kernel: $k(x_i, x_j) = \exp(-\gamma \|x_i - x_j\|)^2, \ \gamma > 0$

Sigmoid kernel: $k(x_i, x_j) = \tanh(\gamma x_i^T x_j + r), \ \gamma > 0$

The SVM model incorporates the parameters C, γ, r, and d. The efficacy of the Support Vector Machine (SVM) model relies on the calibre of the selected configurations for its parameters, which including the kernel parameters. Effectively managing the complexity of the regression model relies heavily on the meticulous selection of the parameters C, γ, and r. However, the process of choosing the most appropriate criteria is further complicated by the vast complexity involved in determining them. In order to expedite the classification process and decrease the dimensionality of the input space, kernel functions are implemented. Exposure to data sets significantly improves the efficacy of the Support Vector Machine (SVM) model, much like the process of enhancing other neural network models.

3.7 Average cat and salp swarm algorithm (AC-SSO)

Despite spending most of their time sleeping, cats maintain a heightened level of alertness and curiosity towards their environment and any moving objects within their vicinity. This behaviour assists cats in observing and catching their prey. In relation to their sleep period, they dedicate an inadequate amount of time to hunting in order to save their energy. Chu and Tsai (2007) developed the CSO algorithm by drawing inspiration from the predatory behaviour of felines. The algorithm has two distinct modes: the "seeking mode" during which cats are in a state of rest, and the "tracing mode" when they are actively following their prey, as seen in the Figure3.10. In the context of Cat Swarm Optimisation (CSO), A collection of cats is generated and uniformly dispersed throughout the M-dimensional solution space. every cat represents a unique solution. The population is divided into two main categories, as seen in the image. The cats in the first subgroup are in a state of quiescence and attentiveness, carefully analysing their

environment (i.e., in a state of searching), whereas the cats in the second grouping are actively in motion and aggressively chasing their prey (i.e., in a state of tracing). By using these two modes, CSO is able to advance towards the global solution inside the solution space that has M dimensions. Since the cats do not spend enough time in the tracing mode, it is essential to restrict the number of cats in the tracing subgroup. The numerical value of this value is determined by the mixing ratio (MR), which is characterised by a tiny magnitude. Once the cats have been categorised into these two groups, will proceed to generate new arrangements and fitness functions. The feline with the best optimal response will be stored in the memory. The process is iterated until the specified termination conditions are met.

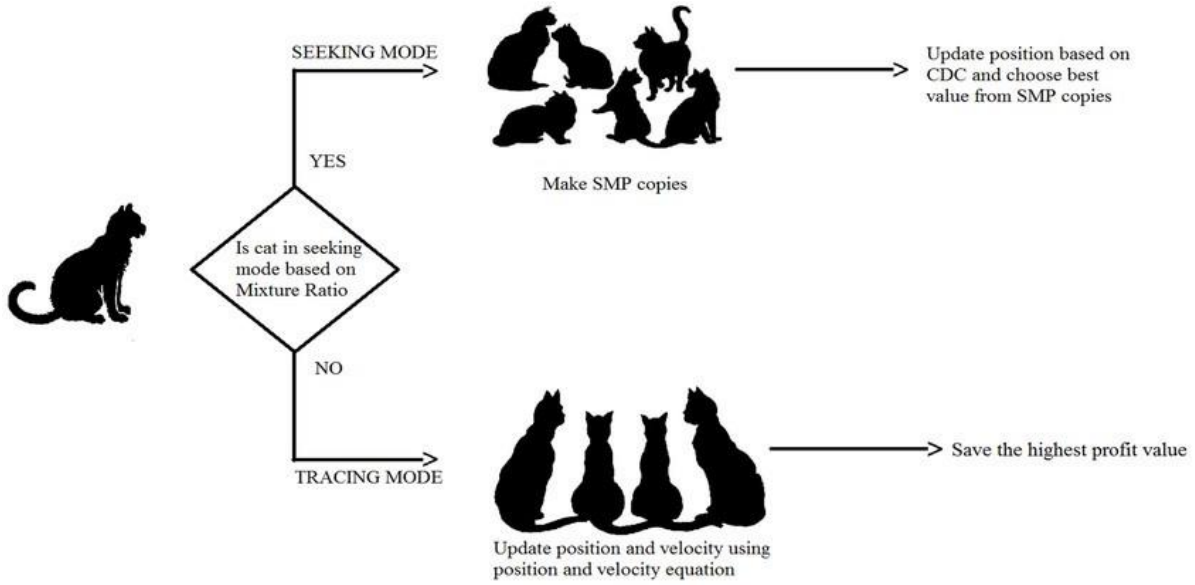

Figure 3.10 Cat swarm optimization (CSO) algorithm. SMP, seeking memory pool; CDC, counts of dimensions to change (Selvakumar et al. 2017)

3.7.1 Seeking mode (Resting)

During this phase, the cat is in a condition of rest while being alert to its surroundings. Upon sensing the presence of prey or danger, the cat assesses the situation and decides on its next course of action. The cat's decision to move is executed with intention and caution. During periods of inactivity, the cat enters a state of focused exploration, meticulously analysing the M-dimensional solution space in order to choose its subsequent course of action. In this situation, the cat has self-awareness about its circumstances, surroundings, and the possible

choices for its movement. The CSO technique employs four factors to characterise these: the searching memory pool (SMP), the seeking range of the selected dimension (SRD), the counts of dimension to alter (CDC), and the self-position consideration (SPC) (Chu and Tsai 2007). SMP stands for the number of copies produced for each cat throughout the search process. The SRD exhibits the most significant discrepancy between the revised and initial values in the selected mutation dimension. The CDC offers data on the quantity of dimensions that will experience mutation. These parameters together dictate the search process of the algorithm. The variable SPC is a Boolean that signifies the present location of the cat as a potential site for migration. Statistical Process Control (SPC) has no impact on the value of Standardised Mean Difference (SMP).

3.7.2 Tracing mode (Movement)

The tracking mode makes feel like a cat chasing its prey. Upon discovering a prey during a period of rest (in seeking mode), the cat determines its velocity and trajectory by taking into account the prey's location and speed.

3.7.3 Termination criteria

The termination criteria establish the point at which the algorithm is concluded. The choice of proper termination criteria is critical in ensuring the algorithm's precise convergence. The CSO is frequently terminated based on the degree of progress made, the number of iterations completed, and the duration of execution. Though conventional Cat swam optimiser (CSO), algorithm imitates the food searching behaviour of cats, scheme involves diverse enhancements but it suffers due to premature convergence etc (Chu et al 2012). Hybrid optimizing models are proficient for specified searching issues, (Elango et al 2020) To overcome the disadvantages of traditional CSO, the theory of Salp Swarm Algorithm (SSA) (Amir and Mirjalili 2017) is included with it to form a new scheme termed as, AC − SSO.

The AC − SSO algorithm emulates the foraging habit of felines. The food is considered the solution space, whereas the global optimum is considered the food. All unique solutions are represented by cats while searching in a certain area. The method begins by assigning the number of cats with position P to velocity. The solution's quality is assessed by use of a fitness function for each cat. The behaviour of a cat is determined by the concepts of curiosity-driven exploration (CDC), sensory-motor primitives (SMP), and self-regulated decision-making (SRD) in its seeking mode. The SMP stands for the number of cats that are counted more than once,

CDC is for the dimensions that need to be changed, and SRD stands for the variability of the selected dimensions. The following are the stages involved in this procedure for j^{th} cat.

(i) Generate a replica of SMP copies of j^{th} cat.

(ii) For all copies (k^{th}cat, $k = 1,2 \ldots SMP$) Vary the position in accordance with Equation (3.35)., wherein, Z_{ca} refers to present position and Ψ is a Random integer between [0, 1].

$$Z_{k,\ell} = (1 \pm SRD \times \Psi) \times Z_c \quad (3.35)$$

(iii) Calculate the fitness for each individual and prioritise the one with the highest fitness. (Z_{best}).

(iv) Replace $Z_j$with Z_{best}if $Z_j$is inferior than Z_{best}based on fitness value.

During tracing mode, the cats track the prey and illustrate the relevant process as seen below. Upon detecting the prey, the felines strategize their movement according to the velocity and location of the target (prey). The velocity of catj in dimensionℓ is modelled based on cat's best position, in which ra_1, ra_2denotes a random value between 0 and 1, $Gl_{best.\ell}$ represents global best, $Z_{j,\ell}$ represents cat's position, $V_{j,\ell}$ represents cat's velocity in dimension ℓ.

$$V^*_{j,\ell} = V_{j,\ell} + ra_1 ca_1 \times \left(Gl_{best.\ell} - Z_{j,\ell}\right) \quad (3.36)$$

If cat's velocity is greater than maximum velocity, then the highest possible speed may be provided. In the traditional approach, the novel position is typically updated using the cat's position. However, according to the advanced $AC - SSO$ model, the new velocity of cat $Z_{j,\ell,new}$is updated by taking the harmonic mean of both CSO update and SSA update as shown in Eq. (3.37), where $Z_{j,\ell,old}$ represents present position of cats in dimension ℓ and $V_{j,\ell}$ represents cat's velocity at dimensionℓ, Z_j^i points out position of i^{th}follower salp in j^{th} dimension. The harmonic mean is computed as shown in Eq. (3.38), wherein, n implies the value count in a set of data and we implies the weight. The pseudocode of $AC - SSO$ is shown in Algorithm 1.

$$Z_{j,\ell,new} = HM\left(Z_{j,\ell,old} + V_{j,\ell}\right) and \frac{1}{2}\left(Z_j^i + Z_j^{i-1}\right)$$

(3.37)

$$HM = \frac{n}{\sum\left(\frac{1}{b}\right)} * we \quad (3.38)$$

Algorithm 1: Implemented AC-SSO model

Initialize the population

while do

Compute fitness as shown in Eq. (3.13)

$Z_{best.\ell}$ =cat with optimal solution

For $j = 1,2.,..N$

If $SPC = 1$

Begin seeking mode

Else

Begin tracing mode

Compute velocity based on Eq. (3.14)

Compute position by taking the harmonic mean of both CSO update and SSA update as shown in Eq. (3.15).

end if

end for j

end while

3.8 Opposition based self-adaptive shark smell optimizer (OSA-SSO)

The smell system, found in all mammals, serves as the main sensory system responsible for detecting and reacting to chemical signals originating from a remote source. The olfactory pits, located on the lateral margins of fish heads, contain the olfactory receptors responsible for detecting smells. Each cavity has a set of outside openings via which water is both introduced and expelled. The water flow inside the pit is facilitated by the reciprocal movement of tiny cilia on the cells lining the pit, as well as propulsion created by the swimming movement of fish in the water. The chemicals in solution attach to a folded surface in the nerve terminals of the olfactory system (Abedinia et al. 2014). Vertebrates possess olfactory receptors that form a direct neural link with their brains, bypassing the need for intermediary nerves, which is distinct from other sensory nerves. The olfactory bulb, situated in the anterior portion of the brain, receives the olfactory sensations. Fish has a set of olfactory bulbs, located inside an olfactory pit. The olfactory sense of fish is improved by the provision of a larger surface area to olfactory pits. This results in larger smell nerves and more extensive smell information centres in the

brain (Magnuson 1979). Eels and sharks possess the most sizable olfactory bulbs for the purpose of processing smell information. Sharks appeared some 400 million years ago as proficient predators, cementing their supremacy in the aquatic ecosystem. Sharks' extraordinary olfactory talents are a key role in their survival in their native environment. These qualities allow them to successfully discover and capture prey. Sharks have a highly efficient sense of smell. As a shark moves through water, the liquid flows via its nostrils located on the sides of its snout. After the water reaches the olfactory pits, it continues via the skin's folds that are covered with sensory cells. Some species of sharks have the capacity to detect even the smallest trace of blood due to their sensory cells (Sfakiotakis et al. 1999).

For instance, a shark has the capacity to detect a solitary droplet of blood amongst an extensive swimming pool. Abedinia et al. (2014) reported that sharks had the capability to identify the odour of an injured fish from one kilometre. The shark's smell sense mechanism might be seen as a navigational system for it. The odor emitted from the left side of the shark travels via the left nostril and then reaches the right nostril. This method allows sharks to identify the source of the scent (Wu and Yao-Tsu 1971). Figure 3.11 illustrates the shark's move towards the source of the odour. Focusing is essential in this move to guide the shark towards its prey. In essence, heightened focus results in the shark's physical motion. This property forms the basis for developing an optimisation algorithm that aims to find the most optimal solution to a given problem.

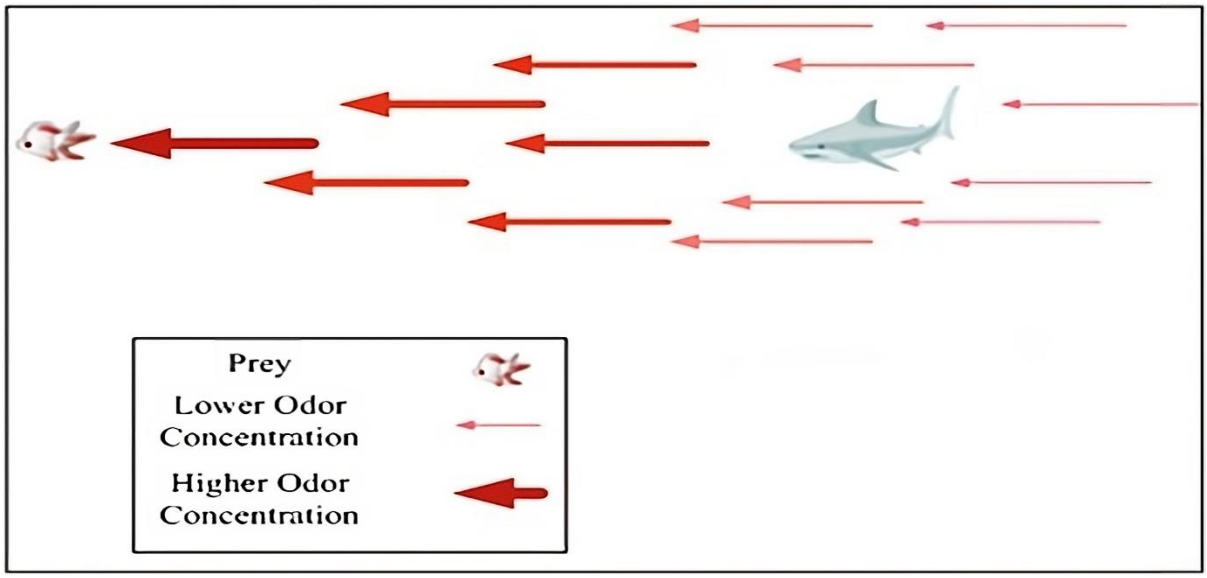

Figure 3.11 Schematic of shark's movement toward the source of the smell (Mohammad et al. 2018)

Mohammad et al. (2018) introduced Shark Smell Optimiser (SSO) model, offers various benefits but it does, however, have certain drawbacks, such as premature convergence. As a consequence, a specialist modification is necessary to solve this problem, and as a result, the opposition based self-adaptive shark smell optimizer (OSA-SSO) was developed. Self-enhancement has been demonstrated to be successful in classical optimisation procedures (Wang et al. 2016; Li et al. 2022). proposed OSA-SSO includes 4 primary phases namely, "initialization, forward movement, rotational movement, and position update".

3.8.1 Initialization

In the OSA-SSO algorithm, the initial solution populations in the searching space are created randomly. Every solution represents a scent particle that indicates a potentially viable location of a shark during the early phase of the search process. The initial solution is depicted in Eq. (3.39) and (3.40), where, $Z_i^1 = i^{th}$ initial Population vector position and np implies size of Population. In addition, objective based solutions are created, that is, opposite solutions are generated in SSO. The generation of opposite solutions ensures better convergence rates, thereby, ensuring the attainment of objectives in a precise manner.

$$Z^1 = \left[Z_1^1, Z_2^1, \ldots . Z_{np}^1\right] \tag{3.39}$$

The related optimization issue is shown in Eq. (3.40), in which, $Z_{i,j}^1 = j^{th}$dimension of i^{th}position of shark and nd implies decision variable count.

$$Z_i^1 = \left[Z_{i,1}^1, Z_{i,2}^1, \ldots . Z_{i,nd}^1\right] \tag{3.40}$$

Forward movement

As blood is diluted in water, the Shark, regardless of its location, moves towards more concentrated odour particles with a velocity (V) in order to get closer to its goal (prey). As a result, Vis computed as exposed in Eq. (3.41) and every V includes a dimensional element as in Eq. (3.42).

$$V_i^1 = \left[V_1^1, V_2^1, \ldots . V_{np}^1\right] \tag{3.41}$$

$$V_i^1 = \left[V_{i,1}^1, V_{i,2}^1, \ldots . V_{i,nd}^1\right] \tag{3.42}$$

Hence, the velocity in all dimensions is evaluated as in Eq. (39), wherein, $k = 1,2,\ldots . k\frac{\partial(obj)}{\partial \chi j}\Big|_{\chi_{i,j}^k}$ specify derivative objat position$\chi_{i,j}^k$,k_{max} specify stage count for shark's

forwarding movement, k specify stage count. Conventionally, the parameters$\Re 1$, $\Re 2$, $\Re 3$, $\alpha_k$and β_k are chosen randomly, however as per proposed $\mathrm{OSA-SSO}$ concept, $\Re 1$, $\Re 2$, $\Re 3$ parameters are computed based on tent map as shown in Eq. (3.43) and $\alpha_k$and β_k are computed based on logistic map as revealed in Eq. (3.44).

$$\Re_{k+1} = \begin{cases} \Re_k / 0.4, 0 < \Re_k \leq 0.4 \\ (1 - \Re_k)/0.6 0.4 < \Re_k \leq 1 \end{cases} \tag{3.43}$$

$$\Re_{k+1} = 4\Re_k(1 - \Re_k) \tag{3.44}$$

$$V_{i,j}^k = \eta_k . \Re 1 . \frac{\partial(\mathrm{obj})}{\partial \chi j}\Big|_{\chi_{i,j}^k} \tag{3.45}$$

The raise in Vis represented by the lift in the intensity of odour. In all phases of $V_{i,j}^k$, the velocity limiter is deployed as exposed in Eq. (3.46), where α_k denotes inertia coefficient.

$$V_{i,j}^k = \eta_k . \Re 1 . \frac{\partial(\mathrm{obj})}{\partial \chi j}\Big|_{\chi_{i,j}^k} + \alpha_k . \Re 2 . V_{i,j}^{k-1} \tag{3.46}$$

The velocity limiter deployed for every phase of $\mathrm{OSA-SSO}$ model is shown in Eq. (3.47), wherein, $\beta_k$implies velocity limiter ratio for phase k.

$$\left|V_{i,j}^k\right| = \left[\left|\eta_k . \Re 1 . \frac{\partial(\mathrm{obj})}{\partial \chi j}\Big|_{\chi_{i,j}^k} + \alpha_k . \Re 2 . V_{i,j}^{k-1}\right|, \left|\beta_k . V_{i,j}^{k-1}\right|\right] \tag{3.47}$$

Owing to shark's forward movement, its novel position $G_i^{k+1}$is portrayed based upon its preceding position $Z_i^k$and velocity (V_i^k), the novel shark position is depicted in Eq. (3.48).

$$G_i^{k+1} = Z_i^k + V_i^k . \Delta t_k \tag{3.48}$$

Here, Δt_kspecify is a time period (around 1).

3.8.2 Rotational movement

The shark includes rotational movement for discovering the strong odour particle. This process is known as local search as revealed in (3.49), wherein, $m = 1,2 \ldots M$.

$$Y_i^{k+1,m} = G_i^{k+1} + \Re 3 . G_i^{k+1} \tag{3.49}$$

3.8.3 Particle position update

The searching path of shark continues with rotational movement as it moves nearer to strong odour particle, which is revealed in Eq. (3.50), here; Y_i^{k+1}signify subsequent position of shark with higherObjvalue.

$$Z_i^{k+1} = \arg\max\{obj(G_i^{k+1}), Obj(Y_i^{k+1,i}), \ldots, Obj(Y_i^{k+1,M})\} \quad (3.50)$$

The course of action will be continued till k attains the utmost value for an optimization crisis.

The pseudo code of $OSA - SSO$ approach is specified in Algorithm 2.

Algorithm 2: OSA-SSO

Start

Initializing populace

Generate OBL based opposite solutions

Assign constraints, np , α_k , $k_{\max}$, η_k and $k = 1,2,....\nu_{\max}$

Compute $\Re 1$, $\Re 2$, $\Re 3$, α_k and β_k based upon tent map and logistic map as per Eq. (3.43) and Eq. (3.45)

Generate primary populace with all individuals

initializing $k = 1$

For $k = 1$: $k_{\max}$

Forward movement

Compute every element of $V_{i,j}$

Attain novel shark position as revealed in Eq. (3.48)

Rotational movement

Attain novel shark position as per rotational movement $Y_i^{k+1,m}$ shown in Eq. (3.49)

Choose subsequent shark position depending upon 2 movements

Carry out cycle cross over operation

End for k

Fix $k = k + 1$

Choose best shark position with higher Obj value shown in Eq. (3.50)

End

3.9 Conclusions

- Genetic programming (GP) is a computational technique that belongs to the broader class of genetic algorithms (GA). It is designed to mimic biological processes and incorporates many operators, including reproduction, crossover, and mutation. Unlike linear regression, Artificial Neural Networks (ANN) provide a comprehensive framework for analysing the output based on the input data. A compromise has to be reached between the intricacy and precision of the procedure. Geotechnical engineering offers just a limited number of applications for GP. Initial study on the utilisation of GP for suction pile uplift capacity has shown that the GP model exhibits superior performance compared to Excel, Linear regression, ANN, and other models. Consequently, the subsequent chapters of this thesis aim to develop models for assessing the likelihood of liquefaction using deterministic, probabilistic, and reliability-based approaches that use Genetic programming (GP).
- The Support Vector Machine (SVM), Deep Belief Network (DBN), Long Short-Term Memory (LSTM), and Bidirectional Gated Recurrent Unit (Bi − GRU) are highly resilient models that surpass simpler models like Artificial Neural Networks (ANN) and linear regression. They provide a comprehensive representation of the output based on the input data, enabling more in-depth research. DBN is a hybrid model that integrates Restricted Boltzmann Machines (RBMs) with Deep Belief Networks (DBNs) to tackle challenges encountered by traditional neural networks in deep hierarchical structures. Deep Belief Networks (DBNs) consist of many unsupervised neural networks that determine the binary states of the hidden layers in the positive phase by evaluating the probability of weights and visible units. The vanishing gradient is a significant problem in recurrent neural networks (RNNs) since it rapidly diminishes or amplifies in the first layers, hence hindering the RNN′s ability to retain information from longer sequences. Consequently, Recurrent Neural Networks (RNNs) have limited memory capacity, since they might overlook crucial information due to challenges with gradient propagation and fail to transfer knowledge from earlier time steps to subsequent ones. In order to resolve this matter in order to address the problem of the vanishing gradient, LSTM (Long Short-Term Memory) and Bi − GRU (Bidirectional Gated Recurrent Unit) were developed.
- Swarm intelligence originates from the collective behaviour seen in natural swarms. Gradient descent is used to optimise the problem and reduce convergence towards local

minima. The Cat Swam Optimiser and Shark Smell Optimiser algorithms demonstrate premature convergence. In order to tackle this problem, two novel algorithms have been implemented: the Average Cat and Salp Swarm Algorithm ($AC-SSO$) and the Opposition-based Self-Adaptive Shark Smell Optimizer ($OSA-SSO$).

CHAPTER 4

DETERMINISTIC MODELS FOR EVALUATION OF LIQUEFACTION

4.1 Introduction

The stress-based approach is the most commonly utilised method for determining the liquefaction potential of soil, despite the availability of other approaches such as the cycle stress-based approach, the cyclic strain-based approach, and the energy-based approach (Krammer 1996). Although the standard penetration test (SPT) is the most often utilised in situ test-based soil exploration approach for assessing liquefaction risk, it does include a few limitations. These limitations mostly arise from the variation in the implementation of the SPT throughout various regions of the world. The cone penetration test (CPT) is increasingly gaining popularity in the corporate sector due to its consistent and repeatable nature, as well as its ability to identify continuous soil profiles. Data visualisation refers to the visual representation of information and data. Data visualisation tools use visual components such as charts, graphs, and maps to facilitate the examination and understanding of patterns, trends, and outliers within the data in a user-friendly manner. Data visualisation is the field of data analysis that focuses on visually representing data. Furthermore, in addition to graphically representing data, it serves as an effective means of conveying the findings derived from these visualisations. Data visualisation allows us to get a graphical representation of data, providing a comprehensive perspective. The human mind exhibits enhanced cognitive processing and understanding when provided with visual aids such as pictures, maps, and graphs. This is especially advantageous when dealing with massive data sets, when it is difficult to visually inspect all the data, much alone evaluate and understand it manually. Data visualisation is crucial for representing both small and big data sets, but its value is particularly significant when dealing with massive data sets. The creation of liquefaction prediction models using in-situ test datasets has been achieved by using optimisation approaches like genetic programming (GP). These models have been shown to be more efficient than artificial neural networks (ANN), support vector machines (SVM), relevance vector machines (RVM), and statistical approaches. In the first chapter, have already addressed both the favourable and unfavourable features of the tactics that have been previously introduced.

The present study aims to visually represent the data to determine the correlation between the independent variable and other components, as well as the dependent variables. Furthermore, the entropy of the data has been determined to get insight into the transmission of information. In addition, a deterministic model has been developed utilising the post-liquefaction SPT database and the GP method proposed by Hwang and Yang in 2001. A cyclic resistance ratio (CRR) equation has been developed using GP, including both liquefied and non-liquefied scenarios. This equation represents the state of the soil. To assess the liquefaction potential in relation to Fs, the CRR model, in conjunction with the widely used CSR model (Juang et al. 2000), is applied. Using a dataset obtained from an outside source.

4.2 Methodology and simulation setup

The raw post-liquefaction data were collected from various sources, including case studies spanning significant earthquakes, such as the 1944 Tohnankai earthquake, the 2010-2011 Canterbury earthquake in New Zealand, and the Tohoku-oki, Great East Japan earthquake. After gathering the raw data, necessary corrections and modifications were performed following the procedures outlined by Idriss and Boulanger (2010). Additionally, independent data from Faridabad, NCR Delhi, were collected using standard SPT procedures. Laboratory tests were conducted to determine the engineering and index properties, followed by required modifications to the data.

The data preprocessing involved handling outliers using the mean and median method (Livingston, 2004), ensuring that any potential human errors did not impact the analysis. After reviewing the literature, data points with a factor of safety greater than 3 were excluded from further analysis (Upadhyaya et al., 2019).

For the cleaned data, visualization was performed using Python's Matplotlib library to identify trends, such as the coefficient of dependency through Pearson correlation and entropy of variables using pair plots. This analysis provided insights into the data and guided the selection of appropriate models for further study.

The stress-based technique developed by Seed and Idriss (1967), which evaluates the likelihood of liquefaction triggering, was employed. Although extensively used for over 45 years (Seed and Idriss, 1971), liquefaction remains sudden and catastrophic, making improvements critical. In this study, the Cyclic Resistance Ratio (CRR), which represents the soil's resistance to

liquefaction failure, was modified. While previous research has primarily focused on modifying CRR using only ((N1)60CS), very few studies have considered all soil properties in CRR formulations. Here, a new CRR equation was developed using all relevant soil properties and the corrected SPT value ((N1)60CS). Unlike previous methods that relied on Excel curve fitting, this study employed a more advanced methodology—genetic algorithms (GA)—to modify the CRR equation and explore the impact of various variables.

The Gene Expo 5 (2023) software was used for analysis. A dataset of 496 records, comprising five independent variables (Zm, FC, D50, (N1)60CS) and one target variable (CRR), was split into different training sets (50%, 60%, 70%, 80%, and 90%) to optimize the genetic algorithm process. Iterations were performed to identify the best chromosomal crossovers and mutations, leading to the creation of an optimal genetic tree with coefficients and the most influential variables. From this tree, a new CRR equation was derived. This equation forms the basis for the probabilistic analysis and machine learning models discussed in Chapters 5 and 6.

4.3 Data collection

The ongoing investigation used a dataset including measurements obtained from the Standard Penetration Test (SPT). The collection contained post-liquefaction case histories from the Tohnankai earthquake in 1944 to the Chi Chi earthquake in 1999 in Taiwan. The study dataset consisted of 286 liquefied data and 210 non-liquefied data. Furthermore, to validate the models, a total of 30 borehole data obtained from boreholes situated in the Faridabad, National Capital region (NCR) of Delhi. The Faridabad falls Seismic Zone IV, creating moderate damage risk from earthquakes (BIS, 2002). An earthquake hazard map for Haryana state is prepared by Building Materials & Technology Promotion Council (BMTPC, 2007) and printed in Vulnerability Atlas of India (First Revision) is shown in Figure 4.2. The region remains susceptible to earthquakes due to the following faults (Puri and Jain, 2015). In the recent past, no major earthquakes have hit Haryana but shocks are felt whenever an earthquake occurs in areas of Himalayan Thrust System. A longer time ago, a MAG-6.8 earthquake struck on Oct 20, 1991 02:53, 299 kilometers (186 mi) north-east of Faridabad. It is the strongest earthquake near Faridabad in the past 124 years (Data goes back to January 1st, 1900).

The borehole data are collected by using standard penetration test (SPT), a commonly used process for assessing soil qualities at a given location. The standard penetration test (SPT) test consists of 63.5-kilogram hammer is dropped freely from a height of 0.76 metres to drive a split spoon sampler. The sampler has a length of 650 millimetres, an internal diameter of 35 millimetres, and an external diameter of 50 millimetres. Subsequently, the sampler is inserted into the pre-measured soil. The sampler is implanted to a depth of 450 millimetres. The N – SPT value is the parameter being considered in this test precisely determined as the number of impacts needed for the sampler to reach a depth of 300 mm from the surface. A geotechnical examination has been conducted at the area in accordance with the specifications outlined in the IS code. Consequently, samples were acquired throughout the whole process of collecting samples and doing subsequent laboratory testing. Stringent techniques and meticulous attention to detail were consistently used. The model bore hole data and the model data for the study are presented in Table 4.1 and Table 4.2, respectively.

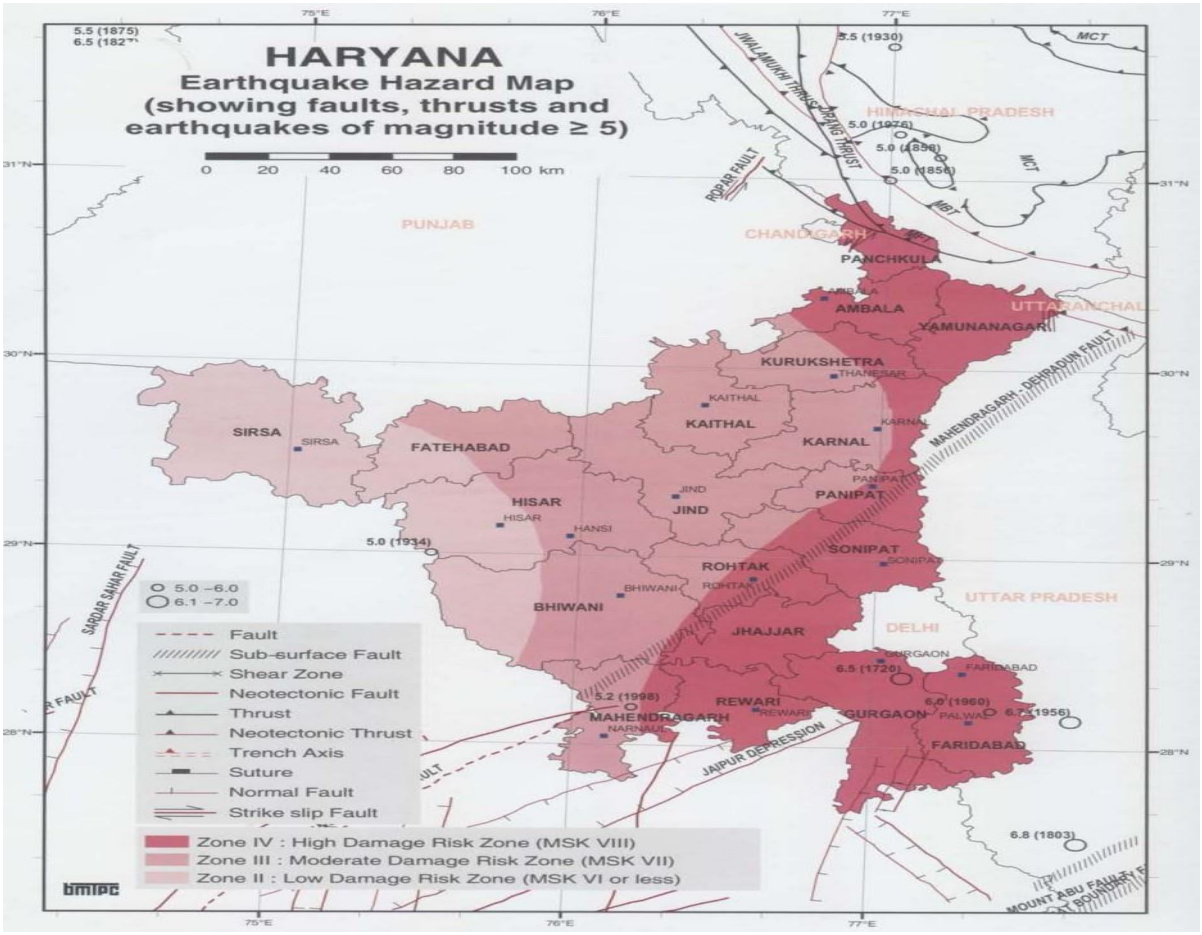

Figure 4.2 Earthquake hazard map of Haryana

Figure 4.2 (a) SPT field set up and (b) Split spoon sample

Table 4.1 Sample bore hole data

Avg Depth	WT	σ_v (kPa)	σ_v' (kPa)	N_m	$(N_1)_{60}$	C_B	C_E	C_N	C_R	C_S	FC	$(N_1)_{60cs}$	$\Delta(N_1)_{60cs}$	γ_{total}	γ'_{total}
2.3	1.2	43	32	4	6.1	1	1.1	1.7	0.8	1	69	11.7	5	19.1	18.5
3	1.2	57	39	6	9.2	1	1.1	1.6	0.9	1	33	14.6	2	19.1	18.5
3.4	1.2	63	42	3	4.6	1	1.1	1.6	0.9	1	33	10.1	1	19.1	18.5
3.7	1.2	69	45	6	8.6	1	1.1	1.5	0.9	1	33	14.1	2	19.1	18.5
3.8	1.2	72	46	13	17.4	1	1.1	1.4	0.9	1	20	21.9	5	19.1	18.5
4.3	1.2	81	51	11	14.4	1	1.1	1.4	0.9	1	20	18.9	2	19.1	18.5
4.6	1.2	87	54	10	14.3	1	1.1	1.3	1	1	20	18.8	5	19.1	18.5
4.9	1.2	92	56	4	5.8	1	1.1	1.4	1	1	33	11.3	2	19.1	18.5
5.2	1.2	98	59	4	5.7	1	1.1	1.3	1	1	33	11.2	1	19.1	18.5
5.3	1.2	101	61	6	8.3	1	1.1	1.3	1	1	33	13.8	5	19.1	18.5
5.5	1.2	104	62	10	13.4	1	1.1	1.3	1	1	33	18.9	2	19.1	18.5
6.1	1.2	116	68	9	11.7	1	1.1	1.2	1	1	33	17.1	1	19.1	18.5
7.1	1.2	133	76	14	16.9	1	1.1	1.1	1	1	33	22.4	2	19.1	18.5
7.6	1.2	87	54	7.1	10.3	1	1.1	1.4	1	1	30	15.7	5.4	19.1	18.5

Table 4.2 Sample trained and test data

Liquefaction	Magnitude (M)	Critical Depth (d)	Fine Content (%)	D50 (mm)	Water Table (m)	PGA (g)	r_d	(N1)60cs	CSR
Yes	7.3	6	61	0.075	2.3	0.428	0.942	8.47	0.451
Yes	7.3	4.2	24	0.2	2.7	0.789	0.959	3.58	0.378
Yes	7.3	9	42	0.1	2.3	0.789	0.886	6.38	0.714
Yes	7.3	2.4	41	0.095	2.3	0.789	0.972	8.71	0.514
Yes	7.3	5	22	0.065	2.2	0.428	0.952	3.67	0.379
Yes	7.3	4.2	62	0.1	1.8	0.211	0.959	4.05	0.417
Yes	7.3	7.7	16	0.22	3.8	0.165	0.915	10.19	0.132
Yes	7.3	8.1	16	0.19	3.1	0.165	0.907	8.48	0.136
Yes	7.3	5.7	16	0.17	2.8	0.165	0.945	8.82	0.139
Yes	7.3	8.1	19	0.17	2.8	0.165	0.907	10.71	0.148
Yes	7.3	3.7	11	0.19	2.3	0.165	0.962	11.57	0.128
Yes	7.3	10	45	0.08	3	0.165	0.85	7.25	0.145
Yes	7.3	7.7	18	0.17	3	0.165	0.915	6.72	0.142
No	7.3	5	14	0.2	0.6	0.124	0.952	23.86	0.137
No	7.3	10	15	0.22	0.6	0.124	0.85	21.98	0.128
No	7.3	9	12	0.2	0.6	0.124	0.886	21.09	0.133
No	7.3	5	14	0.2	0.6	0.124	0.952	18.68	0.138
No	7.3	6	19	0.19	0.6	0.124	0.942	21.97	0.138
No	7.3	10	16	0.17	1.3	0.124	0.85	20.42	0.122
No	7.3	18	22	0.104	2.7	0.165	0.73	9.34	0.142
No	7.3	6	8	0.2	2.7	0.165	0.942	12.07	0.142
No	7.3	16	18	0.14	2.7	0.165	0.76	12.08	0.145
No	7.3	18	32	0.1	2.7	0.165	0.73	10.77	0.142
No	7.3	16	18	0.14	2.7	0.165	0.76	9.06	0.145
No	7.3	4	43	0.09	2.7	0.165	0.96	7.46	0.124
No	7.3	12	8	0.201	2.7	0.165	0.82	10.2	0.149

The sample bore hole data contains depth spans from 2.3 to 7.3m and has a water table depth of 1.2 m, registered SPT no at different depths, and all adjustments are computed according to standard protocols supplied by previous studies. After calculating all variables, 'the corrected blow count (N1)60cs, fines content (FC), mean grain size (D50), peak horizontal ground surface acceleration (amax), magnitude of earthquake (M), shear stress reduction factor (rd), water table depth (WT), critical depth (d), and CSR' were selected for further investigation.

During the ongoing inquiry, this dataset included post-liquefaction case histories ranging from the Tohnankai earthquake of 1944 to the Chi Chi earthquake in Taiwan in 1999. The study dataset consisted of 286 cases of liquefaction and 210 cases of non-liquefaction. In addition, thirty borehole data points were acquired from the Faridabad area, which is part of the National Capital area (NCR) of Delhi, to validate the models. In the development of liquefaction prediction model, carefully selected a range of variables to comprehensively assess the susceptibility of soils to liquefaction under seismic loading conditions. The magnitude of the earthquake (M) and peak horizontal ground surface acceleration (PGA) are fundamental factors influencing the intensity of ground shaking, directly impacting liquefaction potential. Critical depth (d) within the soil profile plays a pivotal role in understanding the depth at which liquefaction is likely to occur. Additionally, variables such as fines content of the soil (FC), D50 representing median particle size, and corrected SPT No. $(N1)_{60cs}$ provide insights into soil composition and resistance, crucial for evaluating liquefaction susceptibility. Groundwater table depth (m) influences soil saturation levels, while the stress reduction coefficient (rd) and cyclic stress ratio (CSR) account for stress changes and cyclic loading during earthquakes, respectively. These variables collectively contribute to a holistic understanding of liquefaction potential, ensuring the robustness and accuracy of proposed prediction model for practical applications in earthquake engineering and hazard mitigation efforts.

The table 4.2 in the research data includes information on soil and seismic parameters such as $(N1)_{60cs}$, fines content (FC), mean grain size (D_{50}), peak horizontal ground surface acceleration (PGA), magnitude of earthquake (M), stress reduction coefficient (r_d) and Cyclic Stress Ratio ($CSR_{7.5}$). The parameters are obtained from the SPT measurements carried out at several worldwide sites, together with field performance observations (LI). The soil under these conditions may consist of sand, silty sand, sandy silt, and clayey silt. The collection includes SPT readings ranging from 1.3 meters to 20.3 meters in depth. The water table depth varies between 0 and 15.30 meters. The range of values for $(N1)_{60cs}$ is 0.93 to 35.22. The fines content (FC) varies between 0% and 92%. The PGA value varies between 0.052 and 1, the $CSR_{7.5}$ value

goes from 0.041 to 0.822, the earthquake magnitude is ranging from 5.90 to 8.30 and the stress reduction coefficient (r_d) is ranges from 0.69 to 0.99. A random sample of the whole data is picked for training and testing the resulting model.

4.4 Results and discussion

This section includes data visualisation and a deterministic model that relies on the liquefaction SPT database. The data visualisation was conducted to determine the level of interdependence and independence among the variables, as well as to assess the entropy of the variables. In addition, the CRR model, created in collaboration with the widely used CSR model by Idriss and Boulanger (2004, 2008), was used to assess the liquefaction potential in terms of Fs. The results are shown in the subsequent order.

4.4.1 Data visualization

The use of data visualization facilitates the comprehension of data trends, the interrelationships and distinctions among several variables employed in the study, and the level of disorder or randomness within the data. This understanding aids in determining appropriate methodologies for data analysis.

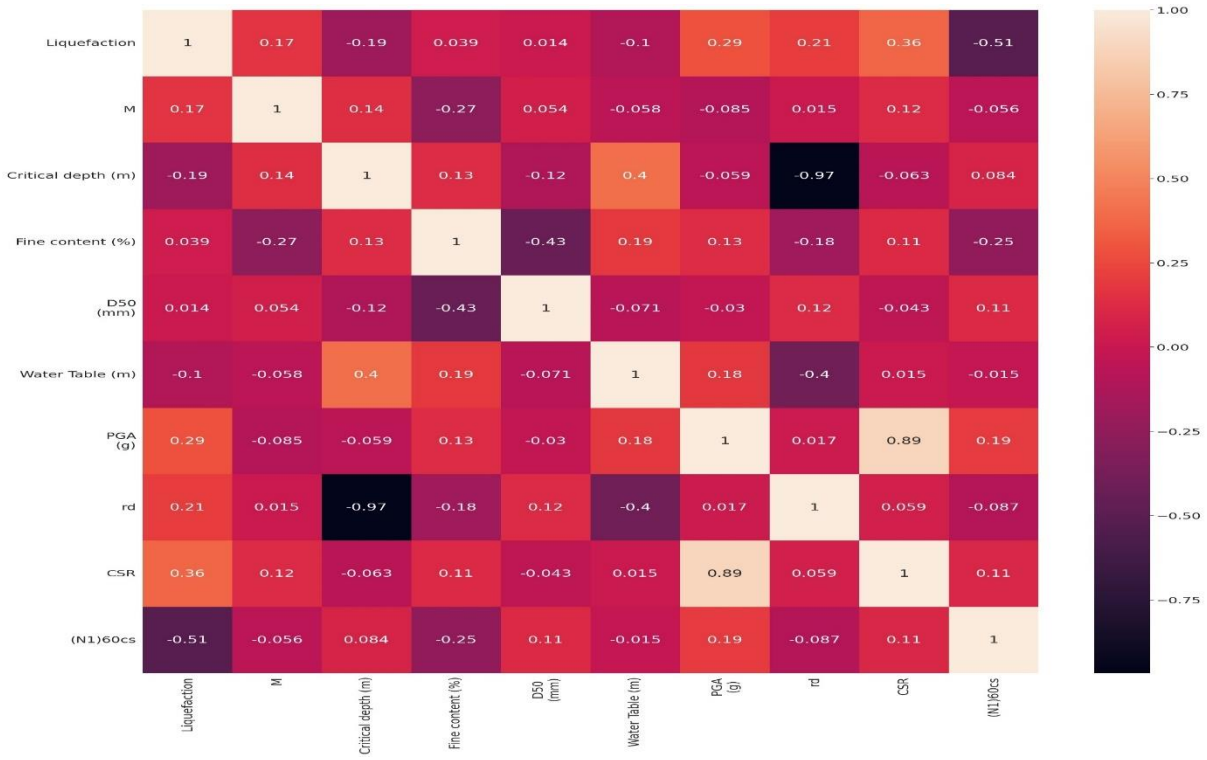

Figure 4.3 Pearson corelation matrix of variables

A heat map of the Spearman's rank correlation coefficient matrix for the input variables is shown in Figure 4.3, with the corresponding correlation coefficients and diagonal element shown the target variable. It can be seen that parameters (Generally speaking, |R|= 0 implies an uncorrelated relationship; |R|< 0.2 implies a very weak correlation; 0.2 <|R|< 0.4 stands for a weak correlation; 0.4 <|R|< 0.6 stands for a moderate correlation; 0.6 <|R|<0.8 implies a strong correlation; 0.8 <|R|<1 implies a very strong correlation; |R|= 1 implies fully correlated.)

The formula for spearman's rank correlation coefficient is follows:

$$R = \frac{COV(\text{rank}\,(X)\text{rank}\,(Y))}{\sigma_{\text{rank}\,(X)}\sigma_{\text{rank}\,(Y)}} = \frac{\Sigma_i(R_X\,(i)-\overline{R_X})(R_Y\,(i)-\overline{R_Y})}{\sqrt{\Sigma_i(R_X\,(i)-\overline{R_X})^2}\sqrt{\Sigma_i(R_Y\,(i)-\overline{R_Y})^2}} \quad (4.1)$$

Where: $\text{rank}\,(X)\text{rank}\,(Y)$ are the ranks of variables X, Y, respectively COV denotes covariance and $\sigma_{\text{rank}\,(X)}\sigma_{\text{rank}\,(Y)}$ are the standard deviations of $\text{rank}\,(X)\text{rank}\,(Y)$, R_X , R_Y represents the average ranks for $\text{rank}\,(X)\text{rank}\,(Y)$, respectively.

Multicollinearity arises when predictor variables exhibit either positive or negative correlation. Positive correlation, as observed between variables X and Y, implies that they move in the same direction; when X increases, Y tends to increase. In regression, this strong positive relationship can lead to multicollinearity, hindering the model's ability to distinguish individual effects. Similarly, negative correlation, such as between variables A and B, involves opposite movements; as A increases, B tends to decrease. High negative correlations in regression may also result in multicollinearity issues, making it challenging to differentiate the impact of A and B on the outcome variable and potentially leading to unreliable estimates.

Figure 4.3 is a data visualisation that uses heat maps to exhibit the Pearson correlation matrix. The variables are organised in a matrix format, with the target variable positioned on the diagonal. This design enables the investigation of the interrelationship between the variables and the desired variable. The variable that exhibits a stronger correlation with the target variable is considered to be a more significant determinant of the target variable. Figure 4.2 demonstrates that none of the factors exhibit a more pronounced correlation with the variables under investigation. To comprehend the intricacies of liquefaction, it is crucial to acknowledge that all elements have equal average importance in determining the aim variable. There is no one factor that has more significance in this study. Due to the interdependence of two distinct variables, the trends associated with each of them may be compared. The level of correlation between the two variables plays a crucial role in determining the extent to which this resemblance exists. To ensure accuracy and minimise the possibility of underfitting during

model training, it is necessary to omit one variable to avoid this problem. The data shown in Figure 4.3 The variables Cyclic Stress Ratio (CSR) and Peak Ground Acceleration (PGA) exhibit a substantial positive correlation with a value of 0.89. This high correlation raises concerns about multicollinearity, suggesting the need to eliminate one of the variables. However, both variables are indispensable in liquefaction studies, necessitating their retention despite the correlation issue. Similarly, the Reduction Factor (rd) and Critical Depth (d) display a notable negative correlation of -0.97, which may also indicate multicollinearity. Despite this challenge, both variables remain crucial in liquefaction studies, and therefore, the decision is to retain both variables while acknowledging the potential impact of their high correlation.

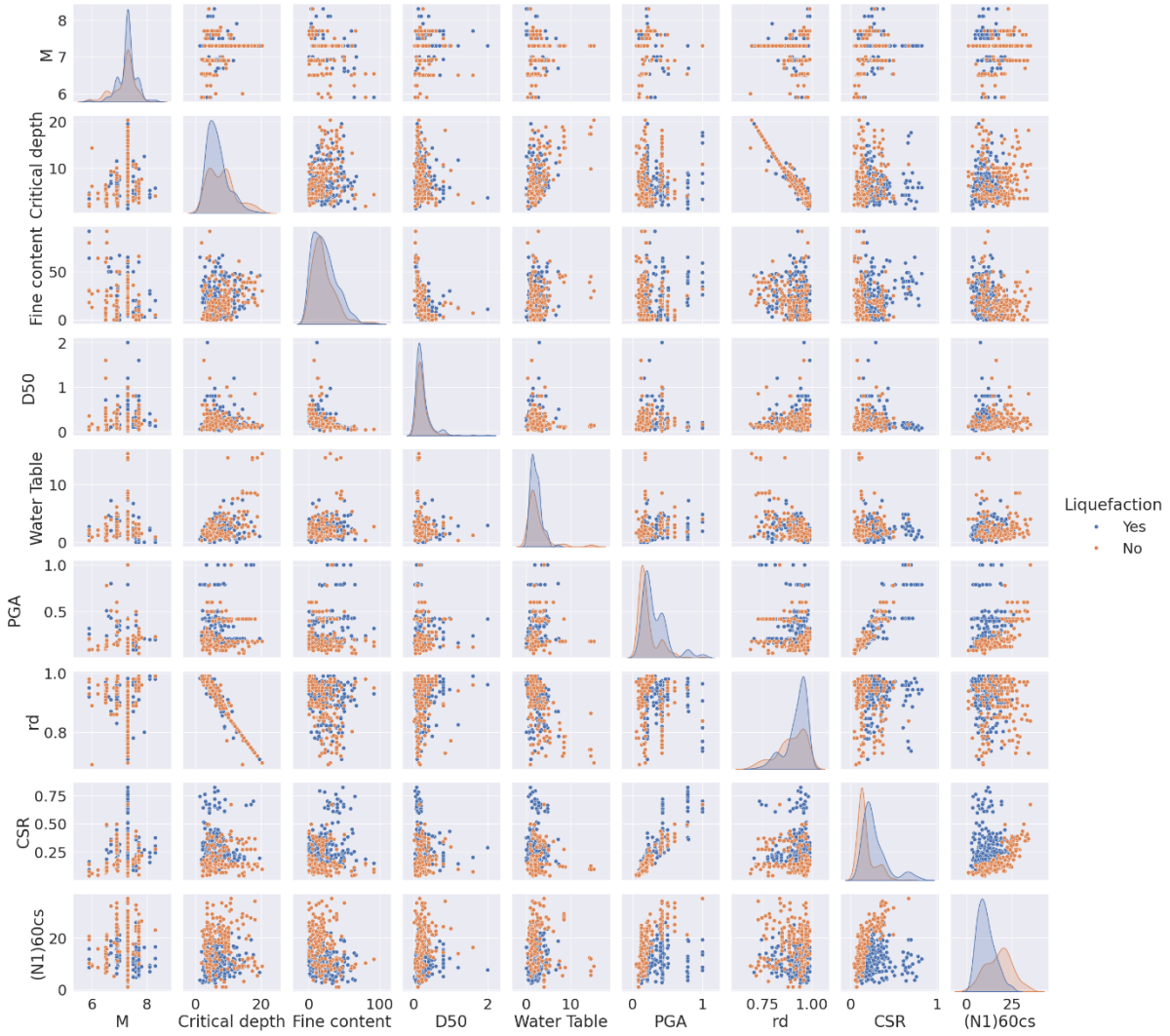

Figure 4.4 Pair plot to determine entropy of variables

In machine learning, entropy is a measure of uncertainty or impurity in a dataset, particularly in classification tasks. It quantifies how mixed the classes are in a given set of data. If the data

is perfectly mixed (e.g., half the data is of one class, and half is of another), the entropy is high, indicating greater disorder. Conversely, if the data is mostly of one class, the entropy is low, signifying lower uncertainty. Entropy is used in decision trees to determine which feature best splits the data, aiming to reduce uncertainty and create more homogeneous groups. Pair graphs are often used to assess the entropy of data. A lower entropy number indicates a substantial level of segregation or classification within the data, but a lower entropy value signifies a higher degree of information transmission. This entropy metric may provide a deeper comprehension of the selection of models, taking into account their categorization complexity and information transmission capabilities. Figure 4.4 depicts the contrast between data that has been liquefied and data that has not been liquefied, with respect to changes in the values of two variables. The picture clearly shows that there is no clear differentiation between the two types of data, suggesting a high level of complexity. Therefore, basic models are inadequate for analysing such intricate data. When faced with such a high degree of complexity, it is advisable to use more advanced models, such as genetic programming and advanced deep learning models, to get beneficial results.

4.5 Genetic programming (GP) model for cyclic resistance ratio (CRR)

The genetic programming (GP) technique is a computational approach used to design computer programmes that can effectively address intricate problems. Dr. Cândida Ferreira, doing her doctoral study at the University of Coimbra in Portugal, first introduced the notion in 1992. The fundamental ideas behind the genetic programming (GP) approach are natural selection and genetics. The iterative process of generating a set of computer codes via various mutation and selection techniques is the mechanism it utilises. The GP approach involves encoding each software as a series of symbols that may undergo various genetic processes, such as combining and modification. All of these operations may be performed on the sequence. The programmes that exhibit superior performance on a particular task are chosen for reproduction in subsequent generations via a process that encompasses numerous generations. This leads to an enhancement in the overall fitness of the programming for the next generation. The ability of GP to handle a large number of objectives concurrently makes it a very valuable tool in the area of optimisation. The GP has been extensively used across several domains, including data analysis, classification, and modelling, among other applications. The empirical evidence indicates that genetic programming (GP) outperforms alternative evolutionary computation techniques, such as genetic programming and evolutionary strategies, in certain problem

domains (Ferreira 2001). In addition, the GEP technique has been revised to include enhanced genetic operators to facilitate the handling of intricate data structures like trees and graphs (Otero et al. 2016). The ability to expand was facilitated by modifying the genetic operators.

The current work utilizes a modeling methodology in which the Cyclic Resistance Ratio (CRR) serves as the objective value. The model has five independent input variables, as elaborated upon in Chapter 3. Utilizing the four fundamental arithmetic operators (+, −, ×, and /), the model was constructed using GeneXproTools 5.0 (2023). The high-quality datasets were randomly allocated to two separate time periods for the purposes of training and testing. The models developed throughout the investigation are shown in Table 4.3. These models vary in their relative proportions of training and testing datasets, program size, and the number of generations used throughout the modeling procedure. The fitness function used to assess model performance was the root-mean-squared error (RMSE) denoted as Ei2. The fitness score (fi) was computed by application of an equation obtained from the expression tree, which considered the cumulative mistakes in relation to the desired values. The genetic components were linked by a straightforward additive technique. The performance of the model was assessed using both ordered and scatter plots, which examined the projected CRR values in comparison to the actual target values. Figures 4.6 and 4.7 demonstrate a robust correspondence between the projected and observed values, with both exhibiting comparable patterns, however some variations are seen at higher CRR levels. The main performance indicators of the model are a R^2 value of 0.955 and a correlation coefficient of 0.977. These values suggest that the model accounts for 95.5% of the variability in the data, underscoring its robust prediction capability. The scatter figure, constructed using the linear regression equation $y=1.063x-0.0008y = 1.063x - 0.0008y=1.063x-0.0008$, provides further evidence of the model's precision, indicating a high level of concordance between the anticipated and actual values. Notwithstanding some underestimations at larger CRR ranges, the findings emphasize the resilience of the genetic programming (GP) model in predicting CRR, indicating its dependability for forecasting liquefaction. The expression tree for the GP model 3 is visualized in Figure 4.8. In this model, the input parameters are represented by the symbols d0 to d5, and the constant value for gene one is denoted by G1c8. To facilitate understanding, a mathematical equation derived from the expression tree is provided for Model 3, establishing the relationship between the input variables and the output (CRR).

This research analysed five independent factors and one target variable of equation 4.2 was derived using just two independent variables, namely $(N1)60cs$ and $D50$. This was conducted

to ascertain the relationship between CRR and input components, which was derived from the Pearson correlation matrix of variables (also referred to as Figure 4.5).

The algebraic equation for CRR has been derived after simplification:

$$\mathrm{CRR} = \tanh\left(\tanh\left(\frac{1}{7.19+6.02(\mathrm{N_1})_{60\mathrm{cs}}-\min(3.471,(\mathrm{N_1})_{60\mathrm{cs}}}\right)\right)+\frac{((\mathrm{N_1})_{60\mathrm{cs}})^{\frac{1}{3}}}{2}+$$

$$\tan^{-1}\left(\frac{\max(\mathrm{D_{50}},6.364)\times 3.89(\mathrm{N_1})_{60\mathrm{cs}}}{4}\right)-1.8221 \qquad (4.2)$$

Table 4.3 Genetic programming (GP) models

Model	Training data Coefficient	Testing data Coefficient	No. of chromosomes	Head size	No. of genes	Gene size	Program size	Literals	No. of generations
GP1	0.6	0.4	40	15	8	39	107	42	356684
GP2	0.5	0.5	40	15	8	39	98	39	270413
GP3	0.7	0.3	40	15	8	39	106	40	163511
GP4	0.8	0.2	40	15	8	39	106	41	260010
GP5	0.9	0.1	40	15	8	39	103	38	275015

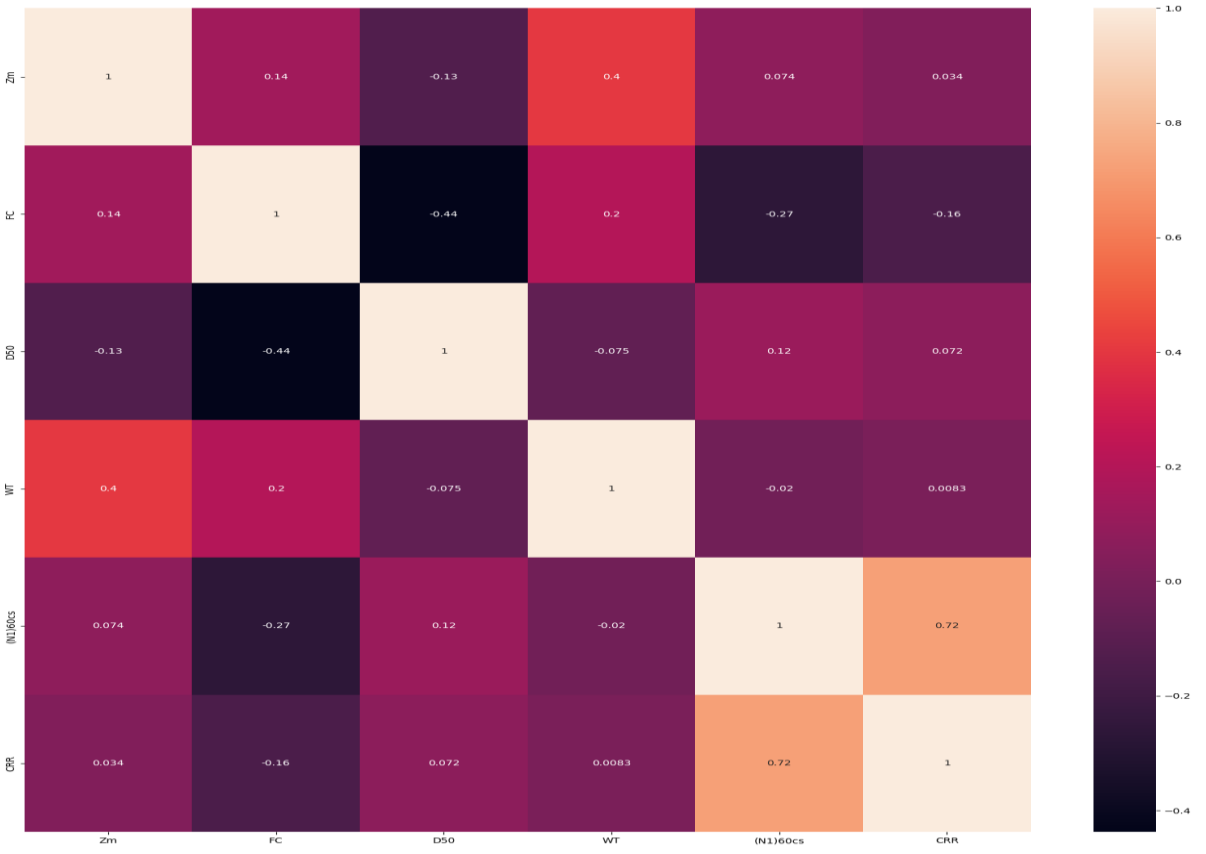

Figure 4.5 Pearson corelation matrix of variables used for GP

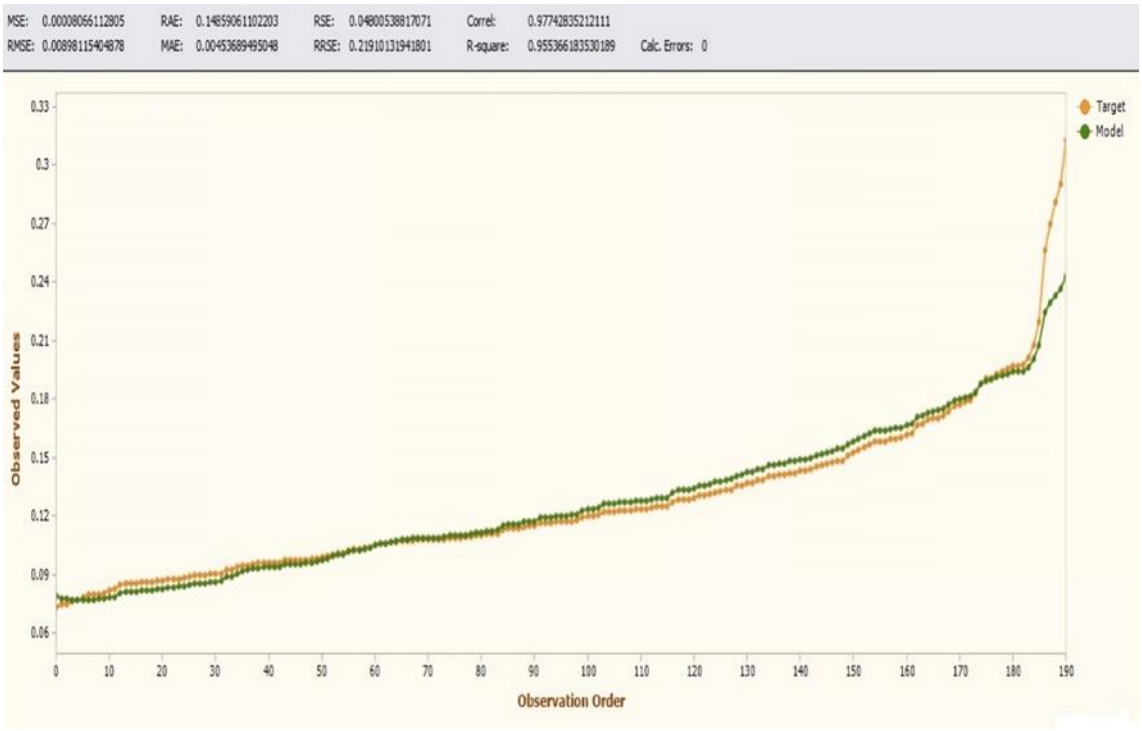

Figure 4.6 Relationship between the maximum and average fitness values as the number of generations increases

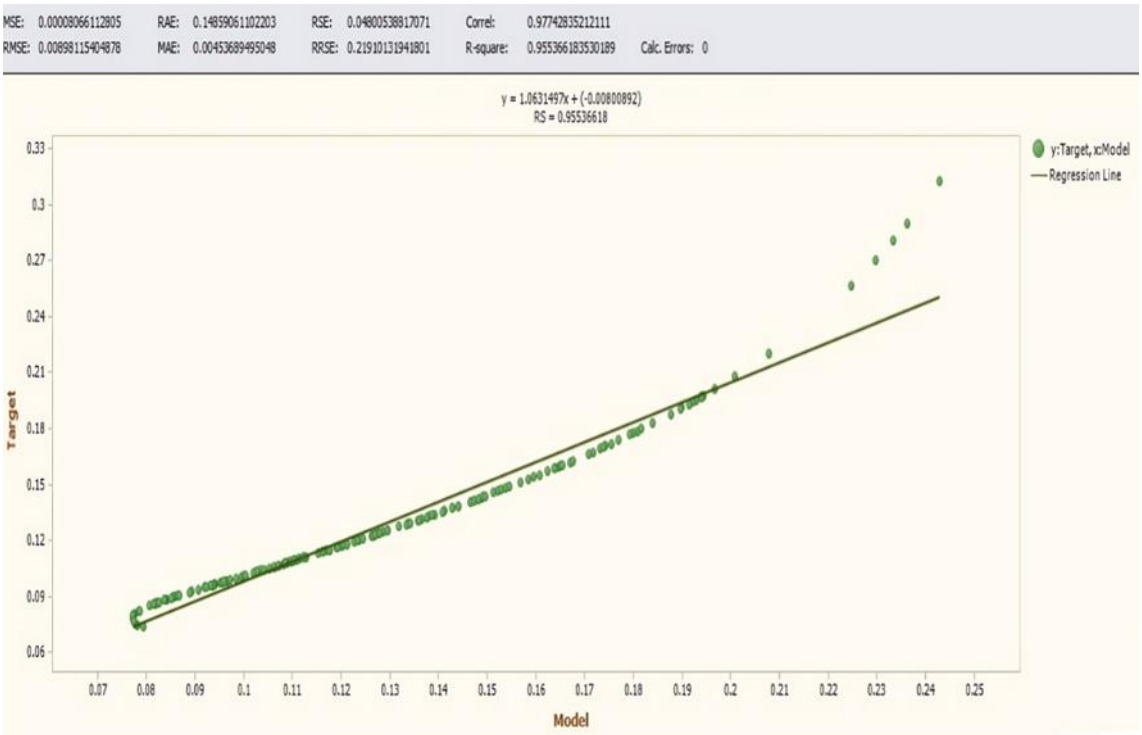

Figure 4.7 R^2 graph of target and model values

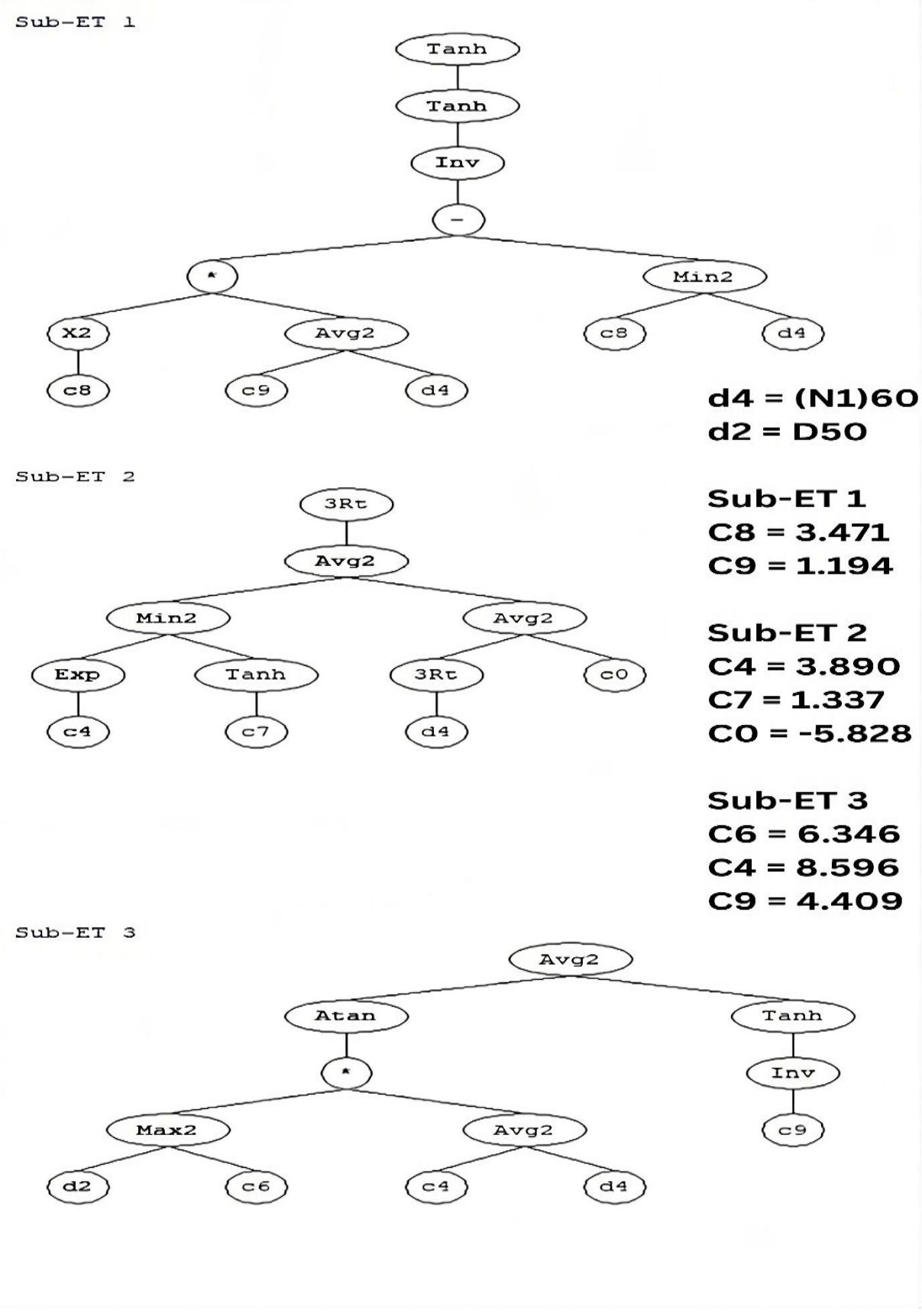

Figure 4.8 Expression tree for CRR

4.6 Conclusion

- The dataset used in this study consisted of a compilation of post-liquefaction case histories, ranging from the 1944 Tohnankai earthquake to the 1999 Chi Chi earthquake in Taiwan. The dataset included 286 instances of liquefaction and 210 instances of non-liquefaction. A collection of 30 borehole data obtained from the Standard Penetration Test (SPT) was gathered inside the Faridabad area, which is located in the National Capital area (NCR) of Delhi, India. The objective of this data collection was to validate the precision and dependability of the used models.
- Data visualisation is essential for improving comprehension of data patterns, relationships and disparities across several study variables, and the level of disorder or unpredictability in the data. The variables Cyclic Stress Ratio (CSR) and Peak Ground Acceleration (PGA) exhibit a substantial positive correlation with a value of 0.89. This high correlation raises concerns about multicollinearity, suggesting the need to eliminate one of the variables. However, both variables are indispensable in liquefaction studies, necessitating their retention despite the correlation issue. Similarly, the Reduction Factor (rd) and Critical Depth (d) display a notable negative correlation of -0.97, which may also indicate multicollinearity. Despite this challenge, both variables remain crucial in liquefaction studies, and therefore, the decision is to retain both variables while acknowledging the potential impact of their high correlation.
- The analysis of entropy in soil liquefaction studies reveals a significant overlap between the two data categories, indicating a high degree of complexity and uncertainty in the variables involved. This suggests that basic models may be inadequate for accurately analyzing such intricate datasets. To address this challenge, it is recommended to employ more advanced approaches, such as Genetic Programming (GP) and cutting-edge deep learning models. These sophisticated techniques have the potential to yield more accurate predictions and improved results in liquefaction analysis, particularly by better capturing the non-linear relationships within the data.
- Genetic Programming (GP) was employed to conduct experiments where multiple models were constructed by varying the number of training and testing datasets, program dimensions, and the number of generations. The fitness function used in this process was the Root Mean Square Error (RMSE). The equation derived from the expression tree of GP Model 3 was transformed into a mathematical formula, enhancing the accuracy of the fitness measure. This transformation led to a stronger correlation

between the input variables, such as soil properties and seismic parameters, and the output variables, resulting in more reliable predictions of soil liquefaction potential.

CHAPTER 5

A PROBABILISTIC APPROACH TO EVALUATING LIQUEFACTION POTENTIAL

5.1 Introduction

The processes described in the preceding chapter are inherently deterministic. These methods include evaluating the soil's susceptibility to liquefaction by determining the factor of safety against liquefaction (Fs). However, because to the uncertainty related to the parameters of the model, having Fs values larger than one does not always indicate the lack of liquefaction. Conversely, it should be noted that a value of Fs less than one does not automatically indicate liquefaction, as previously explained in the first chapter. The deterministic technique reveals that the boundary curve (surface) that distinguishes instances of liquefaction from non-liquefaction situations is inclined towards the conservative side. This bias arises from the inclusion of the bulk of the liquefied instances inside the border curve, as previously discussed in the preceding chapter. Conversely, it is not possible to quantify the level of conservatism. A probabilistic evaluation of liquefaction potential has been conducted to address the issues stated in the deterministic approach. This assessment quantifies the liquefaction potential by measuring the probability of liquefaction (P_L).

Consequently, some studies have attempted to measure the uncertain level of caution that is linked to the limit state function. In addition, they have tried to assess the likelihood of liquefaction (P_L) by using probabilistic techniques. The subject matter has been thoroughly examined in Chapter-II. The present study aims to develop a probability design chart by using a mapping function derived from the post-liquefaction SPT database (Hwang and Yang 2001). To build a relationship between Fs and P_L, the mapping function is generated using the Bayesian theory of conditional probability. This chapter utilises the previously introduced GP −based deterministic model to assess the limit state function for calculating the cyclic resistance ratio (CRR) of soil. This calculation is crucial for estimating the factor of safety (Fs) against liquefaction. Utilising an autonomous liquefaction SPT dataset.

5.2 Methodology and simulation setup

The deterministic approach, which quantifies the liquefaction potential of soil using the factor of safety (F_S), is commonly favored by geotechnical specialists due to its simplicity. However, parametric and model inaccuracies may result in situations where $F_S > 1$ does not necessarily indicate the absence of soil liquefaction, nor does it guarantee that the risk is eliminated. Similarly, an $F_S < 1$ does not always lead to liquefaction. There exists a grey area in the factor of safety that cannot be adequately explained by the deterministic method (Juang et al., 2000b). To address this uncertainty, a probabilistic liquefaction analysis has been conducted.

Using the Cyclic Stress Ratio (CSR) and the newly developed Cyclic Resistance Ratio (CRR), the factor of safety was calculated for each instance. Following this, a probability density function (PDF) was determined for each factor of safety. Various distribution methods were explored, and the best-fit distribution was selected. The distribution values for liquefied and non-liquefied instances were then applied to a Bayesian mapping function. For each instance, the Bayesian mapping function values were analyzed, and a best-fit curve was derived, leading to the creation of a probabilistic equation for predicting liquefaction.

This new probability equation was then compared with existing probabilistic models, such as those proposed by Toprak et al. (1999), Juang et al. (2002), and Idriss & Boulanger (2006). The comparison was performed using Performance Fitness and Error Metrics (PFEMs) designed for binary classification. In the context of liquefaction prediction, binary classification involves both liquefied and non-liquefied cases, yielding four possible outcomes: true negatives (TN), true positives (TP), false positives (FP), and false negatives (FN). A false positive occurs when liquefaction is predicted incorrectly, and a false negative when liquefaction is missed. The results from PFEMs were used to rank the models in terms of prediction accuracy.

Finally, the Gini index (GI) was utilized to assess the relative importance of independent variables in predicting liquefaction. The Gini index was calculated for each independent variable, and their significance in forecasting the likelihood of liquefaction in soil deposits was evaluated. A higher Gini index value indicates a stronger influence of the corresponding variable on the prediction of liquefaction.

5.3 Development of a probabilistic model based on SPT

The deterministic approach using the Standard Penetration Test (SPT), as explained in the preceding section, is adjusted via the use of Bayesian theory of conditional probability and the examination of past instances of post-liquefaction SPT data. The calibration procedure leads to the creation of a probabilistic model called the Bayesian mapping function. This model establishes a correlation between the factor of safety (F_s) and the likelihood of liquefaction (P_L).

5.3.1 Implementation of bayesian mapping function

Based on the research conducted by Juang et al. (1999b), the probability of a case in the database undergoing liquefaction may be estimated using Bayes' theorem of conditional probability, given that the Fs has been calculated.

$$P\left(L/F_s\right) = \left(\frac{P\left(F_s/L\right)P(L)}{P\left(F_s/L\right)P(L)+P\left(F_s/NL\right)P(NL)}\right) \tag{5.1}$$

The equation $P\left(L/F_s\right)$ represents the probability of liquefaction given a certain value of Fs. $P\left(F_s/L\right)$represents the probability of Fs assuming that liquefaction did occur. $P\left(F_s/NL\right)$ represents the probability of Fs assuming that liquefaction did not occur. P(L) represents the prior probability of liquefaction, and P(NL) represents the prior probability of non-liquefaction. $P\left(F_s/L\right)$and $P\left(F_s/NL\right)$ may be derived using equations (5.2a) and (5.2b) correspondingly.

$$P\left(F_s/L\right) = \int_{F_s}^{F_s+\Delta F_s} f_L(x)dx \tag{5.2a}$$

$$P\left(F_s/NL\right) = \int_{F_s}^{F_s+\Delta F_s} f_{NL}(x)dx \tag{5.2b}$$

$f_L(x)$ and $f_{NL}(x)$ represent the probability density functions of Fs for examples in the database where liquefaction occurred and where liquefaction did not occur, respectively. As the change in Fs approaches zero, Equation (5.1) may be rewritten as Equation (5.3).

$$\left(L/F_s\right) = \left(\frac{f_L(F_s)P(L)}{f_L(F_s)P(L)+f_{NL}(F_s)P(NL)}\right) \tag{5.3}$$

Given the established prior probabilities P(L) and P(NL), can be use Equation (5.3) to compute the probability of liquefaction for a certain value of Fs. Without knowing the values of P(L) and P(NL), to deduce that P(L) is likely to be equal to P(NL) based on the principle of maximum entropy (Juang et al. 1999b). Thus, if assume that the probability of L is equivalent to the probability of NL, may express Equation (5.3) as Equation (5.4).

$$P_L = \frac{f_L(F_s)}{f_L(F_s)+f_{NL}(F_s)} \tag{5.4}$$

where, $f_L(x)$ Fs and $f_{NL}(x)$ (Fs) represent the probability density functions (PDFs) of Fs for situations where liquefaction occurs and cases where liquefaction does not occur, respectively.

The Fs values, calculated using the SPT −based deterministic approach explained in the previous chapter, are computed for different cases in the Hwang and Yang (2001) database in this research. The examples are classified according to their observed field performance as either liquefaction (L) or non-liquefaction (NL). The Weibull probability density function is determined to provide the most optimal fitting curves for both the L and NL groups. Figures 5.1 to 5.4 depict this. The Weibull distribution best describes the safety factor of both groups, of scale parameter (λ) and shape parameter (k) values of 0.580 and 2.437, respectively. The probability density functions (PDF) of these Weibull distributions are seen in Figures 5.1 to 5.4 and may be expressed using Equation (5.5).

$$f(x;\lambda,k) = \frac{k}{\lambda}\left(\frac{x}{\lambda}\right)^{k-1} e^{-\left(\frac{x}{\lambda}\right)^{k}}, \qquad x \geq 0 \tag{5.5}$$

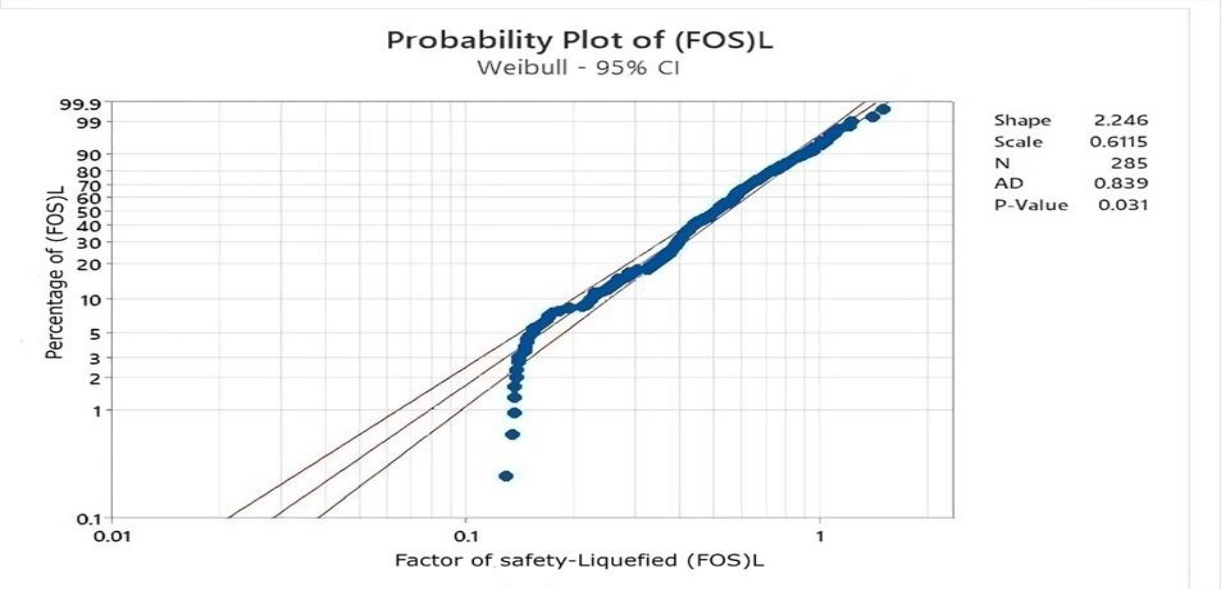

Figure 5.1 Percentage of probability of factor of safety liquefied data

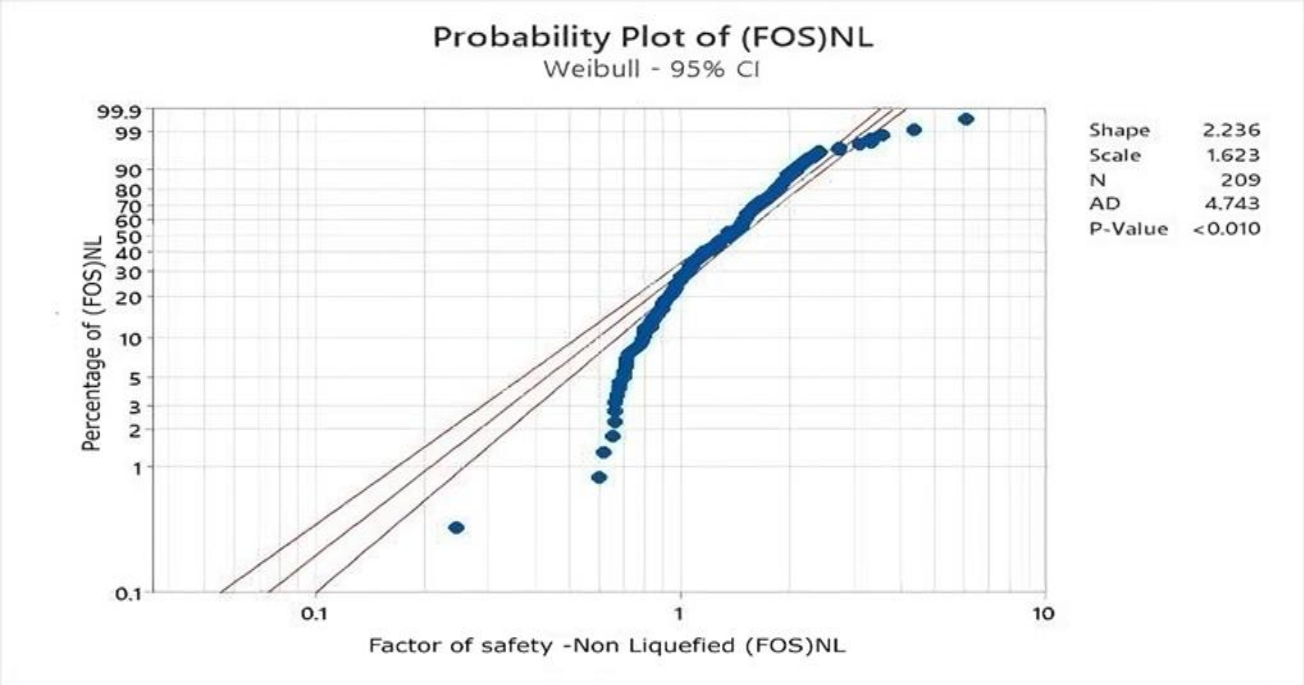

Figure 5.2 Percentage of probability of factor of safety non-liquefied data

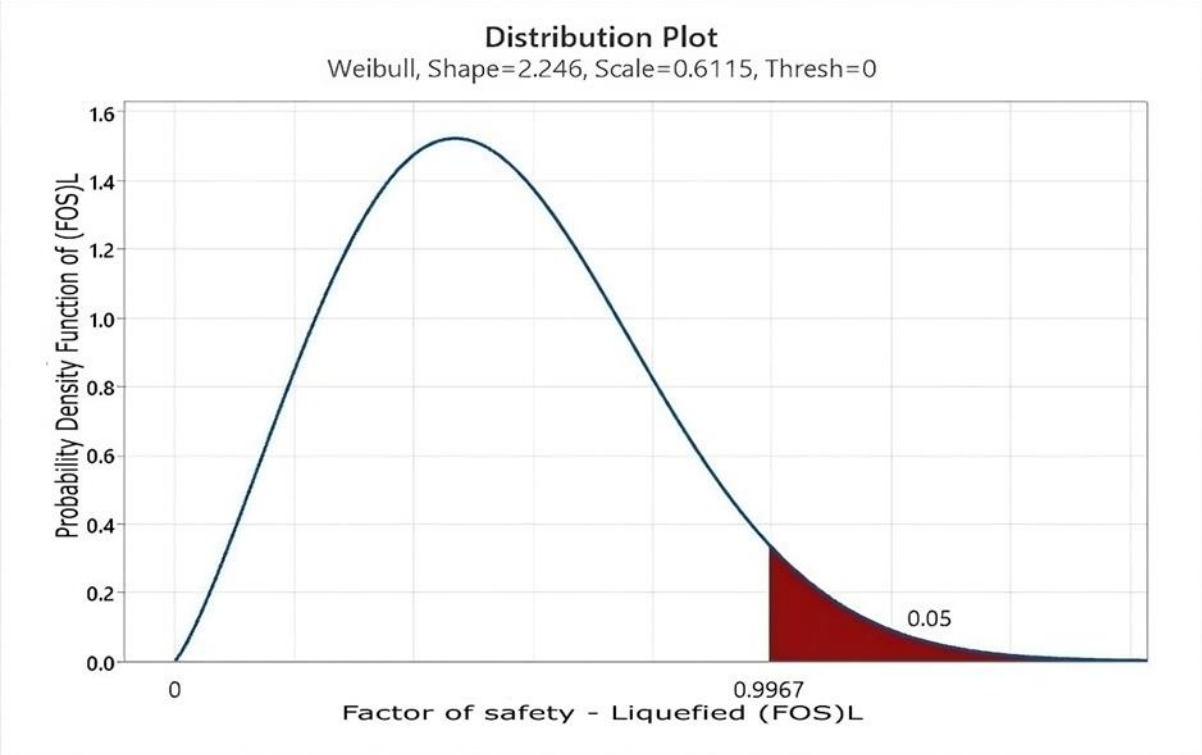

Figure 5.3 Weibull distribution of probability density function of liquefied data

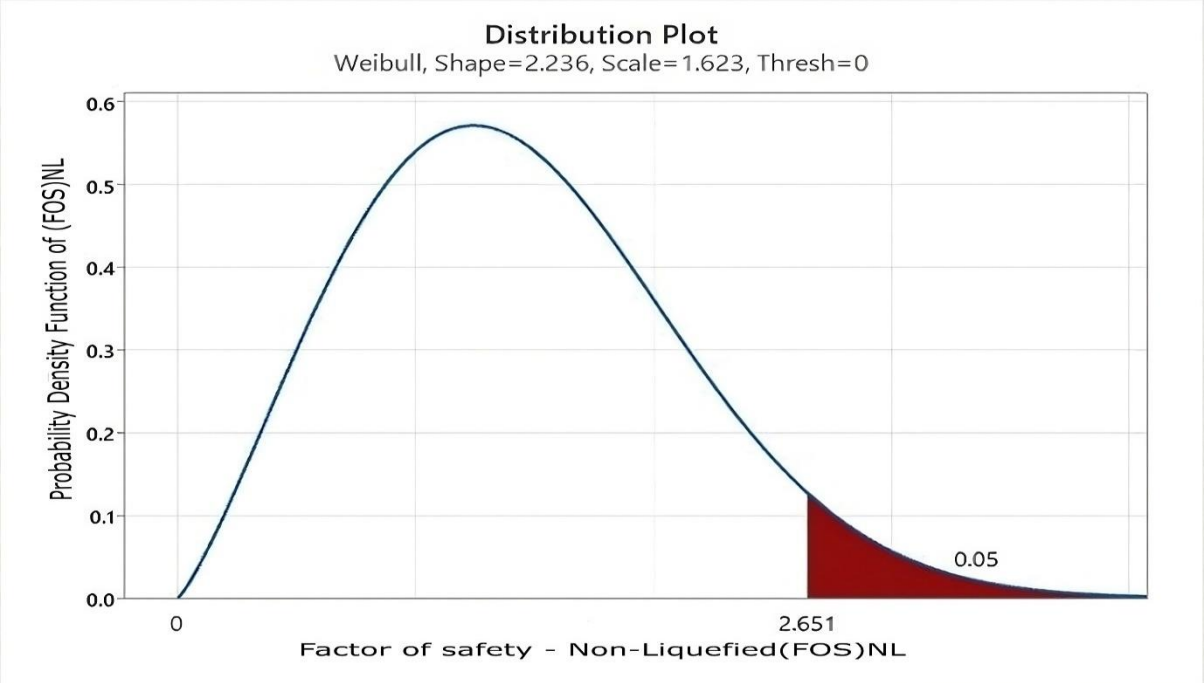

Figure 5.4 Weibull distribution of probability density function of non-liquefied data

5.4 Formulation of equation by bayesian mapping function

The probability of liquefaction (P_L) and probability of non-liquefaction (P_{NL}) for each case in the database is calculated using Equation (5.4), which depends on the probability density functions.

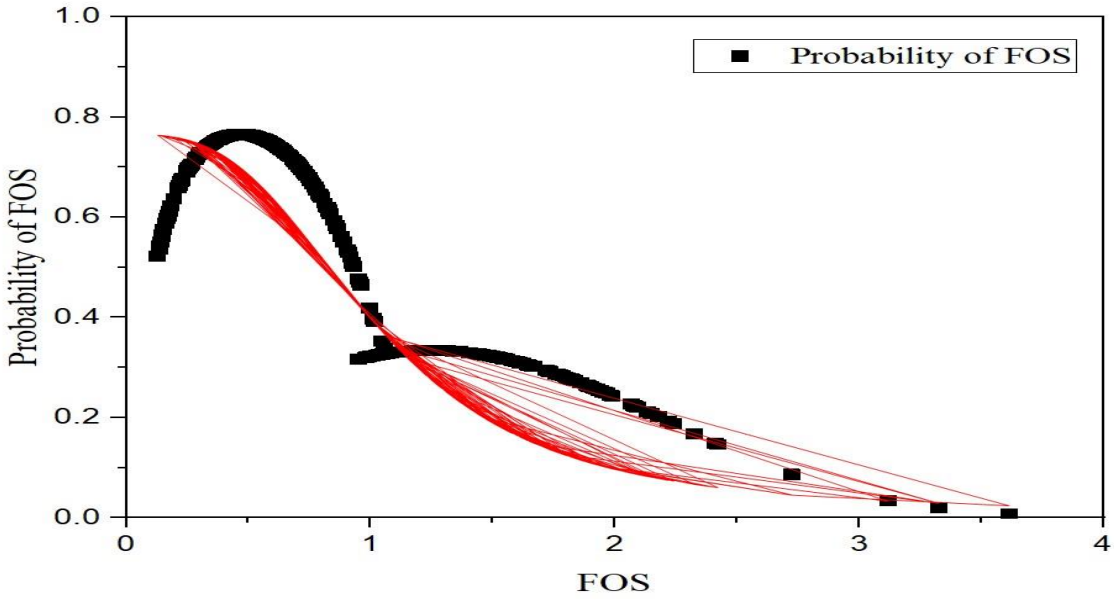

Figure 5.5 Curve fitting of probability of factor of safety

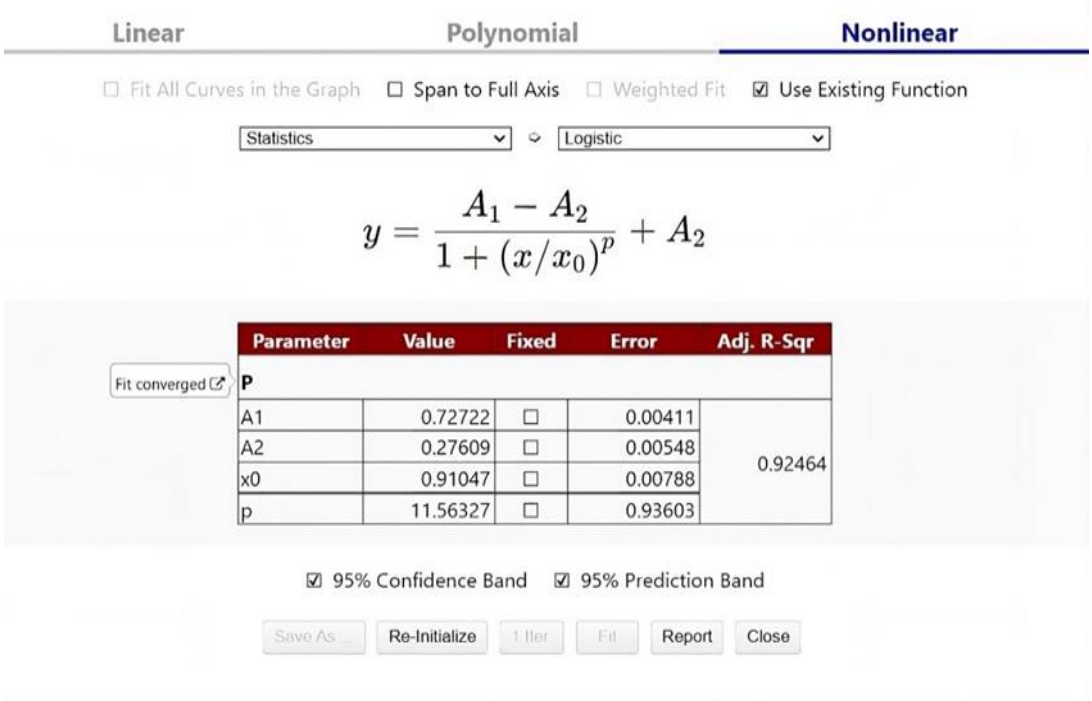

Figure 5.6 Curve fitting equation with constants and variables

The values of the factor of safety (Fs) and probability of liquefaction (P_L) and probability of non-liquefaction (P_{NL}) for each of the 496 samples in the database are shown in Figure 5.5. A mapping function is obtained by the use of curve-fitting methodologies. The equation was formulated using the logistic curve fitting methodology. The derived equation has a coefficient of determination (R^2) value of 0.93. The equation (5.6) formulation presents the coefficients and variables, as seen in Figure 5.6. The derived equation is compared to the equations proposed by Toprak et al. (1999), Juang et al. (2002), and Idriss & Boulanger (2006).

$$P = \frac{0.45113}{1+\left(\frac{FOS}{0.91049}\right)^{11.5632}} + 0.27609 \quad (5.6)$$

5.5 Comparison with existing methods using independent database

Regularly assessing the efficacy of a recently developed method in relation to existing methods is crucial. The present study examines the efficacy of the GP −based probabilistic approach in forecasting liquefied and non-liquefied scenarios, in comparison to the equations proposed by Toprak et al. (1999), Juang et al. (2002), and Idriss & Boulanger (2006), with respect to their success rate. There are 30 databases gathered in the NCR area utilizing SPT tests, and these databases are used to assess the efficacy of the model.

Liquefaction probability (P_L) is determined by calculating its value, where a P_L more than 0.5 indicates liquefied soil, while a P_L less than 0.5 indicates non-liquefied soil.

Table 5.1 Classification criteria for liquefied and non-liquefied

Criteria	Probability of Liquefaction	Liquefaction Classification	Non-Liquefaction Classification
A	$P_L > 0.85$	High Chances of Liquefaction	
B	$P_L > 0.65$	Intermediate Chances of Liquefaction	
C	$P_L > 0.5$	Low Chances of Liquefaction	
D	$P_L < 0.15$		High Chances of Non-Liquefaction
E	$P_L < 0.35$		Intermediate Chances of Non-Liquefaction
F	$P_L < 0.5$		Non-Low Chances of Liquefaction

5.6 Results and discussion

The effectiveness of the suggested techniques, based on real-world data, is assessed by calculating the probability of liquefaction using the three endorsed approaches. The present research assesses the accuracy of the suggested methods based on three criteria (A-C): High probability of liquefaction 0.85-1.0), Intermediate probability of liquefaction (0.65-1.0), and Low probability of liquefaction (0.65-1.0). The range is between 0.5 and 1.0. Criteria (D) is defined as having a high probability of non-liquefaction with a range of 0.15 to 0. Criteria (E) is defined as having an intermediate probability of non-liquefaction with a range of 0.35 to 0. Criteria (F) is defined as having a low probability of non-liquefaction with a range of 0.5 to 0. These criteria are applicable to cases when liquefaction does not occur. The categorization criteria are shown in Table 5.1. The findings are shown in Table 5.2, which categorises the soil

into liquefiable (Criteria A-C) and non-liquefiable (Criteria D-F) based on the accuracy of prediction achieved by each suggested method.

5.6.1 Probability categorization

Table 5.2 Classification results of different models

Criteria	Models							
	Proposed Model		Toprak et al. (1999)		Juang et al. (2002)		Idriss and Boulanger (2006)	
	Count of successful prediction	Rate (%)	Count of successful prediction	Rate (%)	Count of successful prediction	Rate (%)	Count of successful prediction	Rate (%)
Total observed liquefied (285)								
A (P_L > 0.85)	214	75	199	70	208	73	210	74
B (P_L > 0.65)	242	85	208	73	230	81	239	84
C (P_L > 0.5)	254	89	228	80	239	84	242	85
Total observed non-liquefied (211)								
D (P_L < 0.15)	127	60	65	31	105	50	91	43
E (P_L < 0.35)	137	65	89	42	120	57	108	51
F (P_L < 0.5)	154	73	120	57	139	66	129	61

The results are shown in Table 5.2, which classifies the soil that has the potential to liquefy (Criteria A-C) and the soil that does not have the potential to liquefy (Criteria D-F) based on the predictive accuracy of each recommended approach.

The findings from Table 5.2 show that the Proposed Model, which is based on certain criteria, has a higher success rate in predicting liquefaction cases compared to the models developed by Idriss & Boulanger (2006), Juang et al. (2002), and Toprak et al. (1999). Specifically, the

Proposed Model achieved success rates of 75% for A, 85% for B, and 89% for C, whereas the other models achieved lower success rates ranging from 70% to 84%. Furthermore, compared to Idriss & Boulanger (2006) (A = 74%, B = 84% and C= 85%), Juang et al. (2002) (A = 73%, B = 81% and C= 84%) And Toprak et al. (1999) (A = 70%, B = 73% and C= 80%) proposed model has a greater success rate of non-liquefiable case prediction.

5.6.2 Performance fitness and error metrics (PFEMs)

Table 5.3 Comparative analysis of the proposed approach with existing techniques for binary classification

Matrices	Models				
	Proposed Model	Toprak et al. (1999)	Juang et al. (2002)	Idriss and Boulanger (2006)	Range
TPR	0.89	0.762	0.84	0.85	1.0
FNR	0.108	0.237	0.161	0.15	0.0
PPV/Precision	0.817	0.714	0.768	0.746	1.0
NPV	0.832	0.628	0.751	0.75	1.0
FPR	0.270	0.431	0.341	0.388	0.0
FDR	0.183	0.285	0.231	0.253	0.0
FOR	0.168	0.372	0.249	0.25	0.0
F_1 Score	0.852	0.737	0.802	0.794	1.0
MCC	0.634	0.3851	0.508	0.478	-1.0 to + 1.0
Accuracy	0.822	0.682	0.762	0.747	1.0
Sensitivity/Recall	0.891	0.762	0.838	0.849	1.0
Specificity	0.729	0.568	0.658	0.611	---------
$G_{\text{mean error}}$	0.193	0.342	0.257	0.279	0.0
BA	0.81	0.665	0.748	0.730	1.0

Utilising Performance Fitness and Error Metrics (PFEMs) for binary classification. In order to fully evaluate the efficacy of the proposed approaches for classifying liquefaction problems, several Performance Fitness and Error Metrics (PFEMs) are used in this section. Within the binary classification scenario, including both liquefied and non-liquefied instances, there are

four distinct possible outcomes for a single prediction. The terms "true negative" (TN) and "true positive" (TP) refer to accurate classifications. A false positive (FP) occurs when the output is erroneously predicted to be negative, whereas a false negative (FN) arises when the outcome is mistakenly classified as negative. The 2 × 2 confusion matrix seen in Figure 5.7 may be used to assess these matrices. PFEMs are used to elucidate the correspondence between probabilistic forecasts of suggested methodologies and the actual outcome. These measures often pertain to the discrepancy in variance between the predicted and actual data. In this study, used specific Performance Fitness and Error Metrics (PFEMs) to evaluate categorization issues (Naser and Alavi 2021). The mathematical representation of these PFEMs is provided below:

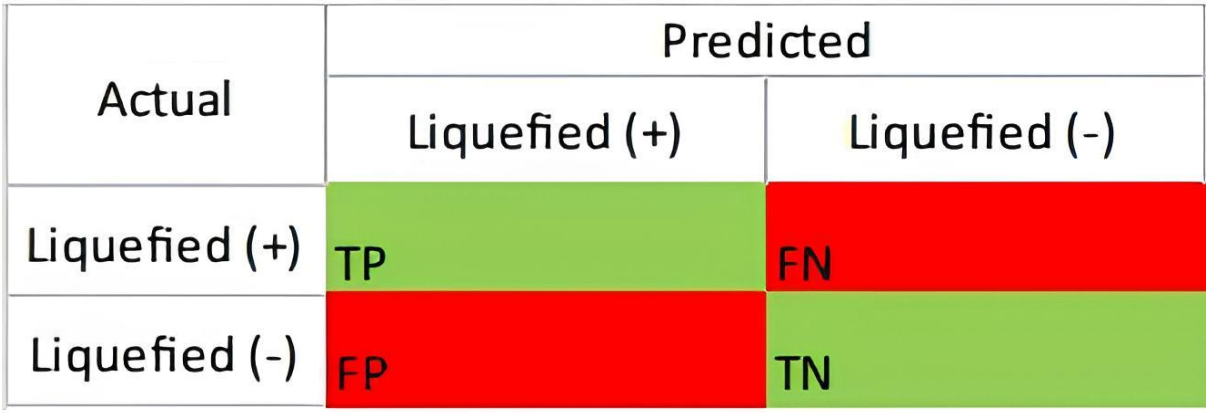

Figure 5.7 Illustration of confusion matrix (2 × 2) for classification problem

$$\mathrm{TPR} = \frac{\mathrm{TP}}{\mathrm{TP+FN}} \tag{5.7}$$

$$\mathrm{FNR} = \frac{\mathrm{FN}}{\mathrm{FN+TP}} \tag{5.8}$$

$$\mathrm{PPV} = \frac{\mathrm{TP}}{\mathrm{TP+FP}} \tag{5.9}$$

$$\mathrm{NPV} = \frac{\mathrm{TN}}{\mathrm{TN+FN}} \tag{5.10}$$

$$\mathrm{FPR} = \frac{\mathrm{FP}}{\mathrm{FP+TN}} \tag{5.11}$$

$$\mathrm{FDR} = \frac{\mathrm{FP}}{\mathrm{FP+TP}} \tag{5.12}$$

$$\mathrm{FOR} = \frac{\mathrm{FN}}{\mathrm{FN+TP}} = 1 - \mathrm{NPV} \tag{5.13}$$

$$\mathrm{F}_{1\ \mathrm{SCORE}} = \frac{2\mathrm{TP}}{2\mathrm{TP+FP+FN}} \tag{5.14}$$

$$\text{MCC} = \frac{\text{TP}\times\text{TN}-\text{FP}\times\text{FN}}{\sqrt{(\text{TP}+\text{FP})(\text{TP}+\text{FN})(\text{TN}+\text{FP})(\text{TN}+\text{PN})}} \quad (5.15)$$

$$\text{Accuracy} = \frac{\text{TP}+\text{TN}}{\text{FN}+\text{TP}+\text{FP}+\text{TN}} \quad (5.16)$$

$$\text{Sensitivity} = \frac{\text{TP}}{\text{FN}+\text{TP}} \quad (5.17)$$

$$\text{Specificity} = \frac{\text{TN}}{\text{FP}+\text{TN}} \quad (5.18)$$

$$\text{G}_{(\text{mean})\text{error}} = 1 - \sqrt{\text{Sensitivity} \times \text{Specificity}} \quad (5.19)$$

$$\text{BA} = 0.5 \times \left(\frac{\text{TP}}{\text{TP}+\text{FN}} + \frac{\text{TN}}{\text{TN}+\text{FP}}\right) \quad (5.20)$$

Table 5.4 Score analysis of the proposed method and existing methods

Matrices	Proposed Model	Toprak et al. (1999)	Juang et al. (2002)	Idriss and Boulanger (2006)
TPR	4	1	2	3
FNR	4	1	2	3
PPV	4	1	3	2
NPV	4	1	3	2
FPR	4	1	3	2
FDR	4	1	3	2
FOR	4	1	3	2
F_1 Score	4	1	3	2
MCC	4	1	3	2
Accuracy	4	1	3	2
Sensitivity	4	1	2	3
Specificity	4	1	3	2
$G_{\text{mean error}}$	4	1	3	2
BA	4	1	3	2
Total Score	56	14	39	31
Rank	1	4	2	3

In this context, True Positives (TP) refer to instances where the model correctly identifies positive examples, specifically liquefied events, meaning the model's prediction aligns with the actual occurrence of liquefaction. True Negatives (TN), on the other hand, represent cases where the model accurately recognizes negative examples, correctly predicting non-liquefied events when no liquefaction occurs. False Negatives (FN) occur when the model fails to detect positive examples, incorrectly classifying actual liquefied events as non-liquefied. Lastly, False Positives (FP) describe situations where the model erroneously predicts liquefaction for instances that are actually non-liquefied. This framework is essential for assessing the model's effectiveness in accurately distinguishing between liquefied and non-liquefied events.

The binary classification predictions were compared with the actual observations by analyzing the PFEM data presented in Table 5.3. This analysis assesses the model's predictive ability across various metrics, specifically for identifying liquefied and non-liquefied events.

The true positive rate (TPR) measures the ratio of accurately detected positive cases to the total number of actual positive cases. In this study it measures the proportion of actual positive cases (liquefied) that are correctly identified by the model. The TPR values of the suggested model (0.89) were found to be higher than those of the Idriss and Boulanger (2006) (0.85), Toprak et al. (1999) (0.762), and Juang et al. (2002) (0.84) approaches.

The positive predictive value (PPV) is a measure that represents the percentage of positive observations that actually result in true positive values. In this study it measures the proportion of positive predictions (liquefied) that are correctly identified. The PPV value obtained for the proposed model (0.817) is higher than the values obtained by Juang et al. (2002) (0.764), Idriss and Boulanger (2006) (0.746), and Toprak et al. (1999) (0.714) techniques.

The optimal and suboptimal values for the Negative Predictive Value (NPV) are 1 and 0, correspondingly. It computes the ratio of incorrect positive results among observations that seem to be negative. In this study it measures the proportion of negative predictions (non-liquefied) that are correctly identified. The suggested model (0.832) outperforms the Juang et al. (2002) (0.751), Idriss and Boulanger (2006) (0.75), and Toprak et al. (1999) (0.628) approaches.

A perfect prediction accuracy would include a False Positive Rate (FPR) of zero, indicating that no negative instances are incorrectly categorised as positive ones. In this study it measures the proportion of actual negative cases (non-liquefied) that are incorrectly classified as positive (liquefied). Although the FPR score of the suggested model (0.270) is lower than that of Juang

et al. (2002) (0.341), Idriss and Boulanger (2006) (0.388), and Toprak et al. (1999) (0.431) approaches.

The False Discovery Rate (FDR) refers to the proportion of individuals who have a positive test result while not having the real ailment. In this study it measures the proportion of positive predictions (liquefied) that are actually incorrect (non-liquefied). The false discovery rate (FDR) obtained in this study for the proposed model (0.183) is lower than that reported by Juang et al. (2002) (0.231), Idriss and Boulanger (2006) (0.253), and Toprak et al. (1999) (0.285). This indicates that the proposed method outperformed the methods employed by Idriss and Boulanger (2006), Toprak et al. (1999), and Juang et al.

The False Omission Rate (FOR) quantifies the proportion of individuals whose test results indicated a negative outcome, although really having a positive condition. In this study It measures the proportion of negative predictions (non-liquefied) that are actually incorrect (liquefied). The suggested technique (0.168) has a lower value compared to the procedures used by Toprak et al. (1999) (0.372), Juang et al. (2002) (0.249), and Idriss and Boulanger (2006) (0.25). The suggested approaches' accuracy is evaluated using the F1 score. The F1-score obtained for the suggested approach (0.852) is greater than that for the Idriss and Boulanger (0.794), Toprak et al. (1999) (0.737), and Juang et al. (2002) methodologies. This indicates that the proposed method is more accurate in forecasting the possibility of liquefaction.

Furthermore, the assessment of a binary classifier's effectiveness involves the use of Balanced Accuracy (BA), miss or false negative rate (FNR), Gmean error, and the Matthews correlation coefficient (MCC).

The definitions of balanced accuracy and G(mean) error may be found in Equation (5.17) and Equation (5.19) accordingly. The miss rate indicates the quantity of liquefied or non-liquefied substances that could have been incorrectly classified as not having the potential to cause tsunamis. Gmean is often used when each class's performance is both remarkable and anticipated to be excellent simultaneously (Kubat and Matwin 1997; Yuan and Liu 2011). The given value is the geometric mean of the correctness of each instance inside each class. To assess the efficacy of the classifier model, some studies have used Gmean as a measure of error rate, in addition to the F1-score.

Matthews (1975) established the Matthews Correlation Coefficient (MCC) to measure the effectiveness of a model when there is a significant difference between the percentage of positive and negative data. The MCC is particularly valuable in such scenarios. The MCC value must fall between the range of -1.0 and +1.0. Conversely, a preference for the greater number indicates a more accurate forecast. When compared to the criteria established by Toprak et al. (1999) (0.385), Juang et al. (2002) (0.508), and Idriss and Boulanger (2006) (0.478), the suggested method's MCC value (0.634) indicates that it outperforms these criteria in predicting liquefaction likelihood.

The False Negative Rate (FNR) accurately predicts cases of liquefaction turning into non-liquefaction. FNR provides a clearer understanding of where sudden failure occurs. In this study, the proposed method (0.108) demonstrates lower FNR values compared to Toprak et al. (1999) (0.237), Juang et al. (2002) (0.161), and Idriss and Boulanger (2006) (0.15). Score analysis is performed to assess the effectiveness of the suggested methods.

The score is calculated for each strategy by considering their performance fitness and error matrices. The score value range is defined by the total number of approaches used in this study, which is 1-4 (with a total of 4 procedures applied). The score value in this study is calculated based on the obtained value of PFEMs. The procedures that possess the most worth for any particular PFEMs, with an optimal value of 1.0, are assigned a maximum score of 4.0. On the other hand, the methods that have the greatest significance for any particular PFEMs with an optimal value of 0.0 are assigned a minimum score of 0. The proposed methodology in this research has received the highest score of 56 in the prediction liquefaction by binary classification, as shown in Table 5.4. Thus, the suggested approach has obtained the highest ranking, with Juang et al. (2002), Idriss and Boulanger (2006), and Toprak et al. (1999) methods following in subsequent positions. Scatter plots are shown for both liquefied and non-liquefied samples, demonstrating all the recommended methods for the parameters $(N1)_{60cs}$, and CSR. The scatter plots in Figures 5.8, 5.9, 5.10, and 5.11 illustrate the correlation between the total number of liquefied and non-liquefied instances for the Proposed Model, Toprak et al. (1999), Idriss and Boulanger (2006), and Juang et al. (2002) techniques. These charts illustrate the comparison between the observed and forecasted values. The scatter plot of the Proposed Model exhibits distinct and improved segregation, aligning closely with the projected value ranges in contrast to the other models. Conversely, the scatter plot for Toprak et al. (1999) demonstrates a substantial degree of inaccuracy in forecasting both liquefied and non-liquefied instances.

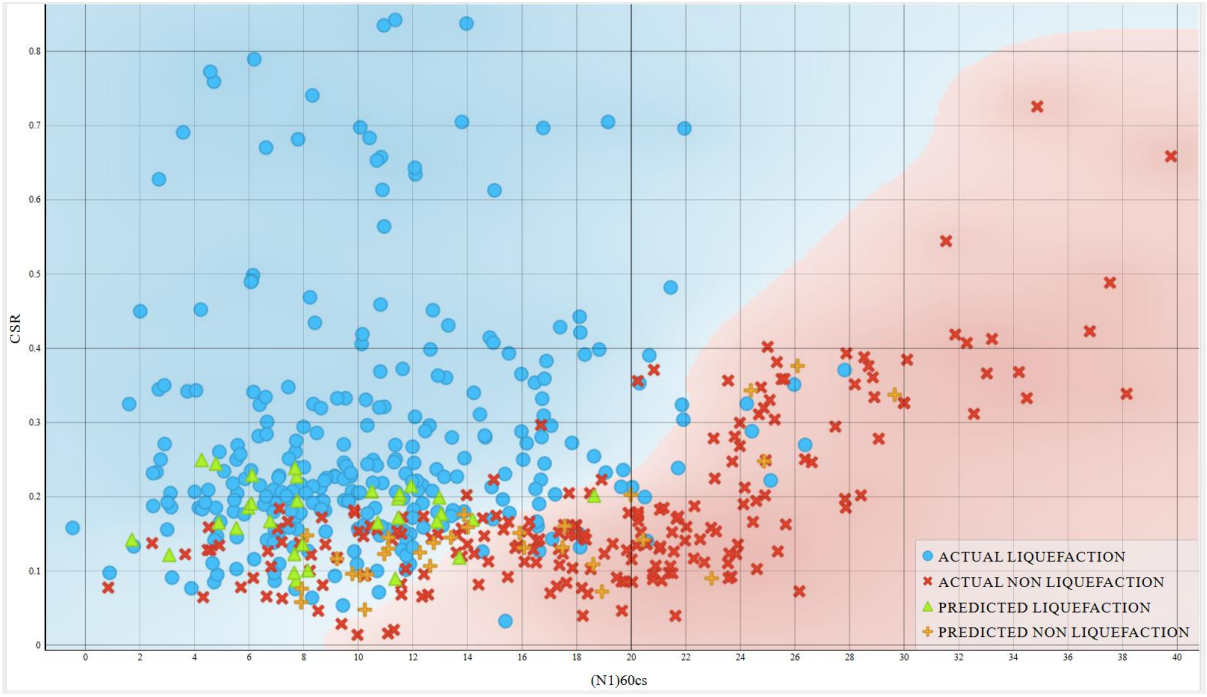

Figure 5.8 Visualisation of observed and forecasted instances using the suggested methodology

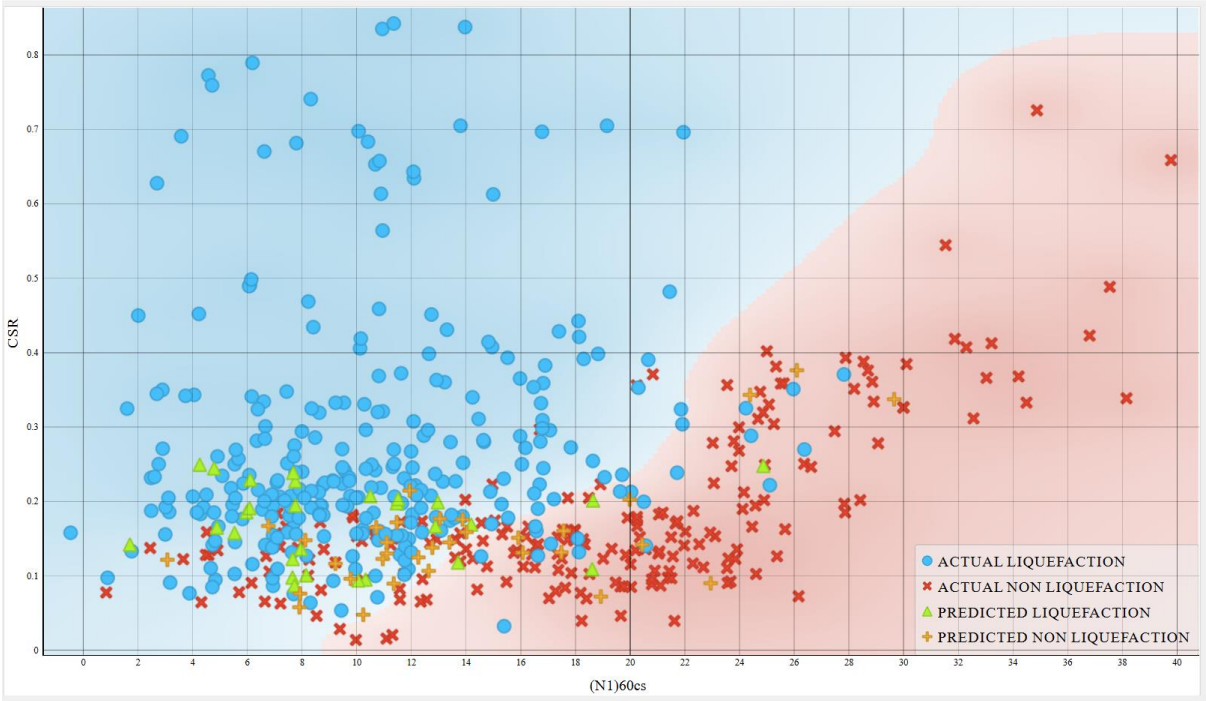

Figure 5.9 Visualisation of observed and forecasted instances of Juang et al. (2002) method

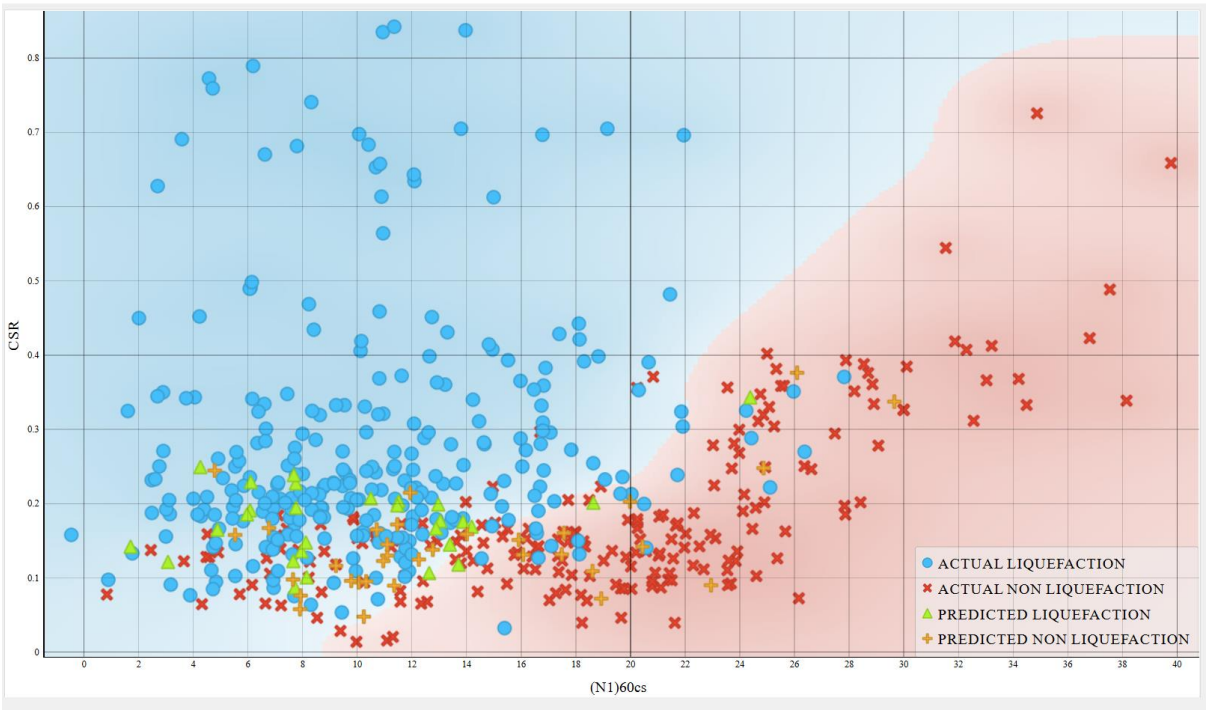

Figure 5.10 Visualisation of observed and forecasted instances of Idriss and Boulanger (2006) method

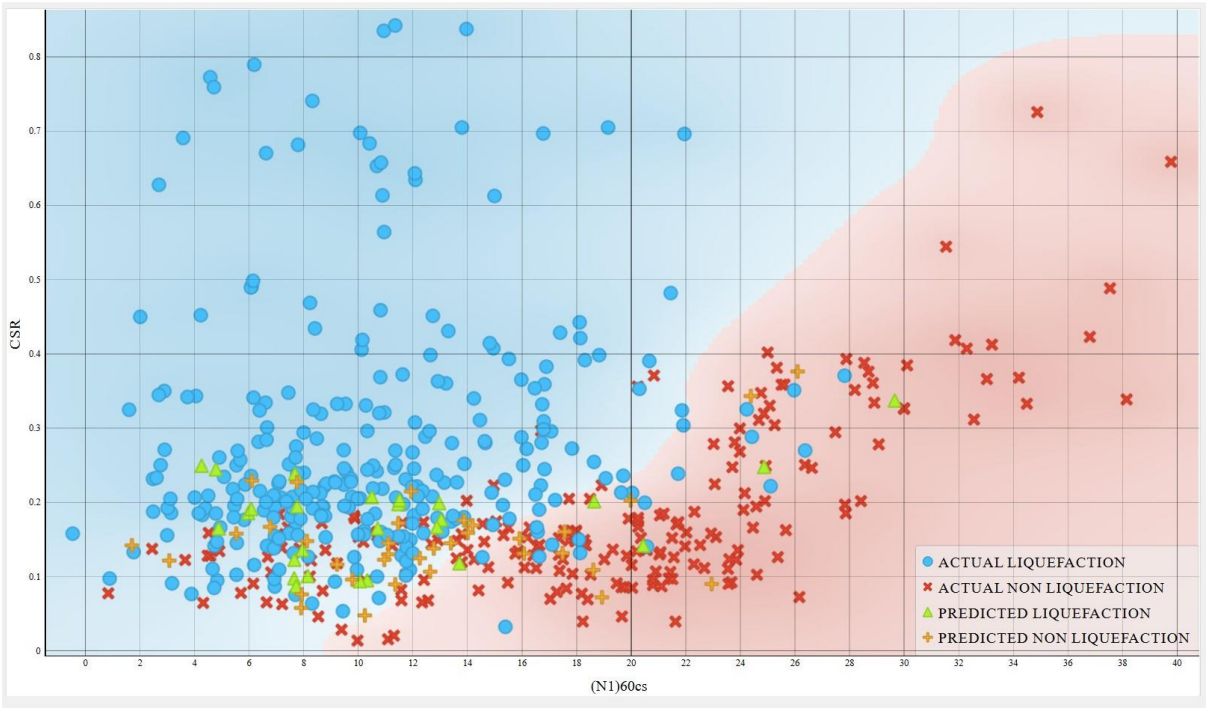

Figure 5.11 Visualisation of observed and forecasted instances of Toprak et al. (1999) method

5.6.3 Evaluating the proportional impact of various criteria on the computation of PL using the Gini Index (GI)

The Gini index (GI) is used to evaluate the relative significance of independent variables in predicting the likelihood of soil deposit liquefaction. The Gini index has been computed for each independent variable, and their relative significance has been evaluated. A higher Gini index value signifies a stronger influence of individual independent elements in forecasting the likelihood of soil liquefaction in a deposit. The Gini index is calculated using the following mathematical equation:

$$GI = \left|\sum_{i=2}^{n} \text{Cum } X_{i-1} \text{Cum } P_{Li} - \sum_{i=2}^{n} \text{Cum } X_i \text{Cum } P_{Li-1}\right| \qquad (5.21)$$

Here, CumX denotes the cumulative value of independent variables, whereas CumPL represents the cumulative value of liquefaction probability for a set of n observed data points. The Gini index values for all three approaches, considering various input variables such as Critical depth, FC, D50, PGA, rd, W.T, CSR, and (N1)60CS, are shown in Table 5.5.

The results shown in Table 5.5 demonstrate that the Gini index value for each independent variable in the proposed technique is lower than the values obtained in the methods used by Juang et al. (2002), Toprak et al. (1999), and Idriss and Boulanger (2006). These findings indicate that each component has a substantial impact on the capacity to estimate the likelihood of liquefaction using the suggested approach.

Table 5.5 Gini index value for all proposed and existing methods

Variables	Proposed Model	Toprak et al. (1999)	Juang et al. (2002)	Idriss and Boulanger (2006)
Critical depth	150.763	208.26	593.07	553.543
FC	336.26	314.6	979.8	811.6
D50	3.1259	4.7289	18.6078	17.0856
W.T	140.165	177.05	296.85	288.44
PGA	2.56265	4.3765	22.9305	20.828
rd	34.0271	37.116	18.033	10.0435
CSR	1.85031	1.0921	7.4296	13.1889
$(N_1)_{60CS}$	1849.761	2180.662	1523.244	1678.829

5.7 Conclusions

- The probability density functions of the Weibull distribution have been computed, and it has been shown that they provide the best fitting curves for both liquefied (L) and non-liquefied (NL). The factor of safety exhibits a better form and distribution when the scale parameter (λ) and shape parameter (k) are set to 0.580 and 2.437, respectively.
- The liquefaction probability was determined by applying Bayesian mapping function to calculate the probability for the given data. The logistic curve fitting method was used to create an equation with an accuracy of 0.93. The resulting equation was then compared to the methods proposed by Juang et al. (2002), Toprak et al. (1999), and Idriss and Boulanger (2006).
- The binary classification was conducted using a confusion matrix and score analysis. The effectiveness of the proposed model was evaluated by comparing its performance with established techniques from Juang et al. (2002), Toprak et al. (1999), and Idriss and Boulanger (2006). In the context of liquefaction studies, the proposed model demonstrated superior performance, consistently achieving better metrics while reducing negative outcomes. This indicates that the model is more reliable and accurate in predicting liquefied and non-liquefied events compared to the existing methodologies.
- The Gini index was calculated for the proposed technique as well as for the existing methods developed by Juang et al. (2002), Toprak et al. (1999), and Idriss and Boulanger (2006). The results demonstrate that all factors considered in the suggested method are significant in predicting the likelihood of liquefaction. This underscores the effectiveness of the proposed approach in accurately identifying key predictors of liquefaction risk.

CHAPTER 6

THE OPTIMISED MACHINE LEARING METHODS TO EVALUATE LIQUEFACTION

6.1 Introduction

Although several methods such as cyclic stress-based, cyclic strain-based, and energy-based techniques are used, the stress-based approach is the predominant way for assessing the potential for soil liquefaction (Krammer 1996). The Standard Penetration Test (SPT) is the predominant approach for assessing the possibility for soil liquefaction via in situ testing. However, it suffers from some limitations, mostly stemming from the inconsistent practices and procedures associated with the SPT across different regions.

Difficulties associated with liquefaction assessment are very non-linear. A team of geotechnical researchers used machine learning techniques to address the difficulties arising from nonlinearity and other intricate factors while predicting the probability of liquefaction. Soft computing methodologies, such as artificial neural network (ANN), support vector machine (SVM), have been used to develop liquefaction prediction models utilising in-situ test datasets. These strategies have shown better efficacy in comparison to statistical methods. The advantages and disadvantages of the solutions have already been evaluated in Chapter-I. This work presents a new model for predicting soil liquefaction, which incorporates enhanced correlation features, chi square, relief characteristics, and technical indicators. To get reliable prediction results, ensemble classifiers such as Deep Belief Networks (DBN), Long Short-Term Memory (LSTM), and Support Vector Machines (SVM) are combined with an optimised Bidirectional Gated Recurrent Unit (Bi − GRU). This study introduces a novel approach for determining the optimal weights in Bi − GRU via the use of a distinctive AC − SSO and OSA − SSO model. The present study used a dataset consisting of measurements acquired from the Standard Penetration Test (SPT). The dataset included of post-liquefaction case histories ranging from the 1944 Tohnankai earthquake to the 1999 Chi Chi earthquake in Taiwan. The dataset consisted of 286 occurrences of liquefaction and 210 occurrences of non-liquefaction. A total of 30 Standard Penetration Test (SPT) borehole data were collected in the Faridabad

region, which is located in the National Capital area (NCR) of Delhi, in order to verify the accuracy of the models.

6.2 Methodology and simulation setup

Forecasting soil liquefaction in geotechnical engineering is a challenging task due to its complex and non-linear interaction with various factors. Conventional methods, while commonly used and straightforward, often fail to yield accurate results due to the unpredictable nature of field conditions and inherent calculation limitations. This highlights the need for more advanced methods to predict soil liquefaction. Over the years, researchers have increasingly turned to machine learning (ML) techniques to address these uncertainties and improve prediction accuracy. Soft computing techniques have gained popularity as a reliable and efficient alternative to traditional methods due to their robustness and predictive capabilities (Xue and Xiao, 2016; Xue and Yang, 2013, 2016).

To overcome the limitations posed by the variability of conventional methods, an enhanced feature selection process was implemented to determine the most significant features based on their coefficients of dependency. According to a literature review, many researchers have used basic models that suffer from reproducibility issues (Beam et al., 2022). To address this, an ensemble deep learning methodology was adopted, integrating Deep Belief Networks (DBN), Long Short-Term Memory (LSTM), and Support Vector Machines (SVM), combined with an optimized Bidirectional Gated Recurrent Unit (Bi-GRU). A novel approach was introduced for determining the optimal weights in Bi-GRU using distinctive AC-SSO (Average Cat and Salp swarm algorithm) and OSA-SSO (Opposition-based self-adaptive shark smell optimizer) models to optimize the process and prevent premature convergence.

The proposed soil liquefaction prediction method was developed using Python, incorporating both EC + AC-SSO and EC + OSA-SSO techniques. A dataset consisting of 496 post-liquefaction case studies was used for training and testing, with an additional 30 SPT borehole data points used for model validation. The learning percentage (LP) was adjusted between 60%, 70%, 80%, and 90% to analyze the model's performance. The efficacy of the proposed model was compared against other existing methods such as EC + SSA (Mirjalili et al., 2017), EC + CSO (Bahrami et al., 2018), EC + GWO (Mirjalili et al., 2014), EC + SSO (Mohammad et al., 2017), EC + PRO (Moosavi and Bardsiri, 2019), and EC + BOA (Arora and Singh, 2019), using various performance metrics.

Convergence analysis was also conducted to evaluate how quickly and accurately the optimization algorithm approaches the optimal solution, studying the rate of improvement in successive iterations. The iterations were continued until the global optima were reached.

6.3 Performance analysis

The recommended $\mathrm{EC} + \mathrm{AC} - \mathrm{SSO}$ and $\mathrm{EC} + \mathrm{OSA} - \mathrm{SSO}$ algorithms are evaluated using current optimisation models with different metrics. Therefore, the assessment was conducted using a dataset. The present study used a dataset consisting of measurements acquired from the Standard Penetration Test (SPT). The collection included post-liquefaction case histories from the 1944 Tohnankai earthquake to the 1999 Chi Chi earthquake in Taiwan. The dataset included 286 occurrences of liquefaction and 210 occurrences of non-liquefaction. A total of 30 Standard Penetration Test (SPT) borehole data were collected in the Faridabad region, which is located inside the National Capital area (NCR) of Delhi, in order to verify the accuracy of the models. The corresponding outcomes are graphed from Figure 6.1 to Figure 6.1.

6.3.1 Model evolution metrics

These metrics provide a thorough comprehension of a model's performance in several dimensions, enabling to evaluate its strengths and shortcomings according to the unique demands of the issue domain. This research primarily focuses on minimising the false negative rate (FNR) rather than enhancing the values of other evolution approaches, taking into account the issue context and dataset characteristics while selecting the matrix. Within the context of this research the FNR indicates the potential for liquefaction, but it forecasts a non-liquefaction outcome, implying the existence of a failure risk (liquefaction) without an actual failure (non-liquefaction) being anticipated.

The proposed $\mathrm{EC} + \mathrm{AC} - \mathrm{SSO}$ and $\mathrm{EC} + \mathrm{OSA} - \mathrm{SSO}$ models are assessed against $\mathrm{EC} + \mathrm{SSA}, \mathrm{EC} + \mathrm{CSO}, \mathrm{EC} + \mathrm{GWO}, \mathrm{EC} + \mathrm{SSO}, \mathrm{EC} + \mathrm{PRO}$, and $\mathrm{EC} + \mathrm{BOA}$ models for various learning rates values ranging from 60 to 90. Essentially, larger positive numbers and smaller negative values indicate a better likelihood of accurate predictions for the scheme. Upon comparing Figure 6.1 to Figure 6.1, it is seen that the outputs of the constructed model rise for all positive measures and decrease for negative measures. Particularly, exceptional results are achieved at the 90th LP for both the current and new designs.

False negative rate (FNR):

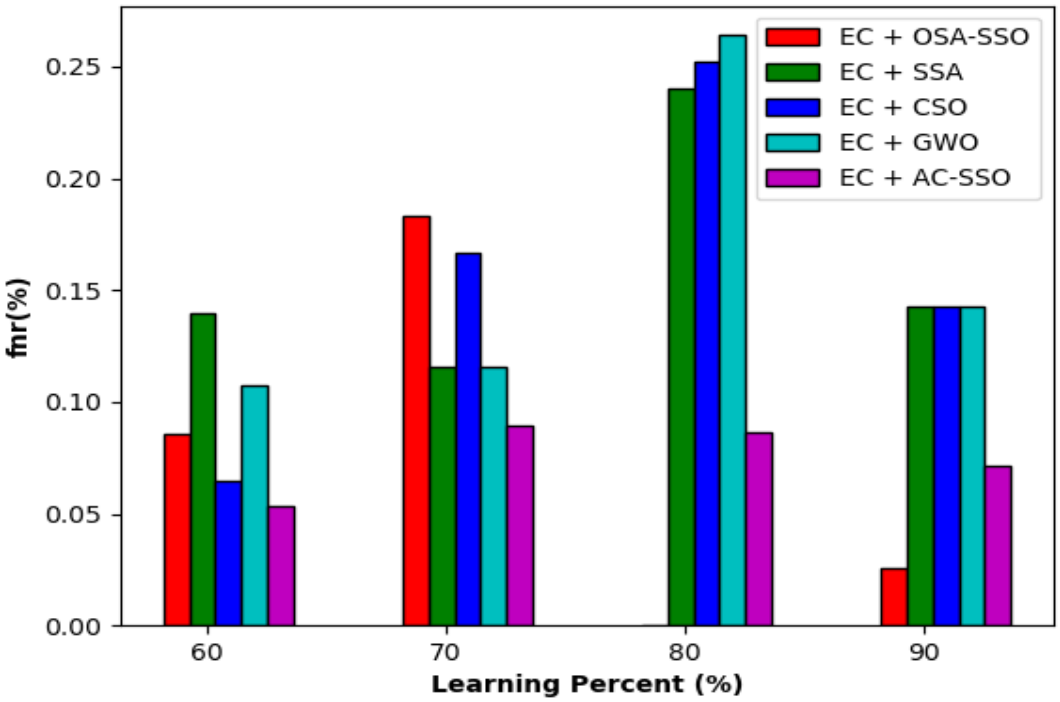

Figure 6.1 Analysing the False Negative Rate (FNR) utilising a newly created technique in comparison to existing optimisation strategies.

Table 6.1 Analysis on developed approach over extant classification of False negative rate (FNR) at various learning percentages

False negative rate (FNR)						
S No	Learning percent (%)	EC + SSA	EC + CSO	EC + GWO	EC + AC-SSO	EC + OSA-SSO
1	60	13.97849	6.451613	10.75269	5.376344	8.602151
2	70	11.53846	16.66667	11.53846	8.974359	18.27957
3	80	24	25.2	26.4	8.62069	0
4	90	14.28571	14.28571	14.28571	7.142857	2.564103

The False Negative Rate (FNR) measures the proportion of true liquefied events that are incorrectly classified as non-liquefied by the model. It is calculated as the ratio of false

negatives to the sum of true positives and false negatives. In the context of liquefaction, a low FNR is particularly important because missing positive instances—where liquefaction is predicted as non-liquefaction can lead to catastrophic failures in soil and structures under dynamic loads. Given the sudden and unpredictable nature of liquefaction, even a few instances of incorrect predictions could result in significant damage.

This study primarily focuses on minimizing the FNR, as opposed to solely improving other evaluation metrics, to ensure the reliability of the model in predicting potential liquefaction. An FNR in this context indicates that while there is a risk of liquefaction (failure), the model incorrectly predicts stability (non-liquefaction), thus overlooking potential dangers. The proposed techniques, EC + OSA-SSO and EC + AC-SSO, demonstrated notably low FNR values at various learning percentages, with EC + OSA-SSO outperforming both the other proposed methods and existing techniques, especially at the 80th and 90th learning percentages. This highlights the effectiveness of the model in accurately identifying liquefaction risks.

False positive rate (FPR)

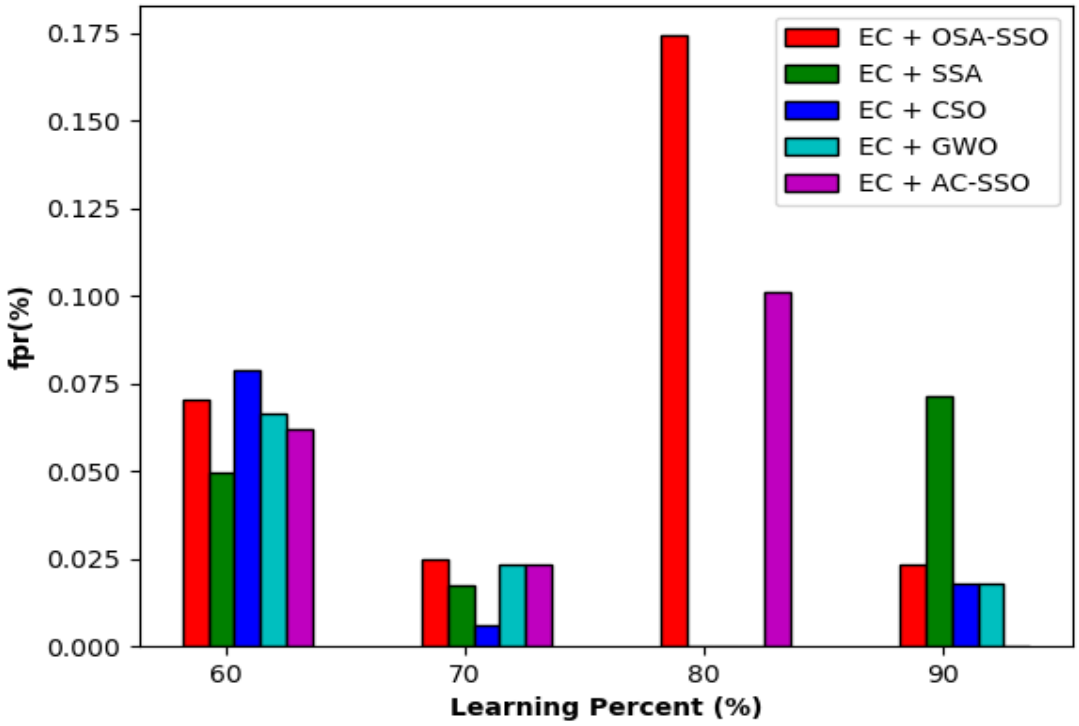

Figure 6.2 Analysing the False positive rate (FPR) utilising a newly created technique in comparison to existing optimisation strategies

Table 6.2 Analysis on developed approach over extant classification of False positive rate (FPR) at various learning percentages

False positive rate (FPR)						
S No	Learning percentage (%)	EC + SSA	EC + CSO	EC + GWO	EC + OSA-SSO	EC + AC-SSO
1	60	4.979253	7.883817	6.639004	7.053942	6.224066
2	70	1.744186	0.581395	2.325581	2.489627	2.325581
3	80	0	0	0	17.43119	10.09174
4	90	7.142857	1.785714	1.785714	2.325581	0

The False Positive Rate (FPR) measures the proportion of true non-liquefied cases that are incorrectly classified as liquefied by the model. It is calculated by dividing the number of false positives by the sum of true negatives and false positives. While minimizing FPR is generally important in many scenarios, its impact on liquefaction studies is somewhat different. In this context, an FPR indicates instances where non-liquefied cases are wrongly identified as liquefied, effectively leading to a more conservative approach by increasing the factor of safety.

In this study, although the proposed models such as EC + SSA, EC + CSO, and EC + GWO showed some FPR values rather than zero or minimal values, this actually contributes positively to the factor of safety in liquefaction assessments. These models demonstrated better predictive performance, particularly at the 80th learning percentage. While a certain level of FPR is present, this cautious overestimation helps ensure that potential liquefaction risks are not underestimated, thereby enhancing the overall safety in liquefaction studies.

Sensitivity (Recall or True positive rate)

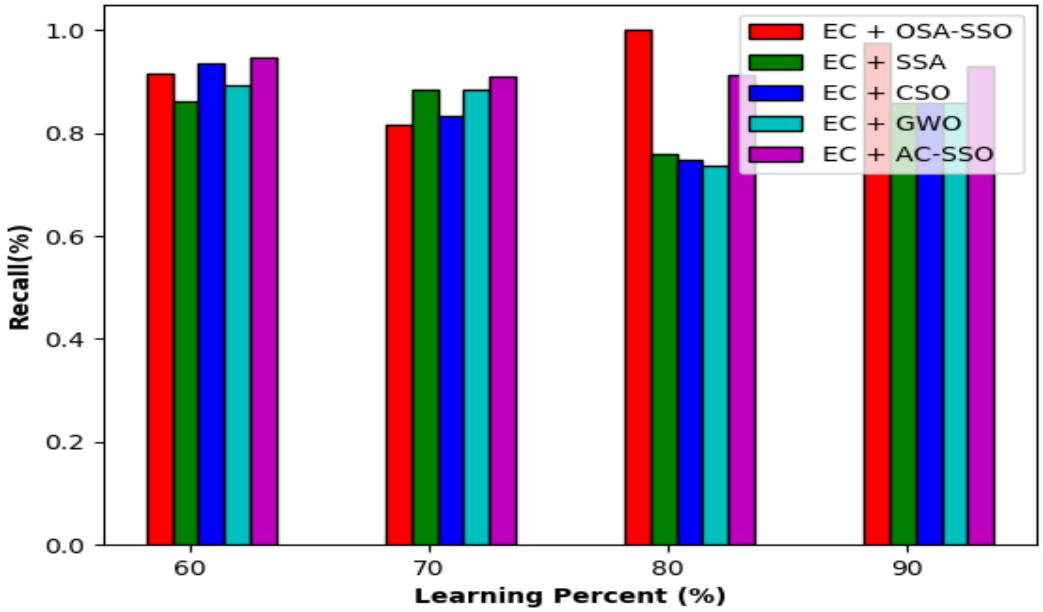

Figure 6.3 Analysis using developed approach over extant optimization schemes regarding Sensitivity or Recall

Table 6.3 Analysis on developed approach over extant classification of Sensitivity or Recall at various learning percentages

Sensitivity or Recall						
S No	Learning percentage (%)	EC + SSA	EC + CSO	EC + GWO	EC + AC-SSO	EC + OSA-SSO
1	60	86.02151	93.54839	89.24731	94.62366	91.39785
2	70	88.46154	83.33333	88.46154	91.02564	81.72043
3	80	76	74.8	73.6	91.37931	100
4	90	85.71429	85.71429	85.71429	92.85714	97.4359

Sensitivity is a critical metric in evaluating the effectiveness of models in liquefaction studies, as it measures the model's ability to correctly identify cases of liquefaction among all instances where liquefaction actually occurs. It is calculated by dividing the number of true positive predictions (correctly identified liquefied cases) by the sum of true positives and false negatives (cases where liquefaction occurred but was not detected by the model).

In the context of liquefaction studies, achieving high sensitivity is crucial because missing cases of potential liquefaction can have severe consequences, such as failing to identify areas at risk of significant ground instability during an earthquake. A highly sensitive model ensures that most, if not all, cases of liquefaction are detected, thus minimizing the risk of overlooking vulnerable zones.

In this study, the EC + OSA-SSO model has demonstrated superior performance in terms of sensitivity, particularly at the 80th and 90th learning percentages. This indicates that as the model's training data increases, it becomes increasingly effective at identifying liquefaction events, outperforming other proposed and existing methods. This finding underscores the importance of sensitivity in model evaluation and highlights the robustness of the EC + OSA-SSO approach in accurately predicting liquefaction.

Precision:

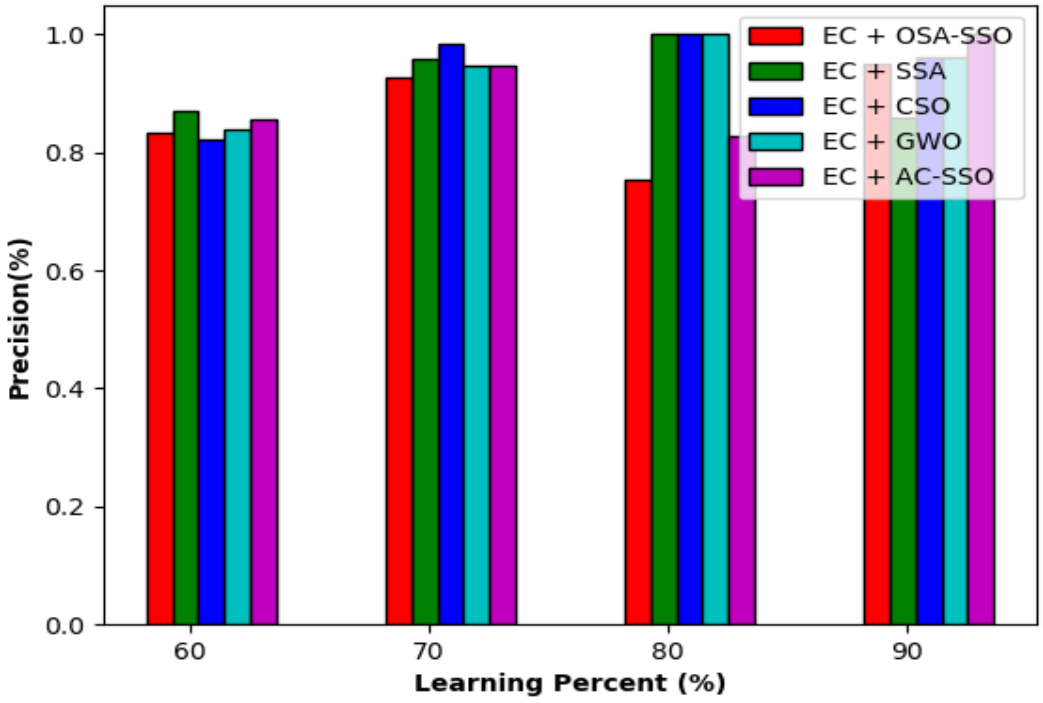

Figure 6.4 Analysing the created technique in comparison to existing optimisation strategies in terms of precision.

Table 6.4 Analysis on developed approach over extant classification of Precision at various learning percentages

Precision						
S No	Learning percentage (%)	EC + SSA	EC + CSO	EC + GWO	EC + AC-SSO	EC + OSA-SSO
1	60	86.95652	82.07547	83.83838	85.43689	83.33333
2	70	95.83333	98.48485	94.52055	94.66667	92.68293
3	80	100	100	100	82.8125	75.32468
4	90	85.71429	96	96	100	95

Precision is a key metric in assessing the accuracy of positive predictions in liquefaction studies, as it measures the proportion of true positive predictions (correctly identified liquefied cases) out of all positive predictions made by the model. It is calculated by dividing the number of true positives by the sum of true positives and false positives (cases where the model incorrectly predicted liquefaction).

In the context of liquefaction, high precision is particularly important when the cost of false positives is high, such as when mistakenly identifying stable areas as prone to liquefaction could lead to unnecessary and costly interventions. Ensuring that the model's positive predictions are highly accurate is crucial to avoid these errors and ensure that resources are allocated effectively.

In this study, the EC + OSA-SSO model has shown superior precision at the 90th learning percentage, indicating its high accuracy in predicting liquefaction when trained with a substantial amount of data. Meanwhile, other models like EC + SSA, EC + CSO, and EC + GWO have demonstrated better precision at the 80th learning percentage. These findings suggest that while EC + OSA-SSO excels with more extensive training, the other models are more effective with a slightly lower amount of data. This variation in performance highlights the importance of selecting the appropriate model and training level depending on the specific requirements of the liquefaction study.

Negative predictive value (NPV):

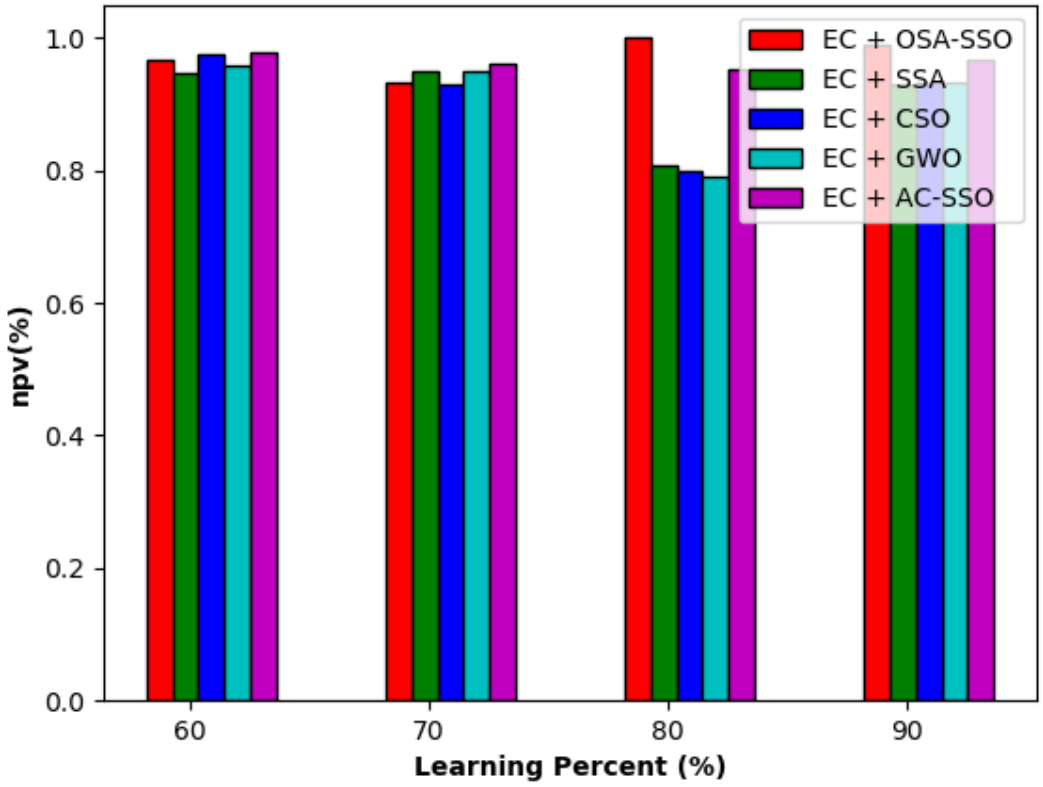

Figure 6.5 Analysis using developed approach over extant optimization schemes regarding Negative predictive value (NPV)

Table 6.5 Analysis on developed approach over extant classification of Negative predictive value (NPV) at various learning percentages

Negative predictive value (NPV)						
S No	Learning percentage (%)	EC + SSA	EC + CSO	EC + GWO	EC + AC-SSO	EC + OSA-SSO
1	60	94.6281	97.36842	95.74468	97.8355	96.55172
2	70	94.94382	92.93478	94.91525	96	93.25397
3	80	80.64516	79.8722	79.11392	95.14563	100
4	90	92.85714	93.22034	93.22034	96.55172	98.82353

Negative Predictive Value (NPV) is a crucial metric in liquefaction studies, as it measures the likelihood that a model's prediction of a negative outcome (non-liquefied) is accurate. It is calculated by dividing the number of true negative predictions (correctly identified non-liquefied cases) by the sum of true negatives and false negatives (cases where liquefaction occurred but was not detected by the model).

In the context of liquefaction, a high NPV is particularly important when it is critical to accurately identify areas that are not at risk of liquefaction. This helps prevent unnecessary concern or intervention in areas that are actually stable, ensuring that resources and efforts are focused where they are truly needed.

In this study, the EC + OSA-SSO model has shown superior NPV at both the 80th and 90th learning percentages, outperforming other proposed and existing methods. This indicates that as the model is trained with more data, it becomes increasingly reliable in correctly identifying non-liquefied areas. These results highlight the robustness of the EC + OSA-SSO model in accurately predicting areas that are not susceptible to liquefaction, which is essential for effective risk management and decision-making in liquefaction studies.

Matthews correlation coefficient (MCC):

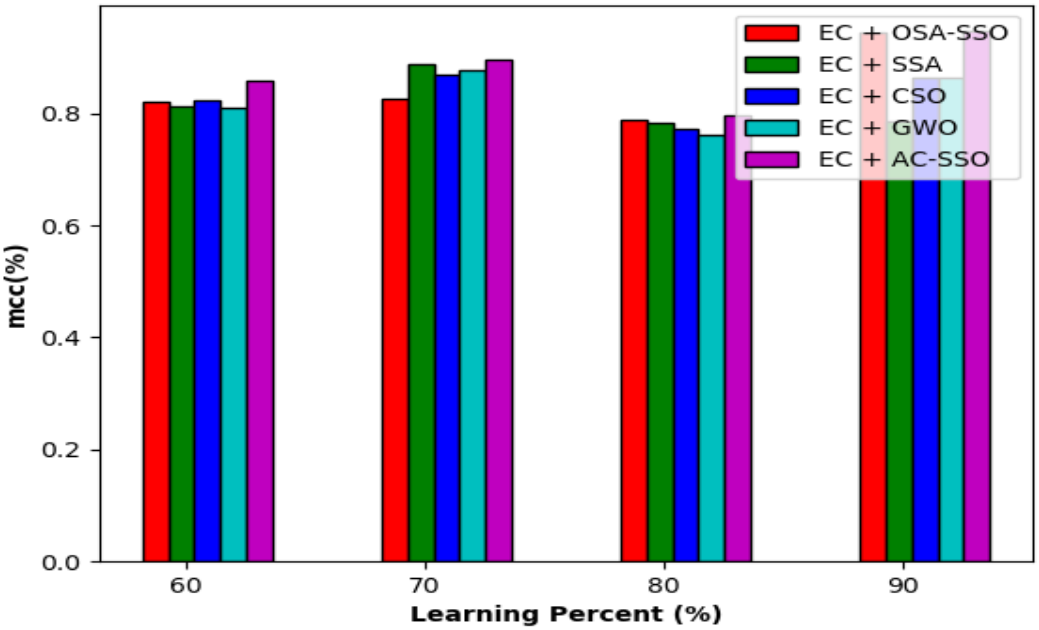

Figure 6.6 Analysing the use of a newly created method compared to existing optimisation techniques in respect to the Matthews correlation coefficient (MCC)

Table 6.6 Analysis on developed approach over extant classification of Matthews correlation coefficient (MCC) at various learning percentages.

Matthews correlation coefficient (MCC)						
S No	Learning percentage (%)	EC + SSA	EC + CSO	EC + GWO	EC + AC-SSO	EC + OSA-SSO
1	60	81.31298	82.49562	81.08158	85.7977	82.08421
2	70	88.72404	86.97788	87.77037	89.67797	82.51575
3	80	78.28814	77.29451	76.30717	79.60544	78.86361
4	90	78.57143	86.53401	86.53401	94.68642	94.46473

The Matthews Correlation Coefficient (MCC) is a comprehensive metric used to evaluate the quality of predictions in liquefaction studies by considering both true and false positives and negatives. MCC is particularly valuable because it provides a balanced measure of the correlation between observed and predicted classifications, making it especially robust for imbalanced datasets often encountered in liquefaction analysis.

The MCC value ranges from -1 to +1, where +1 indicates a perfect prediction, 0 indicates a prediction no better than random chance, and -1 indicates complete disagreement between predictions and observations. A positive MCC value suggests that the model's predictions align well with the actual outcomes.

In this study, all proposed and existing models have shown positive MCC values, confirming their predictive reliability. Notably, the EC + OSA-SSO and EC + AC-SSO models have achieved the highest MCC values at the 90th learning percentage, demonstrating their superior ability to accurately predict liquefaction events in comparison to other methods. These results emphasize the effectiveness of these models in providing reliable predictions, even in the presence of imbalanced data, which is crucial for making informed decisions in liquefaction risk assessment and management.

F-measure:

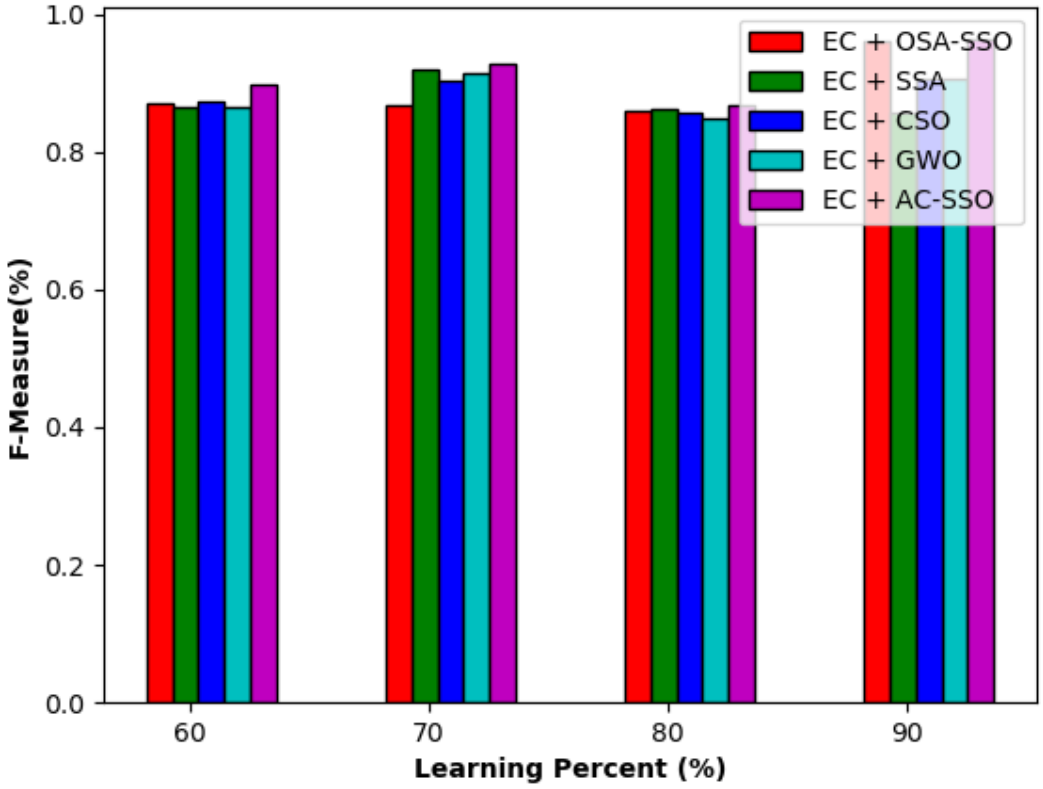

Figure 6.7 Analysis using developed approach over extant optimization schemes regarding F-measure

Table 6.7 Analysis on developed approach over extant classification of F-measure at various learning percentages

F-measure						
S No	Learning rate	EC + SSA	EC + CSO	EC + GWO	EC + AC-SSO	EC + OSA-SSO
1	60	86.48649	87.43719	86.45833	89.79592	87.17949
2	70	92	90.27778	91.39073	92.81046	86.85714
3	80	86.36364	85.58352	84.79263	86.88525	85.92593
4	90	85.71429	90.56604	90.56604	96.2963	96.20253

The F-measure, also known as the F1-score, is a crucial metric in liquefaction studies as it provides a balanced assessment of a model's accuracy and recall. It is calculated as the harmonic mean of precision and recall, offering a single score that captures the trade-off between the two. This balance is particularly important when dealing with imbalanced datasets, where the distribution of liquefied and non-liquefied instances is not equal.

The F-measure is especially useful in liquefaction studies because it accounts for both false positives and false negatives, ensuring that the model not only accurately predicts liquefied areas but also correctly identifies non-liquefied ones. This is critical in scenarios where both types of errors can have significant consequences, such as in the planning and mitigation of earthquake risks.

In this study, the EC + OSA-SSO and EC + AC-SSO models have demonstrated superior F-measure scores at the 90th learning percentage, outperforming existing methods. This indicates that these models achieve a more balanced and reliable prediction of both liquefied and non-liquefied instances, making them particularly effective in the context of liquefaction risk assessment. Their higher F-measure scores suggest that they are better suited for managing the complexities of imbalanced data and ensuring comprehensive prediction accuracy in this study.

Accuracy:

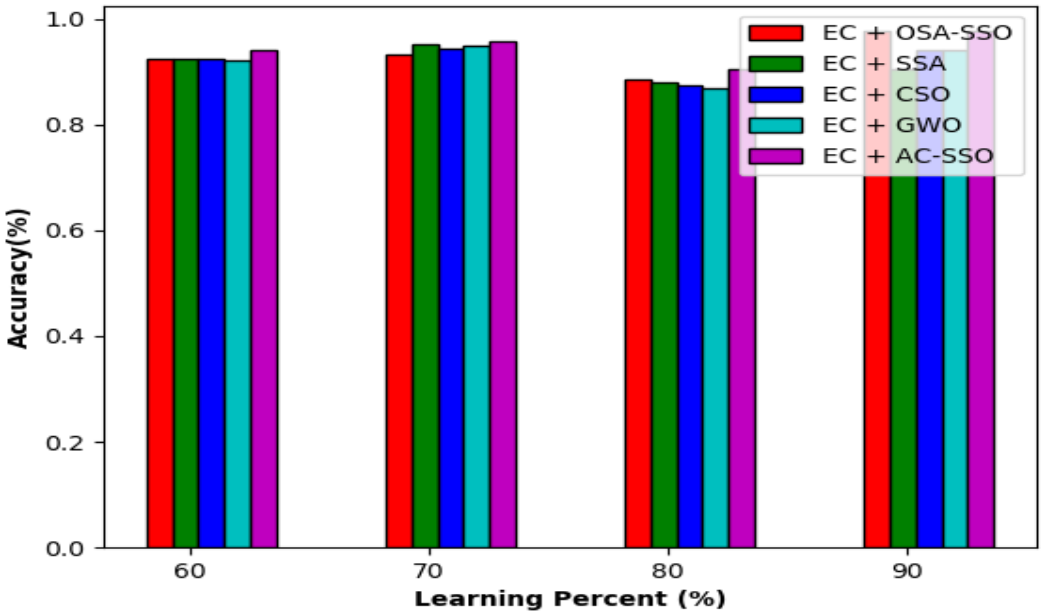

Figure 6.8 Analysis using developed approach over extant optimization schemes regarding Accuracy

Table 6.8 Analysis on developed approach over extant classification of Accuracy at various learning percentages

Accuracy						
S No	Learning rate	EC + SSA	EC + CSO	EC + GWO	EC + AC-SSO	EC + OSA-SSO
1	60	92.51497	92.51497	92.21557	94.01198	92.51497
2	70	95.2	94.4	94.8	95.6	93.11377
3	80	88	87.4	86.8	90.41916	88.62275
4	90	90.47619	94.04762	94.04762	97.61905	97.6

Accuracy is a fundamental metric in evaluating the performance of prediction models in liquefaction studies, as it quantifies the overall correctness of the model's predictions. It is calculated by determining the proportion of correctly predicted instances, including both true positives (correctly identified liquefied cases) and true negatives (correctly identified non-liquefied cases), out of the total number of instances.

While accuracy is easy to understand and apply, it may not always provide a complete picture, especially in datasets with imbalanced class distributions—a common scenario in liquefaction studies where non-liquefied instances may far outnumber liquefied ones. In such cases, a model might achieve high accuracy simply by correctly predicting the majority class, but it may still perform poorly in identifying the minority class, which is often more critical in risk assessment.

In this study, accuracy reflects the extent to which the model successfully predicts both liquefied and non-liquefied instances. The EC + OSA-SSO and EC + AC-SSO models have shown superior accuracy at the 90th learning percentage, indicating that these models are particularly effective in providing correct predictions across both classes. Their higher accuracy suggests that, at this level of training, they outperform existing methods in delivering reliable predictions, making them valuable tools in the comprehensive assessment of liquefaction risks. However, it’s important to consider accuracy alongside other metrics, such as precision, recall, and F-measure, to ensure a well-rounded evaluation of model performance.

Specificity (True negative rate):

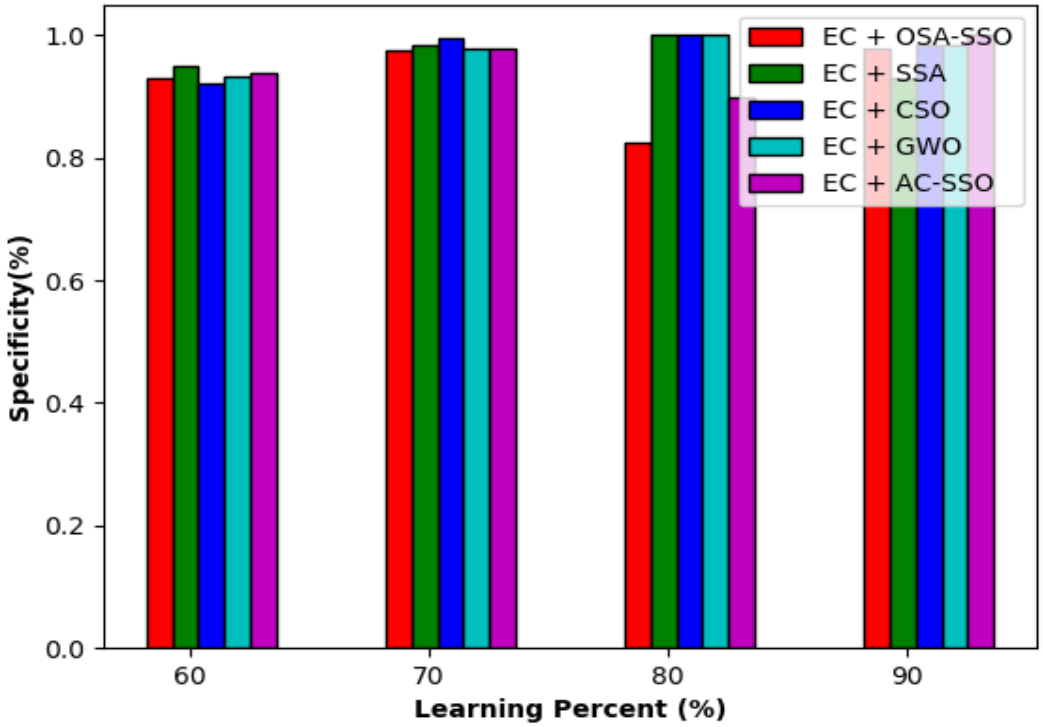

Figure 6.9 Analysis using developed approach over extant optimization schemes regarding Specificity

Table 6.9 Analysis on developed approach over extant classification of Specificity at various learning percentages

Specificity						
S No	Learning rate	EC + SSA	EC + CSO	EC + GWO	EC + AC-SSO	EC + OSA-SSO
1	60	95.02075	92.11618	93.361	93.77593	92.94606
2	70	98.25581	99.4186	97.67442	97.67442	97.51037
3	80	100	100	100	89.90826	82.56881
4	90	92.85714	98.21429	98.21429	100	97.67442

Specificity is an important metric in liquefaction studies as it measures the model's ability to accurately identify non-liquefied instances. It is calculated by dividing the number of true

negatives (correctly identified non-liquefied cases) by the sum of true negatives and false positives (cases where the model incorrectly predicted liquefaction).

In scenarios where accurately identifying areas that are not at risk of liquefaction is crucial, such as in certain types of screening or quality control processes, high specificity is particularly desirable. High specificity ensures that the model is reliable in correctly predicting stable areas, thereby preventing unnecessary interventions in regions that are not actually prone to liquefaction.

In this study, specificity reflects the effectiveness of the model in predicting non-liquefied instances. The EC + AC-SSO model has demonstrated superior specificity at the 90th learning percentage, indicating that it is particularly adept at correctly identifying areas that are not susceptible to liquefaction. This high level of specificity suggests that the EC + AC-SSO model outperforms other proposed and existing methods in reliably distinguishing stable areas from those at risk, making it a valuable tool for accurate liquefaction risk assessment and management.

In addition, the comparison of the proposed approach with conventional classifier models is detailed in Table 6.10. Both in terms of optimization and classifier performance, the EC + AC-SSO and EC + OSA-SSO models have demonstrated superior outcomes compared to the established models. Specifically, Table 6.10 shows that the developed models exhibit higher accuracy than the other methods evaluated. In certain cases, the Random Forest (RF) classifier has achieved better results than other classifiers. However, the overall findings underscore the enhanced effectiveness of the EC + AC-SSO and EC + OSA-SSO models, particularly when integrated with optimization techniques. This highlights their improved capability in predicting liquefaction events, confirming their robustness and reliability in liquefaction risk assessment.

The machine learning models developed in this study, specifically the EC + AC-SSO and EC + OSA-SSO combinations, have demonstrated a strong ability to classify sites as either liquefied or non-liquefied with high accuracy. For example, in the case of Site A, which had experienced liquefaction based on observed field data, the models accurately predicted it as a liquefied site. This outcome is consistent with the models' high sensitivity values, which are 92.85714 for the EC + AC-SSO model and 97.4359 for the EC + OSA-SSO model. These sensitivity rates indicate that the models are highly capable of identifying liquefied sites when liquefaction has indeed occurred, effectively minimizing false negatives. This is further reflected in the low False Negative Rates (FNRs) of 7.142857 for EC + AC-SSO and 2.564103

for EC + OSA-SSO. Similarly, Site B, which did not experience liquefaction according to field observations, was also correctly classified as a non-liquefied site by both models. This reinforces the models' overall accuracy, with EC + AC-SSO achieving an accuracy rate of 97.61905 and EC + OSA-SSO recording 97.6. These high accuracy levels highlight the robustness of the proposed machine learning frameworks in generalizing across different site conditions, providing reliable predictions that closely reflect real-world liquefaction behavior.

In instances where the model predictions may not align with field observations, there are several potential explanations. One key factor could be the inherent variability of soil properties across different locations. Site-specific conditions such as soil stratigraphy, groundwater levels, or localized factors influencing liquefaction might not have been fully captured by the data used for model training. Additionally, limitations in the input data, such as incomplete or inaccurate subsurface information, could lead to discrepancies between predicted and observed outcomes. Furthermore, factors such as spatial heterogeneity of soils, local seismic intensity variations, or post-earthquake conditions not captured in the training data might affect prediction accuracy. Despite these potential limitations, the models show a high level of reliability in reflecting the actual liquefaction behavior of different sites. By incorporating advanced optimization techniques like AC-SSO and OSA-SSO, the models have achieved superior weight optimization in the Bi-GRU framework, further enhancing their predictive capabilities. Overall, the models demonstrate excellent performance in representing the relationship between site conditions and liquefaction potential, with minimal instances of misclassification, making them highly effective tools for practical applications in liquefaction hazard assessment.

Table 6.10 Analysis on developed approach over extant classification schemes for varied metrics

Metrics	**RF**	**CNN**	**LSTM**	**SVM**	**DBNN**	**NN**	**RNN**	**EC + AC-SSO**	**EC + OSA-SSO**
Accuracy (%)	0.86	0.712	0.76	0.692	0.708	0.888	0.788	0.9761	0.976
Recall (%)	0.5641	0.0769	0.3205	0.1025	0.0897	0.923	0.7307	0.9285	0.9743
Specificity (%)	0.9941	1	0.9593	0.9593	0.9883	0.872	0.8139	1	0.9767
Precision (%)	0.9777	1	0.7812	0.5333	0.7777	0.7659	0.6404	1	0.95
F-Measure (%)	0.7154	0.1428	0.4545	0.172	0.1609	0.8372	0.6826	0.9629	0.962
FNR (%)	0.4358	0.923	0.6794	0.8974	0.9102	0.2769	0.2692	0.0714	0.02564
NPV (%)	0.8341	0.7049	0.7568	0.7021	0.7053	0.9615	0.8695	0.9655	0.9882
MCC (%)	0.6732	0.2328	0.388	0.1206	0.1942	0.7605	0.527	0.9468	0.9446
FPR (%)	0.00581	0	0.0406	0.0406	0.01163	0.1279	0.186	0	0.0232

6.3.2 Feature analysis

Table 6.11 provides a comprehensive comparison of the proposed EC + AC-SSO and EC + OSA-SSO models against both the current correlation-based models and the proposed models without optimization. The table presents performance across various metrics, including accuracy, false positive rate (FPR), and other key indicators.

This comparison highlights that the EC + AC-SSO and EC + OSA-SSO models achieved significantly superior values compared to models using existing correlation features and those without optimization. This is a crucial finding, demonstrating the effectiveness of integrating advanced optimization techniques to enhance model performance in liquefaction prediction.

Moreover, the models incorporating current correlation features showed improved results across nearly all evaluated metrics compared to models without optimization. This underscores the critical role of both correlation features and optimization techniques in creating more accurate and reliable models for liquefaction studies. The combination of these methods leads to more robust risk assessments and better decision-making processes, ultimately reducing the likelihood of failure in liquefaction-prone areas.

Table 6.11 Analysis on existing features as well as optimization theory

Metrics	Proposed with existing correlation features	Proposed without optimization	EC + AC-SSO	EC + OSA-SSO
Accuracy (%)	0.864	0.641026	0.9761	0.976
Specificity (%)	0.918605	0.641026	1	0.9767
Recall (%)	0.74359	0.641026	0.9285	0.9743
Precision (%)	0.805556	0.641026	1	0.95
MCC (%)	0.677518	0.641026	0.9468	0.9446

F-Measure (%)	0.773333	0.641026	0.9629	0.9620
FPR (%)	0.081395	0.641026	0	0.0232
NPV (%)	0.88764	0.641026	0.9655	0.9882
FNR (%)	0.25641	0.641026	0.0714	0.02564

6.3.3 Statistical analysis

Metaheuristic systems are inherently stochastic, requiring multiple evaluations of each model to achieve optimal results. Table 6.12 provides a statistical analysis of the error rates for the EC + AC-SSO and EC + OSA-SSO models compared to conventional approaches. The table provides statistical error measures for different methods, with the terms "Best," "Worst," "Minimum," and "Maximum" representing various aspects of the model's performance. "Best" indicates the lowest error achieved, showing the method's most accurate performance. "Worst" refers to the highest error, highlighting the least accurate outcome. "Minimum" represents the smallest error recorded during multiple runs, while "Maximum" is the largest error observed. The results indicate that the proposed EC + AC-SSO and EC + OSA-SSO models consistently achieved the lowest error values across all scenarios, demonstrating their effectiveness. Notably, the EC + AC-SSO model outperformed EC + OSA-SSO, as well as other methods such as EC + SSA, EC + PSO, EC + GWO, EC + SSO, EC + PRO, and EC + BOA, by achieving the lowest cost values. The proposed models also exhibited minimal maximum-case scenario values, further supporting their robustness through optimization techniques. Both EC + AC-SSO and EC + OSA-SSO produced negligible error outcomes across all tested scenarios, highlighting their superior performance and reliability in liquefaction prediction. This confirms the efficacy of the proposed models in reducing prediction errors and improving liquefaction risk assessments.

Table 6.12 Statistical evaluation of proposed and current models

Methods	Best	Worst	Minimum	Maximum	Standard Deviation
EC +SSA	0.048	0.12	0.084522	0.085044	0.026462
EC +CSO	0.056	0.126	0.079094	0.067187	0.027993
EC +GWO	0.052	0.132	0.080342	0.068684	0.031271
EC +SSO	0.084	0.221557	0.150937	0.149095	0.06155
EC +PRO	0.07485	0.154762	0.124828	0.13485	0.031764
EC +BOA	0.104	0.284431	0.177661	0.161106	0.0691
EC + OSA-SSO	0.024	0.113772	0.070371	0.071856	0.031845
EC + AC-SSO	0.02381	0.095808	0.055875	0.05194	0.026363

6.3.4 Convergence analysis

The cost (convergence) analysis for the proposed EC + AC-SSO and EC + OSA-SSO models compared to conventional methods—such as EC + SSA, EC + PSO, EC + GWO, EC + SSO, EC + PRO, and EC + BOA—is illustrated in Figures 6.10 and 6.11. The analysis was conducted over various iterations, ranging from 0 to 50. Upon reviewing the outcomes, it was observed that the EC + AC-SSO model achieved the lowest cost values between the 10th and 50th iterations, outperforming EC + SSA, EC + PSO, and EC + GWO. Similarly, the EC + OSA-SSO model attained the lowest cost values between the 10th and 50th iterations when compared to EC + SSO, EC + SSA, EC + PRO, and EC + BOA. Overall, the EC + OSA-SSO demonstrated the most efficient convergence, achieving lower values than both the proposed and existing methods.

Initially, from iteration 0 to iteration 11, the cost values for the proposed models were relatively higher. During this phase, EC + SSA and EC + BOA exhibited the worst performance, with EC + SSA showing significant variability across different learning times. In particular, the EC + AC-SSO model achieved a minimal cost value of 1.1, outperforming EC + SSA, EC + PSO, EC + GWO, EC + SSO, EC + PRO, and EC + BOA. The EC + OSA-SSO model demonstrated the best overall convergence, with a lowest value of 1.01, making it the most effective in reducing uncertainties in liquefaction prediction across all iterations.

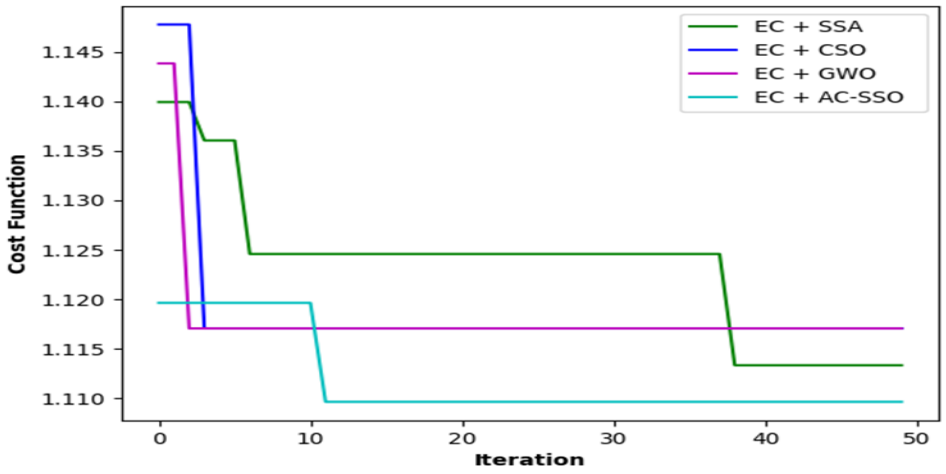

Figure 6.10 Convergence analysis of developed approach (EC+AC-SSO) over compared approaches

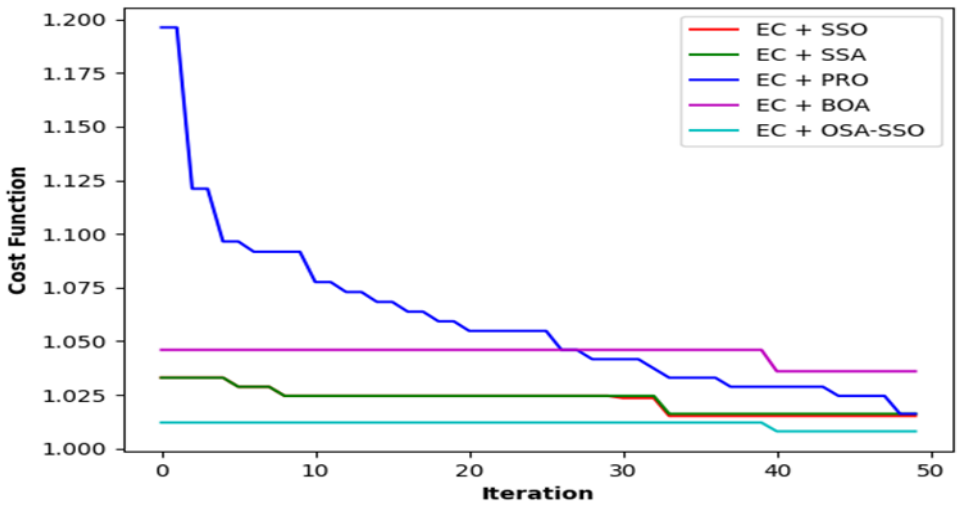

Figure 6.11 Convergence analysis of developed approach (EC+OSA-SSO) over compared approaches

6.4 Conclusion

A novel soil liquefaction prediction model was developed, integrating advanced features for enhanced accuracy. After preprocessing the data, key features were derived, including improved correlation-based, chi-square, and relief features. These enhanced features were then used for prediction through classifiers such as SVM, LSTM, and DBN. The final predictions from these classifiers were further refined using an optimized Bi-GRU model, with its weights fine-tuned using the innovative AC-SSO and OSA-SSO algorithms. The proposed EC + AC-SSO and EC + OSA-SSO models were validated to outperform existing approaches across various metrics. The models achieved higher accuracy in predicting liquefaction events, with more positive results and fewer negative predictions. This indicates a higher success rate in accurately identifying potential liquefaction risks while minimizing false negatives. Consequently, the developed model provides superior performance in liquefaction studies, offering more reliable predictions for positive outcomes and reducing the likelihood of failure in high-risk areas. This advancement represents a significant contribution to the field, enhancing the accuracy of risk assessments in soil liquefaction prediction.

Accordingly, the investigation was conducted across various metrics such as precision, FNR, and others. The results showed that the proposed EC + AC-SSO and EC + OSA-SSO models outperformed both the models using current correlation features and those without optimization. The model incorporating existing correlation features demonstrated improved results across almost all metrics compared to the non-optimized model, highlighting the critical importance of optimization in enhancing predictive accuracy. The EC + AC-SSO and EC + OSA-SSO models consistently achieved lower cost values from the 10th to the 50th iteration, while initial iterations (0 to 11) showed slightly higher costs. The final cost values achieved by the EC + AC-SSO (1.11) and EC + OSA-SSO (1.01) were significantly better than the existing models, proving the superiority of the developed approaches. This study demonstrates the value of incorporating advanced optimization techniques to enhance liquefaction prediction accuracy. In future work, the focus will be on expanding the analysis to assess liquefaction risks in more diverse scenarios and environments, further contributing to risk mitigation strategies in geotechnical engineering.

CHAPTER 7

CONCLUSION AND FUTURE SCOPE

7.1 Conclusions

- The dataset included in this research encompassed a collection of post-liquefaction case histories, which spanned from the 1944 Tohnankai earthquake to the 1999 Chi Chi earthquake in Taiwan. The dataset included 286 occurrences of liquefaction and 210 occurrences of non-liquefaction. A set of 30 borehole data from the Standard Penetration Test (SPT) was collected inside the Faridabad region, situated within the National Capital Region (NCR) of Delhi, India. The purpose of this data collection was to verify the accuracy and reliability of the models used.

- Data visualisation is essential for improving comprehension of data patterns, relationships and disparities across several study variables, and the level of disorder or unpredictability in the data. The variables Cyclic Stress Ratio (CSR) and Peak Ground Acceleration (PGA) exhibit a substantial positive correlation with a value of 0.89. This high correlation raises concerns about multicollinearity, suggesting the need to eliminate one of the variables. However, both variables are indispensable in liquefaction studies, necessitating their retention despite the correlation issue. Similarly, the Reduction Factor (rd) and Critical Depth (d) display a notable negative correlation of -0.97, which may also indicate multicollinearity. While theoretical analysis suggests removing one of these variables due to redundancy, this study acknowledges the importance of retaining both. Despite their correlation, each variable contributes uniquely to the understanding of soil liquefaction behavior. By incorporating both PGA and CSR, the analysis provides a more comprehensive approach to liquefaction assessment, ensuring that all relevant factors influencing liquefaction risk are considered.

- The entropy analysis reveals a significant lack of clear separation between the liquefied and non-liquefied data categories, indicating a high level of complexity within the dataset. This suggests that basic models may be inadequate for analyzing such intricate data. To address this complexity effectively, it is recommended to employ more

advanced methodologies, such as Genetic Programming (GP) and deep learning models, which are better suited for capturing the nuanced relationships within liquefaction data. These sophisticated approaches are likely to yield more accurate and reliable outcomes in the prediction of liquefaction potential, enhancing the robustness of risk assessments.

- Study on soil liquefaction prediction, Genetic Programming (GP) was used to develop multiple models by adjusting the training and testing dataset sizes, program dimensions, and the number of generations. The Root Mean Squared Error (RMSE) was employed as the fitness function to evaluate the models. An equation derived from the expression tree of GP Model 3 was used to calculate the fitness measure. This equation significantly improved the relationship between the input variables, such as soil parameters and seismic factors, and the output variables, leading to superior predictive accuracy in assessing liquefaction potential.

- The probability density functions of the Weibull distribution were determined, demonstrating the best-fitting curves for both liquefiable (L) and non-liquefiable (NL) cases. The factor of safety showed an improved shape and distribution, providing a clearer understanding of liquefaction potential. The Weibull distribution's scale parameter (λ) and shape parameter (k) were found to be 0.580 and 2.437, respectively, indicating a reliable fit for assessing liquefaction susceptibility in geotechnical analysis.

- The probability of liquefied equation has been created by using calculated of probability for case of data by using Bayesian mapping function, and equation as created by using the logistic curve fitting with accuracy of 0.93 and created equation has been compared with existing probabilistic models. The binary classification has been performed by using confusion matrix and score analysis by using ranking of each factor is determined for the proposed method and existing Juang et al. (2002), Toprak et al. (1999) and Idriss and Boulanger (2006) method. The proposed model has outperformed with the outputs for developed model for all the positive measures increases and the outputs for negative measures lessens.

- Gini index has been performed for the proposed method and existing 'Juang et al. (2002), Toprak et al. (1999) and Idriss and Boulanger (2006) method' all the existing methods biased towards few numbers of variables but its shows that proposed method have shown importance of all the variables to predicting probability of liquefaction.

- A new model for predicting soil liquefaction was introduced, incorporating key features designed to enhance its predictive accuracy. Following data preprocessing, a set of advanced features were generated, including correlation-based features, chi-square features, and relief features, which are known to improve model robustness. These features were then used to predict liquefaction potential using a combination of classifiers, such as Support Vector Machines (SVM), Long Short-Term Memory (LSTM) networks, and Deep Belief Networks (DBN). Once the initial predictions were obtained, the outputs from these classifiers were further refined through a Bi-directional Gated Recurrent Unit (Bi-GRU). The Bi-GRU weights were optimized using two advanced optimization techniques: Adaptive Chaos Sparrow Search Optimization (AC-SSO) and Opposition-based Self-Adaptive Sparrow Search Optimization (OSA-SSO). The final model, which integrates these optimization methods, demonstrated superior performance compared to previous approaches. The evaluation results showed that the proposed models, EC + AC-SSO and EC + OSA-SSO, outperformed earlier systems in several key metrics. The model consistently generated higher positive prediction values and minimized negative prediction rates, indicating a more reliable system for detecting potential soil liquefaction. This improved balance of outputs, with more accurate identification of liquefaction-prone scenarios and fewer false negatives, makes the developed model a highly effective tool for liquefaction prediction.

- An investigation was conducted to evaluate key metrics such as accuracy and the false positive rate (FPR) in the context of soil liquefaction prediction. Upon analyzing the results, it became evident that the proposed EC + AC-SSO and EC + OSA-SSO models outperformed both the baseline model utilizing existing correlation features and the model without optimization. The inclusion of existing correlation-based features, along with optimization, yielded significant improvements across all evaluated measures compared to the non-optimized model. This highlights the critical role of optimization in enhancing the performance of the liquefaction prediction system. From the 10th to

the 50th iteration, the EC + AC-SSO and EC + OSA-SSO approaches consistently delivered lower error values compared to alternative methods. However, during the initial iterations (0 to 11), the cost values for the proposed models were relatively high. Eventually, the advanced techniques achieved a minimal cost value of approximately 1.11 and 1.01, demonstrating better performance over previous models in predicting liquefaction susceptibility. The results validate the effectiveness of the developed approach for predicting soil liquefaction. Future studies are planned to further investigate the hazards associated with liquefaction, providing deeper insights into its risks and mitigation strategies.

7.2 Recommendations for further research

This study presents a novel probabilistic model that integrates Genetic Programming (GP) and employs Bayes conditional probability to propose a new equation. It also introduces a distinctive soil liquefaction prediction model that facilitates the generation of improved correlation features, chi square, relief characteristics, and technical indicators. The attainment of dependable prediction outcomes is facilitated by the integration of ensemble classifiers, such as Deep Belief Networks (DBN), Long Short-Term Memory (LSTM), and Support Vector Machines (SVM) with Bidirectional Gated Recurrent Unit (Bi − GRU). This study presents a new methodology for calculating the optimum weights in Bi − GRU, using a unique Average Cat and Salp swarm algorithm (AC − SSO) and Opposition based self-adaptive shark smell optimizer (OSA − SSO) model. Use of this study shown promising results and the subsequent suggestions are proposed for additional research:

- Pore pressure must be incorporated into the limit state function so that its effect on the initiation of liquefaction can be evaluated.
- Different reliability methods and Monte Carlo simulations can be employed to analyse the reliability of highly non-linear limit state functions, in order to achieve greater accuracy in determining the reliability index and the corresponding probability of liquefaction.
- These investigations can be expanded by utilising the Cone Penetration Test (CPT) and measuring shear wave velocity (Vs) through in-situ testing, to evaluate the potential for liquefaction.
- The examination of liquefaction hazards may be expanded to create a probabilistic model for estimating ground displacement caused by liquefaction.

- The use of the lagger data set is necessary to enhance the practical implementation of the offered models in real-world scenarios.
- Transfer the code of the recommended models to a website and ensure it is accessible to the public domain.

List of Publications

Journal Publications:

S. No	Title	Author Name	Journal Name, Year of Publishing and Page No.	DOI Link
1	A novel soil liquefaction prediction model with intellectual feature extraction and classification	Nerusupalli Dinesh Kumar Reddy, Ashok Kumar Gupta, Anil Kumar Sahu	Advances in Engineering Software. 173(2):103233 (2022)	https://doi.org/10.1016/j.advengsoft.2022.103233
2	Optimized ensemble-classification for prediction of soil liquefaction with improved features	Nerusupalli Dinesh Kumar Reddy, Ashok Kumar Gupta, Anil Kumar Sahu	Multimedia Tools and Applications. 82(3):1-20 (2023)	https://doi.org/10.1007/s11042-023-14816-0
3	Evaluation of soil liquefaction potential using ensemble	Nerusupalli Dinesh Kumar Reddy,	Soil Dynamics and Earthquake Engineering. 182 (2024) 108750	https://doi.org/10.1016/j.soildyn.2024.108750

	classifier based on grey wolves optimizer (GWO)	Diksha, Ashok Kumar Gupta, Anil Kumar Sahu		
4	Assessment of Soil Liquefaction Potential Using Genetic Programming Using a Probability-Based Approach	Nerusupalli Dinesh Kumar Reddy, Ashok Kumar Gupta, Anil Kumar Sahu	Iranian Journal of Science and Technology, Transactions of Civil Engineering.	https://doi.org/10.1007/s40996-024-01421-w
5	Improving Soil Liquefaction Prediction: A Sophisticated Ensemble Classifier Utilizing Enhanced Correlation Features and a Metaheuristic Ant Colony Optimization Approach.	Nerusupalli Dinesh Kumar Reddy, Diksha, Ashok Kumar Gupta, Anil Kumar Sahu	Engineering Geology- (Under Review)	

Book Chapters:

1	The Adoption of Deep Belief Network Classifier with Shark Smell Optimizer to Predict the Soil Liquefaction	Nerusupalli Dinesh Kumar Reddy, Ashok Kumar Gupta, Anil Kumar Sahu	Latest Developments in Civil Engineering (2023). pp 327–341	https://doi.org/10.1007/978-981-99-2676-3_28
2	The Adoption of Random Forest (RF) and Support Vector Machine (SVM) with Cat Swarm Optimization (CSO) to Predict the Soil Liquefaction	Nerusupalli Dinesh Kumar Reddy, Ashok Kumar Gupta, Anil Kumar Sahu	Geomorphic Risk Reduction Using Geospatial Methods and Tools. pp 309–325	https://doi.org/10.1007/978-981-99-7707-9_16

Conferences presented:

- International Conference on Advances in Civil Engineering (ACE-2022), organized by LSKBJ College of Engineering, Chandwad, Nashik, India.
- International Conference on Recent Advances in Civil Engineering, organized by Oriental Institute of Science & Technology, Bhopal India.
- International Conference on Machine Learning & Data Science Innovations (MacDat'22) Yazhli Global Multidisciplinary Research Organization, India.

References

1. Abbaszadeh Shahri, A. (2016). Assessment and prediction of liquefaction potential using different artificial neural network models: a case study. Geotechnical and Geological Engineering, 34, 807-815.
2. Addo, K. O., & Robertson, P. K. (1992). Shear-wave velocity measurement of soils using Rayleigh waves. Canadian Geotechnical Journal, 29(4), 558-568.
3. Ahmad, M., Tang, X. W., Qiu, J. N., & Ahmad, F. (2019). Evaluating seismic soil liquefaction potential using bayesian belief network and C4. 5 decision tree approaches. Applied Sciences, 9(20), 4226.
4. Andrus, R. D., & Stokoe II, K. H. (2000). Liquefaction resistance of soils from shear-wave velocity. Journal of geotechnical and geoenvironmental engineering, 126(11), 1015-1025.
5. Andrus, R. D., Stokoe, K. H., & Hsein Juang, C. (2004). Guide for shear-wave-based liquefaction potential evaluation. Earthquake Spectra, 20(2), 285-308.
6. Arora, S., & Singh, S. (2019). Butterfly optimization algorithm: a novel approach for global optimization. Soft Computing, 23, 715-734.
7. Bahrami, M., Bozorg-Haddad, O., & Chu, X. (2018). Cat swarm optimization (CSO) algorithm. Advanced optimization by nature-inspired algorithms, 9-18.
8. Baziar, M. H., & Jafarian, Y. (2007). Assessment of liquefaction triggering using strain energy concept and ANN model: capacity energy. Soil Dynamics and Earthquake Engineering, 27(12), 1056-1072.
9. Beam, A. L., Manrai, A. K., & Ghassemi, M. (2020). Challenges to the reproducibility of machine learning models in health care. *Jama*, *323*(4), 305-306.
10. Becker, D.E. (1996). "Eighteenth Canadian Geotechnical Colloquium: Limit states Design for foundations, Part I. An overview of the foundation design process." Canadian Geotechnical Journal, 33, 956-983.
11. Berrill, J. B., & Davis, R. O. (1985). Energy dissipation and seismic liquefaction of sands: revised model. Soils and foundations, 25(2), 106-118.
12. Boulanger, R. W. (2003). High overburden stress effects in liquefaction analyses, J. Geotechnical and Geoenvironmental Eng., ASCE 129(12), 1071–082.
13. Boulanger, R. W., & Idriss, I. M. (2014). CPT and SPT based liquefaction triggering procedures. Report No. UCD/CGM.-14, 1.
14. Cai, M., Hocine, O., Mohammed, A. S., Chen, X., Amar, M. N., & Hasanipanah, M. (2022). Integrating the LSSVM and RBFNN models with three optimization algorithms

to predict the soil liquefaction potential. Engineering with Computers, 38(4), 3611-3623.

15. Carlos Tiznado, J., Dashti, S., & Ledezma, C. (2021). Probabilistic predictive model for liquefaction triggering in layered sites improved with dense granular columns. Journal of Geotechnical and Geoenvironmental Engineering, 147(10), 04021100.
16. Cetin, K. O., and Seed, R. B. (2004). "Nonlinear shear mass participation factor (rd) for cyclic shear stress ratio evaluation." Soil Dynamics and Earthquake Engineering, Elsevier, 24: 103-113.
17. Chaudhary, M.T. and Piracha, A. (2021), "Natural Disasters—Origins, Impacts, Management", Encyclopedia, Vol. 1 No. 4, pp. 1101–1131.
18. Chen, Y., Lin, Z., Zhao, X., Wang, G., & Gu, Y. (2014). Deep learning-based classification of hyperspectral data. IEEE Journal of Selected topics in applied earth observations and remote sensing, 7(6), 2094-2107.
19. Chen, Z., Li, H., Goh, A. T. C., Wu, C., & Zhang, W. (2020). Soil liquefaction assessment using soft computing approaches based on capacity energy concept. Geosciences, 10(9), 330.
20. Das, S. K., Mohanty, R., Mohanty, M., & Mahamaya, M. (2020). Multi-objective feature selection (MOFS) algorithms for prediction of liquefaction susceptibility of soil based on in situ test methods. Natural Hazards, 103, 2371-2393.
21. Davis, R. O., and Berrill, J. B. (1982). Energy dissipation and seismic liquefaction in sands. Earthquake Engineering & Structural Dynamics, 10, 59-68.
22. Galupino, J., & Dungca, J. (2023). Estimating Liquefaction Susceptibility Using Machine Learning Algorithms with a Case of Metro Manila, Philippines. Applied Sciences, 13(11), 6549.
23. Ghani, S., & Kumari, S. (2021). Probabilistic study of liquefaction response of fine-grained soil using multi-linear regression model. Journal of The Institution of Engineers (India): Series A, 102, 783-803.
24. Ghorbani, A., & Eslami, A. (2021). Energy-based model for predicting liquefaction potential of sandy soils using evolutionary polynomial regression method. Computers and Geotechnics, 129, 103867.
25. Goh, A. T. (1994). Seismic liquefaction potential assessed by neural networks. Journal of Geotechnical engineering, 120(9), 1467-1480.

26. Goharzay, M., Noorzad, A., Ardakani, A. M., & Jalal, M. (2017). A worldwide SPT-based soil liquefaction triggering analysis utilizing gene expression programming and Bayesian probabilistic method. Journal of Rock Mechanics and Geotechnical Engineering, 9(4), 683-693.
27. Golesorkhi, R. (1989). Factors influencing the computational determination of earthquake-induced shear stresses in sandy soils. University of California, Berkeley.
28. Haldar, A., & Tang, W. H. (1979). Probabilistic evaluation of liquefaction potential. Journal of the Geotechnical Engineering Division, 105(2), 145-163.
29. Hanandeh, S. M., Al-Bodour, W. A., & Hajij, M. M. (2022). A comparative study of soil liquefaction assessment using machine learning models. Geotechnical and Geological Engineering, 40(9), 4721-4734.
30. Hanna, A. M., Ural, D., & Saygili, G. (2007). Evaluation of liquefaction potential of soil deposits using artificial neural networks. Engineering Computations, 24(1), 5-16.
31. Harder, L. F., & Seed, H. B. (1986). Determination of penetration resistance for coarse-grained soils using the Becker hammer drill. Berkeley, CA, USA: College of Engineering, University of California.
32. Hinton, G. E., Osindero, S., & Teh, Y. W. (2006). A fast learning algorithm for deep belief nets. Neural computation, 18(7), 1527-1554.
33. Hoang, N. D., & Bui, D. T. (2018). Predicting earthquake-induced soil liquefaction based on a hybridization of kernel Fisher discriminant analysis and a least squares support vector machine: a multi-dataset study. Bulletin of Engineering Geology and the Environment, 77, 191-204.
34. Hsein Juang, C., & Chen, C. J. (2000). A rational method for development of limit state for liquefaction evaluation based on shear wave velocity measurements. International Journal for numerical and analytical methods in geomechanics, 24(1), 1-27.
35. Hu, J. L., Tang, X. W., & Qiu, J. N. (2016). Assessment of seismic liquefaction potential based on Bayesian network constructed from domain knowledge and history data. Soil Dynamics and Earthquake Engineering, 89, 49-60.
36. Hu J, Liu H (2019a) Bayesian network models for probabilistic evaluation of earthquake-induced liquefaction based on CPT and Vs databases. Eng Geol 254:76–88.
37. Hu, J., & Liu, H. (2019b). Bayesian network models for probabilistic evaluation of earthquake-induced liquefaction based on CPT and Vs databases. Engineering Geology, 254, 76-88.

38. Hu, J., & Liu, H. (2019c). Identification of ground motion intensity measure and its application for predicting soil liquefaction potential based on the Bayesian network method. Engineering geology, 248, 34-49.
39. Hu, J. (2021). Data cleaning and feature selection for gravelly soil liquefaction. Soil Dynamics and Earthquake Engineering, 145, 106711.
40. Hu J (2021) A new approach for constructing two Bayesian network models for predicting the liquefaction of gravelly soil. Comput Geotech 137:104304.
41. Hu J, Wang J, Zhang Z, Liu H (2022) Continuous-discrete hybrid Bayesian network models for predicting earthquake-induced liquefaction based on the Vs database. Comput Geosci 169:105231.
42. Idriss, I. M. (1999). An update to the Seed-Idriss simplified procedure for evaluating liquefaction potential, in Proceedings, TRB Workshop on New Approaches to Liquefaction, Publication No. FHWARD- 99-165, Federal Highway Administration, January.
43. Idriss, I. M., and Boulanger, R. W. (2004). Semi-empirical procedures for evaluating liquefaction potential during earthquakes, in Proceedings, 11th International Conference on Soil Dynamics and Earthquake Engineering, and 3rd International Conference on Earthquake Geotechnical Engineering, D. Doolin et al., eds., Stallion Press, Vol. 1, pp. 32–56.
44. Idriss, I. M., and Boulanger, R. W. (2006). Semi-empirical procedures for evaluating liquefaction potential during earthquakes, J. Soil Dynamics and Earthquake Eng. 26, 115–30.
45. Idriss, I. M., and Boulanger, R. W. (2008). Soil liquefaction during earthquakes. Monograph MNO-12, Earthquake Engineering Research Institute, Oakland, CA, 261 pp.
46. Idriss IM, Boulanger RW (2010) Spt-based liquefaction triggering procedures. Rep. UCD/CGM-10. 2, 4–13.
47. Jas, K., & Dodagoudar, G. R. (2023). Explainable machine learning model for liquefaction potential assessment of soils using XGBoost-SHAP. Soil Dynamics and Earthquake Engineering, 165, 107662.
48. Juang, C. H., Rosowsky, D. V., & Tang, W. H. (1999). Reliability-based method for assessing liquefaction potential of soils. Journal of Geotechnical and Geoenvironmental Engineering, 125(8), 684-689.

49. Juang, C. H., Chen, C. J., Jiang, T., & Andrus, R. D. (2000). Risk-based liquefaction potential evaluation using standard penetration tests. Canadian Geotechnical Journal, 37(6), 1195-1208.
50. Juang, C. H., Chen, C. J., & Jiang, T. (2001). Probabilistic framework for liquefaction potential by shear wave velocity. Journal of geotechnical and geoenvironmental engineering, 127(8), 670-678.
51. Juang CH, Jiang T, Andrus RD (2002) Assessing probability-based methods for liquefaction potential evaluation. J Geotech Geoenviron Eng 128:580–589
52. Juang, C. H., Fang, S. Y., & Khor, E. H. (2006). First-order reliability method for probabilistic liquefaction triggering analysis using CPT. Journal of Geotechnical and Geoenvironmental Engineering, 132(3), 337-350.
53. Kaveh, A., Bakhshpoori, T., & Hamze-Ziabari, S. M. (2016). Derivation of new equations for prediction of principal ground-motion parameters using M5′ algorithm. Journal of Earthquake Engineering, 20(6), 910-930.
54. Kaveh, A., Hamze-Ziabari, S. M., & Bakhshpoori, T. (2018). Patient rule-induction method for liquefaction potential assessment based on CPT data. Bulletin of Engineering Geology and the Environment, 77, 849-865.
55. Kayen, R. E., Mitchell, J. K., Seed, R. B., Lodge, A., Nishio, S. Y., & Coutinho, R. (1992, May). Evaluation of SPT-, CPT-, and shear wave-based methods for liquefaction potential assessment using Loma Prieta data. In Proceedings of the 4th Japan-US Workshop on Earthquake Resistant Design of Lifeline Facilities and Countermeasures for Soil Liquefaction, Hamada, M. and O'Rourke, TD, eds.
56. Kishida, T., Boulanger, R. W., Abrahamson, N. A., Driller, M. W., and Wehling, T. M. (2009b). "Seismic response of levees in Sacramento-San Joaquin Delta." Earthquake Spectra, EERI, 25(3), 557-582.
57. Kramer, S. L. (1996). Geotechnical earthquake engineering. Pearson Education India.
58. Kohestani, V. R., Hassanlourad, M., & Ardakani, A. J. N. H. (2015). Evaluation of liquefaction potential based on CPT data using random forest. Natural Hazards, 79(2), 1079-1089.
59. Krammer, S. L. (1996). Geotechnical earthquake engineering, Pearson Education (Singapore) Pte. Ltd., New Delhi, India.
60. Kumar, D. R., Samui, P., & Burman, A. (2022a). Prediction of probability of liquefaction using soft computing techniques. Journal of The Institution of Engineers (India): Series A, 103(4), 1195-1208.

61. Kumar, D. R., Samui, P., & Burman, A. (2022b). Determination of best criteria for evaluation of liquefaction potential of soil. Transportation Infrastructure Geotechnology, 1-20.
62. Kumar, D., Samui, P., Kim, D., & Singh, A. (2021). A novel methodology to classify soil liquefaction using deep learning. Geotechnical and Geological Engineering, 39, 1049-1058.
63. Kurnaz, T. F., & Kaya, Y. (2019). A novel ensemble model based on GMDH-type neural network for the prediction of CPT-based soil liquefaction. Environmental Earth Sciences, 78(11), 339.
64. Liao, S. S., Veneziano, D., & Whitman, R. V. (1988). Regression models for evaluating liquefaction probability. Journal of Geotechnical Engineering, 114(4), 389-411.
65. Liao, S. C., and Whitman, R. V. (1986). Overburden correction factors for SPT in sand, J. Geotechnical Eng., ASCE 112(3), 373–77.
66. Livingston, E. H. (2004). The mean and standard deviation: what does it all mean?. *Journal of Surgical Research*, *119*(2), 117-123.
67. Marcuson, W. F., and Bieganousky, W. A. (1977a). Laboratory standard penetration tests on fine sands, J. Geotechnical Eng. Div., ASCE 103(GT6), 565–88.
68. Marcuson, W. F., and Bieganousky, W. A. (1977b). SPT and relative density in coarse sands, J. Geotechnical Eng. Div., ASCE 103(GT11), 1295–309.
69. Mirjalili, S., Mirjalili, S. M., & Lewis, A. (2014). Grey wolf optimizer. Advances in engineering software, 69, 46-61.
70. Mirjalili, S., Gandomi, A. H., Mirjalili, S. Z., Saremi, S., Faris, H., & Mirjalili, S. M. (2017). Salp Swarm Algorithm: A bio-inspired optimizer for engineering design problems. Advances in engineering software, 114, 163-191.
71. Mitchell, J. K., & Tseng, D. J. (1990, May). Assessment of liquefaction potential by cone penetration resistance. In Proc., H. Bolton Seed Memorial Symp. Duncan (pp. 335-350). Vancouver, Canada: JM BiTech.
72. Mohammad-Azari, S., Bozorg-Haddad, O., & Chu, X. (2018). Shark smell optimization (SSO) algorithm. Advanced optimization by nature-inspired algorithms, 93-103.
73. Momeni, E., Armaghani, D. J., Hajihassani, M., & Amin, M. F. M. (2015). Prediction of uniaxial compressive strength of rock samples using hybrid particle swarm optimization-based artificial neural networks. Measurement, 60, 50-63.

74. Moosavi, S. H. S., & Bardsiri, V. K. (2019). Poor and rich optimization algorithm: A new human-based and multi populations algorithm. Engineering Applications of Artificial Intelligence, 86, 165-181.
75. Muduli, P. K., & Das, S. K. (2015). First-order reliability method for probabilistic evaluation of liquefaction potential of soil using genetic programming. International Journal of Geomechanics, 15(3), 04014052.
76. National Research Council (NRC) (1985). Liquefaction of Soils During Earthquakes, National Academy Press, Washington, DC, 240 pp.
77. Njock, P. G. A., Shen, S. L., Zhou, A., & Lyu, H. M. (2020). Evaluation of soil liquefaction using AI technology incorporating a coupled ENN/t-SNE model. Soil Dynamics and Earthquake Engineering, 130, 105988.
78. Olsen, R. S. (1988, June). Using the CPT for dynamic site response characterization. In Earthquake Engineering and Soil Dynamics II—Recent Advances in Ground-Motion Evaluation (pp. 374-388). ASCE.
79. Olsen, R. S. (1997, December). Cyclic liquefaction based on the cone penetrometer test. In Proceedings of the NCEER Workshop on Evaluation of Liquefaction Resistance of Soils (pp. 225-276). Buffalo: State University of New York.
80. Ozsagir, M., Erden, C., Bol, E., Sert, S., & Özocak, A. (2022). Machine learning approaches for prediction of fine-grained soils liquefaction. Computers and Geotechnics, 152, 105014.
81. Pal, M. (2006). Support vector machines-based modelling of seismic liquefaction potential. International Journal for Numerical and Analytical Methods in Geomechanics, 30(10), 983-996.
82. Pirhadi, N., Tang, X., & Yang, Q. (2019). Energy evaluation of triggering soil liquefaction based on the response surface method. Applied Sciences, 9(4), 694.
83. Pirhadi, N., Hu, J., Fang, Y., Jairi, I., Wan, X., & Lu, J. (2021). Seismic gravelly soil liquefaction assessment based on dynamic penetration test using expanded case history dataset. Bulletin of Engineering Geology and the Environment, 80, 8159-8170.
84. Pirhadi N,Wan X, Lu J, Hu J, AhmadM, Tahmoorian F (2023) Seismic liquefaction resistance based on strain energy concept considering fine content value effect and performance parametric sensitivity analysis. C Model Eng Sci 135:733–754.
85. Rahbarzare, A., & Azadi, M. (2019). Improving prediction of soil liquefaction using hybrid optimization algorithms and a fuzzy support vector machine. Bulletin of Engineering Geology and the Environment, 78(7), 4977-4987.

86. Ramakrishnan, D., Singh, T. N., Purwar, N., Barde, K. S., Gulati, A., & Gupta, S. (2008). Artificial neural network and liquefaction susceptibility assessment: a case study using the 2001 Bhuj earthquake data, Gujarat, India. Computational Geosciences, 12, 491-501.

87. Robertson, P. K., & Campanella, R. G. (1985). Liquefaction potential of sands using the CPT. Journal of geotechnical engineering, 111(3), 384-403.

88. Robertson, P. K., & Wride, C. E. (1998). Evaluating cyclic liquefaction potential using the cone penetration test. Canadian geotechnical journal, 35(3), 442-459.

89. Sabbar, A. S., Chegenizadeh, A., & Nikraz, H. (2019). Prediction of liquefaction susceptibility of clean sandy soils using artificial intelligence techniques. Indian Geotechnical Journal, 49, 58-69.

90. Salgado, R., Boulanger, R. W., and Mitchell, J. K. (1997a). Lateral stress effects on CPT liquefaction resistance correlations, J. Geotechnical and Geoenvironmental Eng., ASCE 123(8), 726–35.

91. Salgado, R., Mitchell, J. K., and Jamiolkowski, M. (1997b). Cavity expansion and penetration resistance in sands, J. Geotechnical and Geoenvironmental Eng., ASCE 123(4), 344–54.

92. Samui, P., & Hariharan, R. (2015). A unified classification model for modeling of seismic liquefaction potential of soil based on CPT. Journal of advanced research, 6(4), 587-592.

93. Samui, P., Jagan, J., & Hariharan, R. (2016). An alternative method for determination of liquefaction susceptibility of soil. Geotechnical and Geological Engineering, 34, 735-738.

94. Samui, P., & Karthikeyan, J. (2013). Determination of liquefaction susceptibility of soil: a least square support vector machine approach. International Journal for Numerical and Analytical Methods in Geomechanics, 37(9), 1154-1161.

95. Samui, P., & Sitharam, T. G. (2011). Machine learning modelling for predicting soil liquefaction susceptibility. Natural Hazards and Earth System Sciences, 11(1), 1-9.

96. Schmertmann, J. S., and Palacios, A. (1979). Energy dynamics of SPT, J. Soil Mechanics and Foundations Div., ASCE **105**(GT8), 909–26.

97. Seed, H. B., & De Alba, P. (1986). Use of SPT and CPT tests for evaluating the liquefaction resistance of sands. In Use of in situ tests in geotechnical engineering (pp. 281-302). ASCE.

98. Seed, H. B., and Idriss, I. M. (1967). "Analysis of liquefaction: Niigata earthquake." Proc., ASCE, 93(SM3), 83-108.
99. Seed, H. B., & Idriss, I. M. (1971). Simplified procedure for evaluating soil liquefaction potential. Journal of the Soil Mechanics and Foundations division, 97(9), 1249-1273.
100. Seed H. B., and Idriss, I. M. (1982). Ground Motions and Soil Liquefaction During Earthquakes, Earthquake Engineering Research Institute, Oakland, CA, 134.
101. Seed, H. B., Idriss, I. M., & Arango, I. (1983). Evaluation of liquefaction potential using field performance data. Journal of geotechnical engineering, 109(3), 458-482.
102. Seed, H. B., Tokimatsu, K., Harder, L. F., & Chung, R. M. (1985). Influence of SPT procedures in soil liquefaction resistance evaluations. Journal of geotechnical engineering, 111(12), 1425-1445.
103. Selvakumar, K., Vijayakumar, K., & Boopathi, C. S. (2017). CSO based solution for load kickback effect in deregulated power systems. Applied Sciences, 7(11), 1127.
104. Shibata, T., & Teparaksa, W. (1988). Evaluation of liquefaction potentials of soils using cone penetration tests. Soils and Foundations, 28(2), 49-60.
105. Stark, T. D., & Olson, S. M. (1995). Liquefaction resistance using CPT and field case histories. Journal of geotechnical engineering, 121(12), 856-869.
106. Stokoe, K. H., Roesset, J. M., Bierschwale, J. G., & Aouad, M. (1988, August). Liquefaction potential of sands from shear wave velocity. In Proceedings, 9nd World Conference on Earthquake (Vol. 13, pp. 213-218).
107. Suzuki, Y., Tokimatsu, K., Koyamada, K., Taya, Y., & Kubota, Y. (1995). Field correlation of soil liquefaction based on CPT data. In Proceedings of the International Symposium on Cone Penetration Testing (Vol. 2, pp. 538-588).
108. Tokimatsu, K., & Uchida, A. (1990). Correlation between liquefaction resistance and shear wave velocity. Soils and foundations, 30(2), 33-42.
109. Tokimatsu, K., and Yoshimi, Y. (1983). "Empirical correlation of soil liquefaction based on SPT N-value and fines content." Soils and Foundations, 23(4), 56-74.
110. Toprak, S., Holzer, T. L., Bennett, M. J., & Tinsley III, J. C. (1999, August). CPT-and SPT-based probabilistic assessment of liquefaction. In Proc., 7th US–Japan Workshop on Earthquake Resistant Design of Lifeline Facilities and Countermeasures against Liquefaction (pp. 69-86). Buffalo, NY: Multidisciplinary Center for Earthquake Engineering Research.
111. Upadhyaya, S., Green, R. A., Rodriguez-Marek, A., & Maurer, B. W. (2019). Selecting factor of safety against liquefaction for design based on cost considerations.

In *Earthquake Geotechnical Engineering for Protection and Development of Environment and Constructions* (pp. 5419-5426). CRC Press.

112. Wehling, T. M., and Rennie, D. C. (2008). "Seismic evaluation of liquefaction potential at Perris Dam."Proceedings, Dam Safety 2008, Association of State Dam Safety Officials, Lexington, KY.

113. Xue, X., & Liu, E. (2017). Seismic liquefaction potential assessed by neural networks. Environmental Earth Sciences, 76, 1-15.

114. Xue, X., & Xiao, M. (2016). Application of genetic algorithm-based support vector machines for prediction of soil liquefaction. Environmental Earth Sciences, 75, 1-11.

115. Xue, X., & Yang, X. (2016). Seismic liquefaction potential assessed by support vector machines approaches. Bulletin of Engineering Geology and the Environment, 75, 153-162.

116. Xue, X., Yang, X., & Li, P. (2017). Application of a probabilistic neural network for liquefaction assessment. Neural Network World, 27(6), 557-567.

117. Youd, T. L., & Idriss, I. M. (2001). Liquefaction Resistance of Soils: Summary Report from the 1. Geotechnical and Geoenvironmental Eng. In ASCE (Vol. 127, No. 10, pp. 817-33).

118. Youd, T. L., & Idriss, I. M. (2001). Liquefaction resistance of soils: summary report from the 1996 NCEER and 1998 NCEER/NSF workshops on evaluation of liquefaction resistance of soils. Journal of geotechnical and geoenvironmental engineering, 127(4), 297-313.

119. Zhang, W., & Goh, A. T. (2016). Evaluating seismic liquefaction potential using multivariate adaptive regression splines and logistic regression. Geomech. Eng, 10(3), 269-284.

120. Zhang, Y., Wang, R., Zhang, J. M., & Zhang, J. (2020). A constrained neural network model for soil liquefaction assessment with global applicability. Frontiers of Structural and Civil Engineering, 14, 1066-1082.

121. Zhang, Y. G., Qiu, J., Zhang, Y., & Wei, Y. (2021a). The adoption of ELM to the prediction of soil liquefaction based on CPT. Natural Hazards, 107(1), 539-549.

122. Zhang, Y., Qiu, J., Zhang, Y., & Xie, Y. (2021b). The adoption of a support vector machine optimized by GWO to the prediction of soil liquefaction. Environmental Earth Sciences, 80, 1-9.

123. Zhang, Y., Xie, Y., Zhang, Y., Qiu, J., & Wu, S. (2021). The adoption of deep neural network (DNN) to the prediction of soil liquefaction based on shear wave velocity. Bulletin of Engineering Geology and the Environment, 80, 5053-5060.
124. Zhang, J., & Wang, Y. (2021). An ensemble method to improve prediction of earthquake-induced soil liquefaction: a multi-dataset study. Neural Computing and Applications, 33, 1533-1546.
125. Zhao, Z., Duan, W., & Cai, G. (2021). A novel PSO-KELM based soil liquefaction potential evaluation system using CPT and Vs measurements. Soil Dynamics and Earthquake Engineering, 150, 106930.
126. Zhou, J., Huang, S., Wang, M., & Qiu, Y. (2021). Performance evaluation of hybrid GA–SVM and GWO–SVM models to predict earthquake-induced liquefaction potential of soil: a multi-dataset investigation. Engineering with Computers, 1-19.

Web References

www.en.wikipedia.org/wiki/Geohazard (2020) Geohazards
www.em-dat.net/ (2020) The International emergency disaster database
www.ngdc.noaa.gov/ (2020) National Geophysical data centre
www.nidm.net/ (2020) National Institute of disaster management
www.saarc-sdmc.nic.in/index.asp (2020) SAARC disaster management centre

APPENDIX

Liquefaction	M	Critical depth (m)	Fine content (%)	D50(mm)	Water Table (m)	PGA(g)	rd	CSR	(N1)60cs	CRR
Yes	7.3	6	61	0.075	2.3	0.428	0.942	0.451	8.47	0.107675
Yes	7.3	4.2	24	0.2	2.7	0.789	0.959	0.378	3.58	0.078208
Yes	7.3	9	42	0.1	2.3	0.789	0.886	0.714	6.38	0.094351
Yes	7.3	2.4	41	0.095	2.3	0.789	0.972	0.514	8.71	0.10927
Yes	7.3	5	22	0.065	2.2	0.428	0.952	0.379	3.67	0.078694
Yes	7.3	4.2	62	0.1	1.8	0.211	0.959	0.417	4.05	0.080771
Yes	7.3	7.7	16	0.22	3.8	0.165	0.915	0.132	10.19	0.11939
Yes	7.3	8.1	16	0.19	3.1	0.165	0.907	0.136	8.48	0.107741
Yes	7.3	5.7	16	0.17	2.8	0.165	0.945	0.139	8.82	0.110005
Yes	7.3	8.1	19	0.17	2.8	0.165	0.907	0.148	10.71	0.123064
Yes	7.3	3.7	11	0.19	2.3	0.165	0.962	0.128	11.57	0.129279
Yes	7.3	10	45	0.08	3	0.165	0.85	0.145	7.25	0.099773
Yes	7.3	7.7	18	0.17	3	0.165	0.915	0.142	6.72	0.096448
Yes	7.3	5.7	15	0.18	2.4	0.165	0.945	0.143	6.62	0.095829
Yes	7.3	7.7	48	0.08	2.4	0.165	0.915	0.15	8.89	0.110474
Yes	7.3	7.7	13	0.18	3.8	0.165	0.915	0.134	5.7	0.090243
Yes	7.3	3.7	17	0.16	1.3	0.165	0.962	0.153	12.63	0.137195
Yes	7.3	3.7	28	0.1	1.6	0.165	0.962	0.148	9.93	0.117576
Yes	7.3	7.7	19	0.17	2.4	0.165	0.915	0.151	6.96	0.097945
Yes	7.3	8.2	17	0.18	3.1	0.165	0.905	0.163	7.04	0.098448
Yes	7.3	2.7	22	0.18	2.7	0.165	0.969	0.105	5.52	0.089175
Yes	7.3	7.2	22	0.18	2.7	0.165	0.925	0.148	6.16	0.093009
Yes	7.3	7.2	13	0.14	2.8	0.165	0.925	0.145	6.05	0.092343
Yes	7.3	10.2	13	0.14	2.8	0.165	0.847	0.145	8.44	0.107477
Yes	7.3	11.7	13	1.2	2.8	0.165	0.825	0.146	8.79	0.109804
Yes	7.3	16	20	0.3	2.8	0.165	0.76	0.152	5.58	0.08953
Yes	7.3	5.7	40	0.08	2.8	0.165	0.945	0.14	6.86	0.09732

Yes	7.3	8.7	42	0.08	2.8	0.165	0.893	0.152	4.31	0.082215
Yes	7.3	5.7	30	0.024	2.8	0.165	0.945	0.136	4.99	0.086079
Yes	7.3	7.2	30	0.024	2.8	0.165	0.925	0.144	4.96	0.085906
Yes	7.3	11.7	48	0.075	2.8	0.165	0.825	0.144	5.68	0.090124
Yes	7.3	8.7	44	0.08	2.8	0.165	0.893	0.148	5.04	0.086368
Yes	7.3	3.8	24	0.138	1.4	0.165	0.962	0.217	13.4	0.143141
Yes	7.3	4.8	29	0.129	1.4	0.165	0.954	0.214	13.11	0.140881
Yes	7.3	12.8	25	0.138	1.3	0.165	0.808	0.174	5.31	0.087939
Yes	7.3	8.8	31	0.125	1.3	0.165	0.891	0.193	11.88	0.131564
Yes	7.3	7.8	46	0.094	1.3	0.165	0.913	0.209	14	0.147901
Yes	7.3	15.4	33	0.18	4.8	1	0.769	0.663	14.48	0.151798
Yes	7.3	8.8	39	0.1	4.8	1	0.815	0.606	7.39	0.100662
Yes	7.3	6.8	59	0.07	4.8	1	0.906	0.633	13.43	0.143376
Yes	7.3	17.6	26	0.2	1.9	1	0.736	0.699	8.61	0.108604
Yes	7.3	3.3	34	0.11	1.9	1	0.964	0.673	19.25	0.197069
Yes	7.3	16.9	49	0.08	3.5	1	0.746	0.67	5	0.086136
Yes	7.3	3	6	0.08	1.1	0.124	0.967	0.12	8.22	0.106028
Yes	7.3	3	12	0.19	1.1	0.124	0.967	0.119	11.86	0.131416
Yes	7.3	9	4	0.22	1.1	0.124	0.886	0.127	3.26	0.076498
Yes	7.3	3	36	0.1	1.1	0.124	0.967	0.118	2.93	0.074766
Yes	7.3	4	36	0.1	1.1	0.124	0.96	0.127	7.27	0.0999
Yes	7.3	4	21	0.14	1.1	0.124	0.96	0.126	5.73	0.090422
Yes	7.3	4	30	0.1	1.1	0.124	0.96	0.124	3.28	0.076604
Yes	7.3	3	9	0.2	1.1	0.124	0.967	0.118	2.39	0.071999
Yes	7.3	6	33	0.16	1.1	0.124	0.942	0.13	11.8	0.130972
Yes	7.3	3	5	0.2	1.1	0.124	0.967	0.121	9.4	0.113927
Yes	7.3	5	20	0.15	4	0.428	0.952	0.296	6.55	0.095396
Yes	7.3	5.8	25	0.15	5	0.428	0.944	0.283	11.62	0.129646
Yes	7.3	8.3	13	0.56	2.8	0.428	0.903	0.386	16.59	0.170085
Yes	7.3	6.3	15	0.27	1.2	0.428	0.938	0.41	10.62	0.122424
Yes	7.3	2.8	22	0.18	0.7	0.428	0.969	0.458	9.75	0.11633

Yes	7.3	7.3	21	0.15	5	0.428	0.923	0.306	6.71	0.096386
Yes	7.3	3	24	0.13	2.4	0.428	0.967	0.3	12.14	0.133499
Yes	7.3	7.5	55	0.08	2.8	0.428	0.919	0.384	4.35	0.082439
Yes	7.3	5.8	35	0.125	2.8	0.428	0.944	0.36	12.04	0.132753
Yes	7.3	5.8	30	0.97	1.5	0.428	0.944	0.433	15.78	0.162815
Yes	7.3	4	26	0.11	2	0.428	0.96	0.362	14.34	0.150653
Yes	7.3	4	11	0.12	2.1	0.428	0.96	0.356	3.02	0.075235
Yes	7.3	2.8	55	0.06	1.5	0.33	0.969	0.271	7.03	0.098385
Yes	7.3	5.8	47	0.08	1.5	0.33	0.944	0.325	8.14	0.105504
Yes	7.3	7.5	47	0.091	0.6	0.211	0.919	0.247	8.14	0.105504
Yes	7.3	7.5	13	0.162	0.5	0.211	0.919	0.248	6.94	0.09782
Yes	7.3	3	26	0.135	0.5	0.211	0.967	0.235	9.58	0.115159
Yes	7.3	3	30	0.127	1.2	0.211	0.967	0.195	9.85	0.117021
Yes	7.3	4.5	26	0.135	1.1	0.211	0.957	0.222	8.33	0.106751
Yes	7.3	12	39	0.108	0.9	0.211	0.82	0.222	9.76	0.116399
Yes	7.3	12	28	0.131	0.6	0.211	0.82	0.238	6.29	0.093801
Yes	7.3	13.5	47	0.091	0.6	0.211	0.798	0.226	6.67	0.096138
Yes	7.3	12	48	0.089	0.6	0.211	0.82	0.232	7.69	0.102583
Yes	7.3	12	41	0.104	0.6	0.211	0.82	0.234	30.44	0.513823
Yes	7.3	13.5	42	0.102	0.6	0.211	0.798	0.228	25.3	0.297288
Yes	7.3	19.5	46	0.093	1	0.211	0.708	0.196	19.59	0.200972
Yes	7.3	12	13	0.162	0.6	0.211	0.82	0.231	23.58	0.259928
Yes	7.3	13.5	14	0.16	0.6	0.211	0.798	0.223	23.49	0.258232
Yes	7.3	4.5	32	0.123	1.1	0.211	0.957	0.221	19.33	0.197976
Yes	7.3	3	38	0.11	1.1	0.211	0.967	0.203	20.43	0.211196
Yes	7.3	6	11	0.167	1.1	0.211	0.942	0.232	17.26	0.176384
Yes	7.3	6	14	0.16	2.1	0.211	0.942	0.193	23.37	0.256005
Yes	7.3	5.8	10	0.36	1.5	0.211	0.944	0.217	22.39	0.239157
Yes	7.3	4.3	9	0.31	1.6	0.211	0.958	0.193	16.43	0.168621
Yes	7.3	5.8	10	0.28	0.8	0.211	0.944	0.231	14.29	0.150246
Yes	7.3	8.8	37	0.11	0.8	0.211	0.891	0.228	21.57	0.226652

Yes	7.3	8.2	10	0.45	2	0.211	0.905	0.202	18.83	0.192414
Yes	7.3	8.8	30	0.1	1.7	0.211	0.891	0.208	14.68	0.153448
Yes	7.3	5.8	34	0.1	2.5	0.211	0.944	0.182	14.92	0.155447
Yes	7.3	10.3	28	0.11	2.3	0.211	0.846	0.191	20.23	0.208681
Yes	7.3	10.3	45	0.1	3.4	0.211	0.846	0.176	24.84	0.286275
Yes	7.3	9.2	49	0.078	1.9	0.211	0.88	0.203	19.91	0.204764
Yes	7.3	11.8	24	0.2	4.5	0.211	0.823	0.165	23.86	0.265351
Yes	7.3	13.3	30	0.11	0.6	0.211	0.801	0.214	21.98	0.232742
Yes	7.3	8.8	46	0.11	2.1	0.211	0.891	0.199	23.86	0.265351
Yes	7.3	13.3	11	0.34	1.5	0.211	0.801	0.2	21.98	0.232742
Yes	7.3	14.8	12	0.21	0.7	0.211	0.778	0.208	21.09	0.219896
Yes	7.3	4.3	10	0.25	2.5	0.211	0.958	0.167	18.68	0.190793
Yes	7.3	7.3	23	0.31	2.5	0.211	0.923	0.208	21.97	0.232589
Yes	7.3	14.8	17	0.17	1.7	0.211	0.778	0.187	20.42	0.211069
Yes	7.3	11.8	13	0.3	0.8	0.211	0.823	0.215	9.34	0.113518
Yes	7.3	2.8	18	0.18	1	0.211	0.969	0.197	12.07	0.132977
Yes	7.3	5.8	47	0.078	0.4	0.211	0.944	0.247	12.08	0.133051
Yes	7.3	10.3	31	0.11	1.4	0.211	0.846	0.207	10.77	0.123492
Yes	7.3	7.3	9	0.49	2	0.211	0.923	0.199	9.06	0.111619
Yes	7.3	3.8	17	0.17	1.1	0.211	0.962	0.208	7.46	0.101109
Yes	7.3	7.3	16	0.21	0.4	0.211	0.923	0.244	10.2	0.11946
Yes	7.3	7.3	18	0.21	2	0.211	0.923	0.201	8.95	0.110877
Yes	7.3	5.8	19	0.5	1.4	0.211	0.944	0.211	9.2	0.112566
Yes	7.3	12.8	26	0.11	3.4	0.211	0.808	0.178	37.49	1.983025
Yes	7.3	4.3	26	0.14	2.5	0.211	0.958	0.165	35.22	1.160671
Yes	7.3	11.8	12	0.61	0.9	0.211	0.823	0.213	15.95	0.164313
Yes	7.3	8.8	25	0.12	2	0.211	0.891	0.201	3.91	0.080001
Yes	7.3	10.3	15	0.38	0.4	0.211	0.846	0.228	1.04	0.065464
Yes	7.3	8.8	24	0.4	1.4	0.211	0.891	0.219	2.87	0.074454
Yes	7.3	11.8	17	0.22	2.1	0.211	0.823	0.194	3.13	0.075812
Yes	7.3	11.8	31	0.13	2.1	0.211	0.823	0.194	3.64	0.078531

Yes	7.3	14.3	14	0.5	7.3	0.211	0.786	0.143	0.93	0.064956
Yes	7.3	4.3	18	0.19	2.1	0.211	0.958	0.177	0.97	0.06514
Yes	7.3	5.3	21	0.23	4.1	0.42	0.94	0.294	5.45	0.088762
Yes	7.3	8.8	38	0.4	4.1	0.42	0.819	0.308	22.7	0.244243
Yes	7.3	5.3	21	0.3	2.9	0.42	0.94	0.339	23.5	0.258419
Yes	7.3	3.6	11	2	2.9	0.42	0.961	0.289	14.1	0.148706
Yes	7.3	5	25	0.8	2.9	0.42	0.945	0.324	35.5	1.232651
Yes	7.3	2.3	29	0.1	1.4	0.42	0.972	0.336	17.6	0.179693
Yes	7.3	3.8	13	0.5	1.4	0.42	0.959	0.391	35.3	1.180608
Yes	7.3	7.4	25	0.18	1.5	0.42	0.885	0.416	23	0.249373
Yes	7.3	5.7	34	0.15	3.5	0.42	0.933	0.322	14.6	0.152786
Yes	7.3	2.2	23	0.15	1.7	0.42	0.973	0.304	14.3	0.150327
Yes	7.3	6.4	16	0.4	1.7	0.42	0.917	0.406	24.4	0.276483
Yes	7.3	2.1	18	0.13	1.3	0.42	0.974	0.33	32.7	0.721321
Yes	7.3	5.5	17	0.7	1.3	0.42	0.937	0.42	14.3	0.150327
Yes	7.3	4.7	29	0.25	2.5	0.42	0.95	0.344	13.6	0.144714
Yes	7.3	7.8	16	0.3	2.5	0.42	0.868	0.363	12.8	0.138493
Yes	7.3	6.2	23	0.13	1.7	0.42	0.922	0.411	15.5	0.16038
Yes	7.3	6.3	30	0.11	2.6	0.42	0.92	0.363	6.7	0.096324
Yes	7.3	10.8	20	0.13	2.6	0.42	0.839	0.376	12.3	0.134699
Yes	7.3	6.5	17	0.3	1.5	0.42	0.912	0.412	14.1	0.148706
Yes	7.3	4.9	29	0.2	3.1	0.42	0.947	0.323	9.6	0.115297
Yes	7.3	10.9	31	0.12	3.1	0.42	0.836	0.355	9.4	0.113927
Yes	7.3	13.2	31	0.1	3.1	0.42	0.802	0.352	8.6	0.108537
Yes	7.3	7.2	18	0.2	3	0.42	0.893	0.349	6.5	0.095088
Yes	7.3	8.1	18	0.2	3	0.42	0.856	0.347	16.3	0.167442
Yes	7.3	2.3	22	0.15	1.3	0.789	0.972	0.641	13.9	0.147099
Yes	7.3	3	45	0.09	1.2	0.789	0.967	0.697	8.1	0.105242
Yes	7.3	7.3	40	0.095	3.2	0.789	0.923	0.644	15.1	0.156962
Yes	7.3	1.3	65	0.055	0.5	0.789	0.982	0.741	22	0.233047
Yes	7.3	6.8	15	0.037	2	0.789	0.931	0.79	17.6	0.179693

Yes	7.3	5.8	22	0.13	1.4	0.789	0.944	0.78	17.8	0.181679
Yes	7.3	5.8	48	0.08	0.9	0.789	0.944	0.822	26.2	0.321486
Yes	7.3	8.8	40	0.1	4.2	0.789	0.891	0.611	24	0.26815
Yes	7.3	2.8	38	0.097	0.9	0.789	0.969	0.76	24.6	0.280849
Yes	7.3	5.8	49	0.075	2.7	0.428	0.944	0.65	21.2	0.221411
Yes	7.3	4.2	27	0.19	2.3	0.428	0.959	0.634	11.7	0.130234
Yes	7.3	5.8	27	0.195	2.8	0.428	0.944	0.659	20.6	0.213376
Yes	7.3	7.2	29	0.185	2.8	0.428	0.925	0.687	15.7	0.162116
Yes	7.3	4.2	34	0.2	2.6	0.428	0.959	0.609	9.6	0.115297
Yes	7.3	2.8	33	0.188	2.7	0.428	0.969	0.506	9.1	0.111889
Yes	7.3	4.2	43	0.143	2.7	0.428	0.959	0.596	10	0.118063
Yes	7.3	4.2	40	0.13	1.9	0.428	0.959	0.672	20.6	0.213376
Yes	7.3	5.8	40	0.16	1.9	0.428	0.944	0.718	10.2	0.11946
Yes	8.1	5.2	10	0.15	2.1	0.2	0.98	0.207	19.3	0.197635
Yes	8.1	4.3	30	0.4	2.4	0.2	0.99	0.159	17	0.173906
Yes	8.1	3.7	27	0.2	2.1	0.2	0.99	0.245	5.1	0.086715
Yes	7	4	0	0.4	1.2	0.4	0.96	0.318	18.1	0.184714
Yes	7	7.5	4	0.55	3.7	0.35	0.9	0.251	18.7	0.191008
Yes	7.6	3.3	5	0.23	1	0.09	0.98	0.086	13.8	0.146301
Yes	7.6	7	2	0.23	0.9	0.16	0.94	0.178	13.1	0.140803
Yes	7.6	5.3	8	0.23	0.9	0.16	0.96	0.188	9.8	0.116675
Yes	7.6	3.8	5	0.23	2	0.162	0.98	0.133	18.9	0.193178
Yes	7.6	10.1	2	0.23	0.9	0.16	0.9	0.182	23.5	0.258419
Yes	7.6	10.1	2	0.43	0.9	0.16	0.9	0.182	23	0.249373
Yes	7.6	4.6	0	0.45	0.6	0.16	0.97	0.176	34.6	1.021474
Yes	7.6	4.3	10	0.3	0	0.16	0.97	0.199	37.3	1.8878
Yes	8.3	5.7	3	0.12	0	0.213	0.98	0.376	20.3	0.209555
Yes	8.3	4	5	0.12	0.6	0.23	0.99	0.304	23.5	0.258419
Yes	8.3	4	20	0.123	0.9	0.2	0.99	0.244	22.5	0.240938
Yes	6.61	6.1	55	0.05	4.6	0.45	0.92	0.246	25.9	0.312996
Yes	6.61	6.1	50	0.06	4.6	0.45	0.92	0.245	17.6	0.179693

Yes	7	8.2	67	0.06	1.5	0.2	0.89	0.175	8.5	0.107874
Yes	7	7.8	48	0.08	1.5	0.3	0.9	0.26	15.7	0.162116
Yes	7	8.2	5	0.15	1.5	0.3	0.89	0.259	7	0.098196
Yes	7.5	10.4	3	0.8	1.5	0.135	0.89	0.125	21.2	0.221411
Yes	7.5	4.6	3	0.8	2.4	0.135	0.97	0.126	11.7	0.130234
Yes	7.6	4.5	12	0.14	1.1	0.13	0.97	0.125	10	0.118063
Yes	7.6	4.4	12	0.1	1.5	0.2	0.97	0.186	8.5	0.107874
Yes	7.6	3.5	3	0.8	1.1	0.22	0.98	0.225	20.6	0.213376
Yes	7.6	5.3	20	0.14	0.9	0.35	0.96	0.357	10.2	0.11946
Yes	7.6	6.1	20	0.145	0.9	0.2	0.95	0.214	19.3	0.197635
Yes	7.5	8.2	20	0.145	4.6	0.2	0.92	0.161	21.4	0.224215
Yes	7.5	11.1	5	0.3	6.7	0.2	0.87	0.169	11	0.12514
Yes	7.5	5.2	50	0.1	1.8	0.2	0.96	0.187	22.6	0.242579
Yes	6.5	2.8	5	0.71	0.5	0.12	0.97	0.087	14.9	0.15528
Yes	7.7	6.4	0	0.35	0.9	0.2	0.95	0.225	21.2	0.221411
Yes	7.7	3.5	10	0.15	1.4	0.2	0.98	0.184	14.7	0.153613
Yes	7.7	3.4	5	0.53	3.1	0.28	0.98	0.187	24.6	0.280849
Yes	7.7	6.1	3	0.35	2.4	0.24	0.96	0.223	34.4	0.981768
Yes	7.7	2.8	5	0.7	0.5	0.32	0.99	0.332	29.2	0.439156
Yes	7.7	3.4	4	0.28	1.3	0.32	0.98	0.299	30.9	0.547335
Yes	7.7	6.4	5	0.34	4.3	0.24	0.95	0.192	32.3	0.675563
Yes	7.7	4	10	0.25	2.4	0.24	0.98	0.192	36.6	1.586053
Yes	7.7	4.3	10	0.25	1.8	0.24	0.97	0.218	22.5	0.240938
Yes	7.7	2.5	7	1.6	1.2	0.24	0.99	0.203	28	0.383595
Yes	7.7	4.3	12	0.12	0.3	0.24	0.97	0.282	27.6	0.367889
Yes	7.7	5.5	60	0.04	1.8	0.24	0.96	0.236	24.5	0.278649
Yes	7.7	4.3	0	0.4	0.9	0.24	0.97	0.258	25	0.290012
Yes	6.53	3.7	18	0.11	1.8	0.78	0.96	0.484	22.5	0.240938
Yes	6.53	2.1	31	0.11	1.5	0.51	0.98	0.271	33.5	0.828773
Yes	6.53	3.4	64	0.05	2.1	0.2	0.96	0.112	38.6	2.68984
Yes	6.53	1.8	80	0.04	0.3	0.24	0.98	0.187	25.1	0.292397

Yes	5.9	4.3	92	0.05	2.7	0.32	0.93	0.151	35.8	1.317052
Yes	5.9	3.4	64	0.07	2.1	0.2	0.95	0.094	37	1.749643
Yes	5.9	4.6	30	0.11	1.2	0.26	0.92	0.164	29.2	0.439156
Yes	7.7	5.7	3	0.25	0	0.116	0.96	0.171	33.5	0.828773
Yes	7.7	4.3	15	0.15	1	0.2	0.97	0.23	31.6	0.605923
Yes	7.7	7.5	1	0.25	0.4	0.227	0.94	0.317	26.5	0.330442
Yes	7.7	3.5	1	0.25	1.7	0.25	0.98	0.222	25.2	0.294822
Yes	7.7	4.3	0	0.24	0.4	0.283	0.97	0.381	27.2	0.353363
Yes	7.7	6.913	3	0.2	1.5	0.205	0.95	0.218	24	0.26815
Yes	7.7	9.799	4	0.2	1.47	0.205	0.91	0.227	18.71	0.191115
Yes	7.7	6.47	8	0.2	1.46	0.205	0.95	0.216	20.72	0.21494
Yes	7.7	7.131	3	0.2	1.45	0.205	0.94	0.219	11.41	0.128109
Yes	7.7	3.783	7	0.3	1.5	0.205	0.98	0.189	21.8	0.23003
Yes	7.7	6.036	2	0.8	1.58	0.205	0.96	0.21	17.04	0.174285
Yes	7.7	5.744	2	0.8	1.51	0.205	0.96	0.209	19.92	0.204885
Yes	7.7	5.21	2	0.314	0.72	0.205	0.96	0.231	17.99	0.183593
Yes	7.7	5.41	2	0.324	1.37	0.205	0.96	0.212	20.52	0.212345
Yes	7.7	5.48	2	0.367	1.35	0.205	0.96	0.213	23.49	0.258232
Yes	7.7	3.91	2	0.4	1.46	0.205	0.98	0.192	21.93	0.231982
Yes	6.54	4.6	30	0.1	1.2	0.206	0.94	0.157	17.97	0.18339
Yes	6.93	6	8	0.2	4.5	0.37	0.93	0.221	21.93	0.231982
Yes	6.93	4.6	3	0.8	2.4	0.28	0.95	0.189	18.03	0.183999
Yes	6.93	3.5	3	0.8	2.5	0.28	0.97	0.167	19.8	0.203447
Yes	6.93	5.3	3	0.8	1.5	0.28	0.94	0.22	17.27	0.17648
Yes	6.93	6.2	32	0.1	4.9	0.39	0.92	0.219	21.87	0.231077
Yes	6.93	7	13	0.13	4.7	0.39	0.91	0.243	18.95	0.193726
Yes	6.93	6	25	0.8	4.4	0.39	0.93	0.243	16.94	0.173341
Yes	6.93	6.3	3	0.189	3	0.28	0.92	0.194	19.89	0.204524
Yes	6.93	6.3	3	0.19	3	0.28	0.92	0.194	20.78	0.21573
Yes	6.93	5.9	50	0.09	3.5	0.18	0.93	0.119	19.04	0.194719
Yes	6.93	3	2	0.19	1.8	0.28	0.97	0.177	19.86	0.204164

Yes	6.93	6.3	8	0.6	3	0.27	0.92	0.189	19.01	0.194387
Yes	6.93	3.4	1	0.23	1.8	0.28	0.97	0.187	20.82	0.216259
Yes	6.93	4.9	1	0.23	2.6	0.28	0.95	0.188	20.7	0.214678
Yes	6.93	6.5	20	0.4	1.5	0.16	0.92	0.137	15.03	0.156372
Yes	6.93	1.8	35	0.16	1	0.28	0.99	0.183	19.62	0.201322
Yes	7.7	7.2	19	0.2	2.3	0.26	0.94	0.245	20.61	0.213506
Yes	7.6	5.2	2	0.34	2	0.4	0.96	0.359	18.44	0.188242
Yes	7.6	3.8	5	0.27	2	0.47	0.98	0.383	15.74	0.162465
Yes	6.69	8.5	50	0.11	7.2	0.8	0.87	0.362	15.99	0.164667
Yes	6.69	7.1	64	0.11	2	0.43	0.91	0.254	9.32	0.113381
Yes	6.69	6.7	33	0.1	4.3	0.51	0.91	0.317	19.55	0.200506
Yes	6.9	8.9	1	0.2	3	0.35	0.88	0.258	17.72	0.180881
Yes	6.9	3.3	0	0.196	3.2	0.4	0.93	0.262	16.09	0.165557
Yes	6.9	5	0	0.197	3	0.5	0.94	0.321	19.31	0.197749
Yes	6.9	4.3	2	0.18	2.8	0.5	0.95	0.313	14.12	0.148868
Yes	6.9	6.8	5	0.16	1.5	0.5	0.91	0.447	11.54	0.129059
Yes	6.9	6.5	15	0.2	2.3	0.5	0.92	0.383	21.72	0.228844
Yes	6.9	5.7	5	0.16	3.7	0.5	0.93	0.312	17.43	0.178029
Yes	6.9	4.5	5	0.165	0.8	0.5	0.95	0.446	21.24	0.221966
Yes	6.9	3.5	0	0.26	2.4	0.5	0.97	0.297	18.12	0.184919
Yes	6.9	3.5	8	0.26	1.8	0.4	0.97	0.27	16.11	0.165735
Yes	6.9	3.8	0	0.4	2	0.4	0.96	0.264	18.35	0.187299
Yes	6.9	7	9	0.27	1.8	0.4	0.91	0.326	11.81	0.131046
Yes	6.9	4.5	6	0.3	2.1	0.5	0.95	0.352	11.43	0.128255
Yes	6.9	5	0	0.4	4	0.35	0.94	0.2	7.95	0.104265
Yes	6.9	8	5	0.3	3	0.5	0.89	0.373	8.19	0.105831
Yes	6.9	4.1	0	0.47	2	0.4	0.96	0.279	7.65	0.102326
Yes	6.9	5	10	0.3	1.2	0.4	0.94	0.352	10.98	0.124996
Yes	6.9	4.7	20	0.13	2.2	0.35	0.95	0.246	8.4	0.107213
Yes	6.9	4	5	0.3	1.6	0.4	0.96	0.308	12.26	0.134398
Yes	7.5	7.1	5	0.15	1.2	0.09	0.9	0.09	8.29	0.106488

Yes	7.5	11.5	8	0.2	1	0.16	0.78	0.16	11.53	0.128986
Yes	7.9	12.5	3	0.25	0	0.21	0.8	0.27	8.98	0.111079
Yes	7.8	7.6	3	0.17	1.5	0.22	0.96	0.24	11.55	0.129133
Yes	6.9	8.8	2	0.32	3.5	0.4	0.88	0.286	8.49	0.107808
Yes	6.9	7.8	20	0.14	2.4	0.34	0.9	0.26	5.5	0.089057
Yes	6.9	10	20	0.16	3	0.34	0.86	0.258	11.84	0.131268
Yes	6.9	7.5	25	0.175	4	0.4	0.9	0.267	5.34	0.088115
Yes	6.9	11.5	20	0.176	4	0.34	0.83	0.246	7.11	0.098888
Yes	6.9	4.7	20	0.181	1	0.25	0.95	0.24	27.8	0.375587
No	7.3	9	14	0.2	1.1	0.124	0.886	0.127	26.28	0.323827
No	7.3	8	24	0.17	1.1	0.124	0.909	0.129	24.34	0.2752
No	7.3	4	15	0.18	1.1	0.124	0.96	0.124	33.43	0.818413
No	7.3	9	10	0.22	1.1	0.124	0.886	0.128	35.34	1.190761
No	7.3	10	16	0.18	1.1	0.124	0.85	0.124	34.18	0.940677
No	7.3	9	12	0.22	1.1	0.124	0.886	0.128	25.9	0.312996
No	7.3	10	10	0.25	1.1	0.124	0.85	0.124	35.09	1.129295
No	7.3	5	31	0.13	1.1	0.124	0.952	0.127	29.28	0.443382
No	7.3	10	14	0.22	1.1	0.124	0.85	0.123	28.47	0.403731
No	7.3	9	6	0.22	1.1	0.124	0.886	0.128	27.73	0.372858
No	7.3	7	8	0.22	1.1	0.124	0.928	0.131	27.04	0.347856
No	7.3	9	7	0.28	1.1	0.124	0.886	0.128	26.67	0.335738
No	7.3	10	11	0.18	1.1	0.124	0.85	0.124	27.92	0.380354
No	7.3	5	17	0.17	1.1	0.124	0.952	0.13	20.82	0.216259
No	7.3	10	7	0.29	1.1	0.124	0.85	0.126	6.34	0.094106
No	7.3	9	9	0.2	1.1	0.124	0.886	0.128	6.6	0.095705
No	7.3	10	12	0.2	1.1	0.124	0.85	0.124	11.4	0.128036
No	7.3	9	15	0.19	1.1	0.124	0.886	0.128	11.53	0.128986
No	7.3	10	17	0.18	1.1	0.124	0.85	0.124	5.61	0.089708
No	7.3	10	11	0.19	1.1	0.124	0.85	0.124	4.94	0.08579
No	7.3	10	14	0.18	1.1	0.124	0.85	0.125	8.82	0.110005
No	7.3	9	9	0.2	1.1	0.124	0.886	0.128	7.79	0.103228

No	7.3	10	18	0.19	1.1	0.124	0.85	0.125	6.03	0.092222
No	7.3	8	13	0.22	1.1	0.124	0.909	0.129	5.24	0.08753
No	7.3	9	14	0.23	1.1	0.124	0.886	0.127	7.46	0.101109
No	7.3	10	14	0.18	1.1	0.124	0.85	0.123	7.22	0.099583
No	7.3	10	21	0.15	1.1	0.124	0.85	0.123	7.98	0.10446
No	7.3	5	46	0.09	1.1	0.124	0.952	0.127	3.94	0.080165
No	7.3	6	9	0.28	1.1	0.124	0.942	0.108	3.31	0.076763
No	7.3	9	16	0.18	1.1	0.124	0.886	0.112	9.87	0.11716
No	7.3	10	13	0.18	1.1	0.124	0.85	0.11	8.59	0.108471
No	7.3	5	14	0.13	1.1	0.124	0.952	0.104	11.49	0.128694
No	7.3	8	13	0.17	1.1	0.124	0.909	0.113	7.88	0.103811
No	7.3	9	10	0.26	1.1	0.124	0.886	0.113	8.58	0.108404
No	7.3	10	23	0.13	1.1	0.124	0.85	0.111	3.86	0.079727
No	7.3	7	20	0.115	1.1	0.124	0.928	0.14	13.29	0.14228
No	7.3	9	13	0.18	1.1	0.124	0.886	0.135	8.94	0.11081
No	7.3	10	40	0.08	1.1	0.124	0.85	0.13	4.87	0.085388
No	7.3	8	13	0.2	1.1	0.124	0.909	0.144	5.31	0.087939
No	7.3	10	28	0.13	1.1	0.124	0.85	0.134	10.81	0.123778
No	7.3	10	20	0.19	1.1	0.124	0.85	0.134	10.81	0.123778
No	7.3	8	16	0.14	1.1	0.124	0.909	0.139	6.53	0.095273
No	7.3	9	29	0.2	1.1	0.124	0.886	0.135	3.85	0.079673
No	7.3	9	14	0.2	1.1	0.124	0.886	0.139	5.6	0.089648
No	7.3	16.2	43	0.113	1	0.128	0.757	0.124	11.32	0.127454
No	7.3	7.2	36	0.126	1	0.128	0.925	0.141	8.65	0.10887
No	7.3	9.8	36	0.126	1	0.128	0.863	0.136	5.76	0.090601
No	7.3	11.8	36	0.126	1	0.128	0.823	0.131	12.54	0.136511
No	7.3	7.8	31	0.135	1	0.128	0.913	0.139	5.94	0.09168
No	7.3	11.3	47	0.106	7.5	0.181	0.831	0.124	7.95	0.104265
No	7.3	12.8	44	0.111	7.6	0.181	0.809	0.126	10.65	0.122637
No	7.3	17.3	39	0.12	14.3	0.181	0.741	0.1	16.15	0.166093
No	7.3	18.8	15	0.164	4.4	0.181	0.719	0.142	7.76	0.103035

No	7.3	14.3	33	0.132	4.6	0.181	0.786	0.147	13.7	0.145506
No	7.3	20.3	30	0.137	15.3	0.181	0.696	0.098	5.13	0.086889
No	7.3	15.8	39	0.12	5.3	0.181	0.764	0.141	10.27	0.119951
No	7.3	14.3	46	0.108	8.8	0.181	0.786	0.12	9.41	0.113995
No	7.3	18.8	45	0.11	14.6	0.181	0.719	0.13	9.57	0.11509
No	7.3	9.8	23	0.149	14.6	0.181	0.864	0.128	5.02	0.086252
No	7.3	18.8	45	0.11	8.2	0.181	0.719	0.123	10.86	0.124135
No	7.3	17.3	23	0.148	14.6	0.181	0.741	0.095	9.86	0.117091
No	7.3	6.5	17	0.28	2.9	0.42	0.913	0.353	7.53	0.101556
No	7.3	7.5	17	0.3	2.9	0.42	0.88	0.354	15.45	0.159949
No	7.3	7.1	15	0.8	2.9	0.42	0.896	0.341	10.63	0.122495
No	7.3	10.6	14	0.3	2.9	0.42	0.841	0.353	8.75	0.109537
No	7.3	18.1	18	0.85	1.4	0.42	0.729	0.367	14.34	0.150653
No	7.3	10.9	21	0.013	3.5	0.42	0.837	0.354	14.4	0.151143
No	7.3	14.3	39	0.08	8.5	0.42	0.785	0.272	7.51	0.101428
No	7.3	15.6	39	0.1	8.5	0.42	0.766	0.274	12.63	0.137195
No	7.3	16.8	39	0.1	8.5	0.42	0.748	0.275	2.69	0.073526
No	7.3	18.1	39	0.08	8.5	0.42	0.729	0.274	18.66	0.190578
No	7.3	12.6	29	0.3	2.5	0.42	0.811	0.368	14.74	0.153945
No	7.3	14.1	35	0.3	2.6	0.42	0.789	0.364	6.99	0.098134
No	7.3	16.2	31	0.3	1.5	0.42	0.758	0.374	7.11	0.098888
No	7.3	10.4	30	0.04	1.5	0.42	0.844	0.406	12.13	0.133425
No	7.3	14.5	18	0.1	3	0.42	0.772	0.322	9.77	0.116468
No	7.3	15.4	18	0.1	3	0.42	0.769	0.337	4.58	0.083734
No	7.3	9.5	17	1	4.2	0.42	0.771	0.296	10.66	0.122708
No	7.3	13	20	0.4	4.2	0.42	0.805	0.331	21.87	0.231077
No	7.3	10	15	0.17	1.1	0.124	0.85	0.134	20.15	0.207689
No	7.3	10	12	0.3	1.1	0.124	0.85	0.135	17.39	0.17764
No	7.3	9	31	0.1	1.1	0.124	0.886	0.139	16.64	0.170546
No	7.3	8	15	0.19	1.1	0.124	0.909	0.138	3.33	0.07687
No	7.3	9	16	0.15	1.1	0.124	0.886	0.139	19.24	0.196956

No	7.3	10	12	0.3	1.1	0.124	0.85	0.134	12.03	0.132678
No	7.3	9	17	0.13	1.1	0.124	0.886	0.14	3.6	0.078315
No	7.3	8	18	0.18	1.1	0.124	0.909	0.143	10.78	0.123563
No	7.3	3	33	0.16	1.1	0.124	0.967	0.156	12.79	0.138416
No	7.3	9	18	0.18	1.1	0.124	0.886	0.141	11.78	0.130824
No	7.3	10	13	0.29	1.1	0.124	0.85	0.135	11.01	0.125212
No	7.3	9	14	0.2	1.5	0.124	0.886	0.122	4.94	0.08579
No	7.3	5	18	0.18	1.5	0.124	0.952	0.119	12.45	0.13583
No	7.3	10	15	0.18	1.4	0.124	0.85	0.118	8.52	0.108006
No	7.3	5	14	0.2	1.3	0.124	0.952	0.137	6.44	0.094719
No	7.3	10	15	0.22	1.3	0.124	0.85	0.128	8.93	0.110743
No	7.3	5	14	0.2	0.6	0.124	0.952	0.137	9.5	0.11461
No	7.3	10	15	0.22	0.6	0.124	0.85	0.128	5.37	0.088291
No	7.3	9	12	0.2	0.6	0.124	0.886	0.133	5.87	0.091259
No	7.3	5	14	0.2	0.6	0.124	0.952	0.138	8.72	0.109337
No	7.3	6	19	0.19	0.6	0.124	0.942	0.138	9.88	0.117229
No	7.3	10	16	0.17	1.3	0.124	0.85	0.122	9.3	0.113245
No	7.3	18	22	0.104	2.7	0.165	0.73	0.142	8.7	0.109203
No	7.3	6	8	0.2	2.7	0.165	0.942	0.142	6.9	0.09757
No	7.3	16	18	0.14	2.7	0.165	0.76	0.145	11.8	0.130972
No	7.3	18	32	0.1	2.7	0.165	0.73	0.142	21.1	0.220033
No	7.3	16	18	0.14	2.7	0.165	0.76	0.145	4.7	0.084416
No	7.3	4	43	0.09	2.7	0.165	0.96	0.124	9.9	0.117368
No	7.3	12	8	0.201	2.7	0.165	0.82	0.149	13	0.14003
No	7.3	13.2	61	0.068	5.3	0.055	0.802	0.042	6.8	0.096946
No	7.3	14.7	25	0.16	5.3	0.055	0.78	0.041	11	0.12514
No	7.3	10.8	32	0.16	4	1	0.838	0.67	17.5	0.178712
No	7.3	2.8	33	0.155	1.8	0.211	0.969	0.161	9.4	0.113927
No	7.3	7.7	24	0.22	4	0.084	0.915	0.068	8.2	0.105897
No	7.3	6.2	42	0.108	4	0.084	0.939	0.064	16.5	0.16926
No	7.3	8.7	23	0.227	4	0.084	0.893	0.07	9.1	0.111889

No	7.3	14.7	39	0.126	4	0.084	0.78	0.071	12	0.132455
No	7.3	4.2	6	0.331	4	0.084	0.959	0.054	9.5	0.11461
No	7.3	9.2	39	0.128	4	0.084	0.88	0.07	13.7	0.145506
No	7.3	8.2	42	0.111	4	0.084	0.905	0.069	13.2	0.141579
No	7.3	6.2	18	0.254	4	0.084	0.939	0.065	19	0.194277
No	7.6	7	2	0.23	1.8	0.18	0.94	0.178	11	0.12514
No	7.6	10.1	2	0.23	1.8	0.18	0.9	0.191	5	0.086136
No	7.6	6.1	0	0.4	2.4	0.18	0.95	0.162	9.7	0.115985
No	7.5	2.89	36	0.25	2	0.242	0.98	0.168	13.8	0.146301
No	8.3	4	5	0.25	0.9	0.23	0.99	0.276	13.5	0.143926
No	7	8.2	50	0.07	1.5	0.2	0.89	0.172	8.5	0.107874
No	7.5	10.7	3	0.8	3.4	0.135	0.89	0.144	24.6	0.280849
No	7.6	3.5	5	0.15	1.1	0.22	0.98	0.211	15	0.156119
No	7.6	5.3	10	0.22	3.1	0.5	0.96	0.389	10.7	0.122993
No	7.5	3.7	4	0.245	1.2	0.2	0.98	0.186	7.6	0.102005
No	7.5	3.1	3	0.245	2.1	0.2	0.98	0.142	11.4	0.128036
No	6.5	6.4	0	0.45	0.9	0.1	0.9	0.076	6.9	0.09757
No	6.5	5.2	20	0.15	2.4	0.14	0.93	0.084	12.8	0.138493
No	6.5	3.5	10	0.15	1.4	0.12	0.96	0.076	15.5	0.16038
No	6.5	3.4	5	0.53	3.1	0.14	0.96	0.065	6.7	0.096324
No	6.5	6.1	3	0.35	2.4	0.14	0.91	0.088	12.3	0.134699
No	6.5	3.4	4	0.28	1.3	0.12	0.96	0.078	14.1	0.148706
No	6.5	6.4	5	0.34	4.3	0.14	0.9	0.075	6.9	0.09757
No	6.5	4	10	0.25	2.4	0.14	0.95	0.077	9.6	0.115297
No	6.5	4.3	10	0.4	1.8	0.12	0.94	0.075	9.4	0.113927
No	6.5	2.5	7	1.6	1.2	0.12	0.96	0.076	8.6	0.108537
No	6.5	4.3	12	1.2	0.3	0.12	0.94	0.097	6.5	0.095088
No	6.5	5.5	60	0.04	1.8	0.12	0.92	0.081	16.3	0.167442
No	6.5	4.3	0	0.4	0.9	0.12	0.94	0.086	13.9	0.147099
No	7.7	4.5	10	0.18	1.4	0.2	0.97	0.183	8.1	0.105242
No	7.7	4.8	0	0.41	3.1	0.28	0.97	0.22	15.1	0.156962

No	7.7	4.6	26	0.12	2.4	0.24	0.97	0.2	7	0.098196
No	7.7	3.4	4	0.28	0.9	0.32	0.98	0.315	10	0.118063
No	7.7	7.3	17	0.35	1.2	0.24	0.94	0.26	8.5	0.107874
No	7.7	5.5	0	0.6	2.1	0.24	0.96	0.22	10.2	0.11946
No	6.53	4	25	0.1	1.8	0.78	0.95	0.493	11.7	0.130234
No	6.53	4.3	92	0.05	2.7	0.13	0.95	0.073	8.5	0.107874
No	6.53	2.3	30	0.09	2.1	0.2	0.98	0.093	15.7	0.162116
No	6.53	4.6	30	0.11	1.2	0.17	0.94	0.129	13.3	0.142358
No	6	6.1	13	0.18	0.9	0.095	0.89	0.067	16.5	0.16926
No	6	14.3	27	0.17	0.9	0.095	0.69	0.061	5.1	0.086715
No	5.9	2.1	31	0.11	1.5	0.09	0.97	0.04	12.4	0.135452
No	5.9	2.3	30	0.11	2.1	0.2	0.97	0.078	16.2	0.166541
No	5.9	1.8	80	0.04	0.3	0.21	0.98	0.138	13.3	0.142358
No	5.9	4.3	18	0.35	0.3	0.21	0.93	0.142	8.7	0.109203
No	6.9	2.4	5	0.11	1.6	0.168	0.98	0.1	6.9	0.09757
No	6.8	4.3	15	0.15	1	0.15	0.95	0.133	10.4	0.120866
No	6.8	9.2	0	0.42	1	0.15	0.86	0.139	13.5	0.143926
No	7.7	2.895	3	0.22	1.75	0.205	0.99	0.159	9.4	0.113927
No	7.7	2.895	3	0.22	1.75	0.205	0.99	0.161	10.2	0.11946
No	7.7	3.338	5	0.2	1.14	0.116	0.98	0.109	11.5	0.128767
No	7.7	4.295	66	0.05	1.6	0.052	0.97	0.049	5.4	0.088467
No	7.7	3.905	3	0.4	1.2	0.205	0.98	0.195	7.4	0.100726
No	7.7	3.42	2	0.4	1.2	0.205	0.98	0.19	5.6	0.089648
No	7.7	2.583	1	0.39	1.2	0.205	0.99	0.176	8.1	0.105242
No	7.7	4.48	2	0.3	1.2	0.205	0.97	0.202	15.7	0.162116
No	7.7	4.543	2	0.4	1.45	0.205	0.97	0.193	10.6	0.122281
No	7.7	6.67	4	0.45	1.6	0.205	0.95	0.211	13.1	0.140803
No	7.7	3.567	0	0.5	1.45	0.205	0.98	0.182	14.9	0.15528
No	6.9	2.895	36	0.11	2	0.268	0.97	0.158	17.6	0.179693
No	6.22	3.4	64	0.05	2.1	0.09	0.96	0.046	15.3	0.158662
No	6.22	4.6	30	0.09	1.2	0.133	0.93	0.092	23.4	0.256558

No	6.54	3.7	18	0.15	1.8	0.15	0.96	0.093	14.9	0.15528
No	6.54	4	25	0.11	1.8	0.13	0.95	0.082	15.4	0.159519
No	6.54	4.3	92	0.05	2.7	0.174	0.95	0.098	17	0.173906
No	6.54	2.1	31	0.11	1.5	0.16	0.98	0.085	10.7	0.122993
No	6.54	3.4	64	0.12	2.1	0.2	0.96	0.113	15.3	0.158662
No	6.54	2.3	30	0.1	2.1	0.18	0.98	0.084	9	0.111214
No	6.54	1.8	80	0.04	0.3	0.19	0.98	0.149	10.3	0.120162
No	6.54	4.3	18	0.15	0.3	0.19	0.95	0.154	18.4	0.187822
No	6.93	2.5	5	0.6	1.4	0.28	0.98	0.182	10.8	0.123706
No	6.93	4.6	30	0.09	3.5	0.14	0.95	0.084	14.6	0.152786
No	6.93	2	1	0.6	2	0.28	0.99	0.14	17.3	0.176769
No	6.93	3.4	1	0.6	1.8	0.28	0.97	0.187	16.4	0.168348
No	6.93	3.4	5	0.5	1.9	0.28	0.97	0.18	25.9	0.312996
No	6.93	3.4	4	0.49	2	0.28	0.97	0.18	18.7	0.191008
No	6.93	8.4	20	0.4	3	0.39	0.89	0.292	14.1	0.148706
No	7.7	5	19	0.2	2.3	0.25	0.97	0.213	17	0.173906
No	7.6	10.8	0	0.24	1.6	0.4	0.89	0.434	6.1	0.092646
No	6.69	9.3	25	0.25	3.9	0.51	0.86	0.349	10.9	0.124422
No	6.9	5.9	21	0.4	2.3	0.4	0.93	0.293	24.1	0.270185
No	6.9	7.5	9	0.14	4.5	0.6	0.9	0.388	12.2	0.133948
No	6.9	5.3	14	0.126	3.2	0.5	0.94	0.316	8.5	0.107874
No	6.9	4.8	19	0.2	3.1	0.5	0.95	0.307	16	0.164756
No	6.9	4.5	5	0.16	2.5	0.6	0.95	0.39	19.2	0.196505
No	6.9	7.5	10	0.206	6.1	0.6	0.9	0.344	21.1	0.220033
No	6.9	3.5	0	0.23	1.7	0.6	0.97	0.412	24.6	0.280849
No	6.9	5	10	0.3	3	0.6	0.94	0.379	21.4	0.224215
No	6.9	3.5	6	0.4	1.4	0.5	0.97	0.367	17.9	0.182683
No	6.9	8	50	0.08	2	0.5	0.89	0.404	25	0.290012
No	6.9	3.5	3	0.3	0.9	0.6	0.97	0.496	18.9	0.193178
No	7.8	7.6	5	0.17	1.5	0.22	0.96	0.22	19.3	0.197635
No	6.9	5.2	18	0.14	3.5	0.4	0.94	0.243	19.1	0.195386

No	6.9	8.5	20	0.18	5	0.4	0.88	0.26	15	0.156119
No	6.9	10	20	0.17	5	0.4	0.86	0.27	13.2	0.141579

Depth	Soil type	Observed SPT	Saturated Density	Submerged Density	Fine content	D50	Earthquake Zone	PGA	Magnitude	Rd	Total overburden Pressure	Effective overburden Pressure	CSR	CN	CE	CH	CB	CR	CS	SPT Corrected	Δ (N1)60cs	Final N160	CRR	K1	K2	MSF	FS	
1.50	SM-ML	9	1.70	1.70	45.00	0.18	IV	0.24	6.80	0.99	2.55	2.55	0.15	1.70	0.75	0.986	1.05	0.75	1.00	8.91	6.78	15.69	0.17	1.00	1.00	1.44	1.56	Non Liquefiable
3.00	SM	11	1.71	1.71	14.00	0.23	IV	0.24	6.80	0.98	5.10	5.10	0.15	1.40	0.75	0.986	1.05	0.85	1.00	10.17	2.63	12.80	0.14	1.00	1.00	1.44	1.31	Non Liquefiable
4.50	SM	12	1.71	1.71	14.00	0.23	IV	0.24	6.80	0.97	7.67	7.67	0.15	1.14	0.75	0.986	1.05	0.95	1.00	10.11	2.63	12.74	0.14	1.00	1.00	1.44	1.32	Non Liquefiable
6.00	SM	17	1.80	1.80	21.00	0.22	IV	0.24	6.80	0.95	10.23	10.23	0.15	0.99	0.75	0.986	1.05	0.95	1.00	12.40	4.85	17.25	0.18	1.00	1.00	1.44	1.77	Non Liquefiable
7.50	SM	20	1.80	1.80	21.00	0.22	IV	0.24	6.80	0.94	12.93	12.93	0.15	0.88	0.75	0.986	1.05	0.95	1.00	12.97	4.9	17.87	0.19	0.95	1.00	1.44	1.76	Non Liquefiable
9.00	SM	26	1.80	1.80	17.00	0.23	IV	0.24	6.80	0.93	15.63	15.63	0.15	0.80	0.75	0.986	1.05	1.00	1.00	16.15	3.98	20.13	0.22	0.90	1.00	1.44	1.93	Non Liquefiable
10.50	CI	22	1.90	1.90	94.00	0.06	IV	0.24	6.80	0.89	18.33	18.33	0.14	0.74	0.75	0.986	1.05	1.00	1.00	12.62	7.52	20.14	0.22	1.00	1.00	1.44	2.25	Non Liquefiable
12.00	CI	33	1.90	1.90	96.00	0.06	IV	0.24	6.80	0.85	21.18	21.18	0.13	0.69	0.75	0.986	1.05	1.00	1.00	17.61	8.52	26.13	0.32	1.00	1.00	1.44	3.42	Non Liquefiable
13.50	CI	36	1.95	1.95	96.00	0.06	IV	0.24	6.80	0.81	24.03	24.03	0.13	0.65	0.75	0.986	1.05	1.00	1.00	18.03	8.61	26.64	0.33	1.00	1.00	1.44	3.73	Non Liquefiable
15.00	CL	39	1.95	1.95	91.00	0.06	IV	0.24	6.80	0.77	26.96	26.96	0.12	0.61	0.75	0.986	1.05	1.00	1.00	18.44	8.69	27.13	0.34	1.00	1.00	1.44	4.09	Non Liquefiable
16.50	CL	38	1.95	1.95	91.00	0.06	IV	0.24	6.80	0.73	29.88	29.88	0.11	0.58	0.75	0.986	1.05	1.00	1.00	17.07	8.41	25.48	0.30	1.00	1.00	1.44	3.80	Non Liquefiable
18.00	CL	56	2.00	2.00	85.00	0.07	IV	0.24	6.80	0.69	32.81	32.81	0.11	0.55	0.75	0.986	1.05	1.00	1.00	24.01	9.8	33.81	NA	1.00	1.00	1.44	>1.0	Non Liquefiable
19.50	CL	65	2.00	2.00	85.00	0.07	IV	0.24	6.80	0.65	35.81	35.81	0.10	0.53	0.75	0.986	1.05	1.00	1.00	26.67	10.34	37.01	NA	1.00	1.00	1.44	>1.0	Non Liquefiable
21.00	ML	55	2.00	2.00	62.00	0.09	IV	0.24	6.80	0.61	38.81	38.81	0.10	0.51	0.75	0.986	1.05	1.00	1.00	21.68	9.34	31.02	NA	0.67	1.00	1.44	>1.0	Non Liquefiable
22.50	ML	57	2.00	2.00	62.00	0.09	IV	0.24	6.80	0.57	41.81	41.81	0.09	0.49	0.75	0.986	1.05	1.00	1.00	21.65	9.33	30.98	NA	0.66	1.00	1.44	>1.0	Non Liquefiable

Depth	Soil type	Observed SPT	Saturated Density	Submerged Density	Fine content		Earthquake Zone	PGA	Magnitude	Rd	Total overburden Pressure	Effective overburden Pressure	CSR	CN	CE	CH	CB	CR	CS	SPT Corrected	Δ (N1)60cs	Final N160	CRR	K1	K2	MSF	FS	
1.50	SM	11	1.80	1.80	30.00	0.19	IV	0.24	6.80	0.99	2.55	2.55	0.15	1.70	0.75	0.986	1.05	0.75	1.00	10.89	6.39	17.28	0.18	1.00	1.00	1.44	1.72	Non Liquefiable
3.00	SM	15	1.80	1.80	23.00	0.2	IV	0.24	6.80	0.98	5.25	5.25	0.15	1.38	0.75	0.986	1.05	0.85	1.00	13.66	5.43	19.09	0.20	1.00	1.00	1.44	1.93	Non Liquefiable
4.50	SM	19	1.80	1.80	23.00	0.2	IV	0.24	6.80	0.97	7.95	7.95	0.15	1.12	0.75	0.986	1.05	0.95	1.00	15.72	5.63	21.35	0.23	1.00	1.00	1.44	2.23	Non Liquefiable
6.00	SM	14	1.79	1.79	14.00	0.22	IV	0.24	6.80	0.95	10.65	10.65	0.15	0.97	0.75	0.986	1.05	0.95	1.00	10.01	2.63	12.64	0.14	0.99	1.00	1.44	1.31	Non Liquefiable
7.50	SM	18	1.79	1.79	14.00	0.22	IV	0.24	6.80	0.94	13.34	13.34	0.15	0.87	0.75	0.986	1.05	0.95	1.00	11.50	2.69	14.19	0.15	0.94	1.00	1.44	1.40	Non Liquefiable
9.00	ML	15	1.79	1.79	80.00	0.07	IV	0.24	6.80	0.93	16.02	16.02	0.15	0.79	0.75	0.986	1.05	1.00	1.00	9.20	6.84	16.04	0.17	0.92	1.00	1.44	1.55	Non Liquefiable
10.50	ML	22	1.80	1.80	80.00	0.07	IV	0.24	6.80	0.89	18.71	18.71	0.14	0.73	0.75	0.986	1.05	1.00	1.00	12.49	7.5	19.99	0.22	0.87	1.00	1.44	1.95	Non Liquefiable
12.00	CL	20	1.85	1.85	88.00	0.06	IV	0.24	6.80	0.85	21.41	21.41	0.13	0.68	0.75	0.986	1.05	1.00	1.00	10.61	7.13	17.74	0.19	1.00	1.00	1.44	2.05	Non Liquefiable
13.50	CL	23	1.85	1.85	88.00	0.06	IV	0.24	6.80	0.81	24.18	24.18	0.13	0.64	0.75	0.986	1.05	1.00	1.00	11.48	7.3	18.78	0.20	1.00	1.00	1.44	2.28	Non Liquefiable
15.00	CL	25	1.89	1.89	90.00	0.06	IV	0.24	6.80	0.77	26.96	26.96	0.12	0.61	0.75	0.986	1.05	1.00	1.00	11.82	7.37	19.19	0.21	1.00	1.00	1.44	2.46	Non Liquefiable
16.50	CL	28	1.90	1.90	90.00	0.06	IV	0.24	6.80	0.73	29.79	29.79	0.11	0.58	0.75	0.986	1.05	1.00	1.00	12.60	7.52	20.12	0.22	1.00	1.00	1.44	2.73	Non Liquefiable
18.00	CL	19	1.91	1.91	90.00	0.06	IV	0.24	6.80	0.69	32.64	32.64	0.11	0.55	0.75	0.986	1.05	1.00	1.00	8.17	6.63	14.80	0.16	1.00	1.00	1.44	2.11	Non Liquefiable
19.50	CL	24	1.91	1.91	90.00	0.06	IV	0.24	6.80	0.65	35.51	35.51	0.10	0.53	0.75	0.986	1.05	1.00	1.00	9.89	6.98	16.87	0.18	1.00	1.00	1.44	2.54	Non Liquefiable
21.00	CL	33	1.95	1.95	83.00	0.07	IV	0.24	6.80	0.61	38.37	38.37	0.10	0.51	0.75	0.986	1.05	1.00	1.00	13.08	7.62	20.70	0.22	1.00	1.00	1.44	3.38	Non Liquefiable
22.50	CL	39	1.95	1.95	83.00	0.07	IV	0.24	6.80	0.57	41.30	41.30	0.09	0.49	0.75	0.986	1.05	1.00	1.00	14.90	7.98	22.88	0.26	1.00	1.00	1.44	4.11	Non Liquefiable

Depth	Soil type	Observed SPT	Saturated Density	Submerged Density	Fine content	D50	Earthquake Zone	PGA	Magnitude	Rd	Total overburden Pressure	Effective overburden Pressure	CSR	CN	CE	CH	CB	CR	CS	SPT Corrected	Δ (N1)60cs	Final N160	CRR	K1	K2	MSF	FS	
1.50	CI	26	2.00	1.00	90.00	0.07	IV	0.24	6.80	0.99	2.85	1.35	0.33	1.70	0.75	0.986	1.05	0.75	1.00	25.74	10.15	35.89	NA	1.00	1.00	1.44	>1.0	Non Liquefiable
3.00	SM-ML	26	2.00	1.00	44.00	0.12	IV	0.24	6.80	0.98	5.85	2.85	0.31	1.70	0.75	0.986	1.05	0.85	1.00	29.17	10.84	40.01	NA	1.00	1.00	1.44	>1.0	Non Liquefiable
4.50	CI	25	2.00	1.00	95.00	0.065	IV	0.24	6.80	0.97	8.85	4.35	0.31	1.52	0.75	0.986	1.05	0.95	1.00	27.96	10.59	38.55	NA	1.00	1.00	1.44	>1.0	Non Liquefiable
6.00	CL	14	1.97	0.97	81.00	0.075	IV	0.24	6.80	0.95	11.85	5.85	0.30	1.31	0.75	0.986	1.05	0.95	1.00	13.50	7.7	21.20	0.33	1.00	1.00	1.44	1.10	Liquefiable
7.50	SM-ML	24	1.98	0.98	31.00	0.18	IV	0.24	6.80	0.04	14.81	7.31	0.30	1.17	0.75	0.986	1.05	0.95	1.00	20.71	8.14	28.85	0.58	1.00	1.00	1.44	1.95	Non Liquefiable
9.00	CI	42	2.02	1.02	95.00	0.07	IV	0.24	6.80	0.93	17.78	8.78	0.29	1.07	0.75	0.986	1.05	1.00	1.00	34.81	11.97	46.78	NA	1.00	1.00	1.44	>1.0	Non Liquefiable
10.50	CI	45	2.02	1.02	95.00	0.07	IV	0.24	6.80	0.89	20.81	10.31	0.28	0.99	0.75	0.986	1.05	1.00	1.00	34.42	11.88	46.30	NA	1.00	1.00	1.44	>1.0	Non Liquefiable
12.00	CL	44	2.02	1.02	82.00	0.07	IV	0.24	6.80	0.85	23.84	11.84	0.27	0.92	0.75	0.986	1.05	1.00	1.00	31.40	11.29	42.69	NA	1.00	1.00	1.44	>1.0	Non Liquefiable
13.50	CL	47	2.02	1.02	82.00	0.074	IV	0.24	6.80	0.81	26.87	13.37	0.26	0.86	0.75	0.986	1.05	1.00	1.00	31.57	11.31	42.88	NA	1.00	1.00	1.44	>1.0	Non Liquefiable
15.00	ML	48	2.01	1.01	69.00	0.098	IV	0.24	6.80	0.77	29.90	14.90	0.24	0.82	0.75	0.986	1.05	1.00	1.00	30.54	11.11	41.65	NA	0.87	1.00	1.44	>1.0	Non Liquefiable
16.50	ML	46	2.01	1.01	69.00	0.092	IV	0.24	6.80	0.73	32.g1	16.41	0.23	0.78	0.75	0.986	1.05	1.00	1.00	27.88	10.58	38.46	NA	0.84	1.00	1.44	>1.0	Non Liquefiable
18.00	CL	57	2.04	1.04	88.00	0.078	IV	0.24	6.80	0.69	35.93	17.93	0.22	0.75	0.75	0.986	1.05	1.00	1.00	33.06	11.61	44.67	NA	1.00	1.00	1.44	>1.0	Non Liquefiable
19.50	CL	48	2.04	1.04	88.00	0.08	IV	0.24	6.80	0.65	38.99	19.49	0.20	0.72	0.75	0.986	1.05	1.00	1.00	30.54	14.51	45.05	NA	1.00	1.00	1.44	>1.0	Non Liquefiable
21.00	SM-ML	42	2.04	1.04	38.00	0.13	IV	0.24	6.80	0.61	42.05	21.05	0.19	0.69	0.75	0.986	1.05	1.00	1.00	34.52	34.71	69.23	NA	0.70	1.00	1.44	>1.0	Non Liquefiable
22.50	SM-ML	42	2.04	1.04	38.00	0.14	IV	0.24	6.80	0.57	45.11	22.61	0.18	0.67	0.75	0.986	1.05	1.00	1.00	34.22	16.64	50.86	NA	0.72	1.00	1.44	>1.0	Non Liquefiable

Depth	Soil type	Observed SPT	Saturated Density	Submerged Density	Fine content	D50	Earthquake Zone	PGA	Magnitude	Rd	Total overburden Pressure	Effective overburden Pressure	CSR	CN	CE	CH	CB	CR	CS	SPT Corrected	Δ (N1)60cs	Final N160	CRR	K1	K2	MSF	FS	
1.50	CI	20	1.99	0.99	88.00	0.08	IV	0.24	6.80	0.99	2.70	1.20	0.35	1.70	0.75	0.986	1.05	0.75	1.00	19.80	8.96	28.76	NA	1.00	1.00	1.44	1.66	Non Liquefiable
3.00	Cl	25	2.00	1.00	91.00	0.06	IV	0.24	6.80	0.98	5.69	2.69	0.32	1.70	0.75	0.986	1.05	0.85	1.00	28.05	10.61	38.66	NA	1.00	1.00	1.44	>1.0	Non Liquefiable
4.50	CI	22	2.00	1.00	91.00	0.06	IV	0.24	6.80	0.97	8.69	4.19	0.31	1.55	0.75	0.986	1.05	0.95	1.00	25.09	10.01	35.10	NA	1.00	1.00	1.44	>1.0	Non Liquefiable
6.00	SM-ML	30	2.00	1.00	42.00	0.13	IV	0.24	6.80	0.95	11.69	5.69	0.31	1.33	0.75	0.986	1.05	0.95	1.00	29.35	10.87	40.22	0.65	1.00	1.00	1.44	>1.0	Non Liquefiable
7.50	SM-ML	34	2.01	1.01	42.00	0.13	IV	0.24	6.80	0.94	14.69	7.19	0.30	1.18	0.75	0.986	1.05	0.95	1.00	29.59	10.92	40.51	0.65	1.00	1.00	1.44	>1.0	Non Liquefiable
9.00	SM-ML	41	2.01	1.01	43.00	0.15	IV	0.24	6.80	0.93	17.70	8.70	0.30	1.07	0.75	0.986	1.05	1.00	1.00	34.13	11.83	45.96	0.62	1.00	1.00	1.44	>1.0	Non Liquefiable
10.50	CI	40	2.03	1.03	94.00	0.075	IV	0.24	6.80	0.89	20.72	10.22	0.28	0.99	0.75	0.986	1.05	1.00	1.00	30.73	11.15	41.88	NA	1.00	1.00	1.44	>1.0	Non Liquefiable
12.00	ML-CL	30	2.00	1.00	86.00	0.71	IV	0.24	6.80	0.85	23.76	11.76	0.27	0.92	0.75	0.986	1.05	1.00	1.00	21.48	9.3	30.78	NA	1.00	1.00	1.44	>1.0	Non Liquefiable
13.50	Cl	38	2.03	1.03	90.00	0.06	IV	0.24	6.80	0.81	26.76	13.26	0.26	0.87	0.75	0.986	1.05	1.00	1.00	25.62	10.13	35.75	NA	1.00	1.00	1.44	>1.0	Non Liquefiable
15.00	ML-CL	56	2.03	1.03	88.00	0.06	IV	0.24	6.80	0.77	29.81	14.81	0.24	0.82	0.75	0.986	1.05	1.00	1.00	35.74	12.14	47.88	NA	1.00	1.00	1.44	>1.0	Non Liquefiable
16.50	ML-CL	61	2.03	1.03	88.00	0.064	IV	0.24	6.80	0.73	32.85	16.35	0.23	0.78	0.75	0.986	1.05	1.00	1.00	37.04	12.41	49.45	NA	1.00	1.00	1.44	>1.0	Non Liquefiable
18.00	CI	60	2.06	1.06	95.00	0.061	IV	0.24	6.80	0.69	35.90	17.90	0.22	0.75	0.75	0.986	1.05	1.00	1.00	34.83	11.96	46.79	NA	1.00	1.00	1.44	>1.0	Non Liquefiable
19.50	CI	65	2.06	1.06	95.00	0.062	IV	0.24	6.80	0.65	38.99	19.49	0.20	0.72	0.75	0.986	1.05	1.00	1.00	36.16	12.23	48.39	NA	1.00	1.00	1.44	>1.0	Non Liquefiable
21.00	SM	50	2.04	1.04	44.00	0.198	IV	0.24	6.80	0.61	42.08	21.08	0.19	0.69	0.75	0.986	1.05	1.00	1.00	26.74	10.35	37.09	0.66	0.78	1.00	1.44	>1.0	Non Liquefiable
22.50	SM	62	2.04	1.04	26.00	0.19	IV	0.24	6.80	0.57	45.14	22.64	0.18	0.66	0.75	0.986	1.05	1.00	1.00	32.00	8.31	40.31	0.63	0.74	1.00	1.44	>1.0	Non Liquefiable

Depth	Soil type	Observed SPT	Saturated Density	Submerged Density	Fine content	D50	Earthquake Zone	PGA	Magnitude	Rd	Total overburden Pressure	Effective overburden Pressure	CSR	CN	CE	CH	CB	CR	CS	SPT Corrected	Δ(N1)60cs	Final N160	CRR	K1	K2	MSF	FS	
1.50	CL	18	1.98	0.98	90.00	0.079	IV	0.24	6.80	0.99	2.85	1.35	0.33	1.70	0.75	0.986	1.05	0.75	1.00	17.82	8.56	26.38	0.32	1.00	1.00	1.44	1.43	Non Liquefiable
3.00	CI	27	2.01	1.01	93.00	0.067	IV	0.24	6.80	0.98	5.82	2.82	0.31	1.70	0.75	0.986	1.05	0.85	1.00	30.2	11.15	41.35	NA	1.00	1.00	1.44	>1.0	Non Liquefiable
4.50	CI	29	2.01	1.01	93.00	0.067	IV	0.24	6.80	0.97	8.84	4.34	0.31	1.52	0.75	0.986	1.05	0.95	1.00	32.49	11.5	43.99	NA	1.00	1.00	1.44	>1.0	Non Liquefiable
6.00	ML	34	2.01	1.01	72.00	0.09	IV	0.24	6.80	0.95	11.85	5.85	0.30	1.31	0.75	0.986	1.05	0.95	1.00	32.79	11.56	44.35	NA	1.00	1.00	1.44	>1.0	Non Liquefiable
7.50	ML	37	2.01	1.01	72.00	0.09	IV	0.24	6.80	0.94	14.87	7.37	0.30	1.17	0.75	0.986	1.05	0.95	1.00	31.80	11.36	43.16	NA	1.00	1.00	1.44	>1.0	Non Liquefiable
9.00	SM	42	2.02	1.02	22.00	0.198	IV	0.24	6.80	0.93	17.88	8.88	0.29	1.06	0.75	0.986	1.05	1.00	1.00	34.61	7.15	41.76	NA	1.00	1.00	1.44	>1.0	Non Liquefiable
10.50	SM	44	2.02	1.02	22.00	0.198	IV	0.24	6.80	0.89	20.91	10.41	0.28	0.98	0.75	0.986	1.05	1.00	1.00	33.49	7.04	40.53	NA	0.99	1.00	1.44	>1.0	Non Liquefiable
12.00	CI	37	2.03	1.03	93.00	0.066	IV	0.24	6.80	0.85	23.94	11.94	0.27	0.92	0.75	0.986	1.05	1.00	1.00	26.29	10.26	36.55	NA	1.00	1.00	1.44	>1.0	Non Liquefiable
13.50	CI	38	2.03	1.03	93.00	0.066	IV	0.24	6.80	0.81	26.99	13.49	0.25	0.86	0.75	0.986	1.05	1.00	1.00	25.41	10.08	35.49	NA	1.00	1.00	1.44	>1.0	Non Liquefiable
15.00	ML	120	2.06	1.06	72.00	0.82	IV	0.24	6.80	0.71	30.03	15.03	0.24	0.82	0.75	0.986	1.05	1.00	1.00	76.00	20.2	96.20	NA	0.82	1.00	1.44	>1.0	Non Liquefiable
16.50	ML	120	2.06	1.06	72.00	0.82	IV	0.24	6.80	0.73	33.12	16.62	0.23	0.78	0.75	0.986	1.05	1.00	1.00	72.28	19.45	91.73	NA	0.78	1.00	1.44	>1.0	Non Liquefiable
18.00	CL	84	2.08	1.08	81.00	0.91	IV	0.24	6.80	0.69	36.21	18.21	0.22	0.74	0.75	0.986	1.05	1.00	1.00	48.33	14.67	63.00	NA	1.00	1.00	1.44	>1.0	Non Liquefiable
19.50	CL	100	2.08	1.08	81.00	0.91	IV	0.24	6.80	0.65	39.33	19.83	0.20	0.71	0.75	0.986	1.05	1.00	1.00	55.14	16.03	71.17	NA	1.00	1.00	1.44	>1.0	Non Liquefiable
21.00	SM	150	2.08	1.08	29.00	0.18	IV	0.24	6.80	0.61	42.45	21.45	0.19	0.68	0.75	0.986	1.05	1.00	1.00	79.53	16.26	95.79	NA	0.68	1.00	1.44	>1.0	Non Liquefiable
22.50	SM	130	2.08	1.08	29.00	0.18	IV	0.24	6.80	0.57	45.57	23.07	0.18	0.66	0.75	0.986	1.05	1.00	1.00	66.68	14.38	81.06	NA	0.66	1.00	1.44	>1.0	Non Liquefiable

Depth	Soil type	Observed SPT	Saturated Density	Submerged Density	Fine content	D50	Earthquake Zone	PGA	Magnitude	Rd	Total overburden Pressure	Effective overburden Pressure	CSR	CN	CE	CH	CB	CR	CS	SPT Corrected	Δ(N1)60cs	Final N160	CRR	K1	K2	MSF	FS	
1.50	CL	22	2.00	1.00	81.00	0.13	IV	0.24	6.80	0.99	2.85	1.35	0.33	1.70	0.75	0.986	1.05	0.75	1.00	21.78	9.36	31.14	NA	1.00	1.00	1.44	>1.0	Non Liquefiable
3.00	SM	26	2.01	1.01	18.00	0.21	IV	0.24	6.80	0.98	5.85	2.85	0.31	1.70	0.75	0.986	1.05	0.85	1.00	29.17	5.17	34.34	0.65	1.00	1.00	1.44	>1.0	Non Liquefiable
4.50	SM	30	2.01	1.01	18.00	0.21	IV	0.24	6.80	0.97	8.87	4.37	0.31	1.51	0.75	0.986	1.05	0.85	1.00	33.50	5.45	38.95	0.63	1.00	1.00	1.44	>1.0	Non Liquefiable
6.00	SM	35	2.01	1.01	20.00	0.21	IV	0.24	6.80	0.95	11.88	5.88	0.30	1.30	0.75	0.986	1.05	0.85	1.00	33.67	6.29	39.96	0.62	1.00	1.00	1.44	>1.0	Non Liquefiable
7.50	SM	41	2.01	1.01	20.00	0.21	IV	0.24	6.80	0.94	14.90	7.40	0.30	1.16	0.75	0.986	1.05	0.95	1.00	35.17	6.41	41.58	0.62	1.00	1.00	1.44	>1.0	Non Liquefiable
9.00	Cl	41	2.03	1.03	92.00	0.070	IV	0.24	6.80	0.93	17.91	8.91	0.29	1.06	0.75	0.986	1.05	1.00	1.00	33.73	11.74	45.47	NA	1.00	1.00	1.44	>1.0	Non Liquefiable
10.50	Cl	46	2.03	1.03	92.00	0.070	IV	0.24	6.80	0.89	20.96	10.46	0.28	0.98	0.75	0.986	1.05	1.00	1.00	34.93	11.99	46.92	NA	1.00	1.00	1.44	>1.0	Non Liquefiable
12.00	ML-CL	200	2.08	1.08	84.00	0.09	IV	0.24	6.80	0.85	24.00	12.00	0.27	0.91	0.75	0.986	1.05	1.00	1.00	141.76	33.36	175.12	NA	1.00	1.00	1.44	>1.0	Non Liquefiable
13.50	ML-CL	120	2.08	1.08	84.00	0.09	IV	0.24	6.80	0.81	27.12	13.62	0.25	0.86	0.75	0.986	1.05	1.00	1.00	79.84	20.97	100.81	NA	1.00	1.00	1.44	>1.0	Non Liquefiable
15.00	ML-CL	100	2.08	1.08	77.00	0.12	IV	0.24	6.80	0.77	30.24	15.24	0.24	0.81	0.75	0.986	1.05	1.00	1.00	62.90	17.58	80.48	NA	1.00	1.00	1.44	>1.0	Non Liquefiable
16.50	ML-CL	100	2.08	1.08	77.00	0.12	IV	0.24	6.80	0.73	33.36	16.86	0.23	0.77	0.75	0.986	1.05	1.00	1.00	59.80	16.96	76.76	NA	1.00	1.00	1.44	>1.0	Non Liquefiable
18.00	CI	60	2.06	1.06	92.00	0.071	IV	0.24	6.80	0.69	36.48	18.48	0.21	0.74	0.75	0.986	1.05	1.00	1.00	34.27	11.86	46.13	NA	1.00	1.00	1.44	>1.0	Non Liquefiable
19.50	CI	64	2.06	1.06	92.00	0.071	IV	0.24	6.80	0.65	39.57	20.07	0.20	0.71	0.75	0.986	1.05	1.00	1.00	35.08	12.01	47.09	NA	1.00	1.00	1.44	>1.0	Non Liquefiable
21.00	CL	76	2.07	1.07	87.00	0.082	IV	0.24	6.80	0.61	42.66	21.66	0.19	0.68	0.75	0.986	1.05	1.00	1.00	40.10	13.02	53.12	NA	1.00	1.00	1.44	>1.0	Non Liquefiable
22.50	SM	88	2.05	1.05	26.00	0.182	IV	0.24	6.80	0.57	45.77	23.27	0.18	0.66	0.75	0.986	1.05	1.00	1.00	44.80	9.88	54.68	0.56	0.69	1.00	1.44	>1.0	Non Liquefiable

Depth	Soil type	Observed SPT	Saturated Density	Submerged Density	Fine content	D50	Earthquake Zone	PGA	Magnitude	Rd	Total overburden Pressure	Effective overburden Pressure	CSR	CN	CE	CH	CB	CR	CS	SPT Corrected	Δ(N1)60cs	Final N160	CRR	K1	K2	MSF	FS	
1.50	ML	21	2.00	1.00	72.00	0.1	IV	0.24	6.80	0.99	2.85	1.35	0.33	1.70	0.75	0.986	1.05	0.75	1.00	20.79	9.16	29.95	0.71	1.00	1.00	1.44	2.06	Non Liquefiable
3.00	SM-ML	18	1.98	0.98	43.00	0.14	IV	0.24	6.80	0.98	5.85	2.85	0.31	1.70	0.75	0.986	1.05	0.85	1.00	20.20	9.04	29.24	0.72	1.00	1.00	1.44	1.94	Non Liquefiable
4.50	SM-ML	23	2.00	1.00	43.00	0.14	IV	0.24	6.80	0.97	8.82	4.32	0.31	1.52	0.75	0.986	1.05	0.95	1.00	25.81	10.17	35.98	0.67	1.00	1.00	1.44	>1.0	Non Liquefiable
6.00	SM	29	2.00	1.00	24.00	0.198	IV	0.24	6.80	0.95	11.82	5.82	0.30	1.31	0.75	0.986	1.05	0.95	1.00	28.04	7.2	35.24	0.66	1.00	1.00	1.44	>1.0	Non Liquefiable
7.50	SM	31	2.00	1.00	24.00	0.198	IV	0.24	6.80	0.94	14.82	7.32	0.30	1.17	0.75	0.986	1.05	0.95	1.00	26.73	7.05	33.78	0.66	1.00	1.00	1.44	>1.0	Non Liquefiable
9.00	SM	30	2.00	1.00	20.00	0.198	IV	0.24	6.80	0.93	17.82	8.82	0.29	1.06	0.75	0.986	1.05	1.00	1.00	24.80	5.59	30.39	0.68	1.00	1.00	1.44	>1.0	Non Liquefiable
10.50	SM	37	2.00	1.00	20.00	0.198	IV	0.24	6.80	0.89	20.82	10.32	0.28	0.98	0.75	0.986	1.05	1.00	1.00	28.28	5.86	34.14	0.66	0.99	1.00	1.44	>1.0	Non Liquefiable
12.00	CL	42	2.02	1.02	85.00	0.07	IV	0.24	6.80	0.85	23.82	11.82	0.27	0.92	0.75	0.986	1.05	1.00	1.00	30.00	11	41.00	NA	1.00	1.00	1.44	>1.0	Non Liquefiable
13.50	CL	49	2.02	1.02	85.00	0.07	IV	0.24	6.80	0.81	26.85	13.35	0.26	0.87	0.75	0.986	1.05	1.00	1.00	32.93	11.59	44.52	NA	1.00	1.00	1.44	>1.0	Non Liquefiable
15.00	CL	200	2.08	1.08	84.00	0.07	IV	0.24	6.80	*0.7T*	29.88	14.88	0.24	0.82	0.75	0.986	1.05	1.00	1.00	127.31	30.46	157.77	NA	1.00	1.00	1.44	>1.0	Non Liquefiable
16.50	CL	85	2.08	1.08	84.00	0.07	IV	0.24	6.80	0.73	33.00	16.50	0.23	0.78	0.75	0.986	1.05	1.00	1.00	51.38	15.28	66.66	NA	1.00	1.00	1.44	>1.0	Non Liquefiable
18.00	CL	59	2.05	1.05	89.00	0.07	IV	0.24	6.80	0.69	36.12	18.12	0.22	0.74	0.75	0.986	1.05	1.00	1.00	34.03	11.81	45.84	NA	1.00	1.00	1.44	>1.0	Non Liquefiable
19.50	CL	64	2.05	1.05	89.00	0.07	IV	0.24	6.80	0.65	39.20	19.70	0.20	0.71	0.75	0.986	1.05	1.00	1.00	35.41	12.08	47.49	NA	1.00	1.00	1.44	>1.0	Non Liquefiable
21.00	SM-ML	100	2.08	1.08	44.00	0.13	IV	0.24	6.80	0.61	42.27	21.27	0.19	0.69	0.75	0.986	1.05	1.00	1.00	53.24	15.65	68.89	0.52	0.70	1.00	1.44	>1.0	Non Liquefiable
22.50	SM-ML	120	2.08	1.08	44.00	0.13	IV	0.24	6.80	0.57	45.39	22.89	0.18	0.66	0.75	0.986	1.05	1.00	1.00	61.59	17.31	78.90	0.50	0.66	1.00	1.44	>1.0	Non Liquefiable

Depth	Soil type	Observed SPT	Saturated Density	Submerged Density	Fine content	D50	Earthquake Zone	PGA	Magnitude	Rd	Total overburden Pressure	Effective overburden Pressure	CSR	CN	CE	CH	CB	CR	CS	SPT Corrected	Δ (N1)60cs	Final N160	CRR	K1	K2	MSF	FS	
1.50	CI	10	1.94	0.94	88.00	0.09	IV	0.24	6.80	0.99	2.85	1.35	0.33	1.70	0.75	0.986	1.05	0.75	1.00	9.90	6.98	16.88	0.37	1.00	1.00	1.44	1.66	Non Liquefiable
3.00	ML	17	1.98	0.98	56.00	0.12	IV	0.24	6.80	0.98	5.76	2.76	0.32	1.70	0.75	0.986	1.05	0.85	1.00	19.07	8.82	27.89	NA	1.00	1.00	1.44	>1.0	Non Liquefiable
4.50	ML	19	1.98	0.98	56.00	0.12	IV	0.24	6.80	0.97	8.73	4.23	0.31	1.54	0.75	0.986	1.05	0.85	1.00	21.55	9.31	30.86	0.27	1.00	1.00	1.44	1.28	Non Liquefiable
6.00	SM	17	1.96	0.96	30.00	0.19	IV	0.24	6.80	0.95	11.70	5.70	0.31	1.32	0.75	0.986	1.05	0.85	1.00	16.61	7.27	23.88	0.29	1.00	1.00	1.44	1.38	Non Liquefiable
7.50	SM	20	1.97	0.97	30.00	0.19	IV	0.24	6.80	0.94	14.64	7.14	0.30	1.18	0.75	0.986	1.05	0.95	1.00	17.46	7.4	24.86	NA	1.00	1.00	1.44	>1.0	Non Liquefiable
9.00	SM	44	2.02	1.02	28.00	0.19	IV	0.24	6.80	0.93	17.60	8.60	0.30	1.08	0.75	0.986	1.05	1.00	1.00	36.85	9.65	46.50	NA	1.00	1.00	1.44	>1.0	Non Liquefiable
10.50	SM	48	2.02	1.02	28.00	0.19	IV	0.24	6.80	0.89	20.63	10.13	0.28	0.99	0.75	0.986	1.05	1.00	1.00	37.04	9.68	46.72	NA	1.00	1.00	1.44	>1.0	Non Liquefiable
12.00	SP-SM	53	2.02	1.02	11.00	0.24	IV	0.24	6.80	0.85	23.66	11.66	0.27	0.93	0.75	0.986	1.05	1.00	1.00	38.12	2.22	40.34	0.36	0.94	1.00	1.44	1.88	Non Liquefiable
13.50	SM-ML	28	1.98	0.98	44.00	0.18	IV	0.24	6.80	0.81	26.69	13.19	0.26	0.87	0.75	0.986	1.05	1.00	1.00	18.93	8.79	27.72	NA	0.93	1.00	1.44	>1.0	Non Liquefiable
15.00	ML	49	2.00	1.00	73.00	0.09	IV	0.24	6.80	0.77	29.66	14.66	0.24	0.83	0.75	0.986	1.05	1.00	1.00	31.43	11.28	42.71	NA	0.87	1.00	1.44	>1.0	Non Liquefiable
16.50	ML	48	2.00	1.00	73.00	0.09	IV	0.24	6.80	0.73	32.66	16.16	0.23	0.79	0.75	0.986	1.05	1.00	1.00	29.32	10.87	40.19	NA	0.85	1.00	1.44	>1.0	Non Liquefiable
18.00	CI	37	2.03	1.03	91.00	0.07	IV	0.24	6.80	0.69	35.66	17.66	0.22	0.75	0.75	0.986	1.05	1.00	1.00	21.62	9.33	30.95	NA	1.00	1.00	1.44	>1.0	Non Liquefiable
19.50	CI	43	2.03	1.03	91.00	0.07	IV	0.24	6.80	0.65	38.70	19.20	0.21	0.72	0.75	0.986	1.05	1.00	1.00	24.10	9.82	33.92	NA	1.00	1.00	1.44	>1.0	Non Liquefiable
21.00	SM-ML	95	2.05	1.05	30.00	0.19	IV	0.24	6.80	0.61	41.75	20.75	0.19	0.69	0.75	0.986	1.05	1.00	1.00	51.21	12.61	63.82	NA	0.71	1.00	1.44	>1.0	Non Liquefiable
22.50	SM-ML	93	2.05	1.05	30.00	0.19	IV	0.24	6.80	0.57	44.82	22.32	0.18	0.67	0.75	0.986	1.05	1.00	1.00	48.34	12.16	60.50	0.37	0.69	1.00	1.44	1.66	Non Liquefiable

Depth	Soil type	Observed SPT	Saturated Density	Submerged Density	Fine content	D50	Earthquake Zone	PGA	Magnitude	Rd	Total overburden Pressure	Effective overburden Pressure	CSR	CN	CE	CH	CB	CR	CS	SPT Corrected	Δ(N1)60cs	Final N160	CRR	K1	K2	MSF	FS	
1.50	CI	15	1.96	0.96	90.00	0.067	IV	0.24	6.80	0.99	2.85	1.35	0.33	1.70	0.75	0.986	1.05	0.75	1.00	14.85	7.97	22.82	0.25	1.00	1.00	1.44	1.13	Non Liquefiable
3.00	ML	21	1.98	0.98	56.00	0.11	IV	0.24	6.80	0.98	5.79	2.79	0.32	1.70	0.75	0.986	1.05	0.85	1.00	23.56	9.71	33.27	NA	1.00	1.00	1.44	>1.0	Non Liquefiable
4.50	ML	25	1.98	0.98	56.00	0.11	IV	0.24	6.80	0.97	8.76	4.26	0.31	1.53	0.75	0.986	1.05	0.95	1.00	28.25	10.66	38.91	NA	1.00	1.00	1.44	>1.0	Non Liquefiable
6.00	SM	31	2.00	1.00	24.00	0.18	IV	0.24	6.80	0.95	11.73	5.73	0.30	1.32	0.75	0.986	1.05	0.95	1.00	30.21	7.43	37.64	NA	1.00	1.00	1.44	>1.0	Non Liquefiable
7.50	SM	34	2.00	1.00	24.00	0.18	IV	0.24	6.80	0.94	14.73	7.23	0.30	1.18	0.75	0.986	1.05	0.95	1.00	29.50	7.35	36.85	NA	1.00	1.00	1.44	>1.0	Non Liquefiable
9.00	SM	42	2.01	1.01	17.00	0.23	IV	0.24	6.80	0.93	17.73	8.73	0.30	1.07	0.75	0.986	1.05	1.00	1.00	34.90	5.11	40.01	NA	1.00	1.00	1.44	>1.0	Non Liquefiable
10.50	SM	48	2.01	1.01	17.00	0.23	IV	0.24	6.80	0.89	20.75	10.25	0.28	0.99	0.75	0.986	1.05	1.00	1.00	36.82	5.23	42.05	NA	0.99	1.00	1.44	>1.0	Non Liquefiable
12.00	ML	43	2.01	1.01	72.00	0.09	IV	0.24	6.80	0.85	23.76	11.76	0.27	0.92	0.75	0.986	1.05	1.00	1.00	30.79	11.16	41.95	NA	0.94	1.00	1.44	>1.0	Non Liquefiable
13.50	ML	55	2.01	1.01	72.00	0.09	IV	0.24	6.80	0.81	26.78	13.28	0.26	0.87	0.75	0.986	1.05	1.00	1.00	37.07	12.41	49.48	NA	0.89	1.00	1.44	>1.0	Non Liquefiable
15.00	ML	136	2.08	1.08	69.00	0.1	IV	0.24	6.80	0.77	29.79	14.79	0.24	0.82	0.75	0.986	1.05	1.00	1.00	87.06	22.42	109.48	NA	0.82	1.00	1.44	>1.0	Non Liquefiable
16.50	ML	126	2.08	1.08	69.00	0.1	IV	0.24	6.80	0.73	32.91	16.41	0.23	0.78	0.75	0.986	1.05	1.00	1.00	76.53	20.3	96.83	NA	0.78	1.00	1.44	>1.0	Non Liquefiable
18.00	CL	21	2.00	1.00	87.00	0.08	IV	0.24	6.80	0.69	36.03	18.03	0.22	0.74	0.75	0.986	1.05	1.00	1.00	12.14	7.43	19.57	0.21	1.00	1.00	1.44	1.40	Non Liquefiable
19.50	CL	32	2.02	1.02	87.00	0.08	IV	0.24	6.80	0.65	39.03	19.53	0.20	0.72	0.75	0.986	1.05	1.00	1.00	17.78	8.56	26.34	0.32	1.00	1.00	1.44	2.27	Non Liquefiable
21.00	SM-ML	75	2.03	1.03	41.00	0.18	IV	0.24	6.80	0.61	42.06	21.06	0.19	0.69	0.75	0.986	1.05	1.00	1.00	40.13	13.02	53.15	NA	0.73	1.00	1.44	>1.0	Non Liquefiable
22.50	SM-ML	100	2.05	1.05	41.00	0.18	IV	0.24	6.80	0.57	45.11	22.61	0.18	0.67	0.75	0.986	1.05	1.00	1.00	51.64	15.33	66.97	NA	0.68	1.00	1.44	>1.0	Non Liquefiable

Depth	Soil type	Observed SPT	Saturated Density	Submerged Density	Fine content	D50	Earthquake Zone	PGA	Magnitude	Rd	Total overburden Pressure	Effective overburden Pressure	CSR	CN	CE	CH	CB	CR	CS	SPT Corrected	Δ (N1)60cs	Final N160	CRR	K1	K2	MSF	FS	
1.50	CI	12	1.97	0.97	90.00	0.065	IV	0.24	6.80	0.99	2.85	1.35	0.33	1.70	0.75	0.986	1.05	0.75	1.00	11.88	7.38	19.26	0.21	1.00	1.00	1.44	0.70	Liquefiable
3.00	ML	7	1.97	0.97	66.00	0.093	IV	0.24	6.80	0.98	5.75	2.75	0.32	1.70	0.75	0.986	1.05	0.85	1.00	7.85	6.57	14.42	0.15	1.00	1.00	1.44	0.70	Liquefiable
4.50	ML	17	1.97	0.97	66.00	0.093	IV	0.24	6.80	0.97	8.64	4.14	0.31	1.55	0.75	0.986	1.05	0.85	1.00	19.49	8.9	28.39	0.38	1.00	1.00	1.44	1.76	Non Liquefiable
6.00	SM	22	1.97	0.97	20.00	0.2	IV	0.24	6.80	0.95	11.60	5.60	0.31	1.34	0.75	0.986	1.05	0.85	1.00	21.70	5.33	27.03	0.34	1.00	1.00	1.44	1.59	Non Liquefiable
7.50	SM	27	2.00	1.00	20.00	0.2	IV	0.24	6.80	0.94	14.55	7.05	0.30	1.19	0.75	0.986	1.05	0.95	1.00	23.72	5.5	29.22	0.42	1.00	1.00	1.44	2.00	Non Liquefiable
9.00	SM	30	2.00	1.00	19.00	0.2	IV	0.24	6.80	0.93	17.55	8.55	0.30	1.08	0.75	0.986	1.05	1.00	1.00	25.19	5.27	30.46	NA	1.00	1.00	1.44	>1.0	Non Liquefiable
10.50	SM	33	2.00	1.00	19.00	0.2	IV	0.24	6.80	0.89	20.55	10.05	0.29	1.00	0.75	0.986	1.05	1.00	1.00	25.56	5.29	30.85	NA	1.00	1.00	1.44	>1.0	Non Liquefiable
12.00	SM	36	2.00	1.00	23.00	0.2	IV	0.24	6.80	0.85	23.55	11.55	0.27	0.93	0.75	0.986	1.05	1.00	1.00	26.01	6.67	32.68	NA	0.95	1.00	1.44	>1.0	Non Liquefiable
13.50	SM	56	2.05	1.05	23.00	0.2	IV	0.24	6.80	0.81	26.55	13.05	0.26	0.88	0.75	0.986	1.05	1.00	1.00	38.06	7.88	45.94	NA	0.90	1.00	1.44	>1.0	Non Liquefiable
15.00	ML	120	2.05	1.05	69.00	0.09	IV	0.24	6.80	0.77	29.63	14.63	0.24	0.83	0.75	0.986	1.05	1.00	1.00	77.05	20.41	97.46	NA	0.83	1.00	1.44	>1.0	Non Liquefiable
16.50	ML	130	2.05	1.05	69.00	0.09	IV	0.24	6.80	0.73	32.70	16.20	0.23	0.79	0.75	0.986	1.05	1.00	1.00	79.57	20.92	100.49	NA	0.79	1.00	1.44	>1.0	Non Liquefiable
18.00	CL	40	2.04	1.04	83.00	0.08	IV	0.24	6.80	0.69	35.78	17.78	0.22	0.75	0.75	0.986	1.05	1.00	1.00	23.30	9.66	32.96	NA	1.00	1.00	1.44	>1.0	Non Liquefiable
19.50	CL	55	2.05	1.05	83.00	0.08	IV	0.24	6.80	0.65	38.84	19.34	0.20	0.72	0.75	0.986	1.05	1.00	1.00	30.71	11.15	41.86	NA	1.00	1.00	1.44	>1.0	Non Liquefiable
21.00	CL	61	2.05	1.05	80.00	0.08	IV	0.24	6.80	0.61	41.91	20.91	0.19	0.69	0.75	0.986	1.05	1.00	1.00	32.76	11.55	44.31	NA	1.00	1.00	1.44	>1.0	Non Liquefiable
22.50	CL	62	2.05	1.05	80.00	0.08	IV	0.24	6.80	0.57	44.99	22.49	0.18	0.67	0.75	0.986	1.05	1.00	1.00	32.11	11.42	43.53	NA	1.00	1.00	1.44	>1.0	Non Liquefiable

Depth	Soil type	Observed SPT	Saturated Density	Submerged Density	Fine content	D50	Earthquake Zone	PGA	Magnitude	Rd	Total overburden Pressure	Effective overburden Pressure	CSR	CN	CE	CH	CB	CR	CS	SPT Corrected	Δ (N1)60cs	Final N160	CRR	K1	K2	MSF	FS	
1.50	CI	12	1.94	0.94	95.00	0.06	IV	0.24	6.80	0.99	2.70	1.20	0.35	1.70	0.75	0.986	1.05	0.75	1.00	11.88	7.38	19.26	0.21	1.00	1.00	1.44	>1.0	Non Liquefiable
3.00	CI	11	1.94	0.94	94.00	0.065	IV	0.24	6.80	0.98	5.61	2.61	0.33	1.70	0.75	0.986	1.05	0.85	1.00	12.34	7.47	19.81	0.21	1.00	1.00	1.44	>1.0	Non Liquefiable
4.50	CI	31	2.00	1.00	94.00	0.065	IV	0.24	6.80	0.97	8.52	4.02	0.32	1.58	0.75	0.986	1.05	0.95	1.00	36.07	12.21	48.28	NA	1.00	1.00	1.44	>1.0	Non Liquefiable
6.00	CI	5	1.92	0.92	95.00	0.06	IV	0.24	6.80	0.95	11.52	5.52	0.31	1.35	0.75	0.986	1.05	0.85	1.00	4.96	6	10.96	0.12	1.00	1.00	1.44	>1.0	Non Liquefiable
7.50	CI	9	1.92	0.92	95.00	0.06	IV	0.24	6.80	0.94	14.40	6.90	0.31	1.20	0.75	0.986	1.05	0.95	1.00	7.99	6.6	14.59	0.16	1.00	1.00	1.44	>1.0	Non Liquefiable
9.00	SP-SM	36	2.01	1.01	9.00	0.24	IV	0.24	6.80	0.93	17.28	8.28	0.30	1.10	0.75	0.986	1.05	1.00	1.00	30.72	1.08	31.80	NA	1.00	1.00	1.44	>1.0	Non Liquefiable
10.50	SP-SM	44	2.01	1.01	11.00	0.24	IV	0.24	6.80	0.89	20.30	9.80	0.29	1.01	0.75	0.986	1.05	1.00	1.00	34.52	2.12	36.64	NA	1.00	1.00	1.44	>1.0	Non Liquefiable
12.00	SM	54	2.01	1.01	14.00	0.24	IV	0.24	6.80	0.85	23.31	11.31	0.27	0.94	0.75	0.986	1.05	1.00	1.00	39.43	3.87	43.30	NA	0.95	1.00	1.44	>1.0	Non Liquefiable
13.50	ML	60	2.01	1.01	72.00	0.08	IV	0.24	6.80	0.81	26.33	12.83	0.26	0.88	0.75	0.986	1.05	1.00	1.00	41.14	13.23	54.37	NA	0.90	1.00	1.44	>1.0	Non Liquefiable
15.00	ML-CL	64	2.03	1.03	84.00	0.08	IV	0.24	6.80	0.77	29.34	14.34	0.25	0.84	0.75	0.986	1.05	1.00	1.00	41.50	13.3	54.80	NA	1.00	1.00	1.44	>1.0	Non Liquefiable
16.50	ML-CL	41	2.03	1.03	84.00	0.08	IV	0.24	6.80	0.73	32.39	15.89	0.23	0.79	0.75	0.986	1.05	1.00	1.00	25.26	10.05	35.31	NA	1.00	1.00	1.44	>1.0	Non Liquefiable
18.00	CL	32	2.02	1.02	82.00	0.08	IV	0.24	6.80	0.69	35.43	17.43	0.22	0.76	0.75	0.986	1.05	1.00	1.00	18.82	8.76	27.58	0.36	1.00	1.00	1.44	2.33	Non Liquefiable
19.50	CL	37	2.02	1.02	82.00	0.09	IV	0.24	6.80	0.65	38.46	18.96	0.21	0.73	0.75	0.986	1.05	1.00	1.00	20.86	9.18	30.04	NA	1.00	1.00	1.44	>1.0	Non Liquefiable
21.00	CL	39	2.02	1.02	87.00	0.08	IV	0.24	6.80	0.61	41.49	20.49	0.19	0.70	0.75	0.986	1.05	1.00	1.00	21.16	9.23	30.39	NA	1.00	1.00	1.44	>1.0	Non Liquefiable
22.50	CL	42	2.03	1.03	87.00	0.08	IV	0.24	6.80	0.57	44.52	22.02	0.18	0.67	0.75	0.986	1.05	1.00	1.00	21.98	9.39	31.37	NA	1.00	1.00	1.44	>1.0	Non Liquefiable

Depth	Soil type	Observed SPT	Saturated Density	Submerged Density	Fine content	D50	Earthquake Zone	PGA	Magnitude	Rd	Total overburden Pressure	Effective overburden Pressure	CSR	CN	CE	CH	CB	CR	CS	SPT Corrected	Δ (N1)60cs	Final N160	CRR	K1	K2	MSF	FS	
1.50	Filled up	50	1.80	0.80	87.00	0.08	IV	0.24	6.50	0.99	2.70	1.20	0.35	1.70	0.75	0.986	1.05	0.75	1.00	49.50	14.9	64.40	NA	1.00	1.00	1.44	>1.0	Non Liquefiable
3.00	CI	22	1.9g	0.99	90.00	0.08	IV	0.24	6.50	0.98	5.40	2.40	0.34	1.70	0.75	0.986	1.05	0.85	1.00	24.68	9.94	34.62	NA	1.00	1.00	1.44	>1.0	Non Liquefiable
4.50	CI	20	1.99	0.99	90.00	0.08	IV	0.24	6.50	0.97	8.39	3.89	0.33	1.60	0.75	0.986	1.05	0.95	1.00	23.67	9.73	33.40	NA	1.00	1.00	1.44	>1.0	Non Liquefiable
6.00	SM	21	1.97	0.97	34.00	0.18	IV	0.24	6.50	0.95	11.37	5.37	0.32	1.36	0.75	0.986	1.05	0.95	1.00	21.14	8.91	30.05	NA	1.00	1.00	1.44	>1.0	Non Liquefiable
7.50	SM	24	1.97	0.97	34.00	0.18	IV	0.24	6.50	0.94	14.33	6.83	0.31	1.21	0.75	0.986	1.05	0.95	1.00	21.43	8.97	30.40	NA	1.00	1.00	1.44	>1.0	Non Liquefiable
9.00	SM	30	1.99	0.99	29.00	0.18	IV	0.24	6.50	0.93	17.28	8.28	0.30	1.10	0.75	0.986	1.05	1.00	1.00	25.60	8.38	33.98	NA	1.00	1.00	1.44	>1.0	Non Liquefiable
10.50	SM	34	1.99	0.99	29.00	0.18	IV	0.24	6.50	0.89	20.27	9.77	0.29	1.01	0.75	0.986	1.05	1.00	1.00	26.72	8.54	35.26	NA	1.00	1.00	1.44	>1.0	Non Liquefiable
12.00	ML	37	2.00	1.00	80.00	0.08	IV	0.24	6.50	0.85	23.25	11.25	0.28	0.94	0.75	0.986	1.05	1.00	1.00	27.09	10.41	37.50	NA	0.96	1.00	1.44	>1.0	Non Liquefiable
13.50	ML	39	2.01	1.01	80.00	0.08	IV	0.24	6.50	0.81	26.25	12.75	0.26	0.89	0.75	0.986	1.05	1.00	1.00	26.82	10.36	37.18	NA	0.92	1.00	1.44	>1.0	Non Liquefiable
15.00	ML	120	2.04	1.04	82.00	0.08	IV	0.24	6.50	0.77	29.27	14.27	0.25	0.84	0.75	0.986	1.05	1.00	1.00	78.01	20.61	98.62	NA	0.84	1.00	1.44	>1.0	Non Liquefiable
16.50	ML	85	2.04	1.04	82.00	0.08	IV	0.24	6.50	0.73	32.33	15.83	0.23	0.79	0.75	0.986	1.05	1.00	1.00	52.47	15.49	67.96	NA	0.80	1.00	1.44	>1.0	Non Liquefiable
18.00	CL	44	2.04	1.04	82.00	0.08	IV	0.24	6.50	0.69	35.39	17.39	0.22	0.76	0.75	0.986	1.05	1.00	1.00	25.91	10.18	36.09	NA	1.00	1.00	1.44	>1.0	Non Liquefiable
19.50	CL	41	2.04	1.04	82.00	0.08	IV	0.24	6.50	0.65	38.45	18.95	0.21	0.73	0.75	0.986	1.05	1.00	1.00	23.13	9.63	32.76	NA	1.00	1.00	1.44	>1.0	Non Liquefiable
21.00	SM	50	2.01	1.01	32.00	0.17	IV	0.24	6.50	0.61	41.51	20.51	0.19	0.70	0.75	0.986	1.05	1.00	1.00	27.11	9.47	36.58	NA	0.78	1.00	1.44	>1.0	Non Liquefiable
22.50	SM	200	2.08	1.08	32.00	0.17	IV	0.24	6.50	0.57	44.52	22.02	0.18	0.67	0.75	0.986	1.05	1.00	1.00	104.65	22.73	127.38	NA	0.67	1.00	1.44	>1.0	Non Liquefiable

Depth	Soil type	Observed SPT	Saturated Density	Submerged Density	Fine content	D50	Earthquake Zone	PGA	Magnitude	Rd	Total overburden Pressure	Effective overburden Pressure	CSR	CN	CE	CH	CB	CR	CS	SPT Corrected	Δ (N1)60cs	Final N160	CRR	K1	K2	MSF	FS	
1.50	CI	5	1.90	0.90	91.00	0.07	IV	0.24	6.80	0.99	2.70	1.20	0.35	1.70	0.75	0.986	1.05	0.75	1.00	4.95	5.99	10.94	0.12	1.00	1.00	1.44	>1.0	Non Liquefiable
3.00	CI	13	1.96	0.96	92.00	0.07	IV	0.24	6.80	0.98	5.55	2.55	0.33	1.70	0.75	0.986	1.05	0.85	1.00	14.59	7.91	22.50	0.25	1.00	1.00	1.44	>1.0	Non Liquefiable
4.50	CI	15	1.96	0.96	92.00	0.07	IV	0.24	6.80	0.97	8.49	3.99	0.32	1.58	0.75	0.986	1.05	0.95	1.00	17.52	8.5	26.02	0.31	1.00	1.00	1.44	1.17	Non Liquefiable
6.00	CH	17	1.97	0.97	91.00	0.07	IV	0.24	6.80	0.95	11.43	5.43	0.31	1.36	0.75	0.986	1.05	0.95	1.00	17.02	8.4	25.42	0.30	1.00	1.00	1.44	1.14	Non Liquefiable
7.50	CH	14	1.97	0.97	91.00	0.07	IV	0.24	6.80	0.94	14.39	6.89	0.31	1.21	0.75	0.986	1.05	0.95	1.00	12.45	7.49	19.94	0.21	1.00	1.00	1.44	>1.0	Non Liquefiable
9.00	CL	49	2.02	1.02	76.00	0.08	IV	0.24	6.80	0.93	17.34	8.34	0.30	1.10	0.75	0.986	1.05	1.00	1.00	41.66	13.33	54.99	NA	1.00	1.00	1.44	>1.0	Non Liquefiable
10.50	SP-SM	28	2.02	1.02	11.00	0.20	IV	0.24	6.80	0.89	20.37	9.87	0.28	1.01	0.75	0.986	1.05	1.00	1.00	21.88	1.79	23.67	0.27	1.00	1.00	1.44	>1.0	Non Liquefiable
12.00	CL	52	2.04	1.04	87.00	0.07	IV	0.24	6.80	0.85	23.40	11.40	0.27	0.94	0.75	0.986	1.05	1.00	1.00	37.82	12.56	50.38	NA	1.00	1.00	1.44	>1.0	Non Liquefiable
13.50	CL	49	2.04	1.04	87.00	0.07	IV	0.24	6.80	0.81	26.46	12.96	0.26	0.88	0.75	0.986	1.05	1.00	1.00	33.42	11.69	45.11	NA	1.00	1.00	1.44	>1.0	Non Liquefiable
15.00	ML	120	2.06	1.06	81.00	0.08	IV	0.24	6.80	*0.7T*	29.52	14.52	0.25	0.83	0.75	0.986	1.05	1.00	1.00	77.33	20.46	97.79	NA	0.83	1.00	1.44	>1.0	Non Liquefiable
16.50	ML	121	2.06	1.06	81.00	0.08	IV	0.24	6.80	0.73	32.61	16.11	0.23	0.79	0.75	0.986	1.05	1.00	1.00	74.15	19.82	93.97	NA	0.79	1.00	1.44	>1.0	Non Liquefiable
18.00	CL	44	2.04	1.04	83.00	0.08	IV	0.24	6.80	0.69	35.70	17.70	0.22	0.75	0.75	0.986	1.05	1.00	1.00	25.68	10.14	35.82	NA	1.00	1.00	1.44	>1.0	Non Liquefiable
19.50	CL	51	2.04	1.04	83.00	0.08	IV	0.24	6.80	0.65	38.76	19.26	0.21	0.72	0.75	0.986	1.05	1.00	1.00	28.53	10.71	39.24	NA	1.00	1.00	1.44	>1.0	Non Liquefiable
21.00	CL	78	2.07	1.07	71.00	0.09	IV	0.24	6.80	0.61	41.82	20.82	0.19	0.69	0.75	0.986	1.05	1.00	1.00	41.97	13.4	55.37	NA	1.00	1.00	1.44	>1.0	Non Liquefiable
22.50	CL	88	2.08	1.08	71.00	0.09	IV	0.24	6.80	0.57	44.93	22.43	0.18	0.67	0.75	0.986	1.05	1.00	1.00	45.63	14.13	59.76	NA	1.00	1.00	1.44	>1.0	Non Liquefiable

Depth	Soil type	Observed SPT	Saturated Density	Submerged Density	Fine content	D50	Earthquake Zone	PGA	Magnitude	Rd	Total overburden Pressure	Effective overburden Pressure	CSR	CN	CE	CH	CB	CR	CS	SPT Corrected	Δ(N1)60cs	Final N160	CRR	K1	K2	MSF	FS	
1.50	CI	16	1.97	0.97	90.00	0.07	IV	0.24	6.80	0.99	2.70	1.20	0.35	1.70	0.75	0.986	1.05	0.75	1.00	15.84	8.17	24.01	0.27	1.00	1.00	1.44	1.14	Non Liquefiable
3.00	ML	13	1.97	0.g7	68.00	0.09	IV	0.24	6.80	0.98	5.66	2.66	0.32	1.70	0.75	0.986	1.05	0.85	1.00	14.59	7.91	22.50	0.25	1.00	1.00	1.44	1.11	Non Liquefiable
4.50	ML	14	1.97	0.97	68.00	0.09	IV	0.24	6.80	0.97	8.61	4.11	0.32	1.56	0.75	0.986	1.05	0.95	1.00	16.11	8.22	24.33	0.28	1.00	1.00	1.44	1.28	Non Liquefiable
6.00	SM	15	1.96	0.96	24.00	0.198	IV	0.24	6.80	0.95	11.57	5.57	0.31	1.34	0.75	0.986	1.05	0.95	1.00	14.83	5.78	20.61	0.22	1.00	1.00	1.44	1.04	Non Liquefiable
7.50	SM	16	1.96	0.96	24.00	0.198	IV	0.24	6.80	0.94	14.51	7.01	0.30	1.19	0.75	0.986	1.05	0.95	1.00	14.10	5.7	19.80	0.21	1.00	1.00	1.44	1.01	Non Liquefiable
9.00	SM	29	1.99	0.99	23.00	0.198	IV	0.24	6.80	0.93	17.45	8.45	0.30	1.09	0.75	0.986	1.05	1.00	1.00	24.50	6.52	31.02	NA	1.00	1.00	1.44	>1.0	Non Liquefiable
10.50	SM	35	2.00	1.00	23.00	0.198	IV	0.24	6.80	0.89	20.43	9.93	0.29	1.00	0.75	0.986	1.05	1.00	1.00	27.27	6.8	34.07	NA	1.00	1.00	1.44	>1.0	Non Liquefiable
12.00	ML	20	1.97	0.97	80.00	0.09	IV	0.24	6.80	0.85	23.43	11.43	0.27	0.94	0.75	0.986	1.05	1.00	1.00	14.53	7.9	22.43	0.25	0.97	1.00	1.44	1.27	Non Liquefiable
13.50	ML	21	1.97	0.97	80.00	0.09	IV	0.24	6.80	0.81	26.39	12.89	0.26	0.88	0.75	0.986	1.05	1.00	1.00	14.36	7.88	22.24	0.25	0.94	1.00	1.44	1.28	Non Liquefiable
15.00	ML	34	2.00	1.00	82.00	0.09	IV	0.24	6.80	0.77	29.34	14.34	0.25	0.84	0.75	0.986	1.05	1.00	1.00	22.05	9.41	31.46	NA	0.90	1.00	1.44	>1.0	Non Liquefiable
16.50	ML	36	2.00	1.00	82.00	0.09	IV	0.24	6.80	0.73	32.34	15.84	0.23	0.79	0.75	0.986	1.05	1.00	1.00	22.21	9.44	31.65	NA	0.87	1.00	1.44	>1.0	Non Liquefiable
18.00	ML	24	1.96	0.96	74.00	0.08	IV	0.24	6.80	0.69	35.34	17.34	0.22	0.76	0.75	0.986	1.05	1.00	1.00	14.15	7.83	21.98	0.24	0.88	1.00	1.44	1.39	Non Liquefiable
19.50	ML	25	1.96	0.96	74.00	0.08	IV	0.24	6.80	0.65	38.28	18.78	0.21	0.73	0.75	0.986	1.05	1.00	1.00	14.17	7.83	22.00	0.24	0.87	1.00	1.44	1.45	Non Liquefiable
21.00	CI	30	2.03	1.03	92.00	0.07	IV	0.24	6.80	0.61	41.22	20.22	0.20	0.70	0.75	0.986	1.05	1.00	1.00	16.38	8.28	24.66	0.29	1.00	1.00	1.44	2.11	Non Liquefiable
22.50	CI	37	2.03	1.03	92.00	0.07	IV	0.24	6.80	0.57	44.27	21.77	0.18	0.68	0.75	0.986	1.05	1.00	1.00	19.47	8.9	28.37	0.38	1.00	1.00	1.44	3.04	Non Liquefiable

Depth	Soil type	Observed SPT	Saturated Density	Submerged Density	Fine content	D50	Earthquake Zone	PGA	Magnitude	Rd	Total overburden Pressure	Effective overburden Pressure	CSR	CN	CE	CH	CB	CR	CS	SPT Corrected	Δ (N1)60cs	Final N160	CRR	K1	K2	MSF	FS	
1.50	CL	24	2.00	1.00	85.00	0.07	IV	0.24	6.80	0.99	2.70	1.20	0.35	1.70	0.75	0.986	1.05	0.75	1.00	23.76	9.75	33.51	NA	1.00	1.00	1.44	>1.0	Non Liquefiable
3.00	Cl	22	2.00	1.00	90.00	0.07	IV	0.24	6.80	0.98	5.70	2.70	0.32	1.70	0.75	0.986	1.05	0.85	1.00	24.68	9.94	34.62	NA	1.00	1.00	1.44	>1.0	Non Liquefiable
4.50	CI	39	2.03	1.03	90.00	0.07	IV	0.24	6.80	0.97	8.70	4.20	0.31	1.54	0.75	0.986	1.05	0.85	1.00	44.39	13.88	58.27	NA	1.00	1.00	1.44	>1.0	Non Liquefiable
6.00	CI	37	2.03	1.03	93.00	0.07	IV	0.24	6.80	0.95	11.75	5.75	0.30	1.32	0.75	0.986	1.05	0.85	1.00	36.01	12.2	48.21	NA	1.00	1.00	1.44	>1.0	Non Liquefiable
7.50	CI	46	2.04	1.04	93.00	0.07	IV	0.24	6.80	0.94	14.79	7.29	0.30	1.17	0.75	0.986	1.05	0.95	1.00	39.74	12.95	52.69	NA	1.00	1.00	1.44	>1.0	Non Liquefiable
9.00	SM	51	2.01	1.01	19.00	0.21	IV	0.24	6.80	0.93	17.85	8.85	0.29	1.06	0.75	0.986	1.05	1.00	1.00	42.09	6.5	48.59	NA	1.00	1.00	1.44	>1.0	Non Liquefiable
10.50	SM	54	2.01	1.01	19.00	0.21	IV	0.24	6.80	0.89	20.87	10.37	0.28	0.98	0.75	0.986	1.05	1.00	1.00	41.18	6.44	47.62	NA	0.99	1.00	1.44	>1.0	Non Liquefiable
12.00	ML	28	1.99	0.99	72.00	0.08	IV	0.24	6.80	0.85	23.88	11.88	0.27	0.92	0.75	0.986	1.05	1.00	1.00	19.95	8.99	28.94	0.41	0.95	1.00	1.44	2.09	Non Liquefiable
13.50	ML	37	2.00	1.00	72.00	0.08	IV	0.24	6.80	0.81	26.87	13.37	0.26	0.86	0.75	0.986	1.05	1.00	1.00	24.85	9.97	34.82	NA	0.91	1.00	1.44	>1.0	Non Liquefiable
15.00	ML	80	2.03	1.03	74.00	0.08	IV	0.24	6.80	0.77	29.87	14.87	0.24	0.82	0.75	0.986	1.05	1.00	1.00	50.95	15.19	66.14	NA	0.83	1.00	1.44	>1.0	Non Liquefiable
16.50	ML	74	2.03	1.03	74.00	0.08	IV	0.24	6.80	0.73	32.91	16.41	0.23	0.78	0.75	0.986	1.05	1.00	1.00	44.85	13.98	58.83	NA	0.80	1.00	1.44	>1.0	Non Liquefiable
18.00	ML-CL	25	2.00	1.00	89.00	0.075	IV	0.24	6.80	0.69	35.96	17.96	0.22	0.75	0.75	0.986	1.05	1.00	1.00	14.49	7.89	22.38	0.25	1.00	1.00	1.44	1.65	Non Liquefiable
19.50	ML-CL	28	2.00	1.00	89.00	0.075	IV	0.24	6.80	0.65	38.96	19.46	0.20	0.72	0.75	0.986	1.05	1.00	1.00	15.59	8.11	23.70	0.27	1.00	1.00	1.44	1.90	Non Liquefiable
21.00	CL	38	2.03	1.03	87.00	0.075	IV	0.24	6.80	0.61	41.96	20.96	0.19	0.69	0.75	0.986	1.05	1.00	1.00	20.38	9.08	29.46	0.43	1.00	1.00	1.44	3.27	Non Liquefiable
22.50	CL	39	2.03	1.03	87.00	0.075	IV	0.24	6.80	0.57	45.00	22.50	0.18	0.67	0.75	0.986	1.05	1.00	1.00	20.19	9.04	29.23	0.42	1.00	1.00	1.44	3.40	Non Liquefiable

Depth	Soil type	Observed SPT	Saturated Density	Submerged Density	Fine content	D50	Earthquake Zone	PGA	Magnitude	Rd	Total overburden Pressure	Effective overburden Pressure	CSR	CN	CE	CH	CB	CR	CS	SPT Corrected	Δ(N1)60cs	Final N160	CRR	K1	K2	MSF	FS	
1.50	CL	25	2.00	1.00	81.00	0.07	IV	0.24	6.80	0.99	2.85	1.35	0.33	1.70	0.75	0.986	1.05	0.75	1.00	24.75	9.95	34.70	NA	1.00	1.00	1.44	>1.0	Non Liquefiable
3.00	SM	20	1.98	0.98	17.00	0.21	IV	0.24	6.80	0.98	5.85	2.85	0.31	1.70	0.75	0.986	1.05	0.85	1.00	22.44	4.36	26.80	0.70	1.00	1.00	1.44	1.53	Non Liquefiable
4.50	SM	21	1.98	0.98	17.00	0.21	IV	0.24	6.80	0.97	8.82	4.32	0.31	1.52	0.75	0.986	1.05	0.85	1.00	23.57	4.43	28.00	0.69	1.00	1.00	1.44	1.73	Non Liquefiable
6.00	SM	18	1.98	0.98	20.00	0.2	IV	0.24	6.80	0.95	11.79	5.79	0.30	1.31	0.75	0.986	1.05	0.85	1.00	17.45	5	22.45	0.74	1.00	1.00	1.44	1.18	Non Liquefiable
7.50	SM	22	1.98	0.98	20.00	0.2	IV	0.24	6.80	0.94	14.76	7.26	0.30	1.17	0.75	0.986	1.05	0.95	1.00	19.05	5.12	24.17	0.73	1.00	1.00	1.44	1.33	Non Liquefiable
9.00	SM	19	1.98	0.98	16.00	0.21	IV	0.24	6.80	0.93	17.73	8.73	0.30	1.07	0.75	0.986	1.05	1.00	1.00	15.79	3.62	19.41	0.76	1.00	1.00	1.44	1.02	Non Liquefiable
10.50	CI	59	2.05	1.05	95.00	0.065	IV	0.24	6.80	0.89	20.70	10.20	0.28	0.99	0.75	0.986	1.05	1.00	1.00	45.36	14.07	59.43	NA	1.00	1.00	1.44	>1.0	Non Liquefiable
12.00	CI	65	2.06	1.06	96.00	0.065	IV	0.24	6.80	0.85	23.78	11.78	0.27	0.92	0.75	0.986	1.05	1.00	1.00	46.51	14.3	60.81	NA	1.00	1.00	1.44	>1.0	Non Liquefiable
13.50	Cl	71	2.07	1.07	96.00	0.065	IV	0.24	6.80	0.81	26.87	13.37	0.26	0.86	0.75	0.986	1.05	1.00	1.00	47.69	14.53	62.22	NA	1.00	1.00	1.44	>1.0	Non Liquefiable
15.00	ML	158	2.08	1.08	73.00	0.078	IV	0.24	6.80	0.77	29.97	14.97	0.24	0.82	0.75	0.986	1.05	1.00	1.00	100.20	25.04	125.24	0.50	0.82	1.00	1.44	>1.0	Non Liquefiable
16.50	ML	150	2.08	1.08	73.00	0.078	IV	0.24	6.80	0.73	33.09	16.59	0.23	0.78	0.75	0.986	1.05	1.00	1.00	90.43	23.08	113.51	0.50	0.78	1.00	1.44	>1.0	Non Liquefiable
18.00	CL	32	2.03	1.03	86.00	0.07	IV	0.24	6.80	0.69	36.21	18.21	0.22	0.74	0.75	0.986	1.05	1.00	1.00	18.41	8.69	27.10	NA	1.00	1.00	1.44	2.2	Non Liquefiable
19.50	CL	35	2.03	1.03	86.00	0.07	IV	0.24	6.80	0.65	39.26	19.76	0.20	0.71	0.75	0.986	1.05	1.00	1.00	19.34	8.86	28.20	NA	1.00	1.00	1.44	2.68	Non Liquefiable
21.00	CL	46	2.04	1.04	84.00	0.07	IV	0.24	6.80	0.61	42.30	21.30	0.19	0.69	0.75	0.986	1.05	1.00	1.00	24.47	9.9	34.37	NA	1.00	1.00	1.44	>1.0	Non Liquefiable
22.50	CL	53	2.05	1.05	84.00	0.07	IV	0.24	6.80	0.57	45.36	22.86	0.18	0.66	0.75	0.986	1.05	1.00	1.00	27.22	10.44	37.66	NA	1.00	1.00	1.44	>1.0	Non Liquefiable

Depth	Soil type	Observed SPT	Saturated Density	Submerged Density	Fine content	D50	Earthquake Zone	PGA	Magnitude	Rd	Total overburden Pressure	Effective overburden Pressure	CSR	CN	CE	CH	CB	CR	CS	SPT Corrected	Δ (N1)60cs	Final N160	CRR	K1	K2	MSF	FS	
1.50	CL	42	2.02	1.02	89.00	0.07	IV	0.24	6.80	0.99	2.85	1.35	0.33	1.70	0.75	0.986	1.05	0.75	1.00	41.58	13.32	54.90	NA	1.00	1.00	1.44	>1.0	Non Liquefiable
3.00	CL	37	2.02	1.02	90.00	0.065	IV	0.24	6.80	0.98	5.88	2.88	0.31	1.70	0.75	0.986	1.05	0.85	1.00	41.51	13.31	54.82	NA	1.00	1.00	1.44	>1.0	Non Liquefiable
4.50	CL	41	2.02	1.02	90.00	0.065	IV	0.24	6.80	0.97	8.91	4.41	0.30	1.51	0.75	0.986	1.05	0.95	1.00	45.54	14.11	59.65	NA	1.00	1.00	1.44	>1.0	Non Liquefiable
6.00	SM	19	1.97	0.97	22.00	0.21	IV	0.24	6.80	0.95	11.94	5.94	0.30	1.30	0.75	0.986	1.05	0.95	1.00	18.18	5.62	23.80	0.74	1.00	1.00	1.44	1.30	Non Liquefiable
7.50	SM	26	2.00	1.00	22.00	0.21	IV	0.24	6.80	0.94	14.90	7.40	0.30	1.16	0.75	0.986	1.05	0.95	1.00	22.30	6.01	28.31	0.70	1.00	1.00	1.44	1.85	Non Liquefiable
9.00	SM	60	2.05	1.05	24.00	0.2	IV	0.24	6.80	0.93	17.90	8.90	0.29	1.06	0.75	0.986	1.05	1.00	1.00	49.40	9.49	58.89	0.54	1.00	1.00	1.44	>1.0	Non Liquefiable
10.50	SM	66	2.05	1.05	24.00	0.2	IV	0.24	6.80	0.89	20.97	10.47	0.28	0.98	0.75	0.986	1.05	1.00	1.00	50.08	9.57	59.65	0.54	0.98	1.00	1.44	>1.0	Non Liquefiable
12.00	CI	29	2.02	1.02	93.00	0.065	IV	0.24	6.80	0.85	24.05	12.05	0.27	0.91	0.75	0.986	1.05	1.00	1.00	20.52	9.1	29.62	NA	1.00	1.00	1.44	2.40	Non Liquefiable
13.50	CI	33	2.02	1.02	93.00	0.065	IV	0.24	6.80	0.81	27.08	13.58	0.25	0.86	0.75	0.986	1.05	1.00	1.00	21.99	9.4	31.39	NA	1.00	1.00	1.44	>1.0	Non Liquefiable
15.00	ML	87	2.03	1.03	72.00	0.08	IV	0.24	6.80	*0.7T*	30.11	15.11	0.24	0.81	0.75	0.986	1.05	1.00	1.00	54.97	15.99	70.96	0.51	0.82	1.00	1.44	>1.0	Non Liquefiable
16.50	ML	84	2.03	1.03	72.00	0.08	IV	0.24	6.80	0.73	33.15	16.65	0.23	0.77	0.75	0.986	1.05	1.00	1.00	50.55	15.11	65.66	0.53	0.79	1.00	1.44	>1.0	Non Liquefiable
18.00	CL	32	2.02	1.02	90.00	0.065	IV	0.24	6.80	0.69	36.20	18.20	0.22	0.74	0.75	0.986	1.05	1.00	1.00	18.42	8.68	27.10	NA	1.00	1.00	1.44	2.29	Non Liquefiable
19.50	CL	30	2.02	1.02	90.00	0.065	IV	0.24	6.80	0.65	39.23	19.73	0.20	0.71	0.75	0.986	1.05	1.00	1.00	16.59	8.31	24.90	NA	1.00	1.00	1.44	2.06	Non Liquefiable
21.00	CL	130	2.10	1.10	85.00	0.07	IV	0.24	6.80	0.61	42.26	21.26	0.19	0.69	0.75	0.986	1.05	1.00	1.00	69.47	18.89	88.36	NA	1.00	1.00	1.44	>1.0	Non Liquefiable
22.50	CL	143	2.10	1.10	85.00	0.07	IV	0.24	6.80	0.57	45.41	22.91	0.18	0.66	0.75	0.986	1.05	1.00	1.00	73.29	19.66	92.95	NA	1.00	1.00	1.44	>1.0	Non Liquefiable

Depth	Soil type	Observed SPT	Saturated Density	Submerged Density	Fine content	D50	Earthquake Zone	PGA	Magnitude	Rd	Total overburden Pressure	Effective overburden Pressure	CSR	CN	CE	CH	CB	CR	CS	SPT Corrected	Δ(N1)60cs	Final N160	CRR	K1	K2	MSF	FS	
1.50	CL	30	2.00	1.00	85.00	0.07	IV	0.24	6.80	0.99	2.85	1.35	0.33	1.70	0.75	0.986	1.05	0.75	1.00	29.70	10.94	40.64	NA	1.00	1.00	1.44	>1.0	Non Liquefiable
3.00	SM	16	1.98	0.98	23.00	0.20	IV	0.24	6.80	0.98	5.85	2.85	0.31	1.70	0.75	0.986	1.05	0.85	1.00	17.95	5.86	23.81	0.27	1.00	1.00	1.44	1.25	Non Liquefiable
4.50	SM	22	1.99	0.99	23.00	0.20	IV	0.24	6.80	0.97	8.82	4.32	0.31	1.52	0.75	0.986	1.05	0.85	1.00	24.69	6.54	31.23	NA	1.00	1.00	1.44	>1.0	Non Liquefiable
6.00	SM	21	1.99	0.99	20.00	0.20	IV	0.24	6.80	0.95	11.81	5.81	0.30	1.31	0.75	0.986	1.05	0.85	1.00	20.33	5.23	25.56	0.30	1.00	1.00	1.44	1.45	Non Liquefiable
7.50	SM	20	1.97	0.97	20.00	0.20	IV	0.24	6.80	0.94	14.79	7.29	0.30	1.17	0.75	0.986	1.05	0.95	1.00	17.28	4.99	22.27	0.25	1.00	1.00	1.44	1.19	Non Liquefiable
9.00	SM	20	1.97	0.97	23.00	0.20	IV	0.24	6.80	0.93	17.75	8.75	0.29	1.07	0.75	0.986	1.05	1.00	1.00	16.61	5.72	22.33	0.25	1.00	1.00	1.44	1.21	Non Liquefiable
10.50	SM	23	1.97	0.97	23.00	0.20	IV	0.24	6.80	0.89	20.70	10.20	0.28	0.99	0.75	0.986	1.05	1.00	1.00	17.68	5.84	23.52	0.27	0.99	1.00	1.44	1.34	Non Liquefiable
12.00	CL	35	2.02	1.02	92.00	0.07	IV	0.24	6.80	0.85	23.66	11.66	0.27	0.93	0.75	0.986	1.05	1.00	1.00	25.17	10.04	35.21	NA	1.00	1.00	1.44	>1.0	Non Liquefiable
13.50	CL	38	2.02	1.02	92.00	0.07	IV	0.24	6.80	0.81	26.69	13.19	0.26	0.87	0.75	0.986	1.05	1.00	1.00	25.70	10.14	35.84	NA	1.00	1.00	1.44	>1.0	Non Liquefiable
15.00	ML	100	2.04	1.04	74.00	0.09	IV	0.24	6.80	0.77	29.72	14.72	0.24	0.82	0.75	0.986	1.05	1.00	1.00	64.01	17.8	81.81	NA	0.82	1.00	1.44	>1.0	Non Liquefiable
16.50	ML	93	2.04	1.04	74.00	0.09	IV	0.24	6.80	0.73	32.78	16.28	0.23	0.78	0.75	0.986	1.05	1.00	1.00	56.60	16.33	72.93	NA	0.79	1.00	1.44	>1.0	Non Liquefiable
18.00	CL	19	1.99	0.99	86.00	0.08	IV	0.24	6.80	0.69	35.84	17.84	0.22	0.75	0.75	0.986	1.05	1.00	1.00	11.05	7.21	18.26	0.19	1.00	1.00	1.44	1.29	Non Liquefiable
19.50	CL	21	2.00	1.00	86.00	0.08	IV	0.24	6.80	0.65	38.82	19.32	0.20	0.72	0.75	0.986	1.05	1.00	1.00	11.73	7.35	19.08	0.20	1.00	1.00	1.44	1.44	Non Liquefiable
21.00	CI	29	2.01	1.01	90.00	0.065	IV	0.24	6.80	0.61	41.82	20.82	0.19	0.69	0.75	0.986	1.05	1.00	1.00	15.61	8.12	23.73	0.27	1.00	1.00	1.44	2.02	Non Liquefiable
22.50	CI	31	2.02	1.02	90.00	0.065	IV	0.24	6.80	0.57	44.84	22.34	0.18	0.67	0.75	0.986	1.05	1.00	1.00	16.11	8.22	24.33	0.28	1.00	1.00	1.44	2.24	Non Liquefiable

Depth	Soil type	Observed SPT	Saturated Density	Submerged Density	Fine content	D50	Earthquake Zone	PGA	Magnitude	Rd	Total overburden Pressure	Effective overburden Pressure	CSR	CN	CE	CH	CB	CR	CS	SPT Corrected	Δ(N1)60cs	Final N160	CRR	K1	K2	MSF	FS	
1.50	CI	51	2.00	1.00	85.00	0.07	IV	0.24	6.80	0.99	2.85	1.35	0.33	1.70	0.75	0.986	1.05	0.75	1.00	50.49	15.1	65.59	NA	1.00	1.00	1.44	>1.0	Non Liquefiable
3.00	ML	86	2.06	1.06	60.00	0.09	IV	0.24	6.80	0.98	5.85	2.85	0.31	1.70	0.75	0.986	1.05	0.85	1.00	96.49	24.3	120.79	NA	1.00	1.00	1.44	>1.0	Non Liquefiable
4.50	ML	87	2.06	1.06	60.00	0.09	IV	0.24	6.80	0.97	8.94	4.44	0.30	1.50	0.75	0.986	1.05	0.95	1.00	96.31	24.26	120.57	NA	1.00	1.00	1.44	>1.0	Non Liquefiable
6.00	SM	19	1.98	0.98	22.00	0.21	IV	0.24	6.80	0.95	12.03	6.03	0.30	1.29	0.75	0.986	1.05	0.95	1.00	18.05	5.61	23.66	0.27	1.00	1.00	1.44	1.07	Non Liquefiable
7.50	SM	20	1.98	0.98	22.00	0.21	IV	0.24	6.80	0.94	15.00	7.50	0.29	1.15	0.75	0.986	1.05	0.95	1.00	17.04	5.51	22.55	0.25	1.00	1.00	1.44	1.01	Non Liquefiable
9.00	SM	20	1.98	0.98	34.00	0.18	IV	0.24	6.80	0.93	17.97	8.97	0.29	1.06	0.75	0.986	1.05	1.00	1.00	16.40	8.02	24.42	0.28	1.00	1.00	1.44	1.15	Non Liquefiable
10.50	SM	24	1.98	0.98	34.00	0.18	IV	0.24	6.80	0.89	20.94	10.44	0.28	0.98	0.75	0.986	1.05	1.00	1.00	18.24	8.36	26.60	0.33	0.99	1.00	1.44	1.38	Non Liquefiable
12.00	CL	47	2.03	1.03	85.00	0.07	IV	0.24	6.80	0.85	23.91	11.91	0.27	0.92	0.75	0.986	1.05	1.00	1.00	33.44	11.69	45.13	NA	1.00	1.00	1.44	>1.0	Non Liquefiable
13.50	CL	41	2.03	1.03	85.00	0.07	IV	0.24	6.80	0.81	26.96	13.46	0.25	0.86	0.75	0.986	1.05	1.00	1.00	27.45	10.48	37.93	NA	1.00	1.00	1.44	>1.0	Non Liquefiable
15.00	ML-CL	36	2.01	1.01	87.00	0.07	IV	0.24	6.80	0.77	30.00	15.00	0.24	0.82	0.75	0.986	1.05	1.00	1.00	22.82	9.57	32.39	NA	1.00	1.00	1.44	>1.0	Non Liquefiable
16.50	ML-CL	32	2.01	1.01	87.00	0.07	IV	0.24	6.80	0.73	33.02	16.52	0.23	0.78	0.75	0.986	1.05	1.00	1.00	19.33	8.87	28.20	0.38	1.00	1.00	1.44	1.97	Non Liquefiable
18.00	CL	33	2.03	1.03	88.00	0.07	IV	0.24	6.80	0.69	36.03	18.03	0.22	0.74	0.75	0.986	1.05	1.00	1.00	19.08	8.82	27.90	0.37	1.00	1.00	1.44	2.02	Non Liquefiable
19.50	CL	53	2.05	1.05	88.00	0.07	IV	0.24	6.80	0.65	39.08	19.58	0.20	0.71	0.75	0.986	1.05	1.00	1.00	29.41	10.89	40.30	NA	1.00	1.00	1.44	>1.0	Non Liquefiable
21.00	SM-ML	167	2.08	1.08	44.00	0.13	IV	0.24	6.80	0.61	42.15	21.15	0.19	0.69	0.75	0.986	1.05	1.00	1.00	88.99	22.79	111.78	NA	0.69	1.00	1.44	>1.0	Non Liquefiable
22.50	SP-SM	176	2.08	1.08	9.00	0.24	IV	0.24	6.80	0.57	45.27	22.77	0.18	0.66	0.75	0.986	1.05	1.00	1.00	90.81	2.1	92.91	NA	0.66	1.00	1.44	>1.0	Non Liquefiable

Depth	Soil type	Observed SPT	Saturated Density	Submerged Density	Fine content	D50	Earthquake Zone	PGA	Magnitude	Rd	Total overburden Pressure	Effective overburden Pressure	CSR	CN	CE	CH	CB	CR	CS	SPT Corrected	Δ(N1)60cs	Final N160	CRR	K1	K2	MSF	FS	
1.50	CL	21	2.00	1.00	86.00	0.07	IV	0.24	6.80	0.99	2.85	1.35	0.33	1.70	0.75	0.986	1.05	0.75	1.00	20.79	9.16	29.95	0.46	1.00	1.00	1.44	2.06	Non Liquefiable
3.00	SM-ML	25	2.01	1.01	35.00	0.16	IV	0.24	6.80	0.98	5.85	2.85	0.31	1.70	0.75	0.986	1.05	0.85	1.00	28.05	10.61	38.66	NA	1.00	1.00	1.44	>1.0	Non Liquefiable
4.50	SM-ML	28	2.01	1.01	35.00	0.16	IV	0.24	6.80	0.97	8.87	4.37	0.31	1.51	0.75	0.986	1.05	0.95	1.00	31.26	11.25	42.51	NA	1.00	1.00	1.44	>1.0	Non Liquefiable
6.00	SM-ML	25	11.98	10.98	34.00	0.16	IV	0.24	6.80	0.95	11.88	5.88	0.30	1.30	0.75	0.986	1.05	0.95	1.00	24.05	9.46	33.51	NA	1.00	1.00	1.44	>1.0	Non Liquefiable
7.50	SM-ML	21	1.98	0.98	34.00	0.16	IV	0.24	6.80	0.94	29.85	22.35	0.20	0.67	0.75	0.986	1.05	0.95	1.00	10.36	6.88	17.24	0.18	0.85	1.00	1.44	1.15	Non Liquefiable
9.00	SP-SM	40	2.01	1.01	12.00	0.21	IV	0.24	6.80	0.93	32.82	23.82	0.20	0.65	0.75	0.986	1.05	1.00	1.00	20.12	2.19	22.31	0.25	0.78	1.00	1.44	1.39	Non Liquefiable
10.50	SP-SM	37	2.01	1.01	12.00	0.21	IV	0.24	6.80	0.89	35.84	25.34	0.20	0.63	0.75	0.986	1.05	1.00	1.00	18.05	2.12	20.17	0.22	0.78	1.00	1.44	1.25	Non Liquefiable
12.00	SP-SM	34	1.99	0.99	10.00	0.24	IV	0.24	6.80	0.85	38.85	26.85	0.19	0.61	0.75	0.986	1.05	1.00	1.00	16.11	1.22	17.33	0.18	0.78	1.00	1.44	1.08	Non Liquefiable
13.50	CL	37	2.02	1.02	88.00	0.07	IV	0.24	6.80	0.81	41.84	28.34	0.19	0.59	0.75	0.986	1.05	1.00	1.00	17.07	8.41	25.48	0.30	1.00	1.00	1.44	2.32	Non Liquefiable
15.00	CL	48	2.03	1.03	88.00	0.07	IV	0.24	6.80	0.77	44.87	29.87	0.18	0.58	0.75	0.986	1.05	1.00	1.00	21.57	9.31	30.88	NA	1.00	1.00	1.44	>1.0	Non Liquefiable
16.50	ML	91	2.03	1.03	71.00	0.08	IV	0.24	6.80	0.73	47.91	31.41	0.17	0.56	0.75	0.986	1.05	1.00	1.00	39.87	12.97	52.84	NA	0.62	1.00	1.44	>1.0	Non Liquefiable
18.00	CL	61	2.05	1.05	85.00	0.08	IV	0.24	6.80	0.69	50.96	32.96	0.17	0.55	0.75	0.986	1.05	1.00	1.00	26.09	10.22	36.31	NA	1.00	1.00	1.44	>1.0	Non Liquefiable
19.50	CL	69	2.05	1.05	85.00	0.08	IV	0.24	6.80	0.65	54.03	34.53	0.16	0.54	0.75	0.986	1.05	1.00	1.00	28.83	10.77	39.60	NA	1.00	1.00	1.44	>1.0	Non Liquefiable
21.00	SM-ML	81	2.00	1.00	48.00	0.12	IV	0.24	6.80	0.61	57.11	36.11	0.15	0.53	0.75	0.986	1.05	1.00	1.00	33.10	11.62	44.72	NA	0.62	1.00	1.44	>1.0	Non Liquefiable
22.50	CL	86	2.08	1.08	88.00	0.07	IV	0.24	6.80	0.57	60.11	37.61	0.14	0.52	0.75	0.986	1.05	1.00	1.00	34.43	11.89	46.32	NA	1.00	1.00	1.44	>1.0	Non Liquefiable

Depth	Soil type	Observed SPT	Saturated Density	Submerged Density	Fine content	D50	Earthquake Zone	PGA	Magnitude	Rd	Total overburden Pressure	Effective overburden Pressure	CSR	CN	CE	CH	CB	CR	CS	SPT Corrected	Δ(N1)60cs	Final N160	CRR	K1	K2	MSF	FS	
1.50	ML	33	2.03	1.03	52.00	0.10	IV	0.24	6.80	0.99	2.70	1.20	0.35	1.70	0.75	0.986	1.05	0.75	1.00	32.67	11.53	44.20	NA	1.00	1.00	1.44	>1.0	Non Liquefiable
3.00	Cl	31	2.03	1.03	85.00	0.07	IV	0.24	6.80	0.98	5.75	2.75	0.32	1.70	0.75	0.986	1.05	0.85	1.00	34.78	11.96	46.74	NA	1.00	1.00	1.44	>1.0	Non Liquefiable
4.50	CL	21	2.00	1.00	87.00	0.07	IV	0.24	6.80	0.97	8.79	4.29	0.31	1.53	0.75	0.986	1.05	0.85	1.00	23.65	9.73	33.38	NA	1.00	1.00	1.44	>1.0	Non Liquefiable
6.00	CL	26	2.00	1.00	87.00	0.07	IV	0.24	6.80	0.95	11.79	5.79	0.30	1.31	0.75	0.986	1.05	0.95	1.00	25.20	10.05	35.25	NA	1.00	1.00	1.44	>1.0	Non Liquefiable
7.50	ML	18	1.98	0.98	72.00	0.08	IV	0.24	6.80	0.94	14.79	7.29	0.30	1.17	0.75	0.986	1.05	0.95	1.00	15.55	8.11	23.66	0.27	1.00	1.00	1.44	1.29	Non Liquefiable
9.00	Cl	20	1.99	0.99	93.00	0.065	IV	0.24	6.80	0.93	17.76	8.76	0.29	1.07	0.75	0.986	1.05	1.00	1.00	16.59	8.32	24.91	0.29	1.00	1.00	1.44	1.42	Non Liquefiable
10.50	Cl	22	2.00	1.00	93.00	0.065	IV	0.24	6.80	0.89	20.75	10.25	0.28	0.99	0.75	0.986	1.05	1.00	1.00	16.88	8.37	25.25	0.30	1.00	1.00	1.44	1.52	Non Liquefiable
12.00	SM	34	2.00	1.00	18.00	0.21	IV	0.24	6.80	0.85	23.75	11.75	0.27	0.92	0.75	0.986	1.05	1.00	1.00	24.36	4.85	29.21	0.42	0.95	1.00	1.44	2.14	Non Liquefiable
13.50	SM	42	2.00	1.00	18.00	0.21	IV	0.24	6.80	0.81	26.75	13.25	0.26	0.87	0.75	0.986	1.05	1.00	1.00	28.34	5.11	33.45	NA	0.91	1.00	1.44	>1.0	Non Liquefiable
15.00	ML	58	2.01	1.01	67.00	0.09	IV	0.24	6.80	0.77	29.75	14.75	0.24	0.82	0.75	0.986	1.05	1.00	1.00	37.09	12.42	49.51	NA	0.86	1.00	1.44	>1.0	Non Liquefiable
16.50	ML	62	2.01	1.01	67.00	0.09	IV	0.24	6.80	0.73	32.76	16.26	0.23	0.78	0.75	0.986	1.05	1.00	1.00	37.75	12.55	50.30	NA	0.82	1.00	1.44	>1.0	Non Liquefiable
18.00	CL	54	2.04	1.04	83.00	0.07	IV	0.24	6.80	0.69	35.78	17.78	0.22	0.75	0.75	0.986	1.05	1.00	1.00	31.45	11.29	42.74	NA	1.00	1.00	1.44	>1.0	Non Liquefiable
19.50	CL	60	2.05	1.05	83.00	0.07	IV	0.24	6.80	0.65	38.84	19.34	0.20	0.72	0.75	0.986	1.05	1.00	1.00	33.50	11.71	45.21	NA	1.00	1.00	1.44	>1.0	Non Liquefiable
21.00	CL	65	2.05	1.05	86.00	0.07	IV	0.24	6.80	0.61	41.91	20.91	0.19	0.69	0.75	0.986	1.05	1.00	1.00	34.90	11.98	46.88	NA	1.00	1.00	1.44	>1.0	Non Liquefiable
22.50	CL	68	2.06	1.06	86.00	0.07	IV	0.24	6.80	0.57	44.99	22.49	0.18	0.67	0.75	0.986	1.05	1.00	1.00	35.21	12.04	47.25	NA	1.00	1.00	1.44	>1.0	Non Liquefiable

Depth	Soil type	Observed SPT	Saturated Density	Submerged Density	Fine content	D50	Earthquake Zone	PGA	Magnitude	Rd	Total overburden Pressure	Effective overburden Pressure	CSR	CN	CE	CH	CB	CR	CS	SPT Corrected	Δ(N1)60cs	Final N160	CRR	K1	K2	MSF	FS	
1.50	ML	24	2.00	1.00	70.00	0.08	IV	0.24	6.80	0.99	2.70	1.20	0.35	1.70	0.75	0.986	1.05	0.75	1.00	23.76	9.75	33.51	NA	1.00	1.00	1.44	>1.0	Non Liquefiable
3.00	CI	24	2.00	1.00	81.00	0.07	IV	0.24	6.80	0.98	5.70	2.70	0.32	1.70	0.75	0.986	1.05	0.85	1.00	26.93	10.38	37.31	NA	1.00	1.00	1.44	>1.0	Non Liquefiable
4.50	CI	22	2.00	1.00	81.00	0.07	IV	0.24	6.80	0.97	8.70	4.20	0.31	1.54	0.75	0.986	1.05	0.95	1.00	25.04	10.01	35.05	NA	1.00	1.00	1.44	>1.0	Non Liquefiable
6.00	CI	26	2.01	1.01	82.00	0.07	IV	0.24	6.80	0.95	11.70	5.70	0.31	1.32	0.75	0.986	1.05	0.95	1.00	25.40	10.08	35.48	NA	1.00	1.00	1.44	>1.0	Non Liquefiable
7.50	ML	27	2.00	1.00	76.00	0.08	IV	0.24	6.80	0.94	14.72	7.22	0.30	1.18	0.75	0.986	1.05	0.95	1.00	23.45	9.69	33.14	NA	1.00	1.00	1.44	>1.0	Non Liquefiable
9.00	ML	30	2.00	1.00	80.00	0.07	IV	0.24	6.80	0.93	17.72	8.72	0.30	1.07	0.75	0.986	1.05	1.00	1.00	24.95	9.99	34.94	NA	1.00	1.00	1.44	>1.0	Non Liquefiable
10.50	Cl	31	2.02	1.02	91.00	0.065	IV	0.24	6.80	0.89	20.72	10.22	0.28	0.99	0.75	0.986	1.05	1.00	1.00	23.82	9.76	33.58	NA	1.00	1.00	1.44	>1.0	Non Liquefiable
12.00	CI	37	2.02	1.02	93.00	0.065	IV	0.24	6.80	0.85	23.75	11.75	0.27	0.92	0.75	0.986	1.05	1.00	1.00	26.51	10.3	36.81	NA	1.00	1.00	1.44	>1.0	Non Liquefiable
13.50	ML	56	2.02	1.02	81.00	0.07	IV	0.24	6.80	0.81	26.78	13.28	0.26	0.87	0.75	0.986	1.05	1.00	1.00	37.74	12.55	50.29	NA	0.89	1.00	1.44	>1.0	Non Liquefiable
15.00	CL	52	2.05	1.05	91.00	0.065	IV	0.24	6.80	0.77	29.81	14.81	0.24	0.82	0.75	0.986	1.05	1.00	1.00	33.18	11.64	44.82	NA	1.00	1.00	1.44	>1.0	Non Liquefiable
16.50	CL	59	2.05	1.05	91.00	0.065	IV	0.24	6.80	0.73	32.88	16.38	0.23	0.78	0.75	0.986	1.05	1.00	1.00	35.80	12.15	47.95	NA	1.00	1.00	1.44	>1.0	Non Liquefiable
18.00	ML	58	2.05	1.05	80.00	0.07	IV	0.24	6.80	0.69	35.96	17.96	0.22	0.75	0.75	0.986	1.05	1.00	1.00	33.61	11.72	45.33	NA	0.80	1.00	1.44	>1.0	Non Liquefiable
19.50	ML	69	2.05	1.05	80.00	0.07	IV	0.24	6.80	0.65	39.03	19.53	0.20	0.72	0.75	0.986	1.05	1.00	1.00	38.34	12.67	51.01	NA	0.76	1.00	1.44	>1.0	Non Liquefiable
21.00	ML	63	2.05	1.05	71.00	0.08	IV	0.24	6.80	0.61	42.11	21.11	0.19	0.69	0.75	0.986	1.05	1.00	1.00	33.67	11.74	45.41	NA	0.76	1.00	1.44	>1.0	Non Liquefiable
22.50	CL	75	2.07	1.07	71.00	0.08	IV	0.24	6.80	0.57	45.18	22.68	0.18	0.66	0.75	0.986	1.05	1.00	1.00	38.67	12.73	51.40	NA	1.00	1.00	1.44	>1.0	Non Liquefiable

Depth	Soil type	Observed SPT	Saturated Density	Submerged Density	Fine content	D50	Earthquake Zone	PGA	Magnitude	Rd	Total overburden Pressure	Effective overburden Pressure	CSR	CN	CE	CH	CB	CR	CS	SPT Corrected	Δ(N1)60cs	Final N160	CRR	K1	K2	MSF	FS	
1.50	ML-CL	16	1.95	0.95	71.00	0.08	IV	0.24	6.80	0.99	2.70	1.20	0.35	1.70	0.75	0.986	1.05	0.75	1.00	15.84	8.17	24.01	0.27	1.00	1.00	1.44	1.14	Non Liquefiable
3.00	SM-ML	19	1.98	0.98	42.00	0.12	IV	0.24	6.80	0.98	5.63	2.63	0.33	1.70	0.75	0.986	1.05	0.85	1.00	21.32	9.26	30.58	NA	1.00	1.00	1.44	>1.0	Non Liquefiable
4.50	SM-ML	23	2.00	1.00	42.00	0.12	IV	0.24	6.80	0.97	8.60	4.10	0.32	1.56	0.75	0.986	1.05	0.85	1.00	26.51	10.31	36.82	NA	1.00	1.00	1.44	>1.0	Non Liquefiable
6.00	CI	24	2.01	1.01	93.00	0.065	IV	0.24	6.80	0.95	11.60	5.60	0.31	1.34	0.75	0.986	1.05	0.85	1.00	23.67	9.73	33.40	NA	1.00	1.00	1.44	>1.0	Non Liquefiable
7.50	CI	37	2.03	1.03	93.00	0.065	IV	0.24	6.80	0.94	14.61	7.11	0.30	1.19	0.75	0.986	1.05	0.95	1.00	32.37	11.47	43.84	NA	1.00	1.00	1.44	>1.0	Non Liquefiable
9.00	CL	33	2.03	1.03	92.00	0.065	IV	0.24	6.80	0.93	17.66	8.66	0.30	1.07	0.75	0.986	1.05	1.00	1.00	27.54	10.51	38.05	NA	1.00	1.00	1.44	>1.0	Non Liquefiable
10.50	CL	33	2.03	1.03	92.00	0.065	IV	0.24	6.80	0.89	20.70	10.20	0.28	0.99	0.75	0.986	1.05	1.00	1.00	25.37	10.08	35.45	NA	1.00	1.00	1.44	>1.0	Non Liquefiable
12.00	CL	43	2.04	1.04	95.00	0.065	IV	0.24	6.80	0.85	23.75	11.75	0.27	0.92	0.75	0.986	1.05	1.00	1.00	30.81	11.16	41.97	NA	1.00	1.00	1.44	>1.0	Non Liquefiable
13.50	CL	43	2.04	1.04	95.00	0.065	IV	0.24	6.80	0.81	26.81	13.31	0.26	0.87	0.75	0.986	1.05	1.00	1.00	28.95	10.79	39.74	NA	1.00	1.00	1.44	>1.0	Non Liquefiable
15.00	ML	45	2.01	1.01	78.00	0.08	IV	0.24	6.80	0.77	29.87	14.87	0.24	0.82	0.75	0.986	1.05	1.00	1.00	28.66	10.73	39.39	NA	0.87	1.00	1.44	>1.0	Non Liquefiable
16.50	ML	48	2.01	1.01	78.00	0.08	IV	0.24	6.80	0.73	32.88	16.38	0.23	0.78	0.75	0.986	1.05	1.00	1.00	29.12	10.83	39.95	NA	0.84	1.00	1.44	>1.0	Non Liquefiable
18.00	ML	52	2.01	1.01	81.00	0.07	IV	0.24	6.80	0.69	35.90	17.90	0.22	0.75	0.75	0.986	1.05	1.00	1.00	30.18	11.04	41.22	NA	0.81	1.00	1.44	>1.0	Non Liquefiable
19.50	ML	53	2.01	1.01	81.00	0.07	IV	0.24	6.80	0.65	38.91	19.41	0.20	0.72	0.75	0.986	1.05	1.00	1.00	29.54	10.91	40.45	NA	0.79	1.00	1.44	>1.0	Non Liquefiable
21.00	CL	54	2.05	1.05	89.00	0.07	IV	0.24	6.80	0.61	41.93	20.93	0.19	0.69	0.75	0.986	1.05	1.00	1.00	28.99	10.79	39.78	NA	1.00	1.00	1.44	>1.0	Non Liquefiable
22.50	CL	65	2.05	1.05	89.00	0.07	IV	0.24	6.80	0.57	45.00	22.50	0.18	0.67	0.75	0.986	1.05	1.00	1.00	33.65	11.73	45.38	NA	1.00	1.00	1.44	>1.0	Non Liquefiable

Depth	Soil type	Observed SPT	Saturated Density	Submerged Density	Fine content	D50	Earthquake Zone	PGA	Magnitude	Rd	Total overburden Pressure	Effective overburden Pressure	CSR	CN	CE	CH	CB	CR	CS	SPT Corrected	Δ(N1)60cs	Final N160	CRR	K1	K2	MSF	FS	
1.50	ML-CL	18	1.98	0.98	73.00	0.08	IV	0.24	6.80	0.99	2.85	1.35	0.33	1.70	0.75	0.986	1.05	0.75	1.00	17.82	8.56	26.38	0.32	1.00	1.00	1.44	1.43	Non Liquefiable
3.00	ML	23	2.00	1.00	66.00	0.085	IV	0.24	6.80	0.98	5.82	2.82	0.31	1.70	0.75	0.986	1.05	0.85	1.00	25.81	10.16	35.97	NA	1.00	1.00	1.44	>1.0	Non Liquefiable
4.50	ML	35	2.02	1.02	66.00	0.085	IV	0.24	6.80	0.97	8.82	4.32	0.31	1.52	0.75	0.986	1.05	0.85	1.00	39.28	12.86	52.14	NA	1.00	1.00	1.44	>1.0	Non Liquefiable
6.00	CI	44	2.03	1.03	93.00	0.065	IV	0.24	6.80	0.95	11.85	5.85	0.30	1.31	0.75	0.986	1.05	0.85	1.00	42.44	13.48	55.92	NA	1.00	1.00	1.44	>1.0	Non Liquefiable
7.50	CI	36	2.03	1.03	93.00	0.065	IV	0.24	6.80	0.94	14.90	7.40	0.30	1.16	0.75	0.986	1.05	0.95	1.00	30.88	11.18	42.06	NA	1.00	1.00	1.44	>1.0	Non Liquefiable
9.00	CL	29	2.02	1.02	94.00	0.065	IV	0.24	6.80	0.93	17.94	8.94	0.29	1.06	0.75	0.986	1.05	1.00	1.00	23.82	9.76	33.58	NA	1.00	1.00	1.44	>1.0	Non Liquefiable
10.50	CL	37	2.02	1.02	94.00	0.065	IV	0.24	6.80	0.89	20.97	10.47	0.28	0.98	0.75	0.986	1.05	1.00	1.00	28.08	10.61	38.69	NA	1.00	1.00	1.44	>1.0	Non Liquefiable
12.00	CI	71	2.07	1.07	95.00	0.065	IV	0.24	6.80	0.85	24.00	12.00	0.27	0.91	0.75	0.986	1.05	1.00	1.00	50.33	15.06	65.39	NA	1.00	1.00	1.44	>1.0	Non Liquefiable
13.50	Cl	95	2.08	1.08	95.00	0.065	IV	0.24	6.80	0.81	27.11	13.61	0.25	0.86	0.75	0.986	1.05	1.00	1.00	63.24	17.65	80.89	NA	1.00	1.00	1.44	>1.0	Non Liquefiable
15.00	ML	58	2.03	1.03	77.00	0.07	IV	0.24	6.80	0.77	30.23	15.23	0.24	0.81	0.75	0.986	1.05	1.00	1.00	36.50	12.3	48.80	NA	0.85	1.00	1.44	>1.0	Non Liquefiable
16.50	ML	64	2.03	1.03	77.00	0.07	IV	0.24	6.80	0.73	33.27	16.77	0.23	0.77	0.75	0.986	1.05	1.00	1.00	38.37	12.68	51.05	NA	0.81	1.00	1.44	>1.0	Non Liquefiable
18.00	CL	51	2.05	1.05	91.00	0.065	IV	0.24	6.80	0.69	36.32	18.32	0.21	0.74	0.75	0.986	1.05	1.00	1.00	29.26	10.85	40.11	NA	1.00	1.00	1.44	>1.0	Non Liquefiable
19.50	CL	55	2.05	1.05	91.00	0.065	IV	0.24	6.80	0.65	39.39	19.89	0.20	0.71	0.75	0.986	1.05	1.00	1.00	30.28	11.06	41.34	NA	1.00	1.00	1.44	>1.0	Non Liquefiable
21.00	CL	60	2.05	1.05	89.00	0.065	IV	0.24	6.80	0.61	42.47	21.47	0.19	0.68	0.75	0.986	1.05	1.00	1.00	31.80	11.36	43.16	NA	1.00	1.00	1.44	>1.0	Non Liquefiable
22.50	CL	56	2.05	1.05	89.00	0.065	IV	0.24	6.80	0.57	45.54	23.04	0.18	0.66	0.75	0.986	1.05	1.00	1.00	28.65	10.73	39.38	NA	1.00	1.00	1.44	>1.0	Non Liquefiable

Depth	Soil type	Observed SPT	Saturated Density	Submerged Density	Fine content	D50	Earthquake Zone	PGA	Magnitude	Rd	Total overburden Pressure	Effective overburden Pressure	CSR	CN	CE	CH	CB	CR	CS	SPT Corrected	Δ (N1)60cs	Final N160	CRR	K1	K2	MSF	FS	
1.50	SM-ML	11	1.97	0.97	48.00	0.15	IV	0.24	6.80	0.99	2.85	1.35	0.33	1.70	0.75	0.986	1.05	0.75	1.00	10.89	7.18	18.07	0.19	1.00	1.00	1.44	0.85	Liquefiable
3.00	SM-ML	12	1.97	0.97	31.00	0.19	IV	0.24	6.80	0.98	5.81	2.81	0.32	1.70	0.75	0.986	1.05	0.85	1.00	13.46	6.96	20.42	0.22	1.00	1.00	1.44	1.01	Non Liquefiable
4.50	SM-ML	18	1.97	0.97	31.00	0.19	IV	0.24	6.80	0.97	8.76	4.26	0.31	1.53	0.75	0.986	1.05	0.95	1.00	20.34	8.08	28.42	0.39	1.00	1.00	1.44	1.79	Non Liquefiable
6.00	SM	22	1.99	0.99	19.00	0.21	IV	0.24	6.80	0.95	11.72	5.72	0.31	1.32	0.75	0.986	1.05	0.95	1.00	21.47	4.99	26.46	0.32	1.00	1.00	1.44	1.53	Non Liquefiable
7.50	SM	26	1.99	0.99	19.00	0.21	IV	0.24	6.80	0.94	14.70	7.20	0.30	1.18	0.75	0.986	1.05	0.95	1.00	22.60	5.08	27.68	0.36	1.00	1.00	1.44	1.72	Non Liquefiable
9.00	CL	22	1.99	0.99	94.00	0.065	IV	0.24	6.80	0.93	17.69	8.69	0.30	1.07	0.75	0.986	1.05	1.00	1.00	18.33	8.67	27.00	0.34	1.00	1.00	1.44	1.65	Non Liquefiable
10.50	CL	27	2.00	1.00	94.00	0.065	IV	0.24	6.80	0.89	20.67	10.17	0.28	0.99	0.75	0.986	1.05	1.00	1.00	20.79	9.16	29.95	0.46	1.00	1.00	1.44	2.36	Non Liquefiable
12.00	CI	48	2.03	1.03	96.00	0.065	IV	0.24	6.80	0.85	23.67	11.67	0.27	0.93	0.75	0.986	1.05	1.00	1.00	34.50	11.9	46.40	NA	1.00	1.00	1.44	>1.0	Non Liquefiable
13.50	Cl	51	2.04	1.04	96.00	0.065	IV	0.24	6.80	0.81	26.72	13.22	0.26	0.87	0.75	0.986	1.05	1.00	1.00	34.45	11.89	46.34	NA	1.00	1.00	1.44	>1.0	Non Liquefiable
15.00	ML	60	2.02	1.02	77.00	0.07	IV	0.24	6.80	0.77	29.78	14.78	0.24	0.82	0.75	0.986	1.05	1.00	1.00	38.33	12.66	50.99	NA	0.85	1.00	1.44	>1.0	Non Liquefiable
16.50	ML	66	2.02	1.02	77.00	0.07	IV	0.24	6.80	0.73	32.81	16.31	0.23	0.78	0.75	0.986	1.05	1.00	1.00	40.13	13.03	53.16	NA	0.82	1.00	1.44	>1.0	Non Liquefiable
18.00	ML	68	2.02	1.02	78.00	0.07	IV	0.24	6.80	0.69	35.84	17.84	0.22	0.75	0.75	0.986	1.05	1.00	1.00	39.54	12.9	52.44	NA	0.7g	1.00	1.44	>1.0	Non Liquefiable
19.50	ML	73	2.02	1.02	78.00	0.07	IV	0.24	6.80	0.65	38.87	19.37	0.20	0.72	0.75	0.986	1.05	1.00	1.00	40.73	13.15	53.88	NA	0.76	1.00	1.44	>1.0	Non Liquefiable
21.00	CL	78	2.07	1.07	90.00	0.065	IV	0.24	6.80	0.61	41.90	20.90	0.19	0.69	0.75	0.986	1.05	1.00	1.00	41.90	13.38	55.28	NA	1.00	1.00	1.44	>1.0	Non Liquefiable
22.50	CL	82	2.08	1.08	90.00	0.065	IV	0.24	6.80	0.57	45.00	22.50	0.18	0.67	0.75	0.986	1.05	1.00	1.00	42.45	13.49	55.94	NA	1.00	1.00	1.44	>1.0	Non Liquefiable

Depth	Soil type	Observed SPT	Saturated Density	Submerged Density	Fine content	D50	Earthquake Zone	PGA	Magnitude	Rd	Total overburden Pressure	Effective overburden Pressure	CSR	CN	CE	CH	CB	CR	CS	SPT Corrected	Δ(N1)60cs	Final N160	CRR	K1	K2	MSF	FS	
1.50	ML-CL	16	1.98	0.98	71.00	0.07	IV	0.24	6.80	0.99	2.85	1.35	0.33	1.70	0.75	0.986	1.05	0.75	1.00	15.84	8.17	24.01	0.27	1.00	1.00	1.44	1.21	Non Liquefiable
3.00	CI	18	1.98	0.98	92.00	0.065	IV	0.24	6.80	0.98	5.82	2.82	0.31	1.70	0.75	0.986	1.05	0.85	1.00	20.20	4.04	24.24	0.42	1.00	1.00	1.44	1.83	Non Liquefiable
4.50	CI	21	2.00	1.00	92.00	0.065	IV	0.24	6.80	0.97	8.79	4.29	0.31	1.53	0.75	0.986	1.05	0.95	1.00	23.65	9.73	33.38	NA	1.00	1.00	1.44	>1.0	Non Liquefiable
6.00	SM	24	1.98	0.98	17.00	0.22	IV	0.24	6.80	0.95	11.79	5.79	0.30	1.31	0.75	0.986	1.05	0.95	1.00	23.27	4.41	27.68	0.36	1.00	1.00	1.44	1.71	Non Liquefiable
7.50	SM	28	2.00	1.00	17.00	0.22	IV	0.24	6.80	0.94	14.76	7.26	0.30	1.17	0.75	0.986	1.05	0.95	1.00	24.24	4.47	28.71	0.40	1.00	1.00	1.44	1.92	Non Liquefiable
9.00	CL	33	2.02	1.02	91.00	0.065	IV	0.24	6.80	0.93	17.76	8.76	0.29	1.07	0.75	0.986	1.05	1.00	1.00	27.38	10.47	37.85	NA	1.00	1.00	1.44	>1.0	Non Liquefiable
10.50	CL	38	2.02	1.02	91.00	0.065	IV	0.24	6.80	0.89	20.79	10.29	0.28	0.99	0.75	0.986	1.05	1.00	1.00	29.09	10.81	39.90	NA	1.00	1.00	1.44	>1.0	Non Liquefiable
12.00	CI	45	2.03	1.03	93.00	0.065	IV	0.24	6.80	0.85	23.82	11.82	0.27	0.92	0.75	0.986	1.05	1.00	1.00	32.14	11.43	43.57	NA	1.00	1.00	1.44	>1.0	Non Liquefiable
13.50	CI	51	2.04	1.04	93.00	0.065	IV	0.24	6.80	0.81	26.87	13.37	0.26	0.86	0.75	0.986	1.05	1.00	1.00	34.25	11.85	46.10	NA	1.00	1.00	1.44	>1.0	Non Liquefiable
15.00	ML	115	2.05	1.05	75.00	0.08	IV	0.24	6.80	*0.7T*	29.93	14.93	0.24	0.82	0.75	0.986	1.05	1.00	1.00	73.34	19.66	93.00	NA	0.82	1.00	1.44	>1.0	Non Liquefiable
16.50	ML	128	2.05	1.05	75.00	0.08	IV	0.24	6.80	0.73	33.00	16.50	0.23	0.78	0.75	0.986	1.05	1.00	1.00	77.07	20.42	97.49	NA	0.78	1.00	1.44	>1.0	Non Liquefiable
18.00	ML	100	2.05	1.05	78.00	0.08	IV	0.24	6.80	0.69	36.08	18.08	0.22	0.74	0.75	0.986	1.05	1.00	1.00	57.75	16.56	74.31	NA	0.74	1.00	1.44	>1.0	Non Liquefiable
19.50	ML	100	2.05	1.05	78.00	0.08	IV	0.24	6.80	0.65	39.15	19.65	0.20	0.71	0.75	0.986	1.05	1.00	1.00	55.39	16.08	71.47	NA	0.72	1.00	1.44	>1.0	Non Liquefiable
21.00	SM-ML	100	2.09	1.09	45.00	0.14	IV	0.24	6.80	0.61	42.23	21.23	0.19	0.69	0.75	0.986	1.05	1.00	1.00	53.30	15.66	68.96	NA	0.70	1.00	1.44	>1.0	Non Liquefiable
22.50	SM-ML	120	2.09	1.09	45.00	0.14	IV	0.24	6.80	0.57	45.36	22.86	0.18	0.66	0.75	0.986	1.05	1.00	1.00	61.63	17.32	78.95	NA	0.66	1.00	1.44	>1.0	Non Liquefiable

Depth	Soil type	Observed SPT	Saturated Density	Submerged Density	Fine content	D50	Earthquake Zone	PGA	Magnitude	Rd	Total overburden Pressure	Effective overburden Pressure	CSR	CN	CE	CH	CB	CR	CS	SPT Corrected	Δ(N1)60cs	Final N160	CRR	K1	K2	MSF	FS	
1.50	ML	15	1.99	0.99	61.00	0.09	IV	0.24	6.80	0.99	2.85	1.35	0.33	1.70	0.75	0.986	1.05	0.75	1.00	14.85	7.97	22.82	0.37	1.00	1.00	1.44	1.13	Non Liquefiable
3.00	SM	20	1.9g	0.99	27.00	0.2	IV	0.24	6.80	0.98	5.84	2.84	0.31	1.70	0.75	0.986	1.05	0.85	1.00	22.44	7.4	29.84	0.66	1.00	1.00	1.44	2.10	Non Liquefiable
4.50	SM	23	1.99	0.99	27.00	0.2	IV	0.24	6.80	0.97	8.82	4.32	0.31	1.52	0.75	0.986	1.05	0.95	1.00	25.81	7.85	33.66	NA	1.00	1.00	1.44	>1.0	Non Liquefiable
6.00	SM	24	1.99	0.99	16.00	0.24	IV	0.24	6.80	0.95	11.81	5.81	0.30	1.31	0.75	0.986	1.05	0.95	1.00	23.24	4.02	27.26	0.50	1.00	1.00	1.44	1.65	Non Liquefiable
7.50	CI	19	1.99	0.99	95.00	0.065	IV	0.24	6.80	0.94	14.79	7.29	0.30	1.17	0.75	0.986	1.05	0.95	1.00	16.42	8.28	24.70	0.41	1.00	1.00	1.44	1.38	Non Liquefiable
9.00	CH	25	2.01	1.01	96.00	0.065	IV	0.24	6.80	0.93	17.78	8.78	0.29	1.07	0.75	0.986	1.05	1.00	1.00	20.72	9.15	29.87	0.66	1.00	1.00	1.44	2.25	Non Liquefiable
10.50	CH	28	2.01	1.01	96.00	0.065	IV	0.24	6.80	0.89	20.79	10.29	0.28	0.99	0.75	0.986	1.05	1.00	1.00	21.43	9.29	30.72	NA	1.00	1.00	1.44	>1.0	Non Liquefiable
12.00	CL	59	2.05	1.05	93.00	0.065	IV	0.24	6.80	0.85	23.81	11.81	0.27	0.92	0.75	0.986	1.05	1.00	1.00	42.16	13.44	55.60	NA	1.00	1.00	1.44	>1.0	Non Liquefiable
13.50	CL	62	2.05	1.05	93.00	0.065	IV	0.24	6.80	0.81	26.88	13.38	0.25	0.86	0.75	0.986	1.05	1.00	1.00	41.62	13.32	54.94	NA	1.00	1.00	1.44	>1.0	Non Liquefiable
15.00	CI	58	2.05	1.05	91.00	0.065	IV	0.24	6.80	0.77	29.96	14.96	0.24	0.82	0.75	0.986	1.05	1.00	1.00	36.83	12.36	49.19	NA	1.00	1.00	1.44	>1.0	Non Liquefiable
16.50	ML	70	2.05	1.05	80.00	0.07	IV	0.24	6.80	0.73	33.03	16.53	0.23	0.78	0.75	0.986	1.05	1.00	1.00	42.28	13.45	55.73	NA	0.81	1.00	1.44	>1.0	Non Liquefiable
18.00	ML	64	2.05	1.05	80.00	0.07	IV	0.24	6.80	0.69	36.11	18.11	0.22	0.74	0.75	0.986	1.05	1.00	1.00	36.93	12.39	49.32	NA	0.7g	1.00	1.44	>1.0	Non Liquefiable
19.50	ML	73	2.05	1.05	78.00	0.07	IV	0.24	6.80	0.65	39.18	19.68	0.20	0.71	0.75	0.986	1.05	1.00	1.00	40.41	13.08	53.49	NA	0.75	1.00	1.44	>1.0	Non Liquefiable
21.00	CL	75	2.07	1.07	93.00	0.065	IV	0.24	6.80	0.61	42.26	21.26	0.19	0.69	0.75	0.986	1.05	1.00	1.00	39.94	12.99	52.93	NA	1.00	1.00	1.44	>1.0	Non Liquefiable
22.50	CL	82	2.08	1.08	93.00	0.065	IV	0.24	6.80	0.57	45.36	22.86	0.18	0.66	0.75	0.986	1.05	1.00	1.00	42.11	13.42	55.53	NA	1.00	1.00	1.44	>1.0	Non Liquefiable

Depth	Soil type	Observed SPT	Saturated Density	Submerged Density	Fine content	D50	Earthquake Zone	PGA	Magnitude	Rd	Total overburden Pressure	Effective overburden Pressure	CSR	CN	CE	CH	CB	CR	CS	SPT Corrected	Δ(N1)60cs	Final N160	CRR	K1	K2	MSF	FS	
1.50	ML	18	2.00	1.00	76.00	0.075	IV	0.24	6.80	0.99	2.85	1.35	0.33	1.70	0.75	0.986	1.05	0.75	1.00	17.82	8.56	26.38	0.32	1.00	1.00	1.44	1.43	Non Liquefiable
3.00	CI	27	2.00	1.00	72.00	0.075	IV	0.24	6.80	0.98	5.85	2.85	0.31	1.70	0.75	0.986	1.05	0.85	1.00	30.2	11.15	41.35	NA	1.00	1.00	1.44	>1.0	Non Liquefiable
4.50	ML	30	2.00	1.00	68.00	0.07	IV	0.24	6.80	0.97	8.85	4.35	0.31	1.52	0.75	0.986	1.05	0.95	1.00	33.55	11.71	45.26	NA	1.00	1.00	1.44	>1.0	Non Liquefiable
6.00	SM-ML	34	2.00	1.00	34.00	0.18	IV	0.24	6.80	0.95	11.85	5.85	0.30	1.31	0.75	0.986	1.05	0.95	1.00	32.79	11.11	43.90	NA	1.00	1.00	1.44	>1.0	Non Liquefiable
7.50	SM-ML	38	2.00	1.00	34.00	0.18	IV	0.24	6.80	0.94	14.85	7.35	0.30	1.17	0.75	0.986	1.05	0.95	1.00	32.70	11.08	43.78	NA	1.00	1.00	1.44	>1.0	Non Liquefiable
9.00	ML	28	2.00	1.00	79.00	0.075	IV	0.24	6.80	0.93	17.85	8.85	0.29	1.06	0.75	0.986	1.05	1.00	1.00	23.11	9.62	32.73	NA	1.00	1.00	1.44	>1.0	Non Liquefiable
10.50	ML	34	2.00	1.00	79.00	0.075	IV	0.24	6.80	0.89	20.85	10.35	0.28	0.98	0.75	0.986	1.05	1.00	1.00	25.95	10.19	36.14	NA	0.99	1.00	1.44	>1.0	Non Liquefiable
12.00	CI	42	2.04	1.04	95.00	0.06	IV	0.24	6.80	0.85	23.85	11.85	0.27	0.92	0.75	0.986	1.05	1.00	1.00	29.96	10.99	40.95	NA	1.00	1.00	1.44	>1.0	Non Liquefiable
13.50	CI	48	2.04	1.04	95.00	0.06	IV	0.24	6.80	0.81	26.91	13.41	0.25	0.86	0.75	0.986	1.05	1.00	1.00	32.19	11.43	43.62	NA	1.00	1.00	1.44	>1.0	Non Liquefiable
15.00	ML	71	2.05	1.05	76.00	0.07	IV	0.24	6.80	*0.7T*	29.97	14.97	0.24	0.82	0.75	0.986	1.05	1.00	1.00	45.06	14.01	59.07	NA	0.84	1.00	1.44	>1.0	Non Liquefiable
16.50	ML	77	2.05	1.05	76.00	0.07	IV	0.24	6.80	0.73	33.05	16.55	0.23	0.78	0.75	0.986	1.05	1.00	1.00	46.48	14.3	60.78	NA	0.80	1.00	1.44	>1.0	Non Liquefiable
18.00	CH	85	2.08	1.08	95.00	0.06	IV	0.24	6.80	0.69	36.12	18.12	0.22	0.74	0.75	0.986	1.05	1.00	1.00	49.03	14.81	63.84	NA	1.00	1.00	1.44	>1.0	Non Liquefiable
19.50	CH	100	2.08	1.08	95.00	0.06	IV	0.24	6.80	0.65	39.24	19.74	0.20	0.71	0.75	0.986	1.05	1.00	1.00	55.27	16.05	71.32	NA	1.00	1.00	1.44	>1.0	Non Liquefiable
21.00	ML	115	2.06	1.06	70.00	0.07	IV	0.24	6.80	0.61	42.36	21.36	0.19	0.68	0.75	0.986	1.05	1.00	1.00	61.30	17.26	78.56	NA	0.68	1.00	1.44	>1.0	Non Liquefiable
22.50	ML	130	2.06	1.06	70.00	0.07	IV	0.24	6.80	0.57	45.45	22.95	0.18	0.66	0.75	0.986	1.05	1.00	1.00	66.85	18.38	85.23	NA	0.66	1.00	1.44	>1.0	Non Liquefiable

Depth	Soil type	Observed SPT	Saturated Density	Submerged Density	Fine content	D50	Earthquake Zone	PGA	Magnitude	Rd	Total overburden Pressure	Effective overburden Pressure	CSR	CN	CE	CH	CB	CR	CS	SPT Corrected	Δ(N1)60cs	Final N160	CRR	K1	K2	MSF	FS	
1.50	ML	8	1.94	0.94	73.00	0.08	IV	0.24	6.80	0.99	2.85	1.35	0.33	1.70	0.75	0.986	1.05	0.75	1.00	7.92	6.58	14.50	0.22	1.00	1.00	1.44	0.69	Liquefiable
3.00	CI	11	1.94	0.94	89.00	0.065	IV	0.24	6.80	0.98	5.76	2.76	0.32	1.70	0.75	0.986	1.05	0.85	1.00	12.34	7.47	19.81	NA	1.00	1.00	1.44	>1.0	Non Liquefiable
4.50	CI	12	1.94	0.94	89.00	0.065	IV	0.24	6.80	0.97	8.67	4.17	0.31	1.55	0.75	0.986	1.05	0.95	1.00	13.71	7.74	21.45	NA	1.00	1.00	1.44	>1.0	Non Liquefiable
6.00	CL	27	2.01	1.01	88.00	0.065	IV	0.24	6.80	0.95	11.58	5.58	0.31	1.34	0.75	0.986	1.05	0.95	1.00	26.66	10.33	36.99	NA	1.00	1.00	1.44	>1.0	Non Liquefiable
7.50	SM	29	2.01	1.01	19.00	0.22	IV	0.24	6.80	0.94	14.60	7.10	0.30	1.19	0.75	0.986	1.05	0.95	1.00	25.40	5.28	30.68	NA	1.00	1.00	1.44	>1.0	Non Liquefiable
9.00	CL	31	2.02	1.02	90.00	0.06	IV	0.24	6.80	0.93	17.61	8.61	0.30	1.08	0.75	0.986	1.05	1.00	1.00	25.94	10.19	36.13	NA	1.00	1.00	1.44	>1.0	Non Liquefiable
10.50	CL	35	2.02	1.02	90.00	0.06	IV	0.24	6.80	0.89	20.64	10.14	0.28	0.99	0.75	0.986	1.05	1.00	1.00	26.99	10.4	37.39	NA	1.00	1.00	1.44	>1.0	Non Liquefiable
12.00	Cl	37	2.03	1.03	96.00	0.06	IV	0.24	6.80	0.85	23.67	11.67	0.27	0.93	0.75	0.986	1.05	1.00	1.00	26.59	10.32	36.91	NA	1.00	1.00	1.44	>1.0	Non Liquefiable
13.50	CI	40	2.03	1.03	96.00	0.06	IV	0.24	6.80	0.81	26.72	13.22	0.26	0.87	0.75	0.986	1.05	1.00	1.00	27.02	10.4	37.42	NA	1.00	1.00	1.44	>1.0	Non Liquefiable
15.00	ML	62	2.03	1.03	72.00	0.07	IV	0.24	6.80	0.77	29.76	14.76	0.24	0.82	0.75	0.986	1.05	1.00	1.00	39.63	12.92	52.55	NA	0.85	1.00	1.44	>1.0	Non Liquefiable
16.50	ML	68	2.03	1.03	72.00	0.07	IV	0.24	6.80	0.73	32.81	16.31	0.23	0.78	0.75	0.986	1.05	1.00	1.00	41.35	13.27	54.62	NA	0.81	1.00	1.44	>1.0	Non Liquefiable
18.00	ML-CL	33	2.02	1.02	83.00	0.07	IV	0.24	6.80	0.69	35.85	17.85	0.22	0.75	0.75	0.986	1.05	1.00	1.00	19.18	8.83	28.01	0.53	1.00	1.00	1.44	2.46	Non Liquefiable
19.50	ML-CL	39	2.02	1.02	83.00	0.07	IV	0.24	6.80	0.65	38.88	19.38	0.20	0.72	0.75	0.986	1.05	1.00	1.00	21.75	9.35	31.10	NA	1.00	1.00	1.44	>1.0	Non Liquefiable
21.00	CL	36	2.03	1.03	84.00	0.07	IV	0.24	6.80	0.61	41.91	20.91	0.18	0.69	0.75	0.986	1.05	1.00	1.00	19.33	8.87	28.20	0.54	1.00	1.00	1.44	2.83	Non Liquefiable
22.50	CL	42	2.04	1.04	84.00	0.07	IV	0.24	6.80	0.57	44.96	22.46	0.18	0.67	0.75	0.986	1.05	1.00	1.00	21.76	9.36	31.12	NA	1.00	1.00	1.44	>1.0	Non Liquefiable

Depth	Soil type	Observed SPT	Saturated Density	Submerged Density	Fine content	D50	Earthquake Zone	PGA	Magnitude	Rd	Total overburden Pressure	Effective overburden Pressure	CSR	CN	CE	CH	CB	CR	CS	SPT Corrected	Δ(N1)60cs	Final N160	CRR	K1	K2	MSF	FS	
1.50	ML	16	1.98	0.98	63.00	0.09	IV	0.24	6.80	0.99	2.85	1.35	0.33	1.70	0.75	0.986	1.05	0.75	1.00	15.84	8.17	24.01	0.27	1.00	1.00	1.44	1.21	Non Liquefiable
3.00	SM-ML	23	2.01	1.01	47.00	0.14	IV	0.24	6.80	0.98	5.82	2.82	0.31	1.70	0.75	0.986	1.05	0.85	1.00	25.81	10.16	35.97	NA	1.00	1.00	1.44	>1.0	Non Liquefiable
4.50	SM-ML	26	2.01	1.01	36.00	0.18	IV	0.24	6.80	0.97	8.84	4.34	0.31	1.52	0.75	0.986	1.05	0.95	1.00	29.13	10.83	39.96	NA	1.00	1.00	1.44	>1.0	Non Liquefiable
6.00	SM	25	2.00	1.00	18.00	0.21	IV	0.24	6.80	0.95	11.85	5.85	0.30	1.31	0.75	0.986	1.05	0.95	1.00	24.11	4.83	28.94	0.41	1.00	1.00	1.44	1.95	Non Liquefiable
7.50	SM	27	2.00	1.00	18.00	0.21	IV	0.24	6.80	0.94	14.85	7.35	0.30	1.17	0.75	0.986	1.05	0.95	1.00	23.23	4.78	28.01	0.37	1.00	1.00	1.44	1.79	Non Liquefiable
9.00	ML-CL	26	2.01	1.01	88.00	0.065	IV	0.24	6.80	0.93	17.85	8.85	0.29	1.06	0.75	0.986	1.05	1.00	1.00	21.46	9.29	30.75	NA	1.00	1.00	1.44	>1.0	Non Liquefiable
10.50	ML-CL	30	2.01	1.01	88.00	0.065	IV	0.24	6.80	0.89	20.87	10.37	0.28	0.98	0.75	0.986	1.05	1.00	1.00	22.88	9.58	32.46	NA	1.00	1.00	1.44	>1.0	Non Liquefiable
12.00	Cl	59	2.05	1.05	96.00	0.06	IV	0.24	6.80	0.85	23.88	11.88	0.27	0.92	0.75	0.986	1.05	1.00	1.00	42.03	13.41	55.44	NA	1.00	1.00	1.44	>1.0	Non Liquefiable
13.50	CI	62	2.05	1.05	96.00	0.06	IV	0.24	6.80	0.81	26.96	13.46	0.25	0.86	0.75	0.986	1.05	1.00	1.00	41.50	13.3	54.80	NA	1.00	1.00	1.44	>1.0	Non Liquefiable
15.00	CL	75	2.07	1.07	87.00	0.065	IV	0.24	6.80	0.77	30.03	15.03	0.24	0.82	0.75	0.986	1.05	1.00	1.00	47.50	14.5	62.00	NA	1.00	1.00	1.44	>1.0	Non Liquefiable
16.50	CL	93	2.08	1.08	87.00	0.065	IV	0.24	6.80	0.73	33.14	16.64	0.23	0.78	0.75	0.986	1.05	1.00	1.00	55.99	16.2	72.19	NA	1.00	1.00	1.44	>1.0	Non Liquefiable
18.00	CL	115	2.10	1.10	88.00	0.065	IV	0.24	6.80	0.69	36.26	18.26	0.21	0.74	0.75	0.986	1.05	1.00	1.00	66.31	18.26	84.57	NA	1.00	1.00	1.44	>1.0	Non Liquefiable
19.50	CL	125	2.10	1.10	88.00	0.065	IV	0.24	6.80	0.65	39.41	19.91	0.20	0.71	0.75	0.986	1.05	1.00	1.00	68.79	18.76	87.55	NA	1.00	1.00	1.44	>1.0	Non Liquefiable
21.00	CL	100	2.10	1.10	86.00	0.065	IV	0.24	6.80	0.61	42.56	21.56	0.18	0.68	0.75	0.986	1.05	1.00	1.00	52.89	15.58	68.47	NA	1.00	1.00	1.44	>1.0	Non Liquefiable
22.50	CL	101	2.10	1.10	86.00	0.065	IV	0.24	6.80	0.57	45.71	23.21	0.18	0.66	0.75	0.986	1.05	1.00	1.00	51.48	15.3	66.78	NA	1.00	1.00	1.44	>1.0	Non Liquefiable

Depth	Soil type	Observed SPT	Saturated Density	Submerged Density	Fine content	D50	Earthquake Zone	PGA	Magnitude	Rd	Total overburden Pressure	Effective overburden Pressure	CSR	CN	CE	CH	CB	CR	CS	SPT Corrected	Δ(N1)60cs	Final N160	CRR	K1	K2	MSF	FS	
1.50	SM-ML	9	1.70	1.70	45.00	0.18	IV	0.24	6.80	0.99	2.55	2.55	0.15	1.70	0.75	0.986	1.05	0.75	1.00	8.91	6.78	15.69	0.17	1.00	1.00	1.44	1.56	Non Liquefiable
3.00	SM	11	1.71	1.71	14.00	0.23	IV	0.24	6.80	0.98	5.10	5.10	0.15	1.40	0.75	0.986	1.05	0.85	1.00	10.17	2.63	12.80	0.14	1.00	1.00	1.44	1.31	Non Liquefiable
4.50	SM	12	1.71	1.71	14.00	0.23	IV	0.24	6.80	0.97	7.67	7.67	0.15	1.14	0.75	0.986	1.05	0.95	1.00	10.11	2.63	12.74	0.14	1.00	1.00	1.44	1.32	Non Liquefiable
6.00	SM	17	1.80	1.80	21.00	0.22	IV	0.24	6.80	0.95	10.23	10.23	0.15	0.99	0.75	0.986	1.05	0.95	1.00	12.40	4.85	17.25	0.18	1.00	1.00	1.44	1.77	Non Liquefiable
7.50	SM	20	1.80	1.80	21.00	0.22	IV	0.24	6.80	0.94	12.93	12.93	0.15	0.88	0.75	0.986	1.05	0.95	1.00	12.97	4.9	17.87	0.19	0.95	1.00	1.44	1.76	Non Liquefiable
9.00	SM	26	1.80	1.80	17.00	0.23	IV	0.24	6.80	0.93	15.63	15.63	0.15	0.80	0.75	0.986	1.05	1.00	1.00	16.15	3.98	20.13	0.22	0.90	1.00	1.44	1.93	Non Liquefiable
10.50	CI	22	1.90	1.90	94.00	0.06	IV	0.24	6.80	0.89	18.33	18.33	0.14	0.74	0.75	0.986	1.05	1.00	1.00	12.62	7.52	20.14	0.22	1.00	1.00	1.44	2.25	Non Liquefiable
12.00	CI	33	1.90	1.90	96.00	0.06	IV	0.24	6.80	0.85	21.18	21.18	0.13	0.69	0.75	0.986	1.05	1.00	1.00	17.61	8.52	26.13	0.32	1.00	1.00	1.44	3.42	Non Liquefiable
13.50	CI	36	1.95	1.95	96.00	0.06	IV	0.24	6.80	0.81	24.03	24.03	0.13	0.65	0.75	0.986	1.05	1.00	1.00	18.03	8.61	26.64	0.33	1.00	1.00	1.44	3.73	Non Liquefiable
15.00	CL	39	1.95	1.95	91.00	0.06	IV	0.24	6.80	0.77	26.96	26.96	0.12	0.61	0.75	0.986	1.05	1.00	1.00	18.44	8.69	27.13	0.34	1.00	1.00	1.44	4.09	Non Liquefiable
16.50	CL	38	1.95	1.95	91.00	0.06	IV	0.24	6.80	0.73	29.88	29.88	0.11	0.58	0.75	0.986	1.05	1.00	1.00	17.07	8.41	25.48	0.30	1.00	1.00	1.44	3.80	Non Liquefiable
18.00	CL	56	2.00	2.00	85.00	0.07	IV	0.24	6.80	0.69	32.81	32.81	0.11	0.55	0.75	0.986	1.05	1.00	1.00	24.01	9.8	33.81	NA	1.00	1.00	1.44	>1.0	Non Liquefiable
19.50	CL	65	2.00	2.00	85.00	0.07	IV	0.24	6.80	0.65	35.81	35.81	0.10	0.53	0.75	0.986	1.05	1.00	1.00	26.67	10.34	37.01	NA	1.00	1.00	1.44	>1.0	Non Liquefiable
21.00	ML	55	2.00	2.00	62.00	0.09	IV	0.24	6.80	0.61	38.81	38.81	0.10	0.51	0.75	0.986	1.05	1.00	1.00	21.68	9.34	31.02	NA	0.67	1.00	1.44	>1.0	Non Liquefiable
22.50	ML	57	2.00	2.00	62.00	0.09	IV	0.24	6.80	0.57	41.81	41.81	0.09	0.49	0.75	0.986	1.05	1.00	1.00	21.65	9.33	30.98	NA	0.66	1.00	1.44	>1.0	Non Liquefiable